STUDY OF SURFACE MODIFICATION OF AL ALLOY USING SOLID STATE PLASTIC DEFORMATION

A THESIS SUBMITTED IN FULFILLMENT OF THE REQUIREMENT FOR THE AWARD OF THE DEGREE OF

DOCTOR OF PHILOSOPHY

IN

MECHANICAL ENGINEERING

BY

RAVI BUTOLA
(Roll No. 2K16/Ph.D./ME/56)

UNDER THE SUPERVISION OF

Dr. RANGANATH M. SINGARI
Professor, Department of Mechanical Engineering

Dr. QASIM MURTAZA
Professor, Department of Mechanical Engineering

DEPARTMENT OF MECHANICAL ENGINEERING
DELHI TECHNOLOGICAL UNIVERSITY
MAIN BAWANA ROAD, SHAHABAD DAULATPUR
DELHI- 110042, INDIA

2021

DECLARATION

I hereby declare that the thesis work entitled **"STUDY OF SURFACE MODIFICATION OF AL ALLOY USING SOLID STATE PLASTIC DEFORMATION"** is an original work carried out by me under the supervision of **Dr. Ranganath M. Singari** (Professor, Department of Mechanical Engineering and Head Department of Design Delhi Technological University, Delhi) and **Dr. Qasim Murtaza** (Professor, Department of Mechanical Engineering Delhi Technological University, Delhi). This thesis has been prepared in conformity with the rules and regulations of the Delhi Technological University, Delhi. The research work presented and reported in the thesis has not been submitted either in part or full to any other university or institute for the award of any other degree or diploma.

Ravi Butola
(Registration Number: 2K16/Ph.D./ME/56)
Department of Mechanical Engineering
Delhi Technological University, Delhi

Date: 17/05/2021
Place: New Delhi

CERTIFICATE

This is to certify that the work embodied in this thesis entitled, **"Study of Surface Modification of Al Alloy Using Solid State Plastic Deformation"** being submitted by **Mr. Ravi Butola (Roll No-2K16/Ph.D./ME/56)** for the award of **Doctor of Philosophy Degree** (**Ph.D.**) in Mechanical Engineering at Delhi Technological University, Delhi is an authentic work carried out by him under our guidance and supervision.

It is further certified that the work is based on original research and the matter embodied in this thesis has not been submitted to any other university/institute for award of any degree to the best of our knowledge and belief.

Dr. Ranganath M. Singari
SUPERVISOR
Professor,
Department of Mechanical Engineering,
Head, Department of Design
Delhi Technological University,
Delhi-110042

Dr. Qasim Murtaza
SUPERVISOR
Professor,
Department of Mechanical Engineering,
Delhi Technological University,
Delhi-110042

Dedicated to

My Parents and beloved Wife

ACKNOWLEDGEMENT

While bringing out this thesis to its final form, I came across a number of people whose contributions in various ways helped my field of research and they deserve special thanks. It is a pleasure to convey my gratitude to all of them.

First and foremost, I would like to express my deep sense of gratitude and indebtedness to my parents, wife, supervisors (**Prof. Ranganath M. Singari, Prof. Qasim Murtaza**) for their invaluable encouragement, suggestions and support from an early stage of this research work and providing me extraordinary experiences throughout the research work.

I would like to express my sincere gratitude to **Prof. R.S. Mishra**, Chairman, DRC, Mechanical Engineering Department and **Prof. Samsher**, Head, Mechanical Engineering Department, Delhi Technological University, for their valuable help, motivation and extending all the necessary processing and experimental facilities during my research work.

I am very thankful to **Prof. P.M Pandey, Prof. P.K Jain, Prof. R.S Walia,** and **Prof. S.G Warker** for being the members of my SRC committee. I am also grateful to **Prof. Vipin, Dr. N. Yuvaraj, Dr. Vijay Gautam**, **Dr. Nand Kumar, Dr. Ravi Pratap Singh, and Dr. Mohit Tyagi** for their kind support during this research work. My sincere thanks to all the staff members of Mechanical Engineering Department, Delhi Technological University, for their support during my entire research work. I am very grateful to **Mr. Pratap Singh Rana**, Technical Officer C (DRDO), **Mr. Tek Chand, Mr. O.P Mouria, Mr. Virender Sharma, Mr. Sunil Kumar, Mr. Net Ram** and **Mr. Lallan Sinha** for their valuable technical support.

I would like to extend my sincere gratitude to **Dr. Mohan Singh Mahata**, Department of Physics, Delhi Technological University and **Dr. Prakash Chandra,** Department of Bio-Technology, Delhi Technological University for their valuable help, motivation and extending all the necessary processing and experimental facilities during my research work and for his kind support and continuous motivation to complete my Ph.D.

I am thankful to my students and research scholars of Laser Spectroscopy Laboratory Department of Physics, Delhi Technological University (DTU) who helped me in every possible way to finish this research work.

Ravi Butola

PREFACE

In this thesis the fabrication of surface composites using solid-state techniques has been described through Formation of Self-Assembled Monolayer (SAM) on the Aluminium Alloy surface via Friction Stir Processing techniques. It would help the researchers to understand the technique to get better mechanical properties by minimizing the nanoparticles reinforcement. The contents of the thesis are as follows:

First chapter: - This chapter introduces surface modification and surface composite of the materials; classification of surface modification and various processing technique for modifying the surface of the substrate materials. It gives an idea about various research gaps existing in fabrication of aluminum alloys based matrix surface composites. Further, the research motivation for the present research work is also discussed.

Second chapter: - This chapter is on the literature review of composites and surface composites of aluminum alloy by various solid state processing techniques. It also discusses various methods of filling reinforcement particles for the advancement of aluminum alloy metal matrix surface composites by Friction stir processing. Advantages, limitations and applications of the Friction Stir Processing are discussed. It also includes analysis of research gap, objective of the research work and plan of research work.

Third Chapter: - This chapter discusses the residual stresses analysis of Friction stir processing tool using modelling and simulation through ABAQUS software. It also includes the details of tool materials and fabrication of FSW/FSP tool using CNC machine.

Fourth Chapter: - This chapter deals with the selection of substrate (base) material, FSW/FSP tool material and reinforcement powder. This chapter also includes the preparation of substrate material through Self-Assembled Monolayer (SAM) technique followed by Friction Stir Processing to fabricate the surface composites. The detailed mechanical, microstructure, residual stress and wear testing procedures are presented.

Fifth chapter: - This chapter discusses the details for finding the optimum process parameter and effect of process parameters for obtaining the maximum hardness and tensile properties of the fabricated surface composite through the Taguchi technique. The microstructure, microhardness, and tensile properties of the Al-B_4C surface composite are discussed. This chapter also investigates the measurement of residual stresses and wear properties of fabricated aluminum based metal matrix surface composites.

Sixth chapter: - It summarizes present research investigation for the successfully fabricated aluminum metal matrix surface composites through Self-Assembled Monolayer followed by Friction Stir Processing with B_4C nanoparticle reinforcement, and the effect of tool pin profiles and process parameter. This chapter also introduces the future scope for further research in this field. Significant findings have been drawn from performed experimentation.

TABLE OF CONTENTS

List of Figures

LIST OF TABLES

NOMENCLATURE

AISI	American Iron and Steel Institute
ANOVA	Analysis of variance
AS	Advancing Side
ASTM	American Society for Testing Materials
BM	Base Metal
CDRX	Continuous Dynamic Recrystallization
B4C	Boron Carbide
SAM	Self-Assembled Monolayer
DEE	Di-ethyl ether
CNT	Carbon Nano Tube
CVD	Chemical Vapour deposition
PVD	Physical Vapour Deposition
DDRX	Discontinuous Dynamic Recrystallization
DoE	Design of Experiments
DRV	Dynamic Recovery
EDM	Electrical Discharge Machining
EDS	Energy Dispersive Spectrometer
FE-SEM	Field Emission Scanning Electron Microscope
FSP	Friction Stir Processing
FSW	Friction Stir Welding
HAZ	Heat Affected Zone
PD	Pin Diameter
PL	Pin Length
RS	Retreating Side
SD	Shoulder Diameter
SEM	Scanning Electron Microscope
SP	Single Pass
SZ	Stir Zone
TIG	Tungsten Inert Gas
TMAZ	Thermo Mechanically Affected Zone
TWI	The Welding Institute
UK	United Kingdom
UTS	Ultimate Tensile Strength
VHN	Vickers Hardness Number
XRD	X-Ray Diffraction
FEA	Finite Element Analysis
CNC	Computer Numerical Control
MMC	Metal Matrix Composite

ABSTRACT

Surface modification or surface composites are considered to have a potential for generation of new materials for numerous engineering applications due to their enhanced mechanical and physical properties. Fabrication of surface composites by Friction Stir Processing (FSP) with enhanced surface properties is attracting by researchers owing to improved life of the component. Friction Stir Processing (FSP) is a solid-state technique, which has been used for fabrication of Al-B_4C surface composite. FSP is a relatively new solid-state technique that has been widely utilized for surface modification of Al alloy. The various methods are used for the fabrication of surface composite using different reinforcement applying methods but no research has been carried out on minimizing the reinforcement particles. Surface modification of Aluminium alloy has a wide range of applications in aerospace industries, where high strength to weight ratio is required.

In this research work, the main focus has been made to fabricate Al-B_4C surface composites with minimizing the B_4C nanoparticle reinforcement through the processing and formation of Self-Assembled Monolayer (SAM) over the surface of substrate (base) metal followed by Friction stir processing (FSP) method. Al 7075-T6 alloy was used as a matrix material and B_4C nanoparticles size (<30nm) was used as reinforcement through Self-Assembled Monolayer (SAM). It is very difficult to control the uniform or homogeneous distribution of nanoparticle reinforcement on the substrate (base) metal by other surface modifying technique. So, in the current method, we have modified the surface using B_4C nanoparticles, which is processed through the Self-Assembled Monolayer on the surface of Al-alloy. SAM is widely being used as a linking process on various surfaces. The major advantage of the Self-Assembled Monolayer technique is that it minimizes the quantity of B_4C nanoparticles used in the preparation of surface composite.

Al-B_4C surface composite with reinforced B_4C nanoparticle through single-pass was performed using different tool rotation speed, traverse speed, and tool tilt angle 2^o were constant during Al-B_4C surface composite experimentation. This research investigated the process parameters of FSP such as tool rotational speed, tool traverse speed in accordance with Taguchi's orthogonal array L9 for obtaining better surface properties of Al-B_4C surface composites.

In physical characteristic microstructure, Scanning Electron Microscope, Field Emission Scanning-Electron Microscope (FESEM) and X-Ray Diffraction (XRD) were examined to analyze the fabricated Al-B_4C surface composite. Fractographs analysis was also done to know the fracture nature of the fabricated Al-B_4C nano surface composite.

In mechanical properties microhardness (HV) and ultimate tensile strength (UTS) of the fabricated Al-B_4C surface composites was studied using ANOVA it was observed that in case of both UTS and HV, tool traverse speed had a more significant role than tool rotational speed. The Al-B_4C surface composite sample has obtained higher hardness as compared to the base metal hardness.
Compressive residual stresses are induced during the friction stir processing due to severe plastic deformation of metal.

The wear behavior of the substrate (base) metal and surface composites were studied through a pin on disc tribometer. The maximum wear has been observed in the substrate (base) metal followed by the Al-B_4C surface composites sample processed at tool speeds of 1000 rpm, 1400 rpm and 1200 rpm. Wear resistance has improved by up to 42.6%, the maximum wear resistance improvement in terms of percentage has been seen in the Al-B_4C surface composites sample processed at 1200 rpm and subjected to 20N load. This follows the same pattern as the values from microhardness, which explains this phenomenon.

Frictional and wear analysis highlights the mechanical durability and surface wear of substrate (base) metal and surface composites. Experimental data suggests that Al-B_4C nano surface composite has the least wearing and frictional coefficient due to the effective application and processing of B_4C nanoparticles Self-Assembled Monolayer technique. Substrate (base) metal has been reported to have least durability and highest frictional coefficient. The worn out surfaces of the Al-B_4C surface composites and wear debris were analyzed through SEM studies to understand the wear mechanisms.

CHAPTER 1

INTRODUCTION

1.1 BACKGROUND: SURFACE MODIFICATION AND SURFACE COMPOSITE

Surface modification or surface composite is the process of modifying the surface of a matrix material by using different methods. The increasing demand of surface composite in order to meet the functional and design requirement of customers, toward the development of surface composite. The selection of the right method to fabricate the surface is a crucial part of the step of design of an engineering component. The first step in surface modification is to determine the surface and substrate engineering requirements which involves one or more of the properties like mechanical and wear properties. The various surface treatments generally used in engineering practice and presented as under. Surface engineering includes a wide range of processes, tailoring chemical and structural properties in a thin surface layer of the substrate, by modifying the existing surface to a depth of 0.001 to 1.0 mm such as: ion implantation, sputtering to weld hard facing and other cladding processes, producing typically 1-20 mm thick coatings, usually for wear and corrosion resistance and repairing damaged parts. The importance of Al based surface composites has gained a wide application in recent years. Surface composites (SC) are fast succeeding traditional metallic alloys in many applications like aerospace, defences, automotive industries. The nanoparticles reinforcing materials used in the development of new material. Friction Stir Processing (FSP) is a solid-state processing technique used to modify the surface layer by plastic deformation, in this a high rotating non-consumable tool is plunged into the material and made to travel. It changes the properties of the material without changing the composition of the material. The surface layer thickness formation using FSP can range from micrometres to millimetres. Fig. 1.1 shows the types of surface modification process.

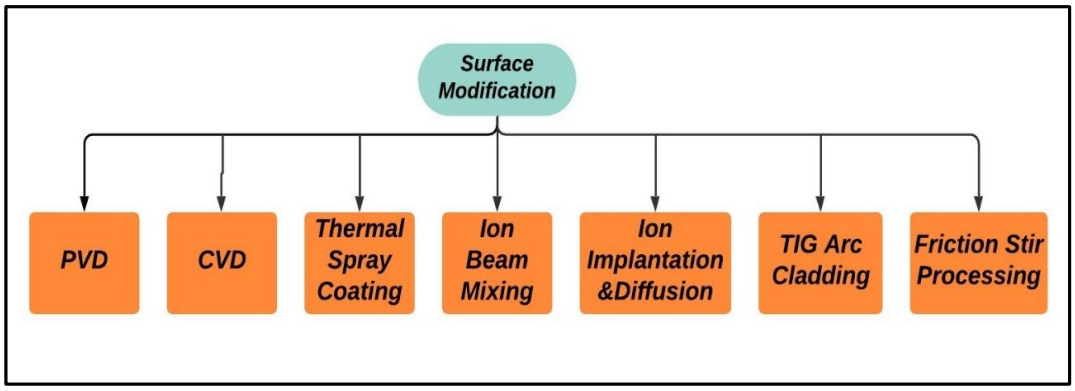

Figure 1.1-Classification of surface modification process

1.2 TYPES OF SURFACE MODIFICATION PROCESSING TECHNIQUES

In the classification of surface modification processes the other deposition processes, such as laser alloying, thermal spraying, cold spraying, liquid deposition methods, anodizing, chemical vapor deposition (CVD), and physical vapor deposition (PVD), are also extensively used in surface engineering. The classification of surface modification methods with respect to the depth and place of interaction on the substrate metal as shown in fig. 1.2.

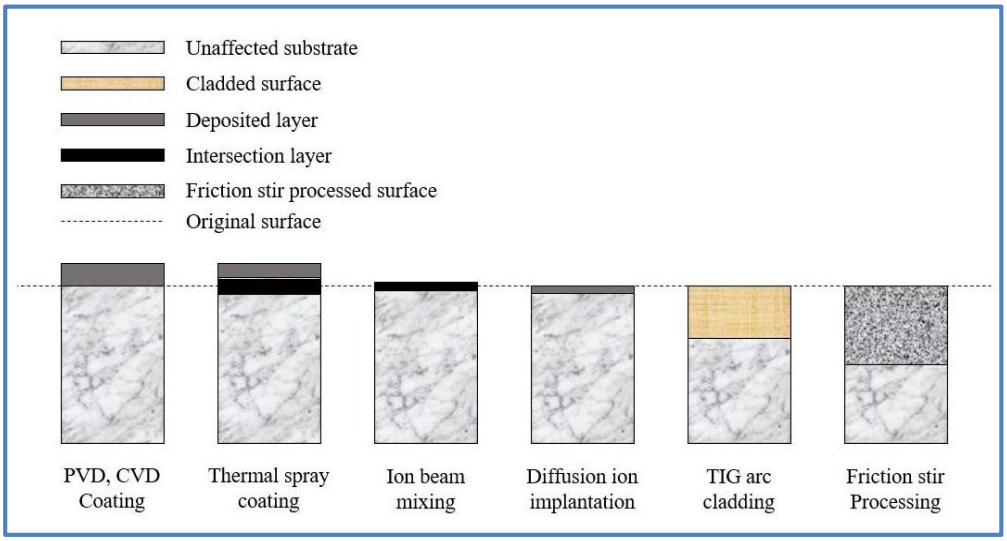

Figure 1.2-Classification of surface modification methods with respect to the depth and place of interaction on the substrate metal (Adopted from) [1]

1.2.1 Physical Vapour Deposition (PVD)

In PVD coating a thin film is deposited on the substrate by vaporizing or atomizing a solid material in a vacuum environment and depositing it on other material, the energy required for vaporization is usually provided from laser beam, heating wire, electron beam etc. [2]. The schematic diagram of the PVD process using electron beam is shown in fig. 1.3. The process is used to produce protective thin film on the corrosion exposed media [3]. Its application ranges from industrial parts to decorative objects [4]. Using the same technique Tanski et al. [5] produced a coating on aluminum alloy and examined it using electron microscope. They found that homogeneous, and crack free uniform thickness coating was produced using PVD process. The main advantage of the process is the on-demand adjustment of the coating layers mechanical, corrosion and aesthetic properties. The coating produced by PVD is thin, so there is always the requirement of multilayering [3].

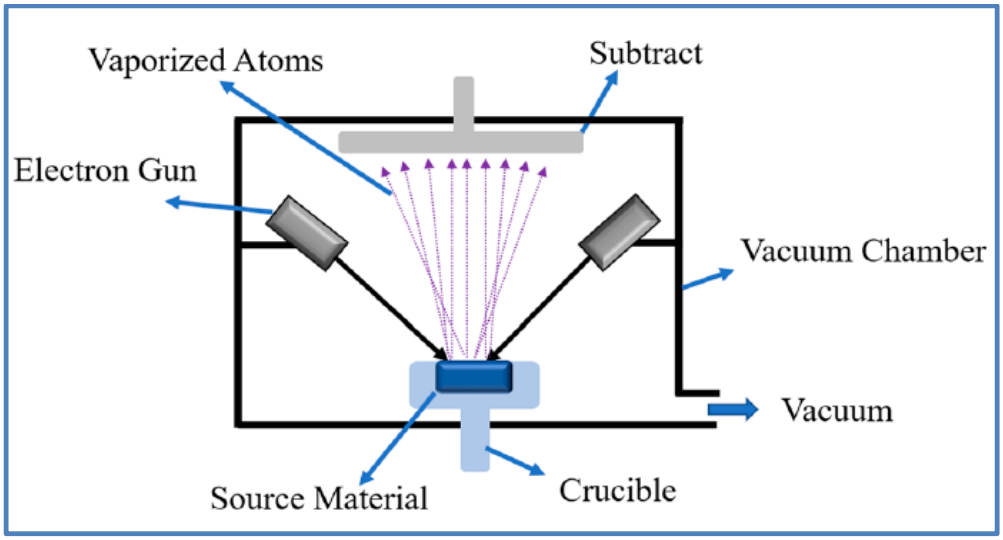

Figure 1.3-Schematic diagram representing PVD coating of a substrate [3]

1.2.2 Chemical Vapour Deposition (CVD)

The CVD process is same like PVD process but instead of vaporizing the solid source, the depositing species are inlet into the coating chamber in a gaseous phase. The schematic diagram of CVD process is shown in fig 1.4. The coating produced by CVD is of high quality and has high resistance, because of the quality it is used in semiconductor industry [6]–[9]. It finds wide application in producing lubricious coating, circuit board, biomedical device implants etc. [10]. Using CVD technique Abidin et, al. [11] deposited carbon fiber along with TiN was deposited on the aluminum substrate, a homogeneous coating was observed and also non-wetting behavior was shown by TiN in contact with CF-Al, but formed excellent adhesion because of the chemical interaction. CVD cannot be performed on the temperature sensitive material, because the substrate is heated to a high temperature [3].

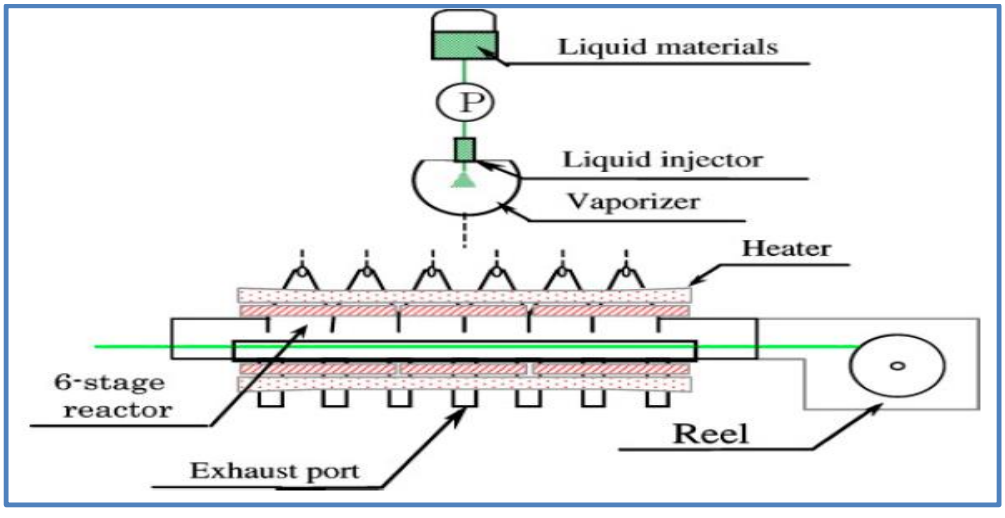

Figure 1.4-Schematic diagram of CVD coating process [12].

1.2.3 Spray Deposition Technique

In spray deposition technique molten metal is sprayed on the substrate material producing a high-quality composite material. There is good interfacial bonding between the substrate and the coating produced using this process [13], the schematic diagram of the thermal spray process is shown in fig. 1.5. The coating produced using thermal spray technique is of higher thickness compared to the coating produced using CVD or PVD [14]. There is high porosity associated with the spray deposition process [13]. Tyagi et, al. [15] on-steel substrate produced carbon coating via thermal spraying HVOF technique, which is one of the spray deposition technique, to enhance the wear resistance and hardness of the material.

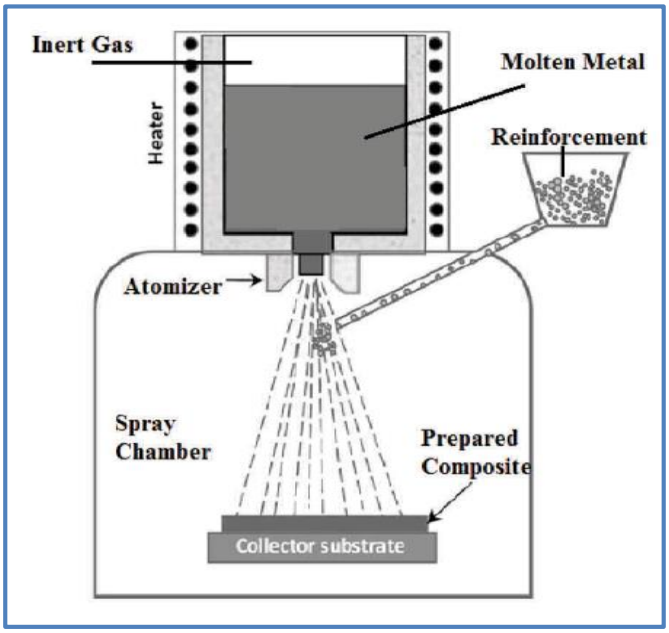

Figure 1.5-Schematic diagram of thermal spray coating process [16]

1.2.4 Ion Beam Mixing Technique

Ion Beam Mixing technique modifies the surface by bombarding the heavy ions on the base material, the ions are accelerated to a high speed and when the ions contacts the surface they slow down producing, ultimately comes to rest forming an implanted impurity. The diagram in fig. 1.6, illustrates the focused ion mixing phenomenon. This process is used in optoelectronic and microelectronic industry [17]. Su et, al. [18] in their study illustrated the temperature dependency of the ion beam mixing in crystalline Fe and amorphous SiOC mixing using Kr ion. They found that intermixing decreased with the increasing temperature. All over the penetrated material there is very uniform composition, but the penetration is only up to a limited depth [19].

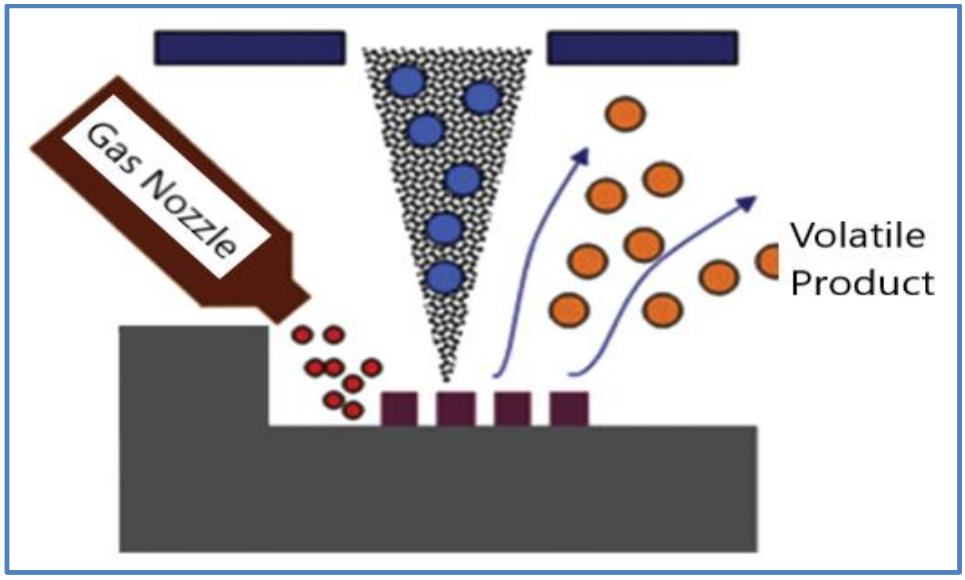

Figure 1.6-Ion Beam mixing process [20]

1.2.5 Ion Implantation Technique

The process of ion implantation is done to introduce the chosen atomic species on the material surface. The advantage of this method is that it requires no thermal assistance. Fig. 1.7 represents the ion implantation phenomenon. With the process thermal distortion is not an issue as the process is intrinsic to low temperature and also the addition done to the surface via this process is quite effective. Dearnaley [21] in his work analyzed the impact of ion implantation on properties of the metals and carbides. He concluded that on doping the material using the process the fatigue endurance and wear resistance of the metals enhanced. The ion implantation process is associated with the doping not with the doping, so there is cohesion of protective layer on the material surface.

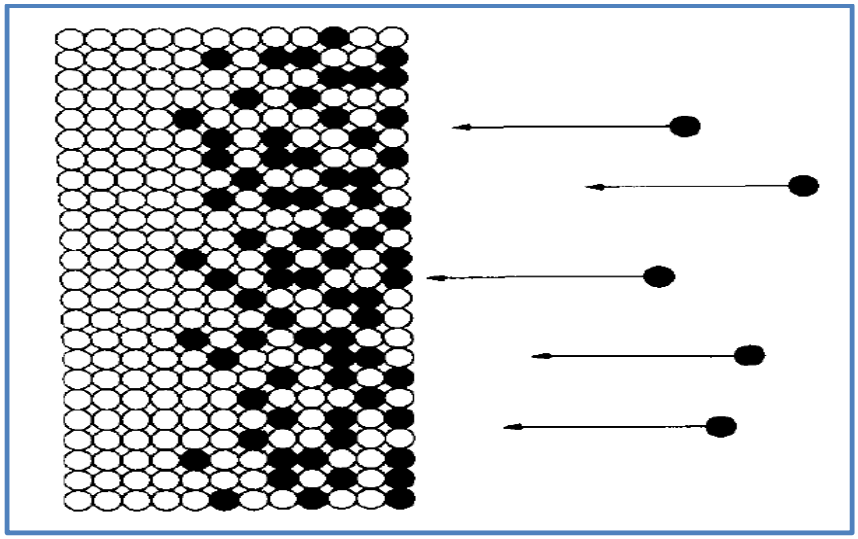

Figure 1.7-Ion implantation phenomenon [19]

1.2.6 TIG Arc Method

The TIG arc method is a surface modification method, used to improve the mechanical, tribological and corrosion properties [22]. The method is used to produce a thick surface composite layer; the schematic diagram of the process is represented by fig. 1.8. It is utilized usually when reactive material are involved. In industries like chemical, mining, petroleum TIG arc surface modification is utilized [1]. Using the same technique Islak et, al. [23] produced the surface composite (FeW/B_4C mix) on the steel substrate and observed the enhanced hardness of the composite produce.

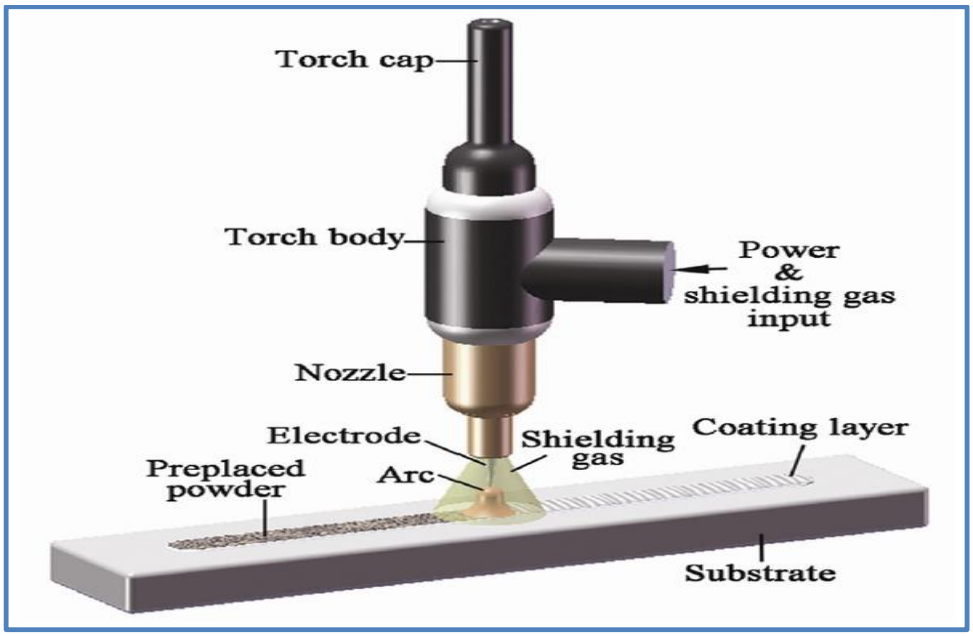

Figure 1.8-TIG arc method for surface modification [23]

1.2.7 Friction Stir Processing (FSP)

Friction stir processing (FSP) involves solid-state processing, in which reinforcement is incorporated into the matrix and a non-consumable tool rotating at a very high rpm is utilized to intermix the matrix and the reinforcement producing the composite, the fig. 1.9 illustrates the same. FSP is widely utilized in industries like aerospace, automotive, railroad, marine etc. [24]. A variety of governed factors in the process makes it more flexible and the major advantage over other processes is that the surface is modified till a depth to which tool is plunged. Kurt et, al.[25] modified the surface of the commercially pure aluminum by integrating SiC into it using FSP and they analyzed the influence of various process parameters on the material. From the study they concluded that increased tool rotational

speed, traverse speed contribute to the more homogenous distribution of the reinforcement and also the properties like hardness and bending strength enhanced on processing.

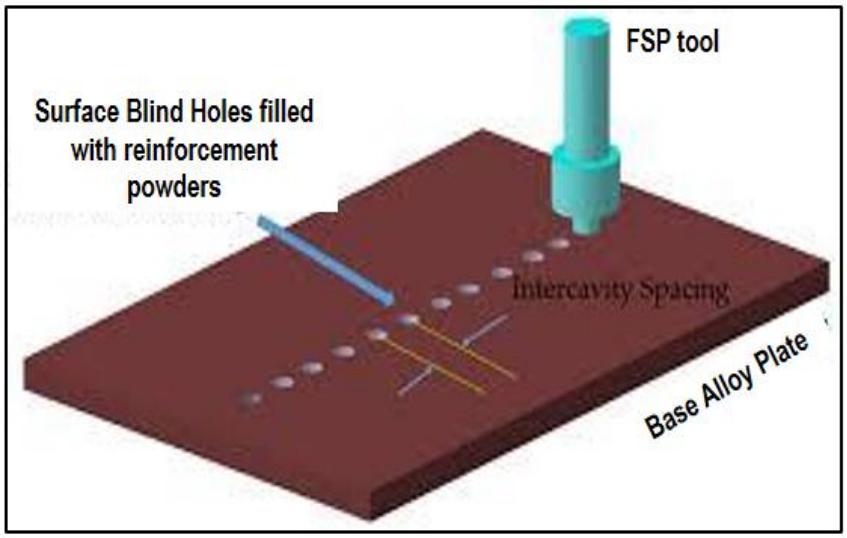

Figure 1.9-Schematic diagram of Friction stir processing technique [26]

1.3 IMPORTANCE OF ALUMINUM ALLOYS BASED SURFACE COMPOSITE FABRICATED USING FRICTION STIR PROCESSING (FSP)

The aluminum-based metal matrix composites are superseding the aluminum alloys owing to their excellent engineering properties like high hardness, wear resistance, strength to weight ratio, stability at high temperature, low thermal expansion and enhanced creep resistance. AMMCs have high hardness, low density and excellent thermo-chemical stability and are hence used to make bicycle frames, bulletproof vests, armorer tanks, containers of nuclear waste, neutron absorbers in nuclear power plants, transportation applications, etc. [27, 28]. AMMCs have been fabricated by several conventional techniques over decades such as casting, squeeze casting, mechanical alloying, etc. Particulate reinforced composite materials are easy to process with conventional fabrication methods due to lower cost, easy fabrication and isotropic in nature [29]. The surface characteristics of a material are crucial to realize longer life of mechanical components. For the surface modification process, the ceramic particles were incorporated in the surface of the matrix material by various techniques to enhance its surface properties. The most common methods include coating, plasma spraying, cladding, laser melt treatment, electron beam irradiation, etc. [30]. These methods are centred around liquid-phase processing at higher temperatures for the processing of surface composites. Because of the recrystallization process, the probability of the development of

some detrimental phases, because of the interfacial reaction between the matrix and reinforcement, are high. In addition, homogeneous dispersal of the nano reinforcement particles on the surface is a difficult task [31]. The aforementioned problems can be solved by conducting the processing under the substrate's melting point. This new surface altering technique is known as Friction Stir Processing.

FSP is capable of creating a surface composite where the surface layer thickness can vary from hundreds of micrometer to several millimeter. FSP is valuable in cases where a fine-grained microstructure is needed and cast defects need to be removed in order to get superior mechanical properties and wear resistance. FSP is also useful for the creation of surface composites as the formation of undesirable intermetallic materials, between reinforcement and matrix, can be avoided.

1.4 RESEARCH MOTIVATION

Nowadays, Aluminium Alloy matrix surface composites are superseding their conventional counterparts expeditiously in almost all of the advanced engineering applications given their improved mechanical properties. In Aluminium alloy-based metal matrix composites, nanoparticles ceramics reinforcements are incorporating into the Al alloy matrix to achieve enhanced mechanical properties but also cost of the composite or nanocomposites will be increases simultaneously due to the cost of nanoparticles reinforcement. Main aim of the fabrication of Al alloy matrix surface composites is to note and develop Self-Assembled Monolayer (SAM), study the consequence of the B_4C nanoparticles on the Al alloy and its mechanical properties of the fabricated surface composite or nanocomposite. The major benefit of Self-Assembled Monolayer technique is that it minimizes the quantity of B_4C nanoparticles used in the preparation of surface composite or nanocomposites and it also improves the property of adhesion of the nanoparticles on the surface of the base metal [32, 33].

1.5 SUMMARY

In preparation of surface composites, the choice of fabrication technology is an integral step of the engineering component design process. The choice of surface and substrate for the component plays a vital role. Aluminium surface composites have emerged in recent times as

significantly more dominant as traditional metallic alloys. Many surface composite techniques exist viz. PVD, CVD, and spray deposition technique, Ion beam mixing technique, Ion implantation and TIG arc method. Being liquid-phase techniques, all of them fall short of the many advantages of Friction Stir Processing, which is a solid-state processing technique. By conducting the processing under the melting point of the substrate, FSP manages to overcome many of the unwanted interfacial reactions that occur due to recrystallization in other techniques. Moreover, by making the microstructure of the substrate finer, FSP removes the cast-defects and results in better mechanical properties and wear resistance in the FSPed substrate. FSP may be used as a surface modification as well as surface fabrication technique.

CHAPTER 2

LITERATURE REVIEW

2.1 INTRODUCTION

This chapter deals with literature review on surface modification and surface composites of aluminum alloy by various solid state processing techniques. It also discusses various filling methods of reinforcement particle to advancement of aluminum alloy metal matrix surface composites by Friction stir processing. Advantages, limitations and applications of the Friction stir processing are discussed. It also includes analysis of research gap, objective of the research work and plane of research work are discussed.

2.2 FABRICATION OF METAL MATRIX COMPOSITES (MMC)

A material is said to be composite when it is the combination of two or more materials which are not soluble in each other and also possess superior properties to one of the component materials [13]. MMCs are a type of composites which are the mixture of alloy metal matrix or ductile metals with other material which can be metal, non-metal or even an organic compound. MMCs are generally known for their amazing properties which makes MMC different from other materials. These properties are the ability to resist High temperature, radiations, moisture, enhanced mechanical properties, thermal and electrical conductivity [34]. Aluminum, Magnesium, Copper, Iron and Titanium are available options for MMCs but aluminum and magnesium are being used most [35]. Aluminum MMCs are known for its lightweight, processing ease with different techniques, high strength to weight ratio, economic feasibility, and excellent corrosion resistance [34]. Similarly, other MMCs have their own merits. In fig. 2.1 shows the types of metal matrix composite production processes.

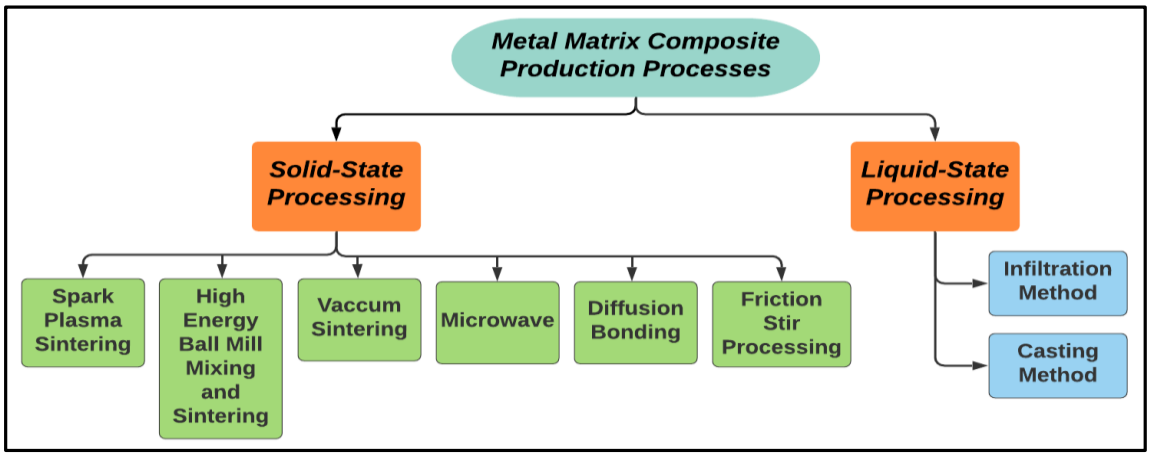

Figure 2.1-Types of metal matrix composite production processes

2.3 SOLID-STATE PROCESSING TECHNIQUES FOR FABRICATION OF COMPOSITES

In this process metal-matrix composites are fabricated and the material matrix is bonded to reinforcements by mutual diffusion which arises between them at higher pressure and temperature [13]. In designing of Ti-based matrix composites, during the situ formation of particles and solution hardening of the matrix both should be taken into consideration simultaneously for alloy formation. Operations like hot forging or heat-treatment can be used for further improvement in properties like fatigue and other application-based properties of powder metallurgy of Ti alloy [36]. The author mechanism for super plasticity in composites is described and it is observed that the probably interface diffusion controls the grain boundary sliding. Aluminum alloys usually have a significant volume fraction of particles in the second phase. Although there is little intentionally added second phase constituents that are formed because of chemistry of the alloy and Al_2O_3 particles are present non-variably. Al_2O_3 particles are present due to the thin alumina layer on the powder surface which is broken down during the process and generally they are uniformly dispersed [37]. The properties of particulate-reinforced composites are highly affected by the distributed reinforcement particles [35]. Powder metallurgy is one of the most common techniques which is used for metal matrix composite's (MMC's) manufacturing [38–41]. Solid-state processing has proved its capability of producing superior property materials as compared to casting techniques. This superiority in properties is due to the powder characteristics to solidify rapidly [38]. Powder metallurgy techniques are being used in automobile industries to manufacture cams, connecting rods, valve seats and many more [42,43]. T. Ozben et. al.[44] in his research studied the machinability and mechanical characteristics of the aluminium MMC reinforced by SiC particles and found the increase in the ratio of reinforcement increases the hardness, density and tensile of aluminium metal matrix composites (MMC).

2.3.1 Plasma Sintering

Sintering of Al_2O_3–SiC where Al_2O_3 is matrix and SiC is reinforcement, the composite was successfully produced by Spark Plasma Sintering. This process is shown in fig. 2.2, the temperature of mould and composite is increased at a very rapid rate. A pressure is applied during this heating process and due to this pressure, sintering happens. The powder is condensed in the mould due to the electrical sparks produced from this electrical current. A plasma environment is produced due to this current [45]**.** The composite which was obtained

showed the maximum hardness of 324.6 HV with 20 weight% Al_2O_3-SiC. The alumina particles which are present in the matrix were homogeneous and were distributed uniformly [46]. Different types of atmosphere are used in powder metallurgy. We can use argon gas, hydrogen gas, air or vacuum as atmosphere. To start the process a pulse current is used and later on after activation level is activated, densification is achieved by external pressure. Generation of plasma requires special conditions and the conductivity of the material changes during the process [47].

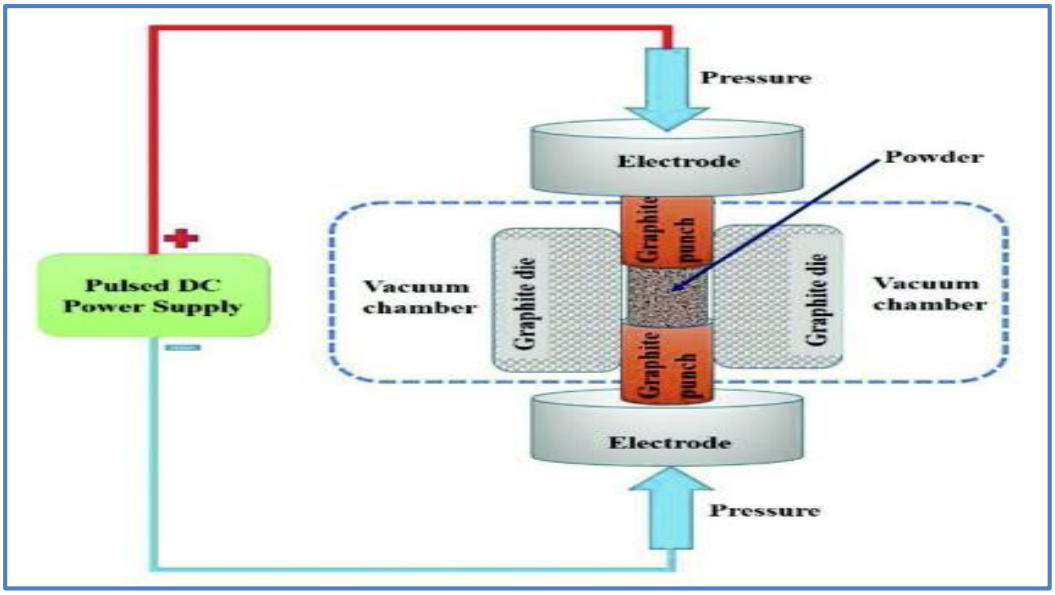

Figure 2.2-Plasma sintering process [13, 45]

2.3.2 High Energy Ball Mill Mixing and Sintering

In High Energy ball mill mixing and sintering is a process that produces a uniformly distributed reinforcement particles which are present in the matrix of the Aluminium. In this process repeated welding and fracturing occurs in the mixture of the powder particles [49]**.** One of the challenges in reinforcement of milled powder metallurgy is to get a fully dense compact material and its nano-scale grain size is retained. The high-energy ball milling and sintering process is shown in fig. 2.3.

The milling speed used by J. Bhatt et. al. [48] was 300rpm and a nano structural metal matrix composite of Aluminium and Magnesium with reinforced Silica particles was successfully produced. The maximum hardness which was observed in the nano-reinforced composite was 145.2 HV which is much more than the hardness of reinforced micro composites in comparison. Their reinforcement particles in the aluminium matrix were uniformly distributed and were homogeneous at 20 h as per Vickers's hardness**.** The top surface of the

mechanically milled aluminum particles was covered with a layer of oxide which gave a rise to some problems in the reinforcement [50]. Di Zhou [51] has worked on a Bi_3NbO_7 ceramic and fabricated it by the process of High energy milling and V_2O_5 was taken to as an additive in the process of fabrication. Structure, and microwave dielectric properties of the material Bi3NbO7 ceramics was analyze and was improved for other applications.

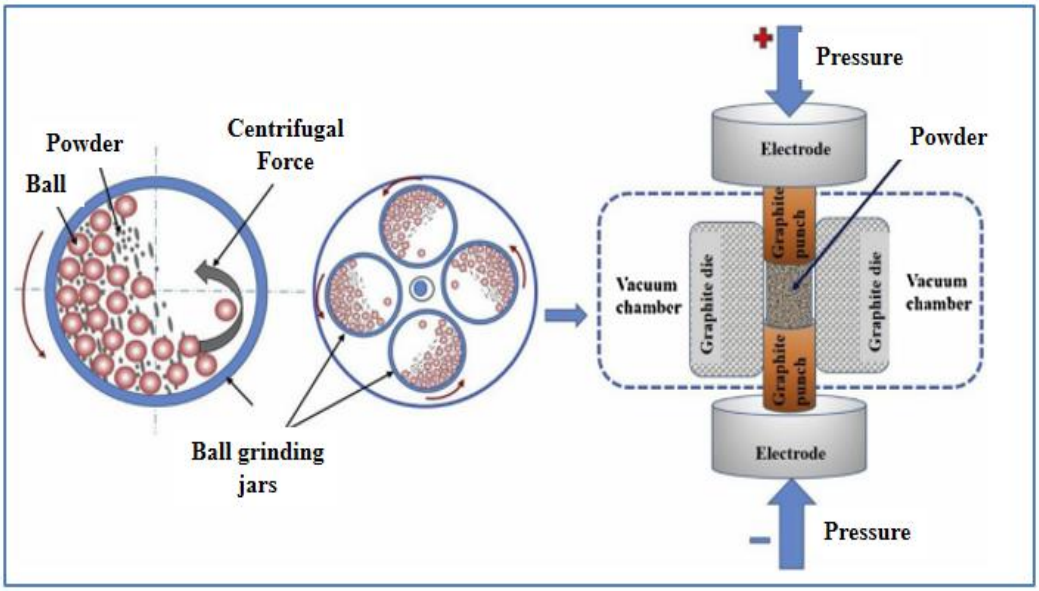

Figure 2.3-High-energy ball milling and sintering process [13, 48]

2.3.3 Vacuum Sintering

Due to its good controllability and large-scale features, this is one of the most commonly used sintering method. Atmosphere is one of the most important characteristics in sintering process [52]. The difference that vacuum atmosphere creates can be seen in the after compacting. Yan Gao [53] observed that as the temperature of sintering increases, and reaches a particular level, a minimum porosity will be observed in the alloys, and also homogeneous microstructure and the best possible hardness will also be. Hence, it was concluded that the microhardness and fracture toughness for a sintered material depends upon the porosity and grain size of the material [54]. The vacuum powder metallurgy is done in two steps; the first step includes cold and hot isostatic pressing of containers and the second step includes developing of HIP-ped ingots to the final product. Powders that have water ionized irregular shaped particles are particularly suitable for uniaxial cold compacting after a soft de-oxidation annealing is performed on it [55]. The Vacuum sintering process is shown in fig. 2.4.

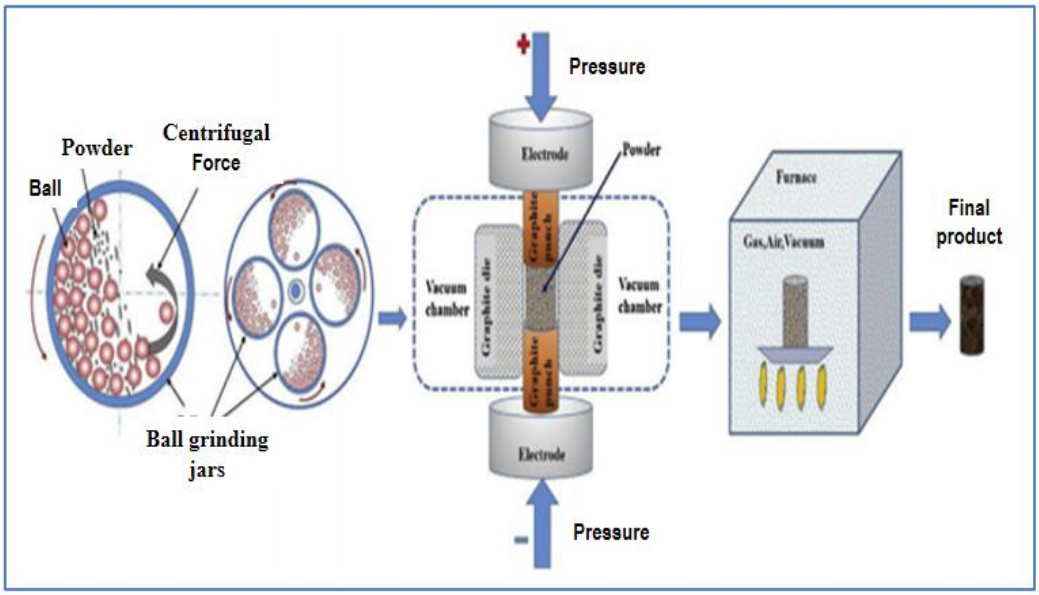

Figure 2.4-Vacuum sintering process [13, 52]

2.3.4 Microwave Sintering Process

In this sintering process, microwave energy is absorbed by the material and within the material body, it gets transformed into heat. This type of sintering has decreased processing time for materials. It is the potential economic sintering process [56]. In microwave heating, electromagnetic energy (frequency range 300MHz to 300GHz) is absorbed by the material volumetrically at the molecular level. This energy is then transformed into heat [56], [57]. In fig. 2.5 shows the Microwave sintering process.

Microwave processing (sintering and heating) has the ability that enables uniform & faster heating, shortened processing time, less energy consumption and enhanced mechanical & physical properties of the material. New material may be formed using microwave processing as microwaves are also capable of initiating a chemical reaction [57,58]. Reddy et. al. [59] found through his research on Ai-SiC nanocomposites which were synthesized using hot Extrusion and microwave sintering techniques: increase in mechanical properties as ultimate tensile strength increased from 119 MPa to 178 MPa of the material & compressive tensile strength of material increased from 105 MPa to 158 MPa. He also found with the increasing amount of SiC particles Young's modulus of elasticity and hardness values increased but ductility decreased. The researchers on adding Al_2O_3 in metal matrix composites synthesized using microwave sintering found increasing compressive strength, better microstructure refinement and better enhanced mechanical properties of MMC. When AA2900 sintered

(microwave) with Al_2O_3 its load-carrying capacity, hardness and compressive strength enhanced [60].

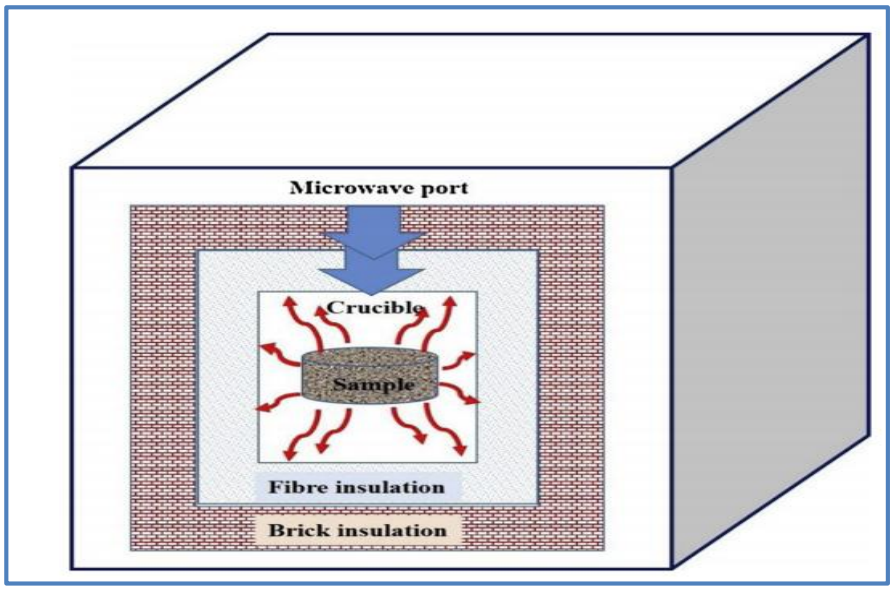

Figure 2.5-Microwave sintering process [13, 56]

2.3.5 Diffusion Bonding

Similar or dissimilar metals can be joined by diffusion bonding process which is a solid-state welding technique. Being a solid-state technique it joins the materials without melting any materials means no liquid fusion and no filler material involved in this process heterogeneous composite materials particularly the metal matrix composites can be joined using this process, therefore, it is being used in advanced applications of engineering, the temperature required for this process is beyond half of melting temperature of joining metals [61]**.** High temperature with high pressure is given to the materials on the conjunction to carry out the diffusion bonding process. Many Alternating layers of thin metals can also be bonded using this process. Due to the high cost of this process, difficulty is done using this process. It is being used in the electronic industry, nuclear industry and aerospace industry [62]. This process is said to be the novel joining process as it includes nearly zero macroscopic distortion and close dimensional tolerances [61]**.** Diffusion bonding diagram is shown in Fig. 2.6. Zhang et. al. [63]in his research on Al/SiCp-MMC diffusion bonding found: with increasing volume percentage of SiCp, the strength of the diffusion bonded joints decreases for both similar and dissimilar type of MMC diffusion bonding and quality of diffusion bonding & joint strength can be increased by suitable soft insert alloy coating layers.

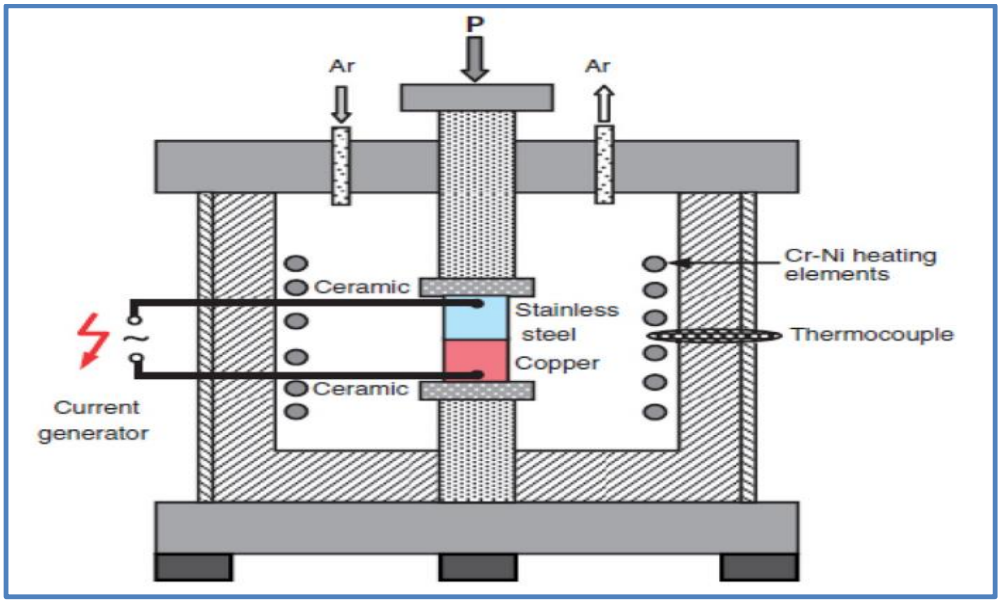

Figure 2.6-Schematic diagram for the diffusion bonding [22]

2.4 SURFACE MODIFICATION VIA FRICTION STIR PROCESSING

The selection of the right method to fabricate the surface is a crucial part of the step of design of an engineering component. The first step in surface modification is to determine the surface and substrate engineering requirements which involves one or more of the properties like wear resistance, corrosion and erosion resistance and thermal resistance, fatigue, creep strength, pitting resistance etc. The concept of FSP, based on FSW, is a new microstructure modification technique, which was invented by The Welding Institute (TWI) of United Kingdom in 1991. Various researchers have contributed immense information in the field of FSW/FSP. An exhaustive literature survey has been done to bring out the research gap in the research area of surface modification using FSP.

Kurt A. et. al. [25]: In this study, SiC particles were fused using Friction Stir Processing (FSP), into commercially pure aluminium to form particulate surface layers. Samples were processed using various tool rotating and traverse speeds with and without SiC powders. Microstructural observations were carried out by employing optical microscopy of the modified surfaces. Mechanical properties like hardness and plate bending were also evaluated. The results showed that a more uniform distribution of SiC particles by increasing rotating and traverse rate. The hardness of processed composite surfaces was enhanced by three times as compared to that of base aluminium.

Shamsipur et. al. [64]: Ti/SiC surface nano-composite layer was successfully fabricated using FSP. The process parameters such as tool rotation and advancing speeds were attuned to produce a defect-free surface composite layer, however, homogeneous dispersion of the nano-size SiC particles in a matrix of titanium was achieved after the second pass.

Rana H.G et. al. [111]: In this paper, Al 7075-T651- B_4C surface composite was manufactured using various combinations of tool rotation, tool travel speed and number of passes, the same being anticipated to improve hardness and thereby wear resistance. Microstructure analysis using image analyser found the friction stir processed zone to have fewer defects. It was also observed that the average hardness of friction stir processed surface composite was 40 – 70% higher than that of parent metal (75–80 HV).

2.4.1 Principle of Friction Stir Processing (FSP)

Friction Stir Processing (FSP) is a relatively new surface modifying technique based on the principles of Friction Stir Welding (FSW). FSW was invented by The Welding Institute (TWI), UK in the year 1991 [65]. FSP is used for contained modification and micro structural control of surface layers of processed metallic components for particular property enhancement [66]. Friction Stir Processing is carried out by a rapidly rotating and a plunging hardened tool steel non-consumable tool, comprising a profiled tool pin and larger diameter shoulder, into the surface and then moving the tool across the surface. FSP uses the same concept and technique as friction stir welding (FSW), but it is used to alter the local microstructure and does not join metals together. Friction between the shoulder and the substrate metal causes localized heating that softens and plasticizes the substrate material at the processing region. The rotating pin produces intense plastic deformation due to the stirring action which results in fine and equiaxed grain structure which is called as stir zone. There is a narrow Thermo Mechanically Affected Zone (TMAZ), Heat Affected Zone (HAZ) and unaffected base material exists [66, 68]. It is an effective method of microstructure refinement, densification and homogenization, as well as for defect removal of cast and forged components such as surface cracks and pores. Modified surfaces have shown an improvement of mechanical properties, such as hardness and tensile strength, better fatigue, corrosion and wear resistance. In contrast, fine microstructures with equi-axed recrystallized grains enhance super plastic behaviour of materials processing and this was confirmed for Aluminium alloys by Nascimento et, al. [69].

A schematic illustration of friction stir processing (FSP) is shown in fig. 2.7. FSP is the most significant technique available for surface modification and it is a green manufacturing technology due to its energy efficient, environmentally friendly, an absence of fumes and versatility.

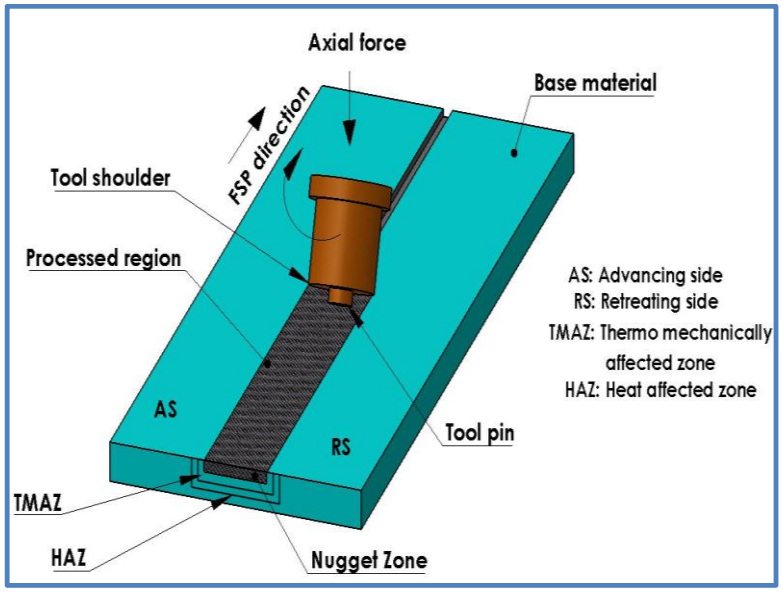

Figure 2.7-Schematic representation of friction stir processing

2.4.1.1 Advantages of FSP

- Low distortion and shrinkage.
- Exceptional mechanical properties in fatigue, tensile and bend tests.
- No arc or fumes, no porosity, no spatter, can operate in all positions and energy efficient.
- Reduction of distortions in materials.
- Production of fine-grained microstructures through the thickness to impart super plasticity.
- It increases ductility and tensile strength of the modified surface of material.

2.4.1.2 Disadvantages of FSP

FSP has some disadvantages such as

- FSP of all structures is not practical; a machine of adequate power is necessary.
- Cost of instruments and tools required and the set up cost.
- Close-fitting among parts and maintaining close concentricity that are required for FSP may be difficult for some cases. Likewise there may be rise in total cost when finishing procedures are required.

2.4.1.3 Applications of FSP

- Metallic parts produced by casting are inexpensive and contain many metallurgical flaws, hence FSP removes the various defects and homogenize it by stirring the cast metal part and reduce the grain size.
- Powder metal objects.
- FSP is used in shipping and marine industries e.g. manufacturing of hulls, aluminium extrusions and off shore accommodations.
- FSP is used in aerospace industries to manufacture the wings.
- FSP is also used in railway industries to build railway tankers and container bodies.
- It is also employed in land transport such as automotive engine chassis, wheel rims, body frames and truck bodies.

2.4.2 Types of tool pin profiles used in FSP

Friction stir tool plays a crucial role in friction stir processing. It is a deciding factor in terms of what kinds of materials is capable of being processed and the dimensions of the workpiece. The shoulder controls the material flow in a certain region, and the pin generates heat and severe plastic deformation. Eventually, the friction stir tool alters the microstructure and mechanical properties of fabricated surface composite. However, little knowledge about the friction stir processing tool geometry was published before, and information on friction stir welding tool could be reference to understand the tool [70-72]. Fig. 2.8 shows the outer and end surface features of different pin profiles.

Elangovan and Balasubramanian [73-75] investigated the effect of pin profile in FSP tool on the development of FSP zone in Al based MMCs using threaded cylindrical, straight cylindrical, triangular, square and tapered cylindrical pin profiles of the tool and concluded that the welds produced by tool having square pin profile when compared to other pin profiled tools are metallurgical flawless and mechanically righteous. Fujii et, al. [76] prospected that circular pin profiled tool fabricated weld with elite mechanical properties for 1050-H24 among circular with and without thread and triangular pin profiled tool used in its FSW. Hashemi and Hussain [77] showed that taper threaded tool with 4 passes produced best wear resistant Al7075-T651 alloy among taper threaded, triangular and square pin profiled tools. Mahmoud et, al. [78] found that square probed tool produced better homogeneous mixture of SiC reinforced with A1050-H24 in nugget zone in contrast to other

pin profiled tools. K. Kumar and Kailas [79] investigated the role of FSW tool on weld formation and material flow to state that among pin and shoulder driven material flows, shoulder transfer the material by bulk while pin transfer layer by layer. A. Kumar and Raju [80] studied the effect of tool pin profiles on microstructure during FSW. Various pin profiles like taper cylindrical, taper threaded and cylindrical, triangular, square, pentagonal and hexagonal, all having same shoulder diameter were utilized to produce the joints. It was observed that joints made by square tool pin profile showed superior mechanical properties in comparison to others. The efficiency of joint made by square pin profile was 85% higher than the base metal. Abolusoro, Akinlabi, and Kailas [81] investigated tool pin geometry in FSW and its impact on mixing at joint interface. Taper threaded and unthreaded pin profiles were utilized. It was seen that more mixing was there in nugget zone at inferior rotational speed with the threaded tool pin. But the reverse happened at medium rotational speed. The tensile strength was superior with threaded tool pin. Ajay Kumar [82] conducted tensile test and found that tool pin profile with square shape gave better results compared to others. Yadav et, al. [83] conducted hardness and tensile test on Al6082-Cu alloy and found that cylindrical threaded tool pin profile provides better result than square tool pin profile. Eftekharinia et, al. [84] employed different pin profile and passes to investigate the tribological and microstructural behaviour of FSPed AA6061/SiC composite and it was showed that composite produced by square pin has higher wear resistance.

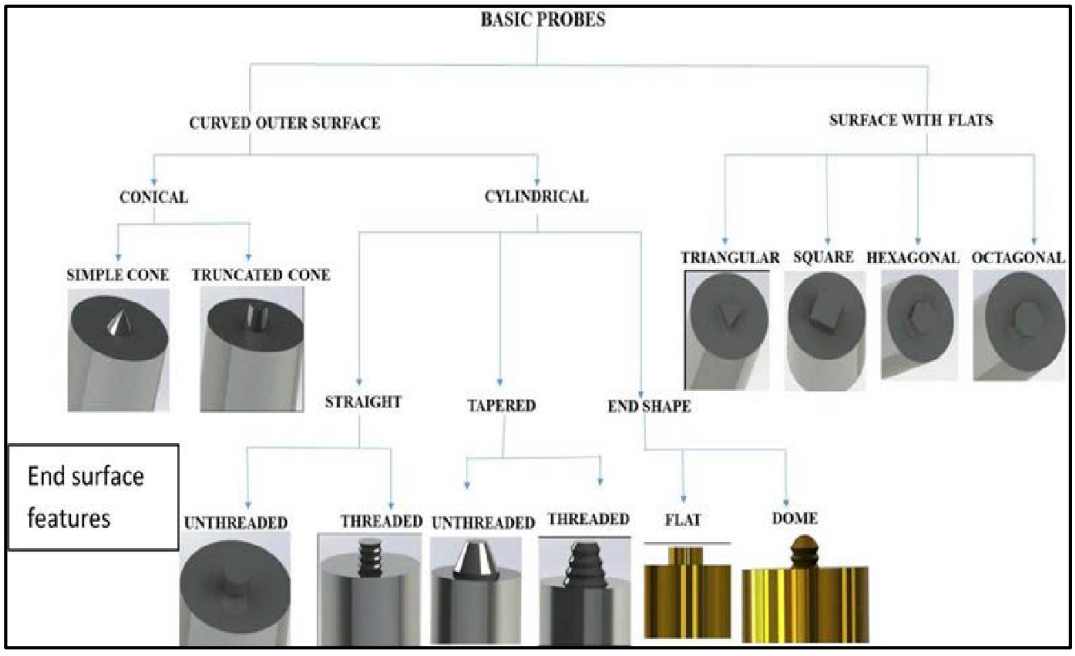

Figure 2.8-Outer and end surface features of pin profiles [85]

2.4.3 Selection of tool pin profiles

Friction stir processing focuses on two components: heat generation and material flow. So different tool profiles are considered to analyse these two components. That is why different pin profiles are considered in our study. The role of the non-consumable rotating tool probe is to stir the plasticize material and transfer the same behind it to have good processed zone. Pin profile plays an important part in material flow and thereby controls the processing speed of the Friction stir processed workpiece [75]. The pin usually has cylindrical, frustum tapered, threaded and flat surfaces. Various tool pin profiles like straight cylindrical, threaded cylindrical, tapered cylindrical, square and triangular have been utilized in the fabrication of the surface composite through FSP. In the present research work we have selected three types of tool pin profile as shown in fig. 2.9.

Pinless: The purpose of pinless tool profile is to make metal matrix consisting of reinforced material. It is intended to use in the initial phase of processing for covering the reinforced materials in the groove or gap formed on the base plate.

Triangle: The purpose of using triangular pin profile tool is that it reduces the amount of transverse welding load required to traverse the pin along the workpiece interface to form an elongate friction stir processed zone. It is also simpler in design and easy to machine as compared to other complicated designs. Quality of friction stir processed zone produced by triangular tool profile is of fine grain and smooth finish. Also it gives a uniform processed structure [100].

Square: The purpose of using square pin profile tool is that it produces defect free friction stir processed region irrespective of welding speed. It is also simpler in design and easy to machine as compared to other complicated designs [32].

Cylinder: It has the simplest construction when the machining operations performed in making the cylindrical pin profile are considered. The focused friction stir processed zone by cylindrical tool profile is akin to the pinless tool profile. It generates a fine grain and smooth surface finish resulting in higher tensile strength and higher hardness [100].

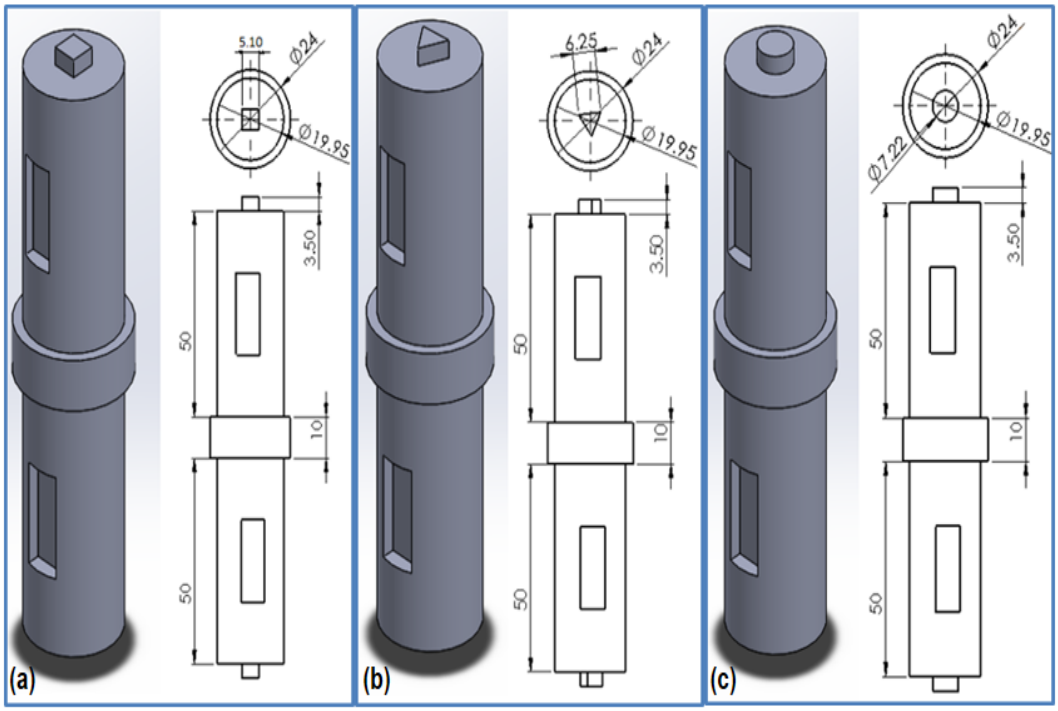

Figure 2.9-Types of tool pin profiles (a) Cylindrical (b) Square (c) Triangular

2.4.4 Tool Geometry

The shape of friction stir process tool play very important role, it consists of tool shoulder and probe. Panaskar and Sharma [86] have been reported the impact of different probe shapes (cylindrical, square, and hexagonal) in taper and untapered profile on the tensile strength of FSW Al/TiB2/10. The joint efficiency made by un-tapered square probe observed max tensile strength of the base materials comparison to other pin profile. This outcome was later confirmed by Fu et, al. [87]. They have been reported that without tapered (square, hexagonal) probe profiles to join aluminium matrix composite (Al- 4%Mg, 1% SiCp and 1% graphite particles). Selvakumar et, al. [88] have been reported that use of threaded conical pin at 800 mm/min high tool travelling rate compared to a flat cylinder to join AA2009/SiC/17p led to an enhancement of the joint efficiency to 97% because of the improvement of the flowability of softened metals. Nattapat et, al. [89] in FSW 5 mm thick Al-12%Si/TiC/10 workpiece, different diameter used (18, 20, and 22 mm) and threaded probe were used as FSW tool. They have been reported that the tensile strength of the joints varied from 124 MPa to 172 MPa depend on the tool type and processing parameter. For obtaining maximum UTS 20 mm shoulder diameter is preferable. A. Kumar and Raju [80] have been reported that tensile strength of 5 mm workpiece. In order to show the impact of three shoulder profile on mechanical properties. The result obtained that the higher heat input as an outcome of higher

contact area b/w surface of shoulder and the sample led to sufficient mixing in the stir zone, as compare with the other two tool profiles. Fig. 2.10-2.12 shows the schematic drawing of square, triangular and cylindrical with groove and holes method.

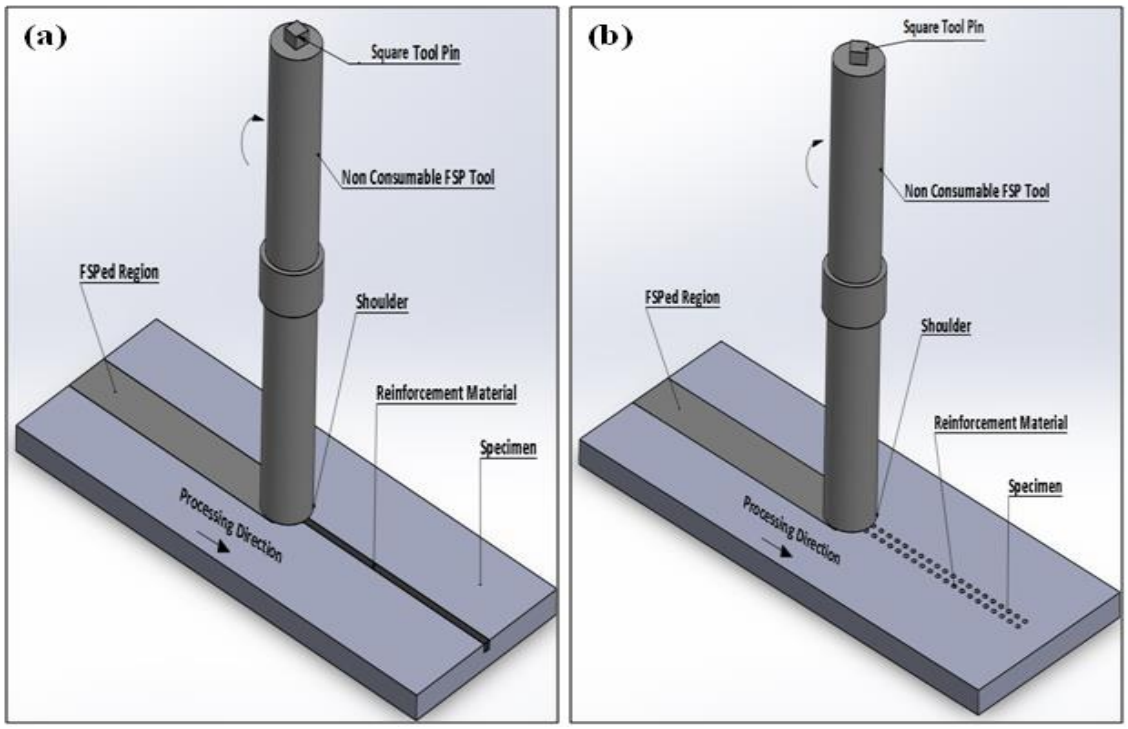

Figure 2.10-(a, b) Schematic drawing of square pin profile with groove and holes methods

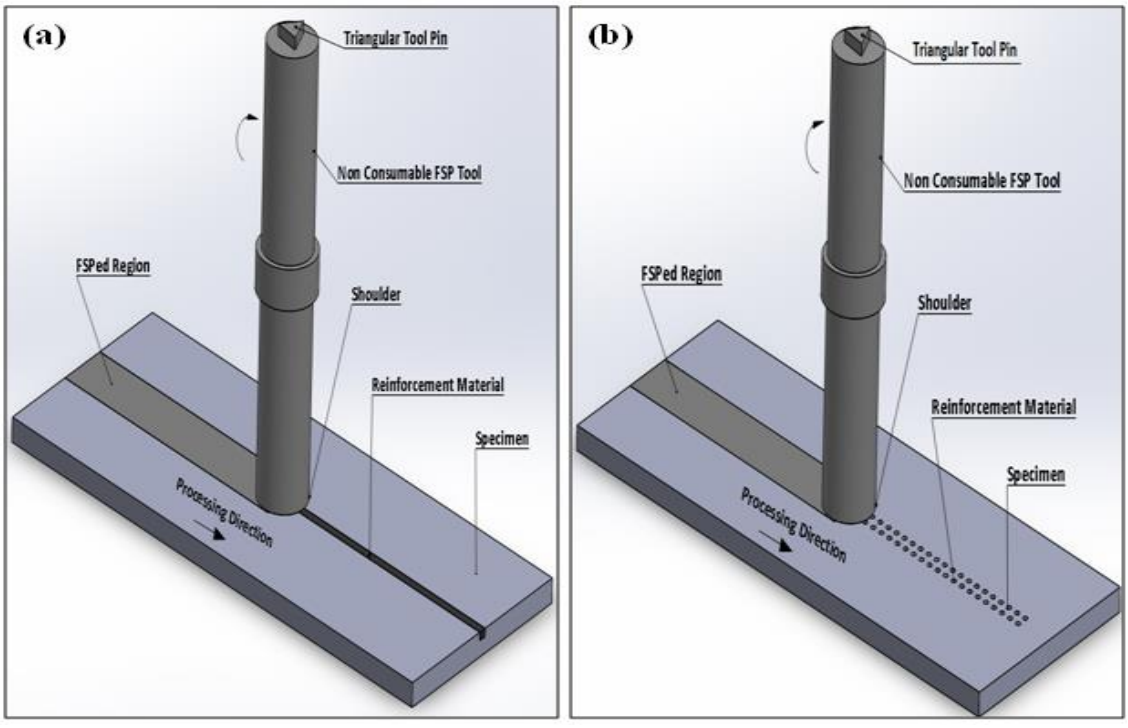

Figure 2.11-(a, b) Schematic drawing of triangular pin profile with groove and holes methods

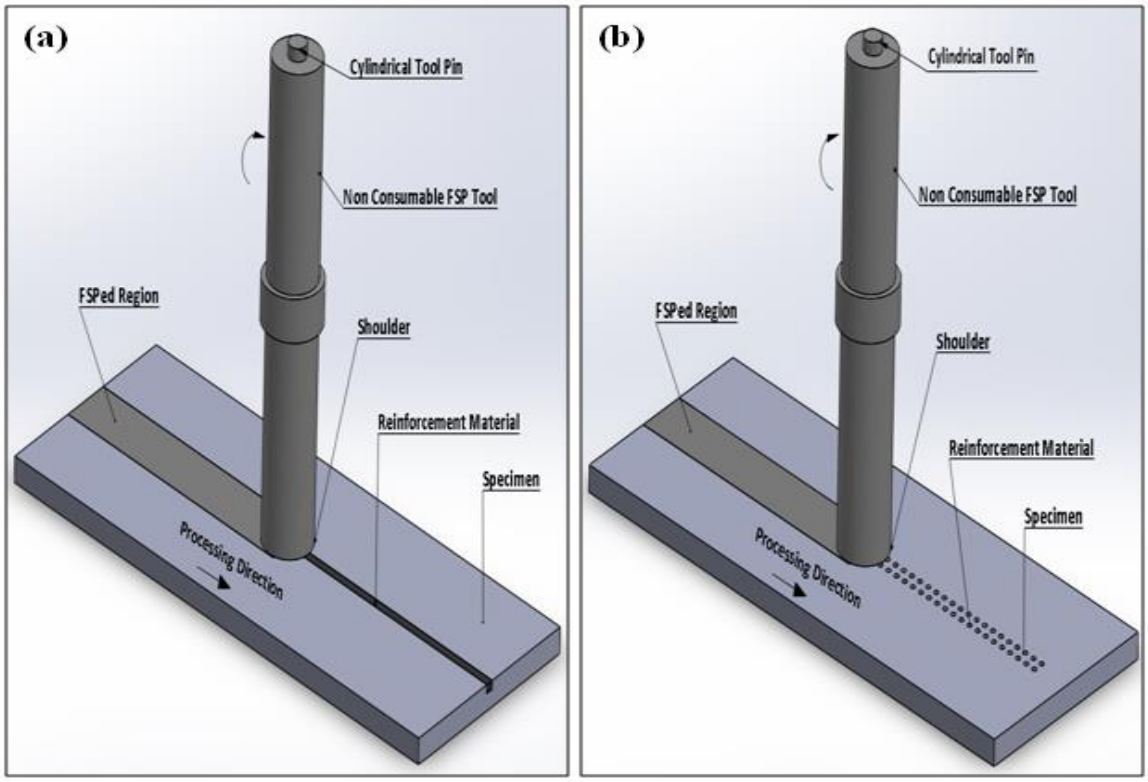

Figure 2.12-(a, b) Schematic drawing of cylindrical tool pin profile with groove and holes methods

Table 2.1:- Effect of Tool geometry of some aluminum surface composites fabricated by FSP

References	**Research Work**	**Tool Geometry(mm)**	**Results**
(García-Bernal et al. 2016)[90]	Studied the influence of tool design on superplastic performance of friction stir processed Al-Mg alloys.	SD=12.5,16mm Major Pin Dia =6,7 mm Minor pin Dia=4,5 mm, PL=3,3.5,5	Superfine microstructures, with grain sizes less than 3 mm, were observed with all the tools. Abnormal grain growth was seen in some of the tools after exposure to high temperature.
(de Jesus et al. 2014) [91]	Influence of tool geometry and process parameters on the mechanical properties of FSW of dissimilar aluminium alloys is experimentally examined.	CSD=10.16 PD=2.55 PL=3 PD=3.08 PL=2.75	Two shoulder profiles produced noteworthy changes in the axial force, the inter dispersion of materials, and the mechanical properties of the joint.
(Srinivas et al. 2013) [92]	Different tool profiles have been used to construct joints and their effect on the mechanical properties of aluminium alloys studied.	SD=20,18,16mm PL= 2.8 ,1.9, 1mm	Longer pin length reduces penetration depth on the rear side of welded plate but increases BHN.

(Radisavljevic et al. 2015) [93]	Studied the collective impact of different pin geometries with rotation and welding speed on the weldability, mechanical and structural properties	Spiral thread= 5.5 mm, SD=25 mm, Taper screw thread pins thread slope $=5^{O}$	Pin geometry had a strong influence on macro structure, hardness distribution, weld formation and mechanical properties
(A. Ramesh, et al, 2016) [94]	Studied the impact of tool design on the mechanical properties in FSW of aluminium alloy	SD=18mm,PD=6mm, PL=5.5mm, Tool inclined angle=2^{o}	Results indicated a significant effect of pin design on the joint structure and the mechanical properties.
(Venkateswarlu et al. 2013) [95]	The impact of threaded FSW tools on AA7039 alloys was investigated with different shoulder diameters, pin diameters, and levels of shoulder surface concavity.	SD=22,19,16mm, PD=8,7,6mm, Shoulder surface concavity =3,2,1	The 7-mm pin diameter was found to yield better results in comparison to 6 and 8 mm. The shoulder diameter was found to not be significant relative to pin diameter for tensile properties of the weld.
(Bozkurt et al, 2018) [96]	Uncoated tool, coated tool with a CrN, AlTiN were utilized for the FSW butt welding of AA2124-T4 alloy matrix MMC.	SD=18 mm, PD=6 mm, Tool tilted= 2°	The tool coated with AlTiN showed the best results and the maximum UTS values.
(Kumar, A. et al. 2014) [97]	Characterization of FSW dissimilar Aluminium alloys AA5052 and AA6061.	SD=16mm,PD=6mm Cylindrical pin tool with 2 threads	Cylindrical threaded pin gave excellent bondage between both alloys (AA5052 and AA6061) by good friction stir joining.
(Elangovan et al, 2008) [73]	Influence of axial force and tool pin profile on FSP zone formation in AA6061 aluminium alloy	SD=15,18,21mm PL=5.5mm PD=6mm	Threaded and square pin profile produced defect free welds with maximum yield and tensile strength. Square and triangular pin profile gave sufficient metal flow because of pulsing action.
(Y. N. Zhang et al. 2012) [98]	Friction stir processing and welding	Flat, concave and convex shoulder end surface.	Flat surface is ineffective for trapping the flowing metal producing material flash while concave resists material extrusion. Convex shoulder is used for very less thickness of plates otherwise it pushes material away.

(Yuvaraj. N, et al., 2015) [99]	Production of AA5083/B4C alloy was done via FSP, with micro- and nano- sized B4C particles as reinforcements.	SD=18mm PL=5mm PD=6mm	In contrast to single pass FSP, an increase in the FSP passes resulted in uniform distribution of nano-particles in the Al matrix thereby leading to improved hardness.
Butola. R, et al., 2019 [100]	Work is carried out for the parametric effects like, TRS, tool profile and reinforcement in friction stir processing of AA7075 on the microhardness and Microstructural analysis.	SD=19.95mm PL=3.5mm SP=Flat	It was found that TRS is the most influential parameter followed by the type of reinforcement and tool profile respectively. The average microhardness of AA7075/B4C composite was found to be increased by 1.5–1.6 times of the base
SD= Shoulder Diameter, CSD=Concave Shoulder Diameter, PL=Pin length, PD=Pin Diameter SP= Shoulder Profile, BM=Base Metal, TRS=Tool Rotational Speed.			

2.5 DIFFERENT METHODS OF REINFORCEMENT INCORPORATION INTO THE MATRIX METAL BY FSP

2.5.1 Groove Filling Method

This was the primary method presented by Mishra et, al.[31]while making Al-based composites. In this technique, a fine groove is shaped on the surface of the piece or plate beforehand FSP and the grove is jam-packed with the reinforcement particles. At that moment FSP is passed out to advance surface composite which is also talked by Ratna Sunil et, al. [101,102] in their papers. Fig. 2.13(a) demonstrations the diagram image of groove filling method. Far ahead, groove filling and closing technique was also stated by Lee, Huang, and Hsieh [103] in which a groove is fashioned on the surface and filled with reinforcement, and the groove is shut by developing the groove using a tool which does not comprise a pin at the shoulder as shown in fig. 2.13(b). Owing to the functional load, heat is produced for the reason of the resistance between the smooth shoulder of the tool and the surface of the job. So, the surface of the groove experiences plastic distortion and is shut to ease the filled particles not to sail away or leak from the groove throughout FSP.

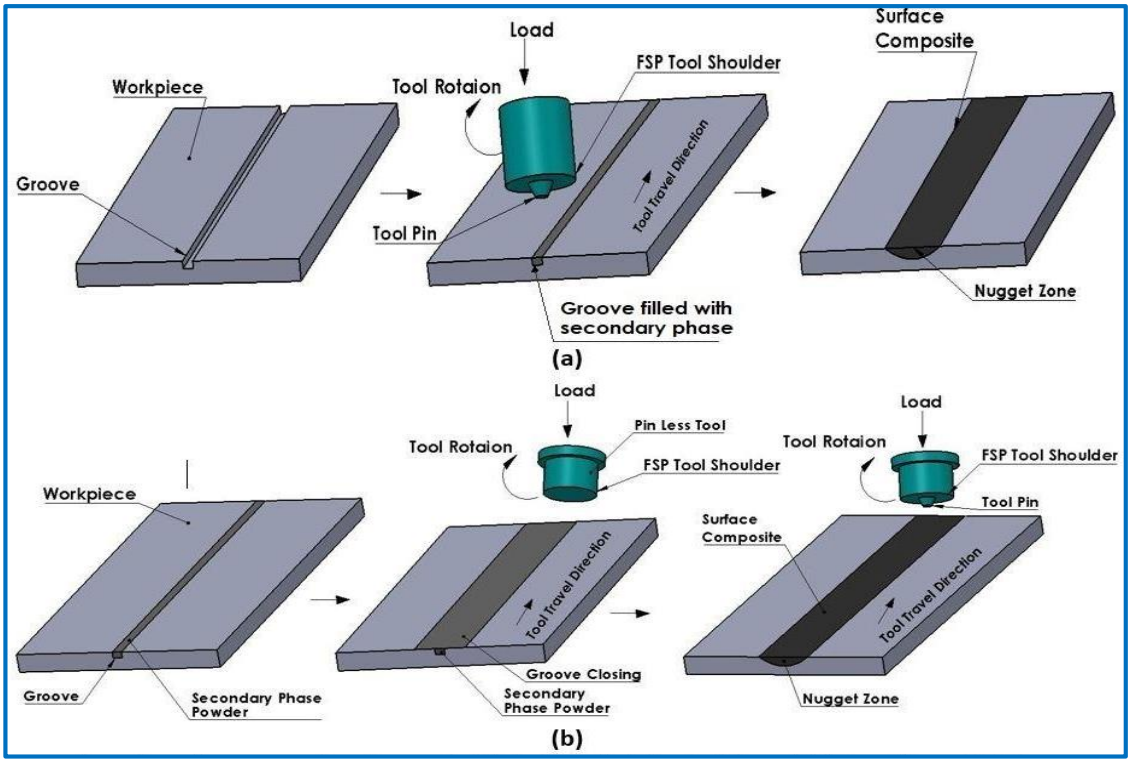

Figure 2.13-(a, b) Schematic representation of surface composite fabrication through groove filling method and groove filling and closing method followed by FSP (Adopted from) [193]

2.5.2 Holes Filling Method

Holes filling method is alternative technique of integrating the reinforcement into the matrix throughout FSP which is used as a method by Yang et, al. [104] and Akramifard et. al. [105] in their studies. Some uncommon small holes are formed on the surface of the material and the holes are jam-packed with the reinforcement, and FSP is passed out to harvest the surface composites as shown in fig. 2.14(a). Alike that of groove filling and closing technique, additional development occurred which was used by Reddy, Rao and Rao [106] in their research and in this method which wants two processing tools that is, one without pin and another with a intended pin at the shoulder. After filling the holes with the reinforcement, the holes are shut with the aid of FSP tool with no pin as shown in fig. 2.14(b) and then FSP is passed out to change surface composites.

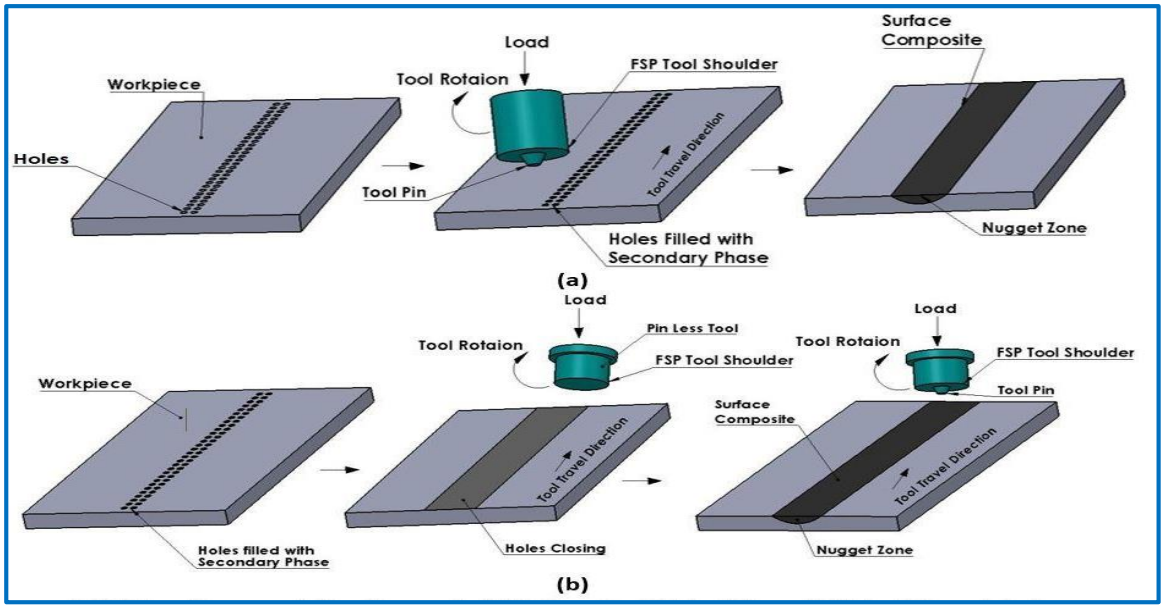

Figure 2.14-(a, b) Schematic representation of surface composite fabrication through holes filling and holes filling and closing method followed by FSP (Adopted from) [193]

2.5.3 Sandwich Method

This is additional way of emerging surface composite using FSP. Firstly, the method was elucidated by Mertens et, al. [107]. In sandwich technique, reinforcement is positioned in the arrangement of a coating or lamina amid sheets or plates of material and FSP is done. Owing to the stirring and traverse movement of the tool, the reinforcement layer or lamina is fragmented into small units. Fig. 2.15 shows diagram depiction of sandwich method.

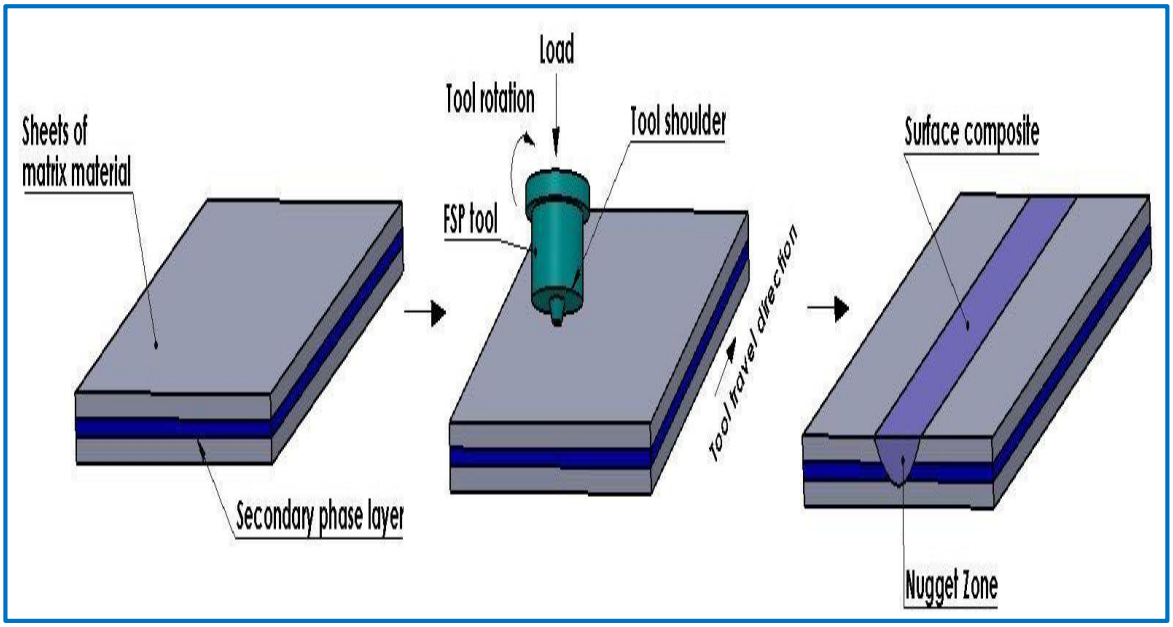

Figure 2.15-Schematic representation of surface composite fabrication through sandwich method followed by FSP (Adopted from) [193]

2.5.4 Direct Friction Stir Processing (DFSP) Tool Method

T. Wang et, al. [108] planned a novel type of FSP tool containing a hole along the longitudinal axis through which powder is delivered and termed it as direct friction stir processing (DFSP) tool. Figure 4 shows the illustration of DFSP process. In this scheme, during the procedure, tributary phase elements are provided through an uninterrupted hole in the DFSP tool itself. The operation behind the composite development using this reformed tool has been enlightened by the authors. Contrasting from the FSP, the reinforcement elements are not presented into the exterior of the base metal before processing but delivered through the hole which is planned within the DFSP tool. As the tool progresses in the cross direction at the exterior of the work piece, the reinforcement particles are directly positioned in the space fashioned between the shoulder of the DFSP tool and the workpiece. Therefore, the particles cannot escape in between the process but are ensnared between the concave spaces. Then, these trapped particles are stimulated and pressed into the workpiece homogeneously to produce the surface composite. As pronounced by the authors, in a single pass, supplementary amount of secondary phase can be presented into the matrix using DFSP tool compared with that of FSP tool. Fig. 2.16 shows the schematic representation of surface composite fabrication through DFSP tool method.

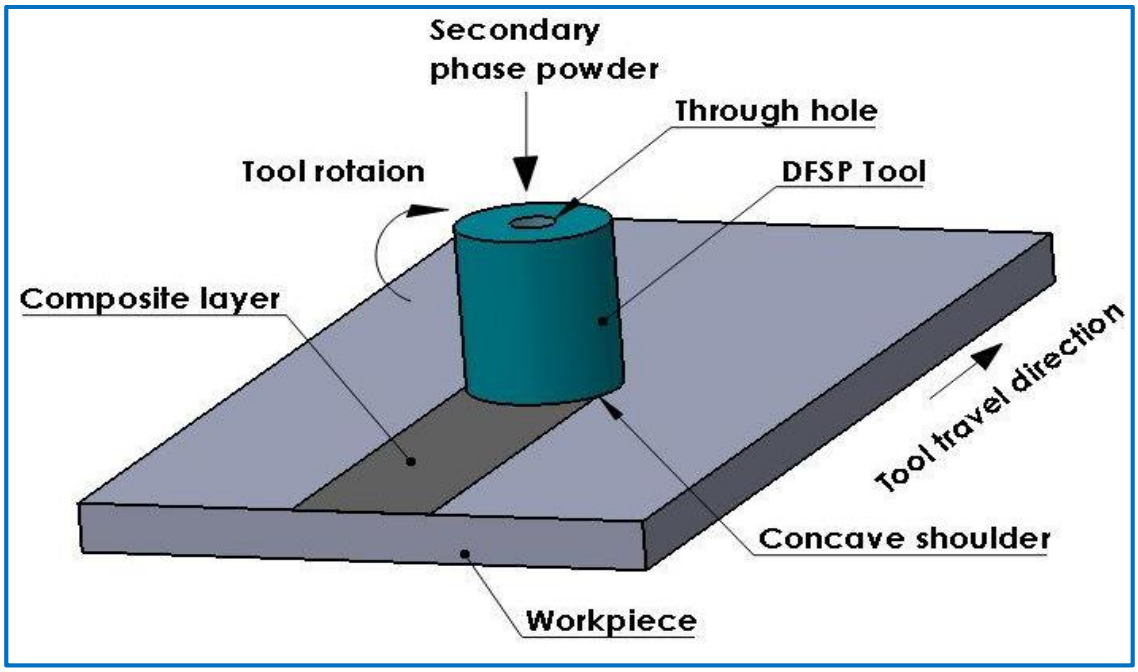

Figure 2.16-Schematic representation of surface composite fabrication through DFSP tool method (Adopted from) [193]

2.5.5 Surface Coating Followed by FSP Method

Applying surface coatings before FSP is an alternative tactic to integrate the secondary phases into the matrix material. Secondary phase is layered on the exterior by any appropriate coating method before FSP. Then the coated sheet is treated using an FSP tool as shown in fig. 2.17. Plastic deformation and material flow lead to matrix material and secondary phase getting appropriately mixed and results in a composite layer.

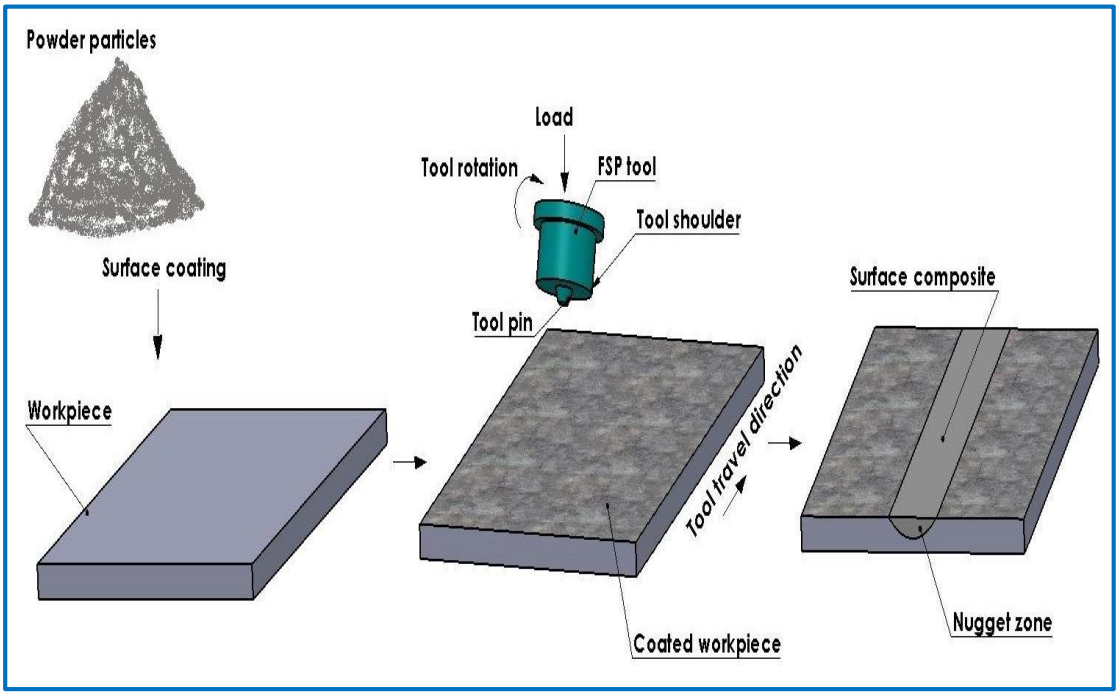

Figure 2.17-Schematic representation of surface composite fabrication through surface coating followed by FSP (Adopted from) [193]

Table 2.2:-Effect of Process Parameter of AA7075 Surface composites fabricated by FSP

Reference	Research Work	FSP Process Parameters	Results
(García-Vázquez et al., 2016) [109]	Nano-particles of TiC (2% w/w) were added to AA7075-T651 alloy to fabricate a surface composite.	TRS= 1000 rpm TTS = 300 mm/min	Chosen FSP variables influenced the area of surface composite, dispersion of TiC particles and micro-hardness of the surface composites.
(Sert A., Celik 2014) [110]	Al7075-T651 alloy's surface is modified with SiC ceramic particles via FSP	TRS=710,1000 ,1400 rpm TTS=20,40, 56 mm/min. Tilt angle=2.5º	An enhancement in the grain structure and wear properties of the FSP-modified specimens is observed; the average hardness decreased despite the SiC particle reinforcement

(Rana, Badheka, and Kumar 2016) [111]	FSP used for the production of surface composites, AA7075 used as base metal with Boron Carbide (B4C) powder as reinforcement particle.	TRS= 545 rpm TTS=50, 78, 120mm/min Tool tilt angle =3 degree	The average hardness of FSPed surface composite was 40 – 70% higher than that of base metal. This increase may be attributed to B_4C particles dispersion in aluminium matrix and grain strengthening mechanisms.
(Bisadi and Abasi 2012) [112]	FSP was used to successfully distribute and embed TiB_2 particles with global size of 2.62 μm in AA7075.	TRS= 450, 825, 1115 rpm, TTS = 32, 60 mm/min Tilt angle = 3°	Increasing the rotational speed caused TiB_2 particles to be dispersed more uniformly.
(Kashani-Bozorg et al. 2009) [113]	Al/B_4C surface nano-composite layers were achieved on commercial AA7075 substrate via FSP.	TRS= 1000rpm TTS=35-210 mm/min.	Increasing the number of passes resulted in better dispersion of B4C particles, reduction of matrix grain size and increase in the micro hardness value of the surface composite layers.
(Mouli, A.Sarath, and Maheswara 2017) [114]	SiC particles were homogeneously dispersed into the AA7075 matrix, promoting grain refinement; further, microscopic structure and hardness properties were increased as well.	TRS=1120 rpm, TTS=20 mm/min Tilt angle= 1degree	SiC particle in AA7075 region showed fine grains even at elevated temperatures (400ºC) consequentially leading to the pinning effect by the SiC for FSPed AA7075 particles.
(Ku et al. 2011) [115]	FSP was performed on 7075-T6 Al alloy plates and then natural aging was performed to investigate the impact of various tool rotation speeds on the microstructures and tensile fracture properties	TRS=1230, 145, 1670 rpm TTS=0.58mms^{-1} Tool angle. =1.5 degree	Grain size became equiaxially fine and the average grain sizes were 5.2, 5.1, and 4.2 mm corresponding too low to high tool rotation speeds in the stir zone. The tensile strength was different for different rotation speeds of FSP.
(R and N 2013) [116]	Fabrication of AA7075-T651 B_4C surface composite was done via FSP and improved surface hardness was observed.	TRS=425, 500, 575rpm TTS= 40, 50,60mm/s	A good surface composite produced at rotational speed of 500 rpm, traverse speed of 60 mm/min using three passes.
(Al-Ghamdi, Hussain, and Hashemi 2017) [117]	Investigated a suitable set of FSP parameters to form AA7075-T651/TiN nano composite.	TRS=1250 r/min Traverse feed = 40 mm/min. Tilt angle = 2.5^O	Increasing the number of passes improved various characteristics of the composite (i.e. distribution of TiN particles, grain refinement and mechanical properties).
(Singh et al. 2018) [118]	B4C (Holes of diameter 2 mm) BM: Magnesium alloy AZ91	TRS= 900 rpm; TTS=45mm/min , Depth of cut = 0.3mm	Improved microhardness, wear resistance. As the size of particle was increased, microhardness was also increased.

(Deore et al. 2020) [119]	SiC (Holes with 2 mm dia & 3 mm depth) BM: AA7075	TTS=60 mm/min TRS= 800 rpm Tilt angle = 3^o	Remarkable increase in impact toughness, microhardness & wear resistance; acute grain refinement; Under impact loading, effective fracture mode is ductile.
(Akbari et al. 2017) [120]	B4C of size 10 µm (square groove of depth = 3.5 mm; width = 1.4 mm) BM: A356 cast alloy	TRS=800/1200/1600rpm, TTS= 8, 32 and 80 mm/min.	UTS improved; Hardness first increased and then decreased; Deduction in size of Si particle & tool axial force occurs due to either decrease in traverse speed or increase in rotation speed of tool;
(Paidar et al. 2019) [121]	Composite of Al-2%B4C	TRS=900rpm, TTS=100mm/min No of passes = 1 to 8	Inverse relationship between average grain size & no. of tool passes. Improved tensile strength, Improved resilience, wear rate & coefficient of friction reduced by increasing the no. of tool pass; Primary fracture found to be ductile.
(G. M. Reddy, Rao, and Rao 2013) [106]	B_4C size of 40 µm [Holes with 2mm dia and 2mm depth were drilled in a line at equal distance of 1mm], BM: Ti-6Al-4V	TRS=1200rpm TTS=50mm/min	Wear resistance increased over 134 times.
(Navaser and Atapour 2017) [122]	Friction stir process on the pitting corrosion and the intergranular attack of 7075 aluminum alloy was investigated.	TTS=100 mm/min TRS=630,1000 ,1600 rpm	Microstructural analysis reveals that the processed zones obtained very fine and equiaxed grain micro structure. It has also found that grain size increased as the tool rotational speed varied.
(Ikumapayi, et al.,2019) [123]	AA7075-T651 & WFA, CSA, CFA, PKSA & CBA	TRS=1500 TTS=20 mm/min, Tilt angle=3^0 PD=0.3 mm	Hardness and Tensile Strength improved majorly. Friction & wear properties, and corrosion behaviour were improved.
(Abrahams, Mikhail, and Fasihi 2019) [124]	AA 5005-H34 & AA 7075-T651	TRS=490/970/1200/1500 rpm, TTS=32/64/127/241	The tool with screw-threaded conical pin profile - most suitable tool design; For AA 7075-T651, microhardness, grain boundaries & mechanical properties improved with increase in traverse speeds.
(Sudhakar, Madhusudhan Reddy, and Srinivasa Rao 2016) [125]	The surface composites were produced by incorporating ceramics like SiC, carbides of transition metals and oxides of aluminium via different surface modification techniques.	TRS=925,1000 rpm, TTS= 50 mm/min Plunging speed=30 mm/min	Friction stir processing route is an effective technique for improvement of ballistic performance of AA7075 aluminium alloy which finds extensive applications in defence.
TRS= Tool Rotational Speed, TTS=Tool Traverse speed, PD=Plunge Depth, AA=Aluminium Alloy BM=Base Metal			

2.6 IDENTIFICATION OF RESEARCH GAPS AND RESEARCH OBJECTIVES

Though aluminum based surface composites are being used in numerous applications like aerospace, marine, automobile and defense, however more opportunities are yet to be explored. Lack of knowledge about ceramics nanoparticles applications, suitable process parameter and usages of nanoparticle reinforced into the matrix metal. In addition to this, minimization of nanoparticles and obtaining the better mechanical properties have not reported. Different methods have been reported for applying of reinforcement particle with a volatile liquid mixture (methanol or acetone) by direct filling method and paste method applied over the matrix metal.

2.6.1 Research Gaps

There are several methods related to the development of surface modification of aluminum alloy. However, researchers have not reported the surface modification of Aluminum based matrix through the FSP technique using B_4C nanoparticle reinforcement mixed with Di-ethyl ether (DEE). On thorough analysing of the literature review. Following research gaps are observed:

1. Literature review reveals that several techniques have been developed for surface modification of different metals and alloys such as shot peening, liquid phase processing like plasma spray, CVD, PVD etc. Limited research work has been done through FSP to enhance the properties of surface modification by different technique such as groove, holes and sandwich, DFSP without taking into account of wt% of reinforcements.

2. Many researchers have fabricated surface composites and most of the published work is reported on optimization of processing parameters and effect of reinforcement particles on surface composites and techniques to evaluate the performance of modified surfaces. Very limited research is available on uniform distribution of nanoparticles reinforcement particles in the modified surface.

3. Most of the published work is focused on surface modification or surface composites of material without considered the minimization of nanoparticle reinforcement. There is still needs to developed new technique which minimizes the reinforcement particles for fabrication of surface composites with upgraded mechanical properties using solid-state processing technique like Friction Stir Processing.

2.6.2 Research Objectives

Based on literature survey the following research objective have been drawn for the Surface modification using solid state plastic deformation technique. The following specific objectives are

1. To analyse the different types of tools shape to conduct the surface modification of a material.
2. Selection of suitable non-ferrous alloys and the Reinforcement particles.
3. To investigate the effects of different develop surface shapes by incorporating reinforcement particles for uniform distribution.
4. To study the effect of process parameters of the modified surface.
5. Characterization and mechanical properties of the modified surface such as Microhardness, Ultimate Tensile Strength, SEM, Fractography analysis, XRD and residual stress.

2.6.3 Plan of work

Initially the literature reviews is accomplished and then conduct the surface modification of material for experimentation. Research methodology adopted to fulfil the objective of this research work is listed below. The flow diagram of the plan of experimental work is shown in fig. 2.18.

1. On the basis of literature survey, FSP technique is utilized to modify the surface of the substrate material and it is easy to develop the surface composite layer.
2. From the literature survey and initial trials, it has been observed that tool rotational speed, tool traverse speed are greatly influencing the developed surface composite.
3. Experiments were performed to optimize the process parameters on ultimate tensile strength and hardness of the surface composite.
4. The Micro-hardness, microstructure, tensile, residual stress and wear behaviour of B_4C nano particles Self-assembled monolayer (SAM) surface composite were investigated.
5. The micrograph analysis, nanoparticle distribution, Fractography analysis and wear behaviour analysis of surface composite and base metal were investigated using FE-SEM, SEM analysis

Plan of Work

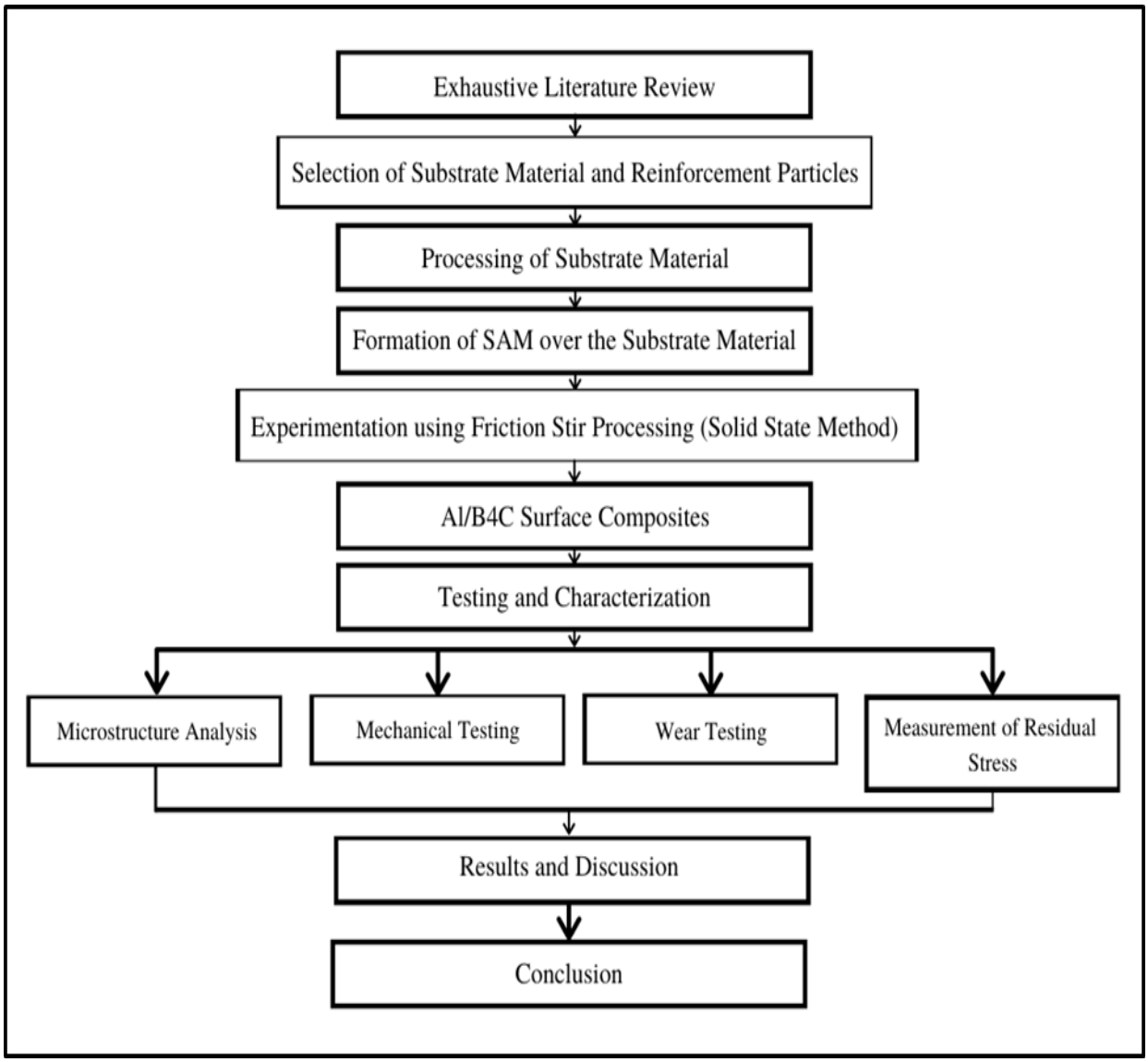

Figure 2.18-Flow diagram of the experimental work

2.7 SUMMARY

MMCs are a type of composites which are the mixture of alloy metal matrix or ductile metals with other material which can be metal, non-metal or even an organic compound. They are usually made with the base metals as Aluminium or Magnesium. Many solid-state fabrication methods have been used for making MMCs. Some notable techniques include plasma sintering, high energy ball milling mixing and sintering, vacuum sintering, microwave sintering, diffusion bonding and FSP. FSP has many advantages over the other techniques, including the enhancement of mechanical properties, no fumes or splatter,

energy efficient etc. Though it also comes with its own sets of disadvantages like space-constraints, higher setup costs etc., they are far outweighed by the benefits. Because of these added benefits, FSP has found applications in a variety of industries like shipping and marine, aerospace, railway and land automotive transports. The processing parameters, especially the tool pin profile, have a significant effect on the amount of heat generation and material flow, which in turn affects the mechanical and microstructural properties of the processed material. Between the cylindrical, triangular and square pin profiles, it has been found that the square pin profile yields the best results. There exist many different methods of adding reinforcement material on top of the metal matrix before FSP is conducted. Some of the major methods include groove filling, hole filling, sandwich method, direct FSP (DFSP) tool method and surface coating method.

CHAPTER 3

ANALYSIS OF TOOL PIN PROFILE

3.1 INTRODUCTION

In the past few years, the use of high-speed steel has accelerated, since its strength to weight ratio is high. In designing a mechanical component from raw material, many machining processes are carried out, which induce residual stresses in the component. Fatigue life is highly affected by the presence of residual stresses. FSP is an adaptation of friction stir welding (FSW), which is a solid-state joining method invented at The Welding Institute of UK in 1991. FSP is a solid state processing and is used in the microstructural modification of the surface of materials. FSP is a solid-state plastic deformation technique which works with the help of a rotating non-consumable tool comprising of a shoulder and a probe at the end [66,100]. Hence, it is crucial to anticipate these residual stresses so as to increase the life of the component. Various methods have been adopted in the past for measuring residual stresses in a component. These include destructive and non-destructive experiments. XRD is the most commonly used process for measurement of the residual stress. However, the initial set-up cost for XRD is very high. Since the present arena is of digital computers, in this research we have used the capabilities of a computer for determining the residual stress. Experimental analysis of surface stresses due to deformation processes such as bending and stretching was done and it was found that during machining, compressive surface residual stresses and informing operation tensile surface residual stresses are formed. They also found that increasing incremental angle results in a decrease in the compressive surface residual stresses using turning process [126]. Hard machining test was conducted on heat-treated AISI4340 steel to investigate the residual stresses and changes in the microstructure. It was suggested that good surface integrity characteristics could be attain with suitable machining parameters [127]**.** Temperature dissemination, bending and residual stress created during plasma arc facing over AISI4140 entryway valve was contemplated utilizing FEA. After simulation, residual stresses were analyzed and estimated by X-Ray diffraction method. Numerical outcomes demonstrated great concurrence with experimental test [128]**.**

Research was carried out to determine the impact of preheating on microstructure, mechanical properties and stress on tool steel SLM parts. It was found that the residual stresses are compressive at low preheating temperatures and on increasing the preheating temperature,

tensile nature increases [129]**.** Some researchers presented an illustrated review report on the machining of stimulated surface probity in titanium and nickel alloys where it was discussed about the increasing use of these alloys, impact of residual stress and surface integrity on the performance, various parameters of machining affecting the microstructure and various methods to reduce the generated residual stress during the machining process [130]**.** A few researchers reported the residual stress generated during the facing of high strength nickel-based superalloys RR1000 by various parameters such as type of tool, coated tool, tool wear, and failure. They obtained medium increment in tool wear leads to highest tensile surface stress, and the round insert in comparison to rhombic insert produce slightly increase in tensile stress [131]**.** In this work a trial and theoretical examination in regards to the impact of the processing factors on residual stress distribution created by milling. The tests are completed on K945 carbon steel. The cutting system is shifted as: v=16 to 1036 m/min; f=375 to 1400 mm/min; DOC= 0.15 to 0.5mm. A small cutting depth (equivalent to 0.15 mm) created the least residual stress. The utilization of high cutting feed (equivalent to 1400 mm/min) lead to huge variations of residual stress [132]. The machining parameter and temperature throughout end milling cutting operation were investigated with various feed rates and DOC and the surface residual stress was measured along acentric direction after turning. It was found that the residual stress along an acentric direction at the middle point was tensile and the mechanical effect represented by cutting forces made the surface residual stress of compressive nature along the eccentric direction [133]. The profile was optimized along with the residual stress by analyzing the effect of DOC on the rearrangement of residual stress during milling of a thin-walled part. It was observed that the depth of cut reduced from roughing to finishing in the operation and the machined surface residual stress decreased [134]. Some researchers studied the residual stress stimulated by orthogonal cutting of tool steel by modelling and simulation using FEM. The residual stresses obtained by modelling were validated using XRD. They obtained that the surface residual stress increased and became more compressive if any of the parameters - cutting speed, uncut chip thickness and tool wear is increased [135]. A report found that the residual stress stimulated by dry turning of H13 tool steel. Residual stress was check out practically in a function of the tool geometry and machining parameter. He found that the maximum and minimum principal residual stress were of tensile and compressive nature respectively. He also found that to minimize the measure of tensile residual stress feed should be decrease and tool-cutting angle is to be increased [135]. Residual stress was analysed in the shaping of AISI 1020 steel. They compared the FEM simulation of single point cutting process with the experimental work

results. XRD technique was utilizing to find out the residual stresses. Process variables were optimized using Taguchi L_9 experimental design and found that rake angle of 12 degree, DOC is 1 mm and cutting speed of 220 m/min was most effective in shaping [136]. Another study dissected SR on CNC turned AISI410 with various coated cutting tool under dry conditions. Multi-layered coated with TiCN+Al_2O_3 of 14 μm embed is utilized for case-I, multi-layered coated with Ti(C, N, B) of 6μm embed is utilized for case-II and single layered coated with (Ti, Al) N of 3μm embed is utilized for case-III. From the outcomes of ANOVA, the feed rate and cutting velocity are the noteworthy cutting factors for influencing the SR with Ti (C, N, B) and (Ti, Al) N. From the consequences of ANOVA, the feed rate and DOC have been found to be the major cutting parameters for influencing the SR with TiCN+Al_2O_3 [137]. Another researcher performed experiments and built the FEM model of orthogonal cutting of 316L steel. It was achieve that the experimental and FEM models gave the similar tendency of residual stresses peak profile [138]. The residual stresses on specimen surface, after cutting process was investigated using FEM modal, and the outcomes were compared with the experiments [139]. In this research, the impacts of a different cooling fluid on residual stresses were studied. To determine residual stress profiles, XRD technique was used. After experiments were performed, the FEM model was applied and compared with the experimental outcome [140]. Analyzed the residual stress in the shaping of AISI1020 and CNC turning of H13 tool steel and, then compared the FEM simulation of single point cutting process. XRD technique and PulsetecμX-360n portable stress analyzer was used to measure residual stress [136], [141], [142]. The conclusion of this research will have a large impact on the fabrication of FSW/FSP tool industry. The forecasting of residual stresses utilizing ABAQUS/CAE 6.14 software gives an opportunity to FSW/FSP tool industries to improve the machining process of FSP tool design before manufacturing the tool. The researchers have presented various ways to use computational power to find out the residual stresses in turning operation. Most of the research work is based on orthogonal cutting and are 2-D simulations. In this research, we have used the explicit dynamics of ABAQUS to simulate the oblique cutting in 3-D environments.

This chapter aims to find out the residual stress on the periphery and tip of the circular and taper circular FSP tool probe. The residual stresses were calculating using PulsetecμX-360n stress analyzer machine. The experiments were done on two different types of tool probe profiles. The experimental results were compared with the outcome got from ABAQUS/CAE simulation of the turning process.

3.2 EXPERIMENTAL PROCEDURE

The material used for conducting experiments was H13 tool steel workpieces (specimen) dimensions 100xØ22 mm as shown in fig. 3.1(a) were used in this investigation. In this study, two work pieces were made with following different probe profile, circular, tapered circular. Machining was done on the CNC Lathe machine set up with the carbide insert as shown in fig. 3.1(b). Feed rate and cutting speeds were 0.15 mm/rev and 1500 m/min, respectively. The circular and taper circular probes were generated in 2 steps turning from an initial 22 mm diameter rod. In the first part of the turning process, the Dia was reduced from 22 mm to 19.95 mm for the complete length of the specimen. In the second part, Dia decreased from 19.65 mm to 7.22 mm for a probe length of 3.5 mm. The taper circular probe was fabricated by using a taper turning attachment and a taper of length 3.5 mm was generated with the Dia gradually decreases from 7.22 mm to 3.5mm. After the completion of the machining process of H13 tool steel, the residual stress on the machined workpieces were determined.

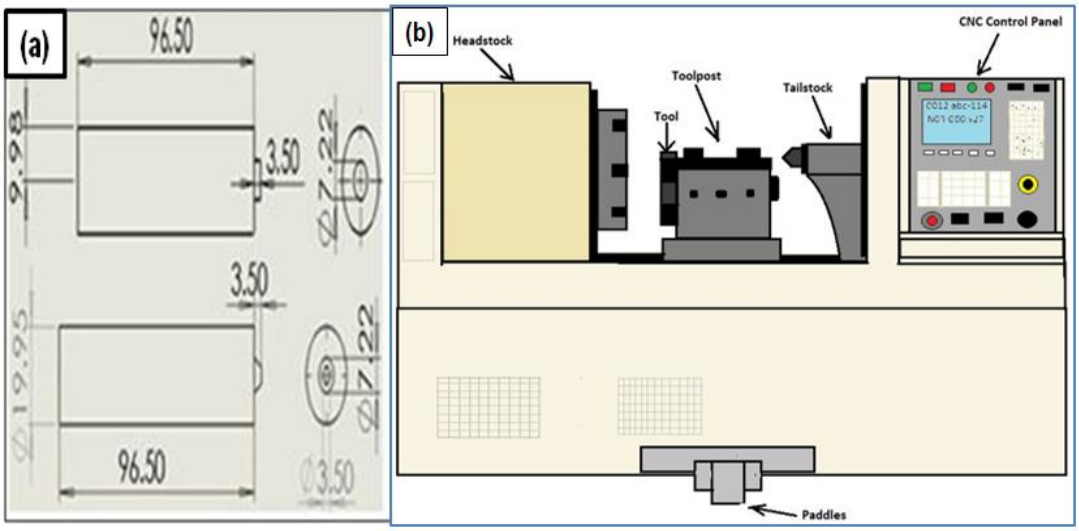

Figure 3.1-(a) Dimension of tool probe (b) CNC lathe machine set up

3.2.1 Measurement Condition

Residual Stresses were measured in two different probes with a portable Stress Analyzer. For each work piece, two tests were done on the circular probe and taper circular probe periphery. Following are the measurement conditions for analysis of residual stress in two different probes are: X-ray tube current=1.00 mA, voltage=30 kV, incidence angle=35 degree, wavelength (K-Alpha) =2.29093[A](Cr), wavelength (K-Beta)=2.08480[A](Cr), temperature = 34.81 degree centigrade.

3.2.2 Set-up and Methodology

In this investigation, residual stresses were estimated utilizing PulsetecμX-360n portable stress analyzer machine set up as shown in fig. 3.2(a-c). These readings were then contrasted and the outcomes got from ABAQUS/CAE simulation of the turning process. The specifications of the machine are maximum measurement distance=51 mm, X-Ray tube voltage & current=30KV/15 mA max, measurement method= Single incident angle method (cosα method), measurement time=60 sec, target material= Ferrite, aluminium, nickel, titanium, ceramics etc. This machine uses cosα method for determining the residual stress. The cosα technique is as promising as $\sin^2\Psi$ technique and with similar errors. However, $\sin^2\Psi$ is the time intensive method and requires a full X-Ray diffractometer setup.

Table 3.1:- Stress Analyzer Specifications

Item	New model (μ X360n)
Collimator Size	Standard: 1mm
Maximum measurement distance (For ferrite Samples)	51 mm
X-Ray tube voltage & current	30KV/ 15mA max.
X-ray tube	Cr/Co/Cu/V/Mn
Measurement Method	Single incident angle method[cosα method]
Target Material	Ferrite, Aluminum, Nickel, Titanium, Ceramics etc.
Weight	Sensor unit: 2.4 Kg, Power Supply Unit : 6.2 kg
Sensor Unit/ Power Supply Unit Size	Sensor unit: W114 × H107× D213 (mm)Power Supply Unit : W159 × H235 × D289 (mm)
Measurement time	60 sec

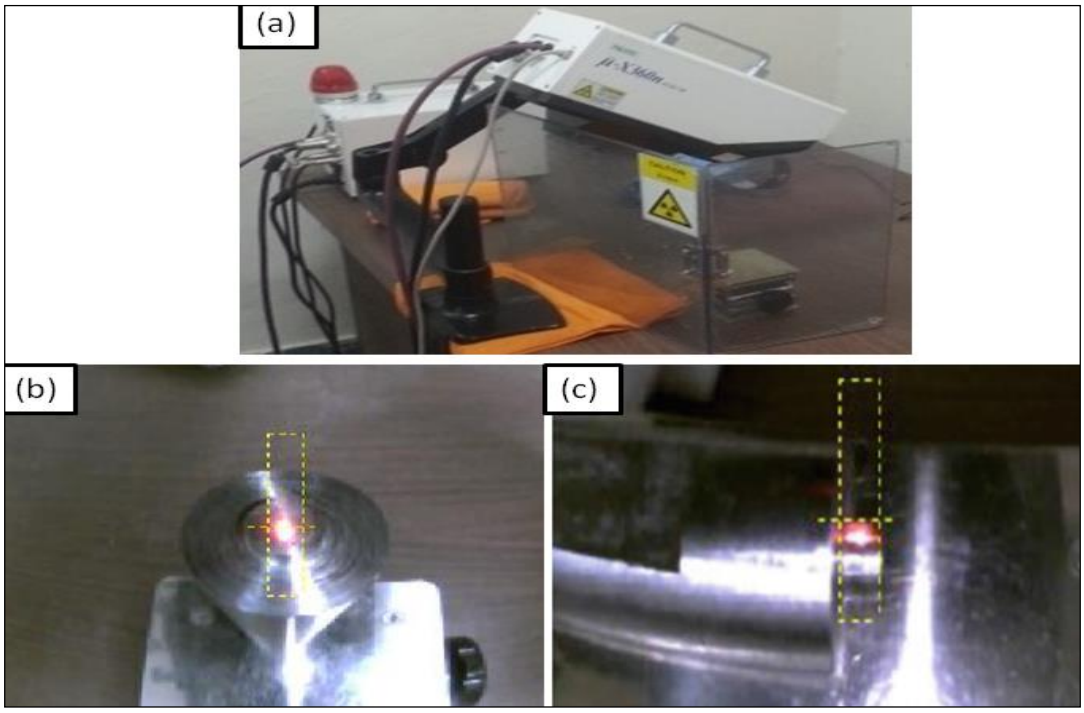

Figure 3.2-(a) Portable stress analyzer setup (b, c) Image captured in circular probe and taper circular probe

3.2.3 Residual Stress Measurement of FSP Tool Probe

The residual stress measurement was done on the specimen, which is made of tool steel material utilizing PulsetecμX-360n stress analyzer machine. Two tests i.e. TEST 1 and TEST 2 were performed on the periphery and the probe tip of the circular probe, while TEST 3 and TEST 4 were performed on the periphery and the probe tip of taper circular probe. The measurements were done by cosα method consisting of a gyro sensor to display the sensor unit angle. The value of diffraction angle 2θ=156.396 degree, Diffraction lattice angle=23.604 degree, interplanar spacing(d)= 1.170, plane(h,k,l)= 2,1,1, crystal structure= BCC, young modulus(E)= 224 GPa, Poisson ratio(v)= 0.280 were taken during measurement.

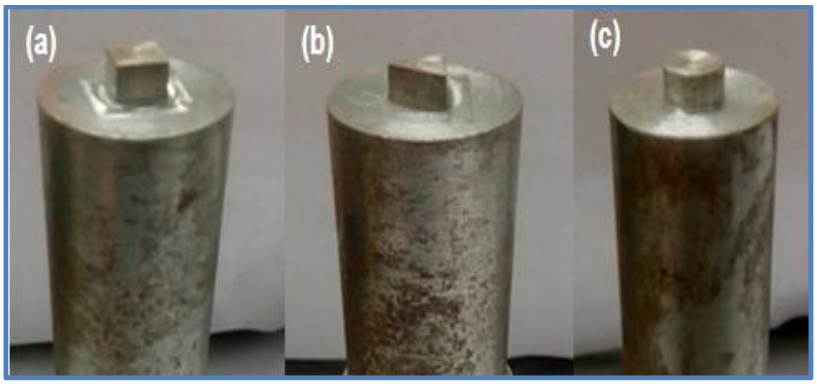

Figure 3.3-(a b, c) Types of FSP tool pin profiles

For measuring the residual Stress, the specimen was kept on the table just below the XRD. Incidence angle Ψ angle was selected as 35 degrees for ferrite material. X- Rays were focused on the pin circumference. After proper adjusting the specimen and XRD, a protecting glass shield was used to cover for prevention against harmful rays. After that two readings were taken on each specimen. Time taken for measuring residual stress on each specimen was 90 seconds. Types of FSP tool pin profiles shown in fig 3.3(a-c).

3.3 SIMULATION

Turning process on lathe machine involves oblique cutting and chip formation. It's therefore, a very complex machining process and so, research is still going on in the search for a formalized methodology to completely simulate the cutting process. The difficulty arises due to the multiple cutting forces involved, the chip formation, temperature changes, varying shear deformation zones and many such factors. Since we need to find out the residual stresses in the H13 tool steel workpiece after it's turned on the CNC lathe machine by a single point cutting tool of carbide insert, naturally, multiple time steps must be input along with a precise degree of mesh accuracy and computational power.

In the 'Materials' module, the material is characterized by adding the properties of specimen, for example, types of material. In the material practices segment properties like conductivity, ductile damage, Shear damage with damage evolution, density, elastic, thermo-viscoplastic properties are characterized. In the current study, Johnson-Cook damage criterion was utilized. In the mesh module, 3D Stress group of explicit, linear geometric order, hex element type was designate to the specimen. Element deletion was picked as we were not intrigued by chip stream and only the stresses on the specimen. In the interaction module, Friction contact coefficient was 0.4. Another material was defined with a density of 100000, a Young's modulus of $1e^{+20}$ and Poisson's ratio of $1e^{-6}$. This material was assigned to the cutting tool to approximate the behaviour of a rigid tool since we are not interested in the residual stresses or deformations in the cutting tool.

3.3.1 Modeling of Circular and Taper Circular FSP Tool Probe

Finite element analysis (FEA) is the modeling of the turning process to create a tapered probe tool. A round sketch of 22 mm range and 30mm deep is drawn. This was raw component of the specimen. Fig. 3.4(a&b) shows the geometry of workpiece radius 22mm and workpiece is extruded to 30mm deep. It is not exactly the definite length of the specimen since we are just

intrigued by the part which is close to the periphery and tip of the tool probe. This assumption is reasonable and spares a considerable amount of meshing and computational time. Next, the part is apportioned into 3 distinct regions. This helps, bettering the mesh quality. Since there is step turning included, various parts can be meshed for a better/coarser quality. A reference point (RP) is also added to the center of the face. Fig. 3.5 (a&b) the material is assigned to the cutting tool to approximate the behavior of a rigid tool since we are not interested in the residual stresses or deformations in the cutting tool. The parts are assembled in the Assembly module. A small gap of 0.5mm between the cutting tool and the specimen is given. Fig. 3.5(c&d) shows the Interaction module, Surface-to-surface contact is selected between the tool and workpiece. Friction contact coefficient of 0.4 is used. Constraints are added of coupling type to the tool and the workpiece, coupled with their respective reference points. A rigid body coupling is also given to the tool. Fig. 3.6(a&b) shows the stress analysis of the circular tool probe, in the load module where the limit constraints are altered, with the goal that the tool traverses in a straight way laterally to the specimen axis.

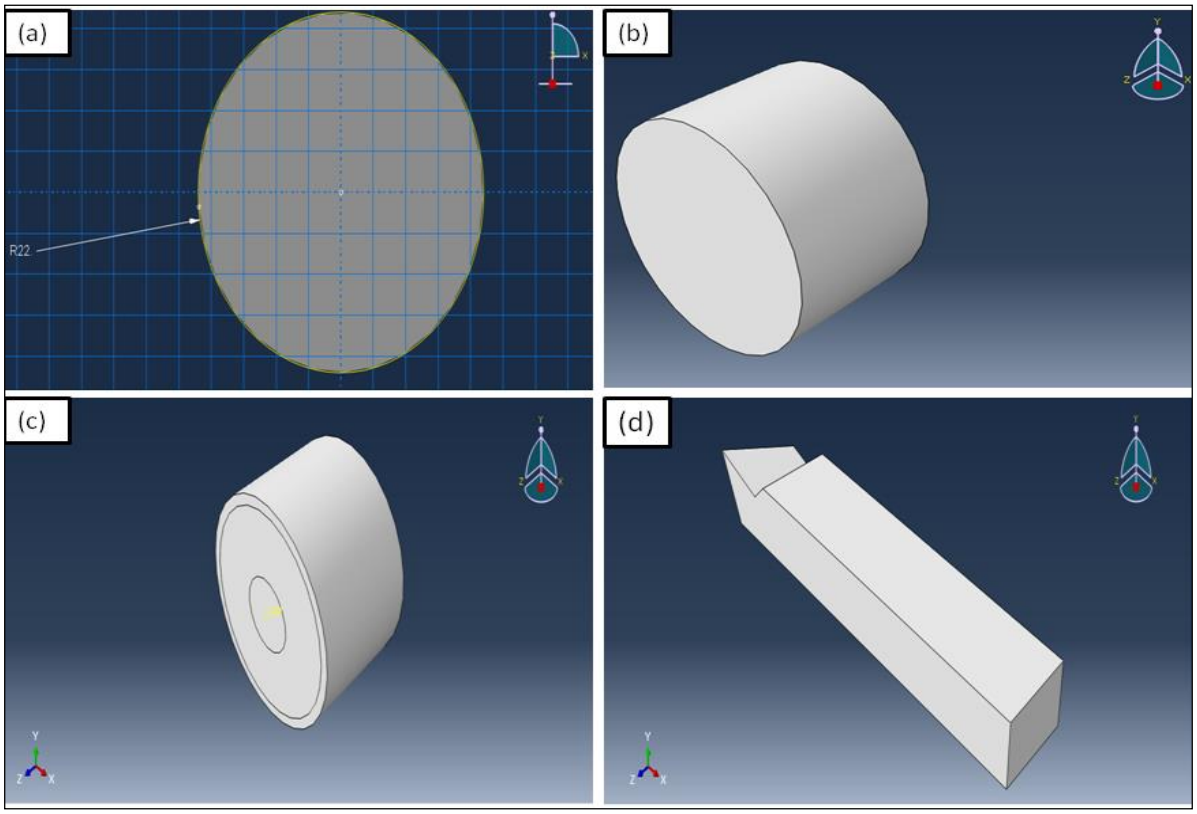

Figure 3.4-(a) Geometry of workpiece R22mm (b) Extruded cylinder workpiece 30mm (c) Partitioned regions in the work piece (d) Single point-cutting tool

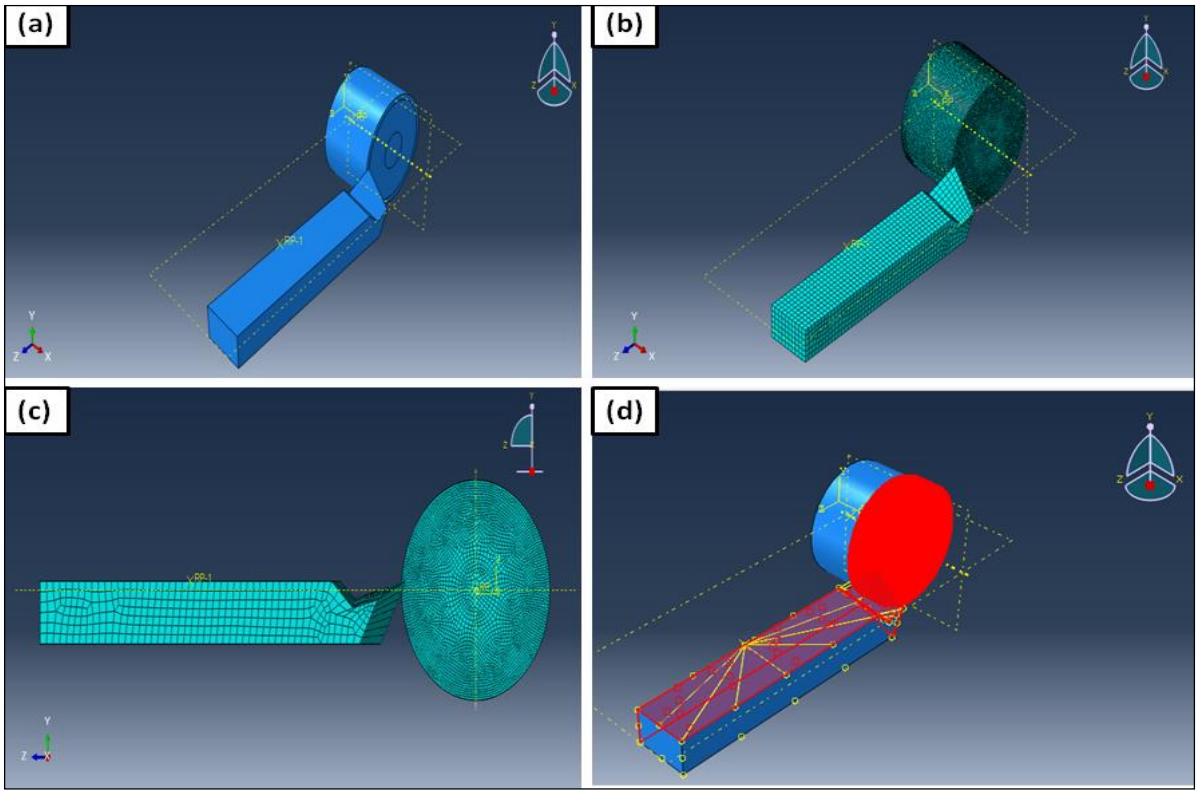

Figure 3.5-(a) Assembly (b) Meshing Top view (c) Meshing Front view (d) Surface to Surface contact

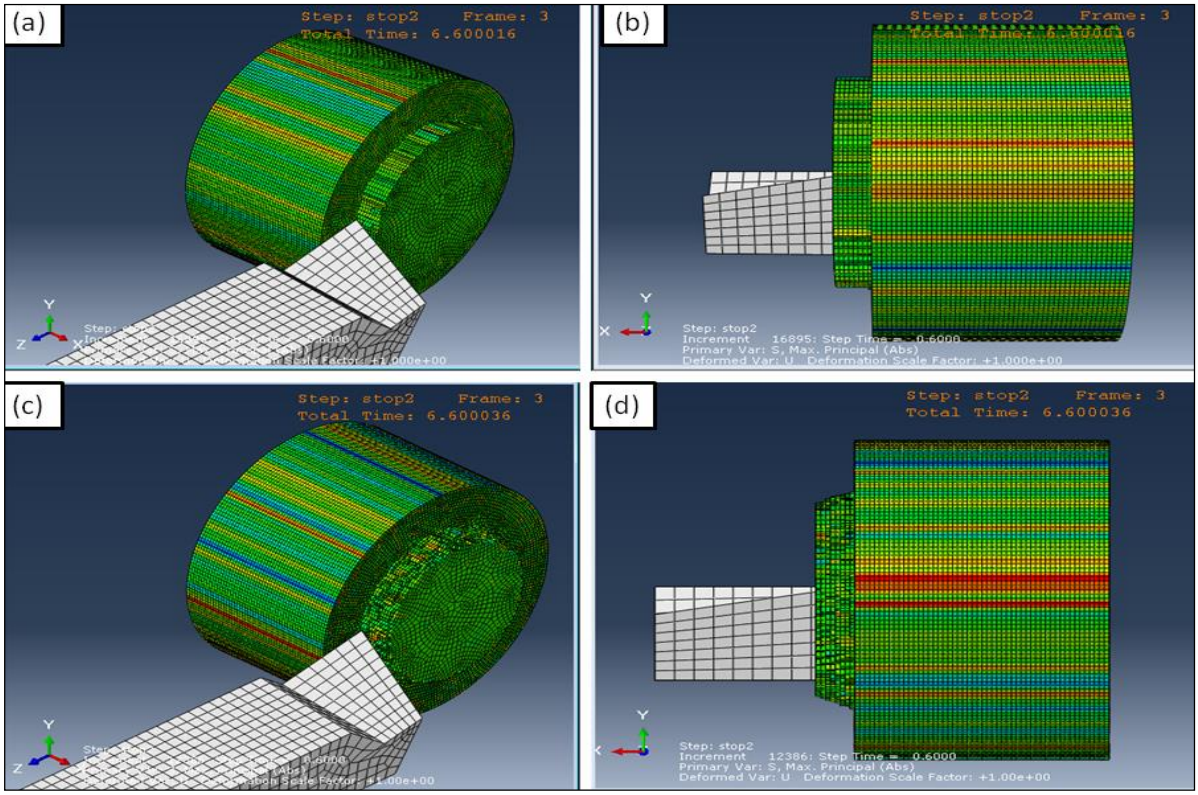

Figure 3.6-Machining visualized with stress contours of (a, b) Circular probe (c, d) Tapered Circular probe

Fig. 3.6 (c&d) shows the stress examination of the taper circular tool probe profile test was like the strategy depicted in the past segment. The main special case i.e., in the load module, boundary conditions are entering. Here, the angular velocity to the specimen, the feed rate and DOC is given to the cutting tool.

3.4 SIMULATION RESULT

Estimation of residual stress due to machining would now be able to be envisioned through simulations as a result of advancements in technology and various ways to use computational power to regulate the residual stresses in turning operation. Most of the research work is based on orthogonal cutting and are 2-D simulations. In this research, we have used ABAQUS explicit dynamics to simulate the oblique cutting in 3-D environments. After turning process completed the next step is to residual stress measurement of machined specimen. Residual stresses data was obtained by utilizing a PulsetecμX-360n stress analyzer machine. A procedure for simulation is formulated which can be applied to similar machining processes. Various manufacturing procedures that alter the shape or change the characteristics of the materials such as deformation of the material, machining operations or other processes contribute to the generation of residual stresses. These can be achieve in a material which hasn't gone through any process, as it depends on various factors and may get generated during manufacturing and operational conditions [143]. Residual stresses may be present on the micro-level and on the macroscopic level. They tend to affect the performance of that material, as it can cause local yielding or plastic deformation. Hence, measurement and analysis of this residual stress in the components becomes vital.

Friction stir processing tool, which is manufactured by H13 tool steel material, plays a vital role in friction stir processing. It selects the kinds of materials that could be processed and the dimension of the workpiece. The shoulder controls the flow of material in certain regions, and the probe generates heat and severe plastic deformation. Ultimately, the friction stir tool impacts the microstructure and mechanical properties. However, little research about the friction stir processing tool geometry has been published until now, and data on friction stir welding tool could be a reference to understand the tool [72], [144], [145]. The result of Test 1 and Test 2 sample of residual stress on the probe periphery and tip of the circular probe was found to be compressive 139 MPa and 109 MPa with a S.D of 9 MPa and 14 MPa respectively. The result of Test 3 and Test 4 sample of Residual Stress on the probe periphery

and tip of tapered circular probe was found to be compressive 199 MPa and 175 MPa with a S.D of 11 and 17 MPa, respectively.

The scattered X-rays are recorded for a family of planes {h,k,l} and using Bragg's law lattice spacing can be found then strain [146] is obtained by Eq. (3.1):

$$\varepsilon_{\varphi\Psi} = \frac{d_{\varphi\Psi} - d_0}{d_0} \quad \ldots\ldots\ldots\ldots\ldots\ldots\ldots\ldots\ldots\ldots\ldots\ldots\ldots\ldots \text{(3.1)}$$

Where, $\varepsilon_{\varphi\Psi}$ is the calculated strain for the {h,k,l} planes for a sample orientation referred by the φ and ψ angles, and d_o is lattice spacing for an unstressed sample**.** In fact, the strain varies with the ψ angle along the normal to the diffraction plane [147]. Equation (3.2) expresses the ε_{α}, the parameter used to calculate the stress [148].

$$\underline{\varepsilon}_{\alpha}^{\{hkl\}} = \frac{1}{2}\left[\left(\varepsilon_{\alpha}^{\{hkl\}} - \varepsilon_{\pi+\alpha}^{\{hkl\}}\right) + \left(\varepsilon_{-\alpha}^{\{hkl\}} - \varepsilon_{\pi-\alpha}^{\{hkl\}}\right)\right] \ldots\ldots\ldots\ldots\ldots\ldots \text{(3.2)}$$

Where, ε_{α}, $\varepsilon_{\pi+\alpha}$, $\varepsilon_{\pi-\alpha}$, $\varepsilon_{-\alpha}$ are strains determined at four points located at 90 degree on the Debye ring. Equation (3.3) provides the stress for the cosα method:

$$\sigma_{\varphi} = \frac{E^{\{hkl\}}}{1+\nu^{\{hkl\}}} \frac{1}{\sin 2\eta \sin 2\Psi_0} \frac{\partial \underline{\varepsilon}_{\alpha}^{\{hkl\}}}{\partial \cos\alpha} = \frac{1}{\frac{1}{2}S_2^{\{hkl\}}} \frac{1}{\sin 2\eta \sin 2\Psi_0} \frac{\partial \underline{\varepsilon}_{\alpha}^{\{hkl\}}}{\partial \cos\alpha} \ \ldots\ldots \text{(3.3)}$$

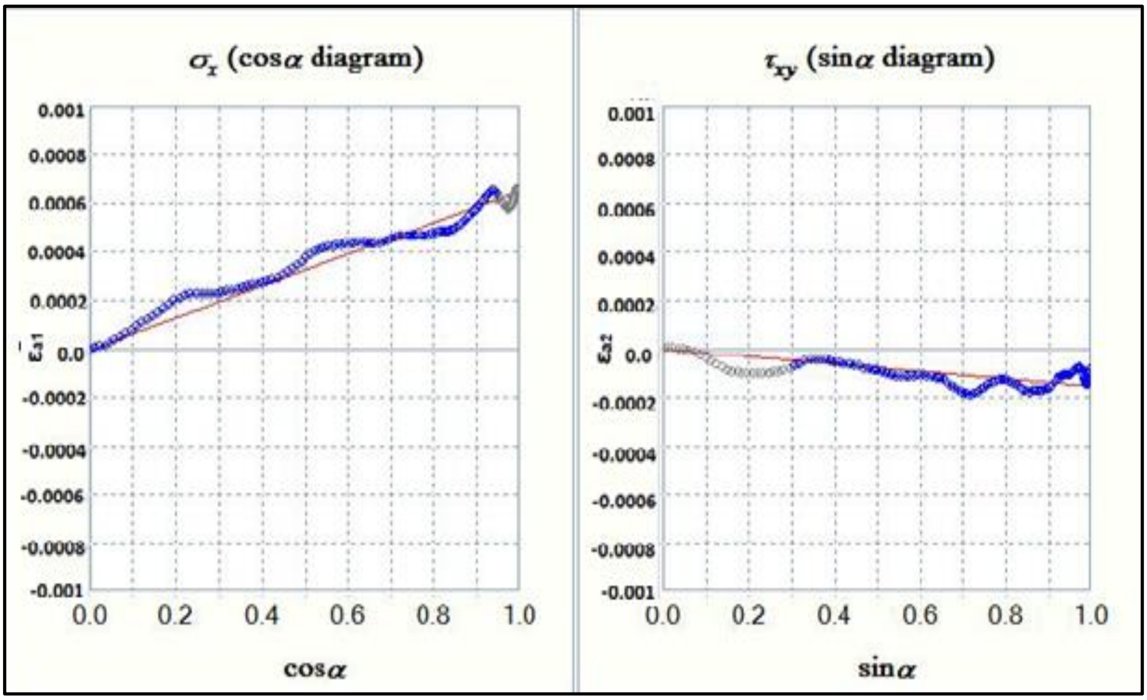

Figure 3.7-Residual Stress Circular probe (Test 1)

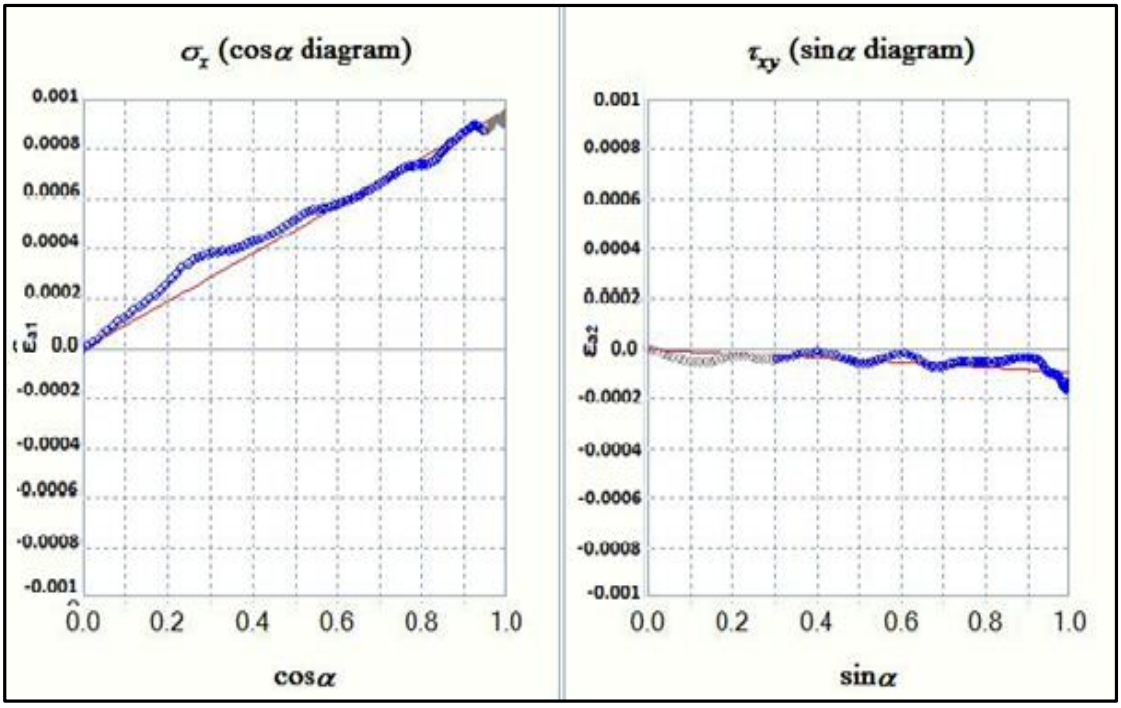

Figure 3.8-Residual Stress Circular probe (Test 2)

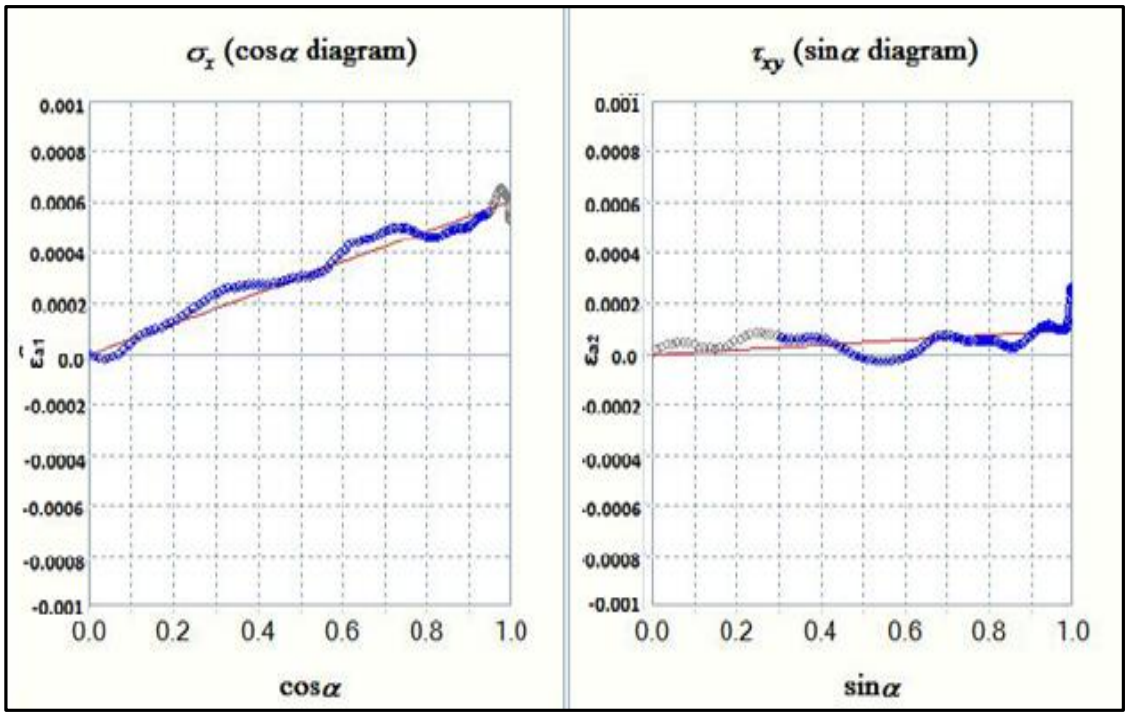

Figure 3.9-Residual Stress Tapered circular probe (Test 3)

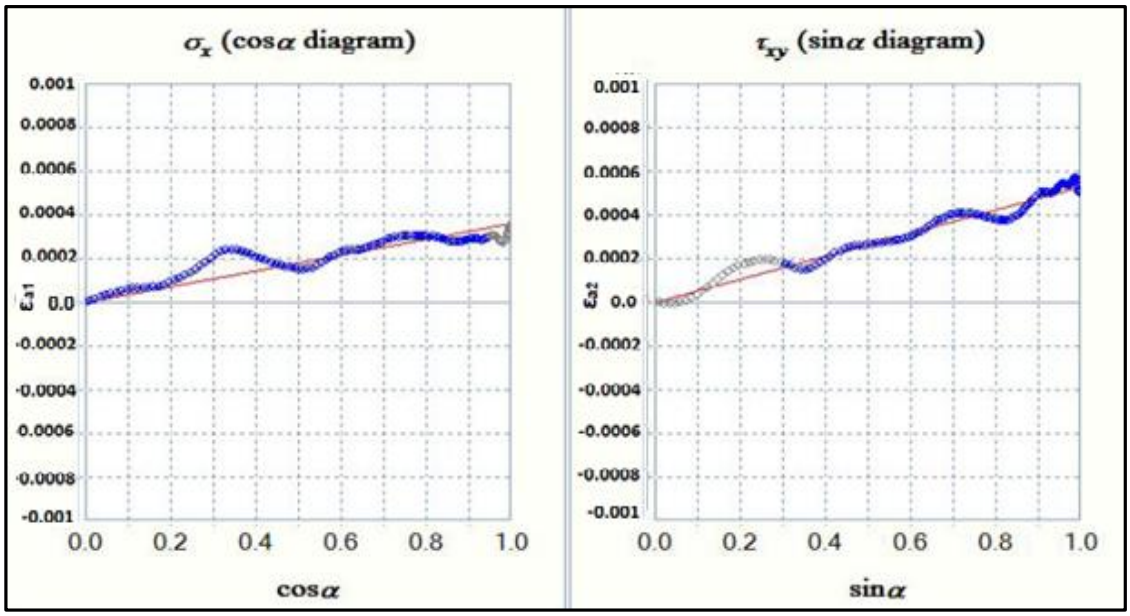

Figure 3.10-Residual Stress Tapered circular probe (Test 4)

Fig. (3.7-3.10) residual stress graphs represent the variation of the parameter a_1 and a_2, which are used for the linear determination of σ_x and T_{xy}, respectively. Following equations (3.4 &3.5) represent the variation of a_1 and a_2 with cosα and sinα, respectively.

$$a_1 = \frac{1+v}{E}\,\sigma_{11} sin2\Psi_0\, sin2\eta\, cos\alpha \qquad \ldots (3.4)$$

$$a_2 = 2\frac{1+v}{E}\,\sigma_{12} sin\Psi_0\, sin2\eta\, sin\alpha \qquad \ldots (3.5)$$

The red line in the above graphs represents the average value of parameters a_1 and a_2 when α varies from 0 to 90 degree. A good linear behavior has been obtained between parameter a_1 and a_2 and angle α as shown in fig. (3.7-3.10).

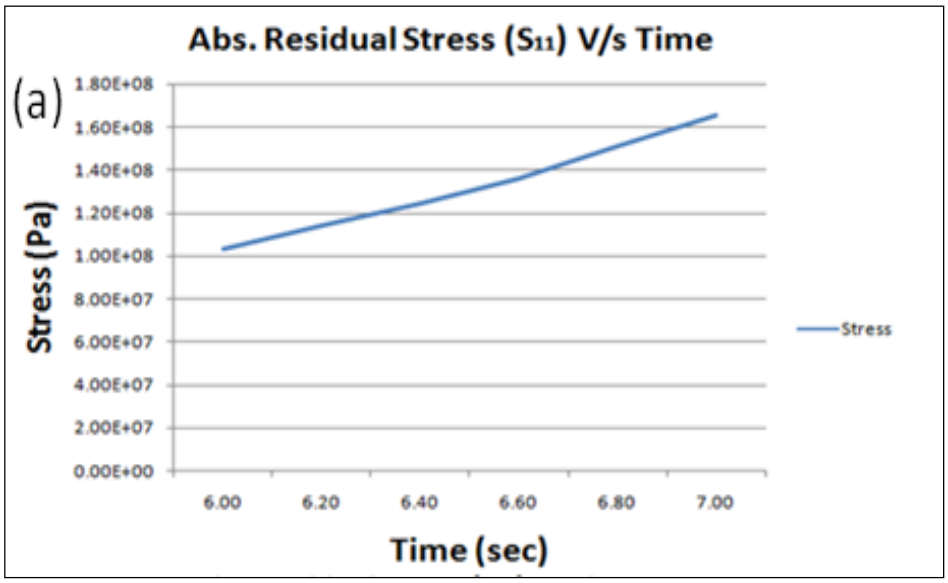

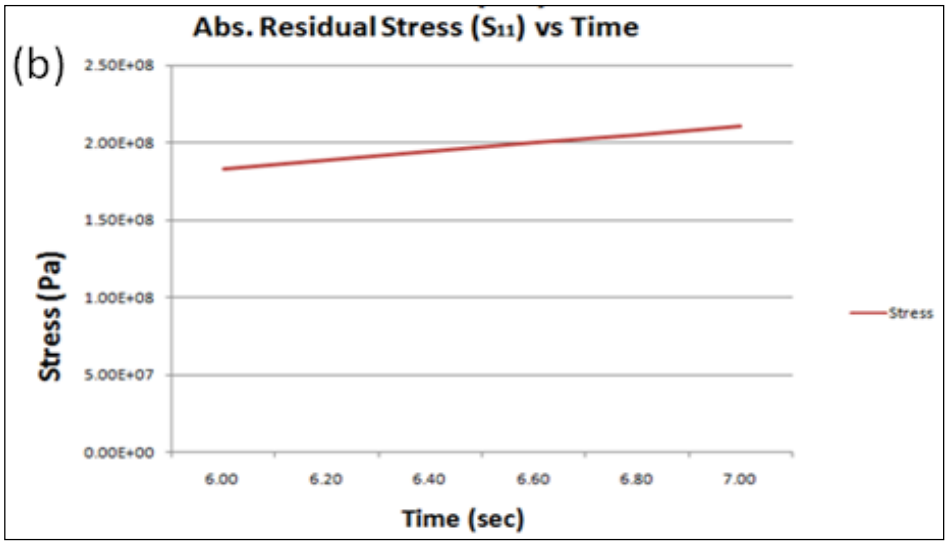

Figure 3.11-Residual Stress v/s time for probe tip (a) Circular probe (b) Taper Circular probe

From fig. 3.11(a) the variation of absolute residual stress versus time for circular probe and it can be noticed that residual stress at the probe tip increase in both the cases with machining time. In fig. 3.11(b) shows the variation of absolute residual stress versus time in the tapered cylinder probe tip in the second pass turning operation. Here the variation is taken from t=6s to t= 7s i.e. the time for the second pass of turning is 1 sec in the simulation. Similarly, as shown in fig. 3.11(a&b) shows that more residual stresses are generated in tapered circular probe profiles, which can be understood from the fact that in turning the probe profile, the diameter of the tapered probe is less at the tip in comparison to the diameter of the tip of a circular probe. In tapered machining, material removal rate decreases from small diameter end to large diameter end of the probe because of which the variation in residual stress in the tapered probe is less as compared to the variation of residual stress in the circular probe.

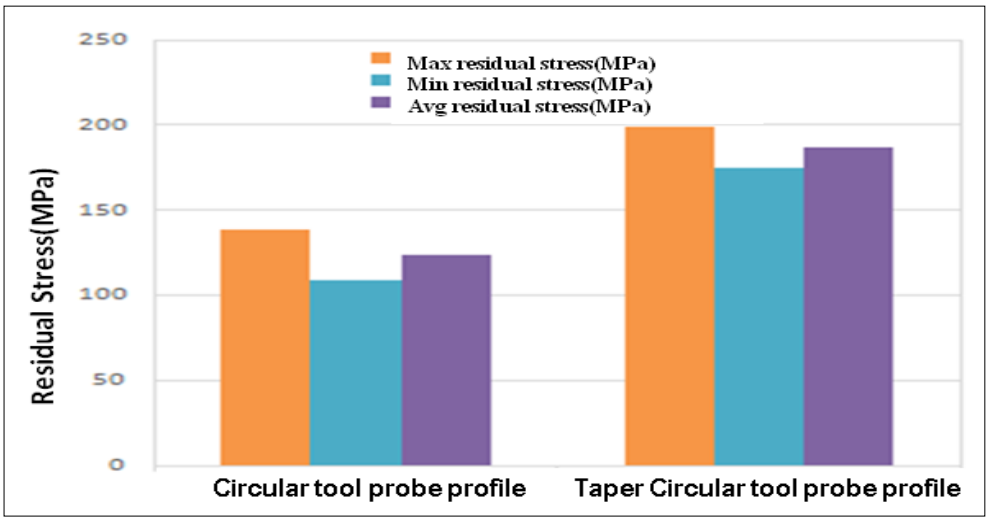

Figure 3.12-Comparison of residual stress on circular and taper circular probe profile

A comparison in the form of a histogram is presented in fig. 3.12 that depicts the residual stresses in different probe profile. It is evident that maximum stress is obtained in taper circular probe profile and the minimum in circular probe profile. The reason for this variation of residual stress is due to the type of machining done in the different specimen. As a result of this, taper circular probe profile faces maximum residual stress. In circular probe profile, only turning was done. But in tapered circular, the diameter was the same as that of the cylinder on one side and less on another side. For the tapered probe, more machining was required as a comparison to the circular probe. Hence, more residual stresses were induced in the tapered circular probe profile.

3.4.1 Experimental Analysis of Residual Stress Tool Probe

From X-Ray Stress Analyzer of residual stress in machining different pin profile we have obtained the value of residual stress given in the table 3.2.

Table 3.2:- Residual stress in different pin profiles

S.No	Tool Pin Profile	Residual Stress [MPa](Absolute)	Average Stress [MPa](Absolute)
1	Square	236	244
2	Square	252	
3	Triangular	211	219
4	Triangular	227	
5	Cylindrical	109	124
6	Cylindrical	139	

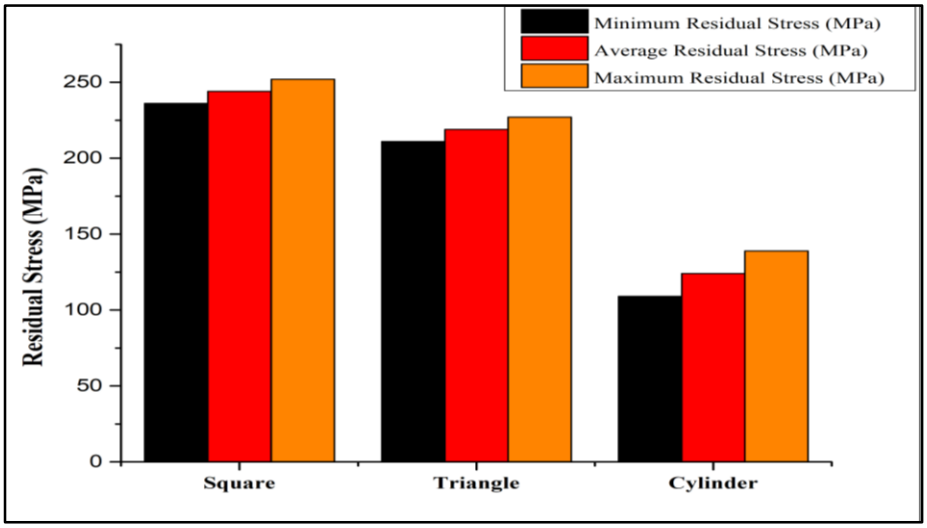

Figure 3.13-Comparison of Residual Stress

A comparison is shown in histogram of residual stress in different pin profile. It can be clearly seen that maximum stress is obtained in square pin profile and minimum in cylinder pin profile. This reason of this variation of residual stress is due to type of machining done in different specimen. In square and rectangle pin profile turning was followed by milling which induces more stress. In square four sides were machined in comparison to triangle in which only three sides were machined. As a result of which square pin profile faces maximum residual stress. In cylinder and tapers pin profile only turning was done. But in tapered the diameter was same as that of cylinder on one side and less on other side. For tapered pin more machining was required as comparison to cylinder. Hence more residual stresses were induced in tapered pin. Stress concentration may also account for more residual stresses in square and triangle pin profile as they were having sharp edges.

3.4.2 Validation

Before residual stresses measurement was done on the workpiece surface, the machining parameters and Abaqus/CAE **s**imulation were observed. The experiment and simulation results for the machining parameter and the residual stresses were compared and are a strong testimony for the validation of the current model. From X-Ray stress analyzer of residual stress in machining, different probe profile developed a residual stress and the values are given in table 3.3.

Table 3.3:-Residual stress in circular and tapered circular probe profile

S.NO	Tool Pin Profile	Residual Stress [MPa](Absolute)	Average Stress [MPa](Absolute)
1	Circular	109	124
2	Circular	139	
5	Tapered circular	175	187
6	Tapered circular	199	

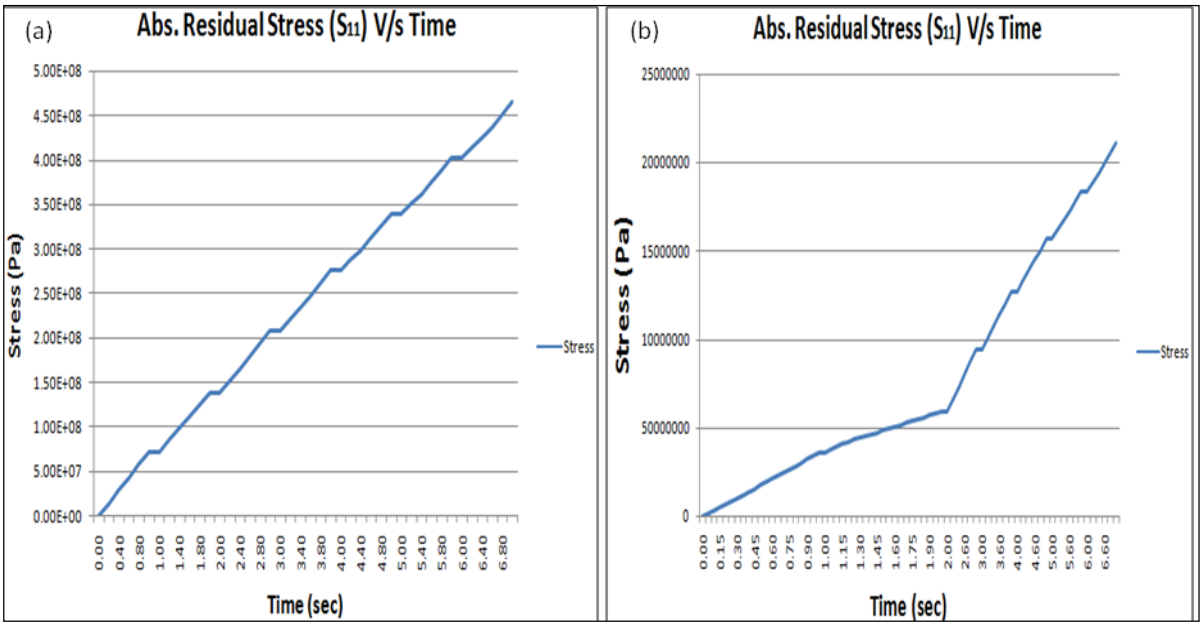

Figure 3.14-Residual Stress v/s time for probe periphery (a) Circular probe (b) Taper circular probe

From the fig. 3.14, residual stress verses time graphs, obtained from ABAQUS/ CAE simulation, we can infer that stress is found to increase during the turning process and the increase is linear in both cases. For the circular probe, the average residual stress is found from simulation to be compressive 130 MPa approximately. This suggests compressive stress on the probe periphery. From experimental readings, the average residual stress was found out compressive 124 MPa. So the percent error is 8.06%. For the tapered circular probe, the average residual stress is found from simulation to be compressive 199 MPa approximately. This also suggests compressive stress on the probe periphery. From experimental readings, the average residual stress was found out compressive 187 MPa. So the percent error is 6.41%.

Since the error value is found to be within an acceptable range, it can be concluded that the experimental readings obtained for the circular and tapered circular tool probe complement the FEA model simulation results.

3.5 SUMMARY

FSP is a solid state plastic deformation method which works with the help of a rotating non-consumable tool comprising of a shoulder and a probe at the end. It is crucial to anticipate the residual stresses induced so as to increase the life of the component. There are many methods to measure the residual stresses in a component (destructive and non-destructive) and the

most common method is XRD. In the present study, the residual stress on the periphery and tip of the circular and taper circular FSP tool probe were measured using the PulsetecμX-360n stress analyzer machine. The experiments were performed using two different types of tool probe profiles and compared with the outcome got from ABAQUS/CAE simulation of the turning process. More residual stresses were generated in tapered circular probe profiles, which can be understood from the fact that in turning the probe profile, the diameter of the tapered probe is less at the tip in comparison to the diameter of the tip of a circular probe. Maximum stress was obtained in taper circular probe profile and the minimum in circular probe profile. Furthermore, maximum stress was obtained in square pin profile and minimum in cylinder pin profile, while more residual stresses were induced in tapered pin. The experimental readings obtained for the circular and tapered circular tool probe complement the FEA model simulation results.

CHAPTER 4

EXPERIMENTAL DETAILS

4.1 MATERIAL SELECTION

The selection of substrate material, FSP tool material and reinforcement powder is very important for the fabrication of surface metal matrix composite. Aluminium alloy 7075 used as the matrix material in this research work.

4.1.1 Substrate Material

Aluminium surface metal matrix composites are preferred aluminium has a very low density, high tensile strength, and higher toughness. Among the series of Aluminium alloys, Al 7075 is exceedingly corrosion resistant, displays high strength and thus finds many applications in the aerospace industry and marine fields. It is one of the strongest and stiffest aluminium alloys among all of the Aluminium series. It is so because it is an alloy with zinc as the next most superior material after Aluminium. The mechanical properties that it exhibits are excellent and includes good ductility, toughness, and strength. Aluminium alloy is preferred as matrix material in surface metal matrix composite. Fig. 4.1 shows the dimension and design of groove and holes method of substrate metal used for the experiments.

The Al7075 alloy consists of many elements, the most prominent of them being aluminium, followed by zinc in terms of weight percentage. The chemical composition and mechanical properties of matrix metal are shown in table 4.1 and 4.2.

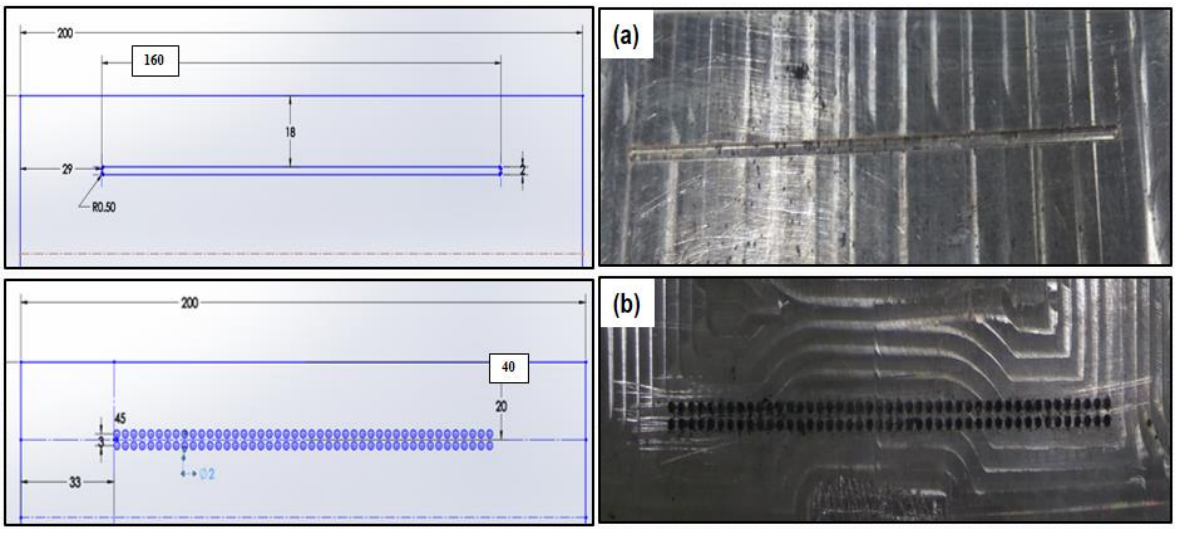

Figure 4.1-Dimensions and design of (a) Groove method (b) Holes method of substrate metal used for the experiment

Table 4.1:- Chemical Composition of AA7075-T6

Alloy	Zn	Mg	Cu	Fe	Mn	Ti	Cr	Si	Al
Wt. %	2.273	2.4	1.3	0.18	0.04	0.08	0.18	0.06	Rest

Table 4.2:- Mechanical Properties of AA7075-T6

Modulus of Elasticity E(GPa)	Tensile Strength (MPa)	Yield Strength (MPa)	Elongation (%)
71.0	544	502	21.5

4.1.2 Tool Material

The FSW/FSP tool was fabricated from H13 tool steel and has a hardness of 55-65HRC. H13 Tool Steel is extensively used in hot work die and cold work applications. It is used for both ferrous and non-ferrous casting e.g. Al and Mg die-casting and in the plastic moulding operation. It possesses high hardness value and strength even at high temperatures and has good hardenability. It is a good thermal resistant and wear resistant. Chances of thermal fatigue cracking due to cyclic cooling and heating cycles are low because of the high hot hardness of H13 tool steel. It is favoured over other tool steel for hot work applications because of its high toughness and thermal fatigue cracking resistant properties. Its application in cold working applications is due to its better stability in heat treatment and high toughness. Improvement in chemical homogeneity, carbide-grain-size-refinement, relatively fatigue and mechanical properties is due to the remelting process.

AISI H13 is the most commonly used tool steel for the processing of aluminium alloys. Though alloys with better strength, ductility and excellent creep and corrosion resistance (like nickel and cobalt superalloys) may be considered as a better alternative, they have a major drawback viz. the difficulty one faces while machining complex features like flutes and flats on the surface of the tools made with them. Many refractory metals like tungsten, molybdenum, niobium and tantalum, due to their single phase structure, show high temperature strength and have stable mechanical properties up to 1000-1500°C, rendering them as good alternatives as tool material; however, their fabrication process (powder processing) is a relatively expensive technique. Carbide materials are frequently used as tool

material at applications involving elevated temperatures due to their remarkable wear resistance and fracture toughness. Ceramic-reinforced MMCs have been considered as tool material as well, though their brittle nature increases the probability of fracture during the penetration phase. Furthermore, the high manufacturing costs, size limitation and poor machinability of polycrystalline cubic boron nitride, PCBN has limited their use as an FSP/FSW tool despite their exceptional mechanical and thermal properties [149].

4.1.3 Tool Pin Profile

Friction stir processing focuses on two components: heat generation and material flow. So different tool profiles are considered to analyze these two components. That is why different pin profiles are considered in this research study. The non-consumable rotating tool probe stirs the plasticized material and moves the same behind it to have a good processed zone. Tool pin profile has a significant impact on material flow and in turn controls the processing speed of the Friction Stir Processed workpiece. Three types of tool pin profiles as shown in fig. 4.2 i.e. square, triangular, and cylindrical pin profiles have been used to process the aluminium based metal matrix at different welding and travelling speeds.

The tool had two sides, with a total length of 117 mm. The side of the square pin profile was 5.10mm, Triangular pin profile was 6.25mm and the diameter of the cylindrical pin profile was 7.22mm. The tool shank diameter was 19.95mm. The length of the all pin profiles was 3.5mm. A tool profile must be such that it has less amount of flashes. The material needs to be well distributed by the tool to form a good processing zone and due to this, it stops the formation of chips. All the tool pin profiles design and dimension used in FSP are shown in fig. 4.3(a-c).

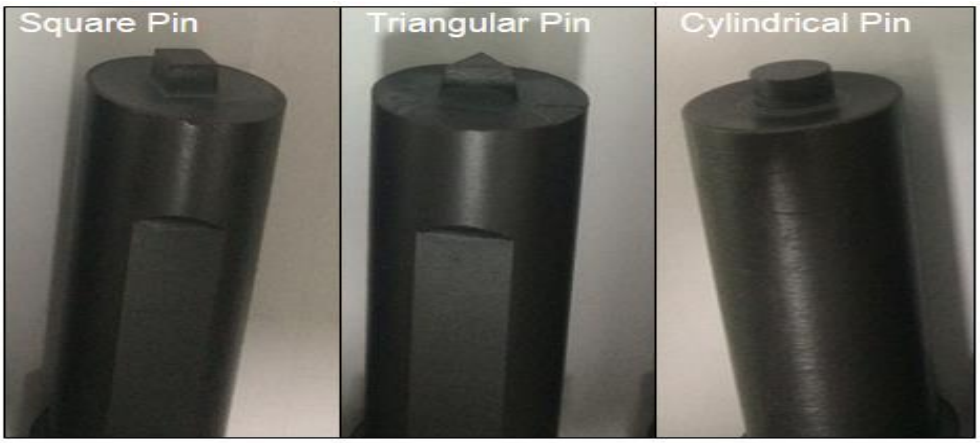

Figure 4.2-Different types of tool pin profiles used in FSP

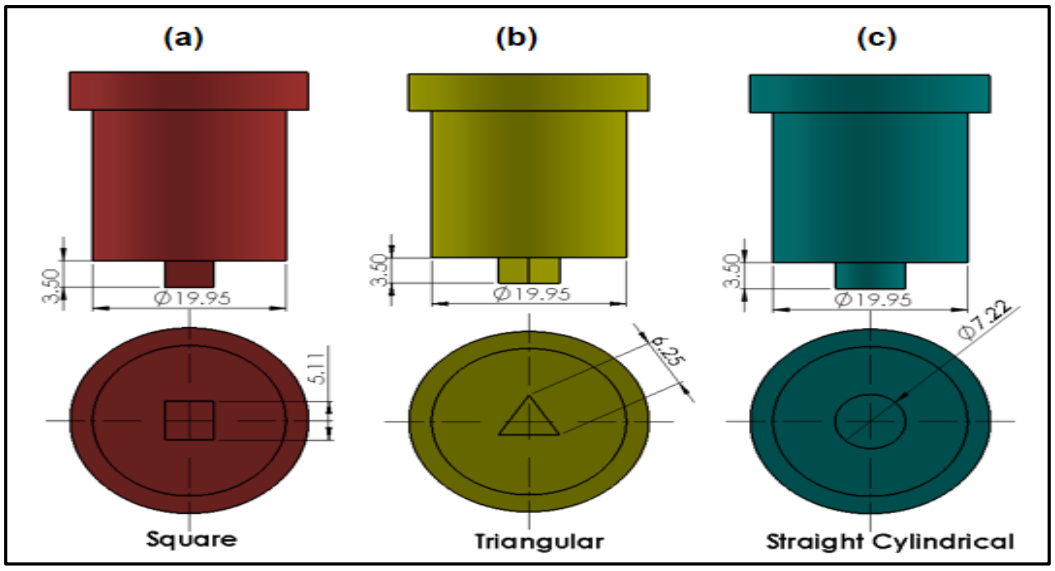

Figure 4.3-Tool pin profiles design and geometry of a FSP tool (a) Square pin (b) Triangular pin (c) Cylindrical pin

4.1.4 Reinforcement powder

Most critical factors in realizing the perfect properties from the fabricated surface metal matrix composite is the selection of the reinforcement powder. Boron Carbide (B_4C) used as the material for the reinforcement particle in this research study. B_4C, owing to its good chemical and thermal stability, is the most appealing reinforcement material and it has a lower density and higher hardness in comparison to Al_2O_3 and SiC [100,150, 151]. Fracture surface analysis of B_4C reinforced aluminium surface composite display a better interfacial bonding in comparison to Al_2O_3 and SiC. Furthermore, B_4C have neutron absorbing capability and therefore B_4C reinforced aluminium surface metal matrix composite suited for operation in nuclear reactors [152,153]. Reinforcing particles strengthen the composite and improve its heat resistance or conduction, resistance to corrosion and rigidity. A reinforcement particle can perform all or one of these functions, as per the requirement of the surface. A reinforcement that increases the matrix strength must be stronger and stiffer than the matrix and have the capability to change the failure mechanism to the advantage of the composite. This means that the ductility should be minimal and the composite must behave as brittle as possible. The B_4C nanoparticles of 99.9% purity with the particle size of (<30nm) were used as reinforcement materials and purchased from Intelligent Materials Pvt. Ltd. (Nanoshel). The SEM micrograph of the nanoparticles and Elemental composition are shown in fig. 4.4. The SEM micrograph reveals the morphology of B_4C reinforcement particles (RPs).

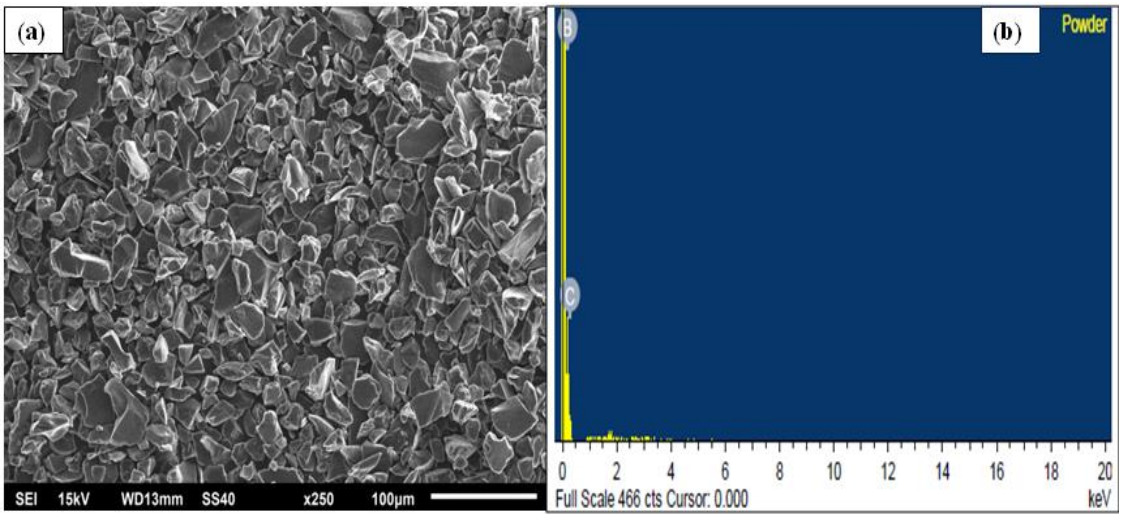

Figure 4.4-(a) SEM micrograph and (b) EDX of Boron carbide reinforcement particles (RPs)

4.2 SUBSTRATE PREPARATION

4.2.1 Ultra Sonic Bath

These ultrasonic baths or cleaners have large transducer areas and tanks that produce a high-powered ultrasonic intensity throughout the entire oscillating tank. Ultrasonic transducers are placed in the unit that create microscopic bubbles in the solution placed in the bath. The act of cavitation is the rapid formation and collapse of millions of tiny bubbles in a liquid. The sonication process was carried out in different rounds; the initial few rounds were performed using a cleaning detergent solution while in the next few rounds clean distilled water was used. Ultra sonic bath using Sonicator is shown in fig. 4.5.

Figure 4.5-Ultra sonic bath using Sonicator

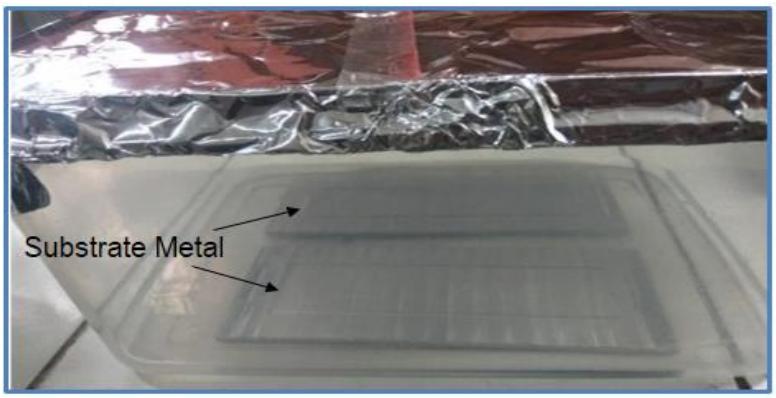

Figure 4.6 Base (substrate) metal plates dipped in Ethanol

The above (fig. 4.6) depicts the sonicated plate dipped in ethanol. The purpose was to prepare the substrate plate surface for further chemical bonding reaction. The plates were thoroughly cleaned and sonicated to depict clean surface with no impurities or particles and were then dipped in ethyl alcohol overnight. To perform coating of monolayer active OH- groups must be available, which could be provided by the ethyl alcohol group. The base (substrate) metal plates dipped in Ethanol is shown in fig. 4.6.

4.2.2 Magnetic stirrer

One of the major challenges in the experiment was to prepare a stable solution of boron carbide nano powder in a solvent. Boron carbide being a hard and dense particle is not completely soluble in any of the commonly used solvents. For the current experiment the solvent used was Diethyl Ether, a temporarily dispersed solution of B_4C in Diethyl Ether could be prepared but needed constant stirring. For this purpose, a magnetic stirrer was employed. A magnetic stirrer works on the principle that a rotating magnetic field can cause a stir bar immersed in a liquid to spin very quickly by stationary electromagnets, thus stirring it. In fig. 4.7(a-c) shows the wt% of nanoparticles, Diethyl Ether (DEE), Magnetic stirrer.

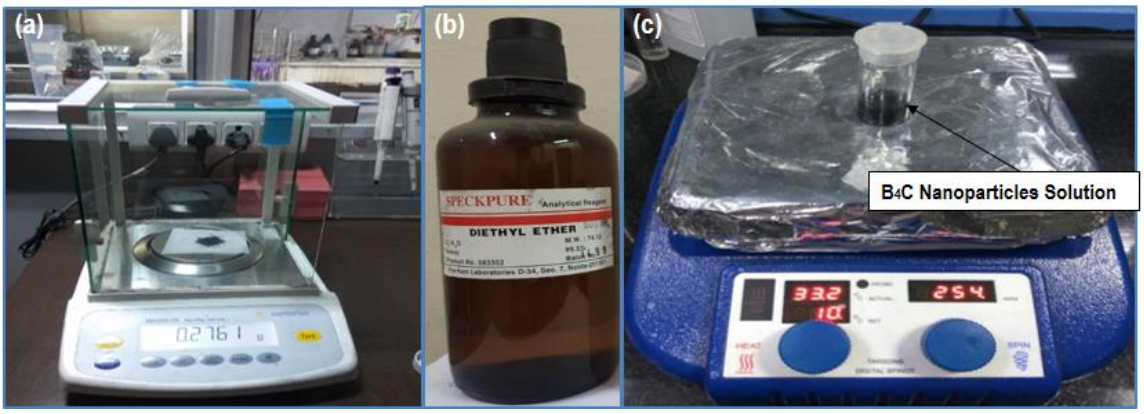

Figure 4.7-(a) Wt% of nanoparticles (b) Diethyl Ether (c) Magnetic stirrer

4.2.3 Micropipette

Micropipette are high precision devices to transfer liquids, its application is usually limited to lab usages for solutions of high quality and value. The current study was focused upon minimizing the wastage of the reinforcement particles and minimum utilization of the same during the nanoparticle reinforcement filling process. A calculated amount of solution was to be coated in the groove and holes on the substrate plates as shown in fig. 4.8(a-c). Use of micropipette seemed ideal in this situation, as only controlled amount of solution had to be dropped and spread evenly using a glass slide.

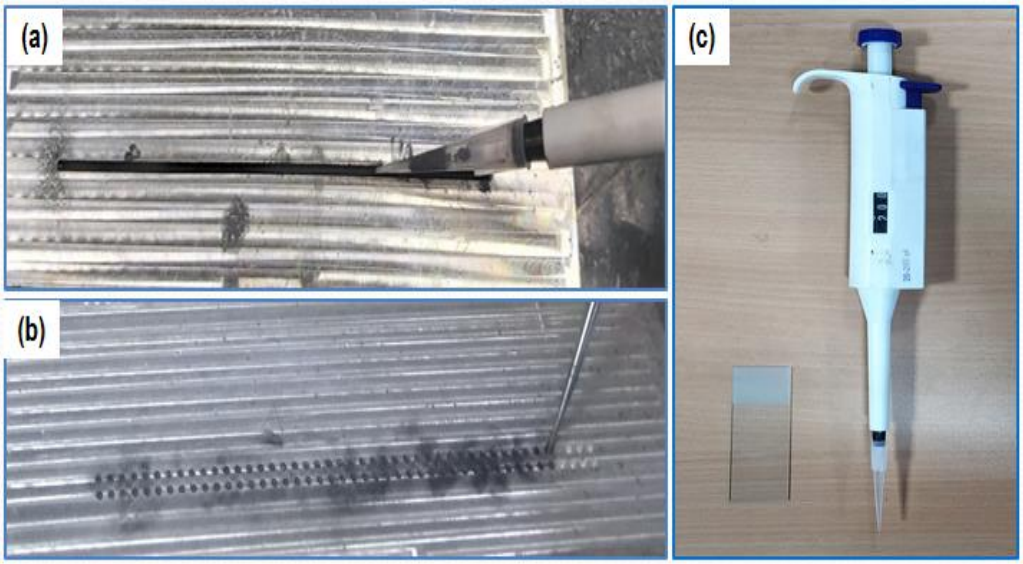

Figure 4.8 (a-c)-Filling of nanoparticles reinforcement in the groove and holes using Micropipette

4.2.4 Fume Hood

Designed to guarantee laboratory conditions and protect against flammable or toxic chemicals. Laboratory fume hoods act as protection devices that have clear sashes that slide horizontally or vertically into place and support high working visibility. The fume hoods circulate and filter air to eliminate possible vapours produced. Constructed for maximum chemical resistance, the leak-proof enclosures will not corrode even with heavy routine use and corrosive spills. However, the current research work had a different purpose of using a fume hood- the motive was to isolate the coated plate from the high moisture content and other gaseous substance that might affect the chemical composition. The substrate is dried on a hot plate inside the fume hood to strengthen the bond. Any foreign particle through air is cut out using the chemical vacuum hood. The Fume Hood set up is shown in fig. 4.9.

Figure 4.9-Fume Hood set up

4.2.5 Hot Plate

Hot Plate are table top portable surfaces used to heat laboratory samples safely. The use of hot plates in the current research work was made inside the fume hood to dry the substrate plate. The coated plate must be dried to strengthen the bond. The same had to be performed in the absence of moisture therefore a hot plate placed inside the vacuum hood was chosen to dry the plate at the earliest and avoid minimal contact of the substrate with moisture or other impurities. Hot Plate setup is shown in fig. 4.10.

Figure 4.10-Hot plate setup

4.2.6 Formation of Self-Assemble Monolayer (SAM)

To get the uniformity and homogeneous layer of B_4C nanoparticles onto the AA7075-T6 substrate a Self-assembled monolayer of B_4C nanoparticles was prepared. Before starting the formation of the self-assembled monolayer, process on the matrix materials the first step of the AA7075-T6 plate surface had to be cleaned by following the sonication technique. Primary sonication was done with a 5% chemical detergent solution in distilled water. The sonicator was switched on for periods of 30mins and left to soak for a 15-minute interval, repeated twice. The secondary sonication was performed by only using distilled water with similar cycles of sonication and soaking repeated 3 times. The sonicated plates were immediately dipped into ethanol and leftover for 24 hours in an airtight container to prevent any further reaction or accumulation of moisture on its surface as shown in fig. 4.11(a). B_4C nanoparticles is uncreative to Di-ethyl ether (DEE) solvent; hence, it requires constant stirring to form a colloidal solution. According to the dimension of groove and holes, we have selected that 0.5 molar concentration of B_4C nanoparticle for the uniformity and homogeneity of B_4C nanoparticle on the Aluminium substrate.

Using a micropipette solution dropped onto the specimen and following the smearing technique, spread across the plate using a glass slide. The active -OH- bonds on a sample from ethanol were prepared to receipt the uniform layer of (B_4C-Diethyl ether) solution and form a temporary bond onto the substrate. The sample was then kept on a hot plate to dry inside a chemical hood with temperature ranging from 75- 200^{o}c for 10 to 15minuts as shown in fig. 4.11(c). Keeping least contact with moisture or any other agent the sample plates immediately placed in an airtight container for carrying out the further process. The B_4C nanoparticle blended with Di-ethyl ether (DEE) and filled in the groove dimensions of 160mm length, 2mm width and 1.5mm depth. Holes dimension was made an aggregate of 2 lines and 90 holes in two lines of each row 45 holes and the length of each line was 145 mm. The dimension of the holes was 2 mm Dia and 1.5 mm depth was machined utilizing CNC vertical milling machine on a center of the matrix metal shown in fig. 4.11(b). Schematic representation of SAM process shown in fig. 4.12(a, b).

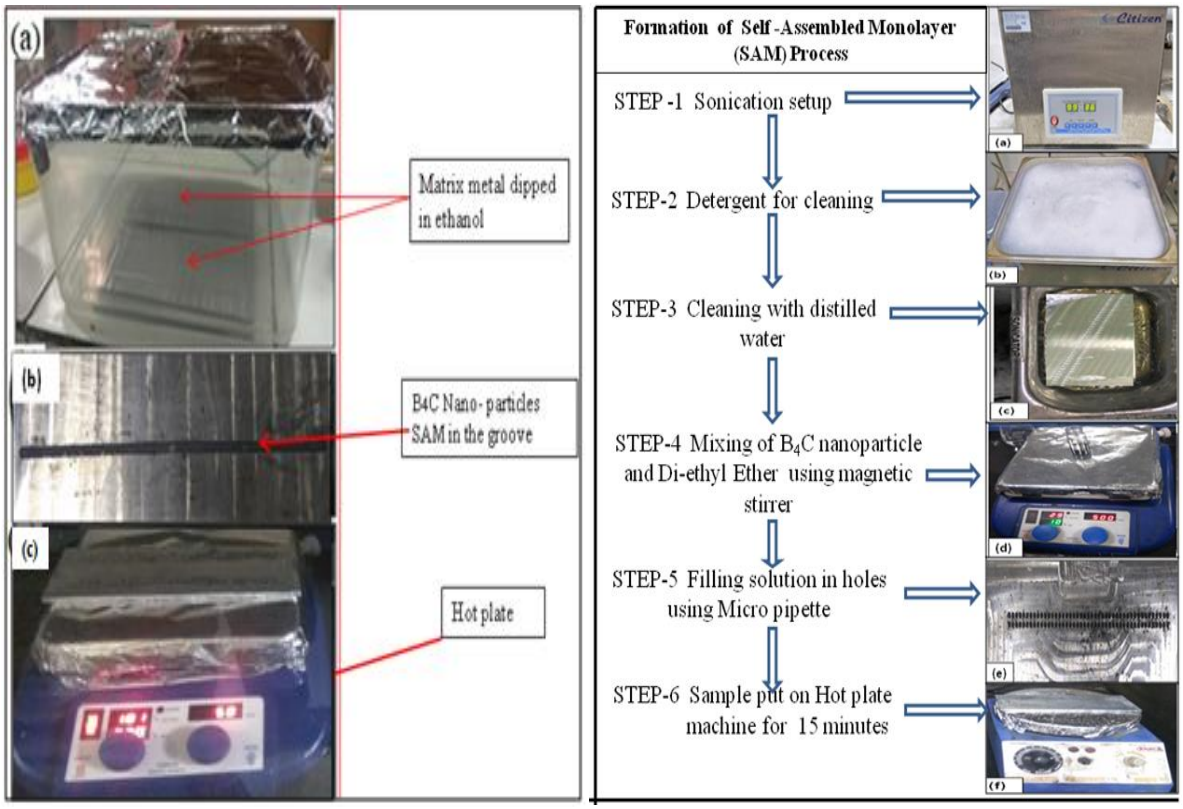

Figure 4.11-Formation of SAM process (a) Matrix metal dipped in ethanol for 24hr(b) filled B_4C nano ceramic particles in the groove (c) Samples kept on hot plate for the evaporation of the solvent and proper adsorption of nanoparticles to the base metal

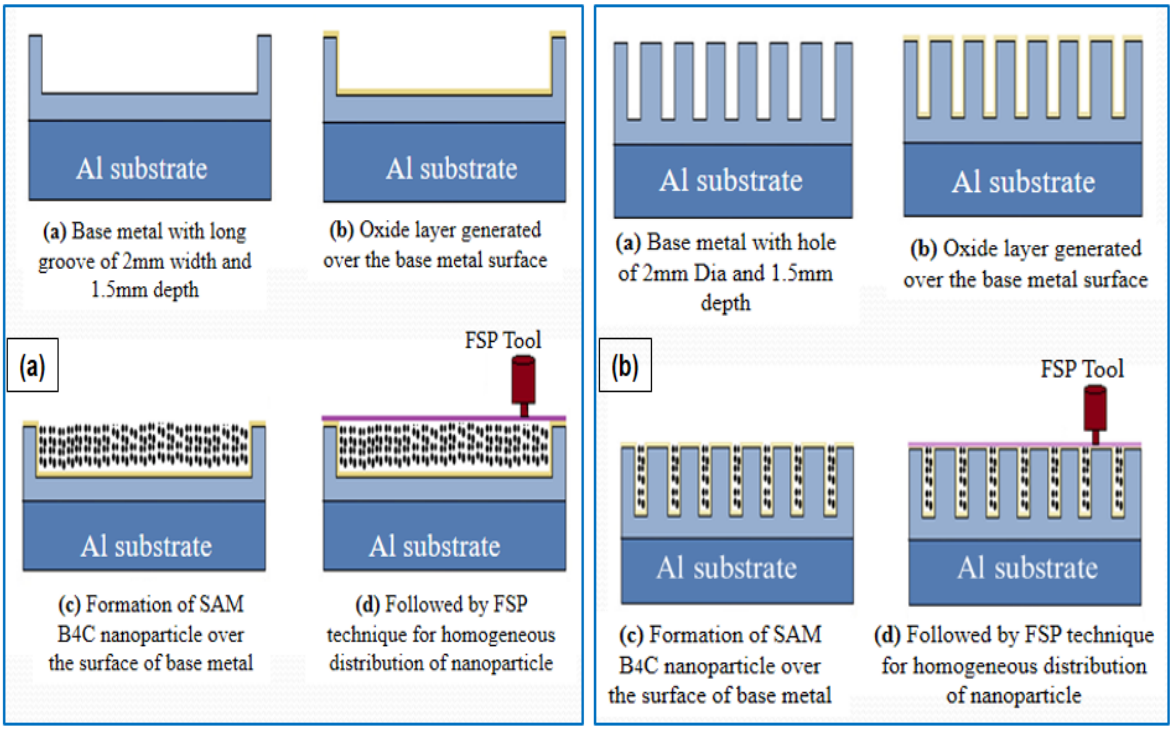

Figure 4.12-Step by Step schematic representation of SAM process (a) Groove method (b) Hole method

4.3 FRICTION STIR WELDING/PROCESSING MACHINEAND PARAMETERS

The Friction stir processing method of aluminum matrix surface composite fabrication was carried out on Friction Stir Welding machine of capacity 11kW, 40kN (Made by RV machine tools, Coimbatore, India), equipped with a hydraulic fixture. The FSW machine setup is shown in fig. 4.13, and the specifications of the machine are presented in table 4.3.

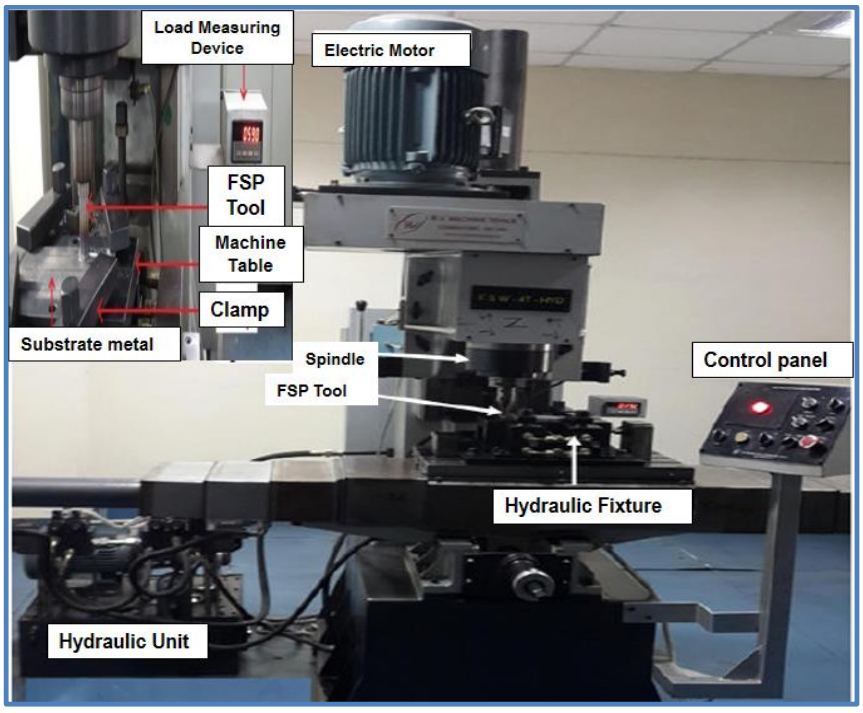

Figure 4.13-Friction Stir Welding/Processing machine setup

Table 4.3:-FSW/FSP machine specification

S.No	Parameters	Specifications
1	Power	11kW
2	Spindle Motor	11KW/ 1440rpm/ 440(AC Drive)
3	Z- Axis Stroke(auto)	300mm
4	Z-Axis cylinder	Diameter 100mmx300mm (Hydraulic operated)
5	Z-Axis thrust	4000kgf(Max)
6	X-Axis Feed	0 to 500mm/min
7	X-Axis cylinder	Diameter 80mmx600mm
8	X-Axis thrust	2500kgf(Max)
9	Y-Axis stroke	200mm
10	Table	600x400mm
11	Hydraulic Power Pack motor	2.2kw/440V
12	Tool holder	ISO 40 Arbor
13	Work holder	Hydraulic Fixture with clap

4.4 DESIGN OF EXPERIMENTS

Design of Experiments plays an important role in process development and process problem- solving to improve efficiency. It is a powerful problem-solving method that helps engineers for tackling process quality problems effectively and cost efficiently. DOE consists of a purposeful change of the inputs of a process to observe the corresponding change in the output. Thus, DOE is a scientific methodology that permits the investigators to study clearly a process and know how the factors affect the response.

4.4.1 Optimization of FSP Process Parameters Using Taguchi Approach

Taguchi's designs aimed to allow greater understanding of variation than did many of the traditional designs. Taguchi contended that conventional sampling is inadequate here as there is no way of obtaining a random sample of future conditions. Taguchi proposed extending each experiment with an "outer array" or orthogonal array should simulate the random environment in which the experiment would function. This is an experimental design methodology, which permits a higher level of logical uniformity of the extraction parameters employed in the process of extracting bioactive compounds. This design is of immense benefits due to the minimum number of experiments involved, and thus reducing the extraction time and the cost of the sample procurement [100]. Compared to other design, the Taguchi optimization method allows for independent investigation of each factors among others. It acknowledges that not all the parameters with a higher variability can be controlled in real life process. The Design of Experiments Taguchi L_9 Orthogonal array is shown in table 4.4.

Table 4.4: Design of Experiments Taguchi L_9 Orthogonal array

Nomenclature of Sample	Exp. no	Factor A	Factor B
S1	1	1	1
S2	2	1	2
S3	3	1	3
S4	4	2	1
S5	5	2	2
S6	6	2	3

S7	7	3	1
S8	8	3	2
S9	9	3	3

In this experiment Tool Pin Profile, Tool Rotation speed were selected as the variable parameters for the Friction stir processing. Three separate values were taken for all the above-mentioned variables. Applying Taguchi statistical approach for DOE, a L_9 table was formulated for the study using the software Minitab. This was done in order so that there are adequate interactions between the different variables and we can examine the effect of variables on the process and obtain an optimum process criterion.

4.4.2 Process parameters

From the literature survey and trials work it has been found that many factors affect the mechanical, microstructural and wear properties of the surface composite. The various process parameters are tool rotational speed, transverse speed, tool plunge depth, tool shoulder diameter, pin diameter, tool pin profile, tool tilt angle, axial force, the number of passes, etc. The major important process variables such as Tool transverse speed (S), Tool rotational speed (N), were selected for this research work. These parameters greatly influenced the heat generation. The selected process parameters and their levels and design matrix are shown in table 4.5 and 4.6 respectively.

Table 4.5: Process parameters and their levels

Symbol	**Input parameters(Factor)**	**Notation**	**Unit**	**Levels**		
				1	2	3
A	Tool Traverse Speed(TTS)	N	rpm	40	50	60
B	Tool Rotational Speed(RPM)	S	mm/min	1000	1200	1400

4.4.3 Experimental Procedure

4.4.3.1 Experimentation as per design matrix

The Self-Assembled Monolayers (SAM) processed substrate or matrix material was clamped on the hydraulic fixture of the Friction Stir Welding machine. The preparation of

the substrate material to form the B_4C nanoparticle layer using SAM technique is described in section 4.2. The experimental setup and schematic diagram of the FSP experiment is shown in fig. 4.12&4.13 (a) and (b) respectively.

Table 4.6: Design matrix (2 Factors and 3 Levels)

Nomenclature of Sample	Exp. no	Tool Traverse Speed	Tool Rotational Speed
S1	1	40	1000
S2	2	40	1200
S3	3	40	1400
S4	4	50	1000
S5	5	50	1200
S6	6	50	1400
S7	7	60	1000
S8	8	60	1200
S9	9	60	1400

The experimental tests were carried out using FSW/FSP setup. AA7075-T6 matrix materials were cut according to the standard dimension of the FSW/FSP setup. The experiment was conducted in two stages. In the first stage, the formation of the Self-Assemble Monolayer (SAM) on the surface of substrate (base) materials was performed. In the second stage, the capping pass was done with a pin-less tool to cover the self-assembled monolayer, which is bind with each groove or holes of the Aluminium alloy plate and the tool profile and rpm were adjusted as per process parameter.

Nine surface composites samples were fabricated using Al 7075-T6 as metal matrix reinforced with B_4C nanoparticles with the particle size of (<30nm) with adjust tool pin profile and varied process parameter in accordance with the design matrix using Taguchi L_9 orthogonal array through a Frictions stir processing.

In the substrate (base) metal two types of design has been made using CNC vertical milling machine on a center of the base plate. First, design over the surface of the base plate was groove dimension of 160mm length, 2mm width and 1.5mm depth and in second design over the surface base plate was made an aggregate of 2 lines and 90 holes in two lines of each row 45 holes, was machined utilizing CNC vertical milling machine on a center of the base plate. The length of each line was 145 mm. The dimension of the holes was 2 mm Dia and 1.5 mm deep. After the formation of the SAM in the designed base plate followed by Friction stir processing has been done using H13 tool steel heat-treated with 60-65 HRC hardness. H-13 Tool Steel is the most widely used work steel in hot work die and cold work applications.

Single-pass were perform using different tool pin profile of tool rotation and traverse speed of 1000-1400 rpm and 40-60mm/min respectively, tool tilt angle 2^{o} were constant during experimentation. After the fabrication of AA7075-T6 and B_4C surface composite, the sample was prepared from the FSP processed materials and then the sample was cut perpendicular to the processed direction using a wire EDM machine. The samples were prepared according to the dimension of microstructure, SEM.

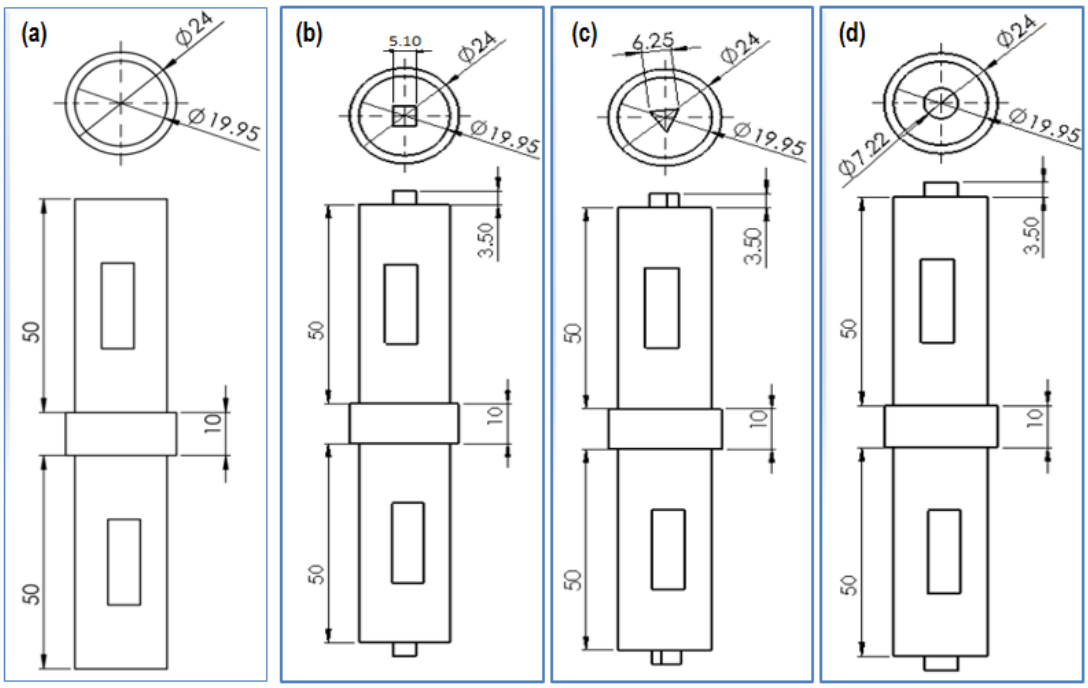

Figure 4.14-Dimension of different FSP tool profiles (a) Pinless (b) Square (c) Triangular (d) Cylindrical

The purpose of pinless tool profile is to stop the scattering of the reinforcement particles during FSP, the B_4C nano-particles filled groove and holes pattern was covered. It is intended

to be used in the initial phase of processing for covering the reinforced materials in the groove or holes formed on the base plate. Fig. 4.14 (a-d) shows the dimension of different FSP tool profiles.

The FSP experimental setup and schematic representation process is depicted schematically with tool tilt angle 2^{o} in fig. 4.15 (a, b). In the middle of the samples, the grooves and holes are contrived with a required depth and formation of a uniform thin layer of B_4C nanoparticles using SAM technique. Initially a pinless tool having shoulder only is employed to cover the top of the groove to prevent the B_4C particles from scattering during FSP. The tool with the pin was plunged at one end of the plate and traversed across the plate as shown in table 4.7 process parameter of FSP. The frictional heat plasticizes the material by the intense stirring action of the tool pin which mixed the B_4C particles of the plasticized material. The rotating tool moves with a considerable amount of forging force to form processed zone for a required length of surface composite layer. The frictional heat and forging force of the rotating tool deform and process the material at elevated temperature. As there is a flow of the material at elevated temperature, the process creates a chance to redistributing the particles in the composites.

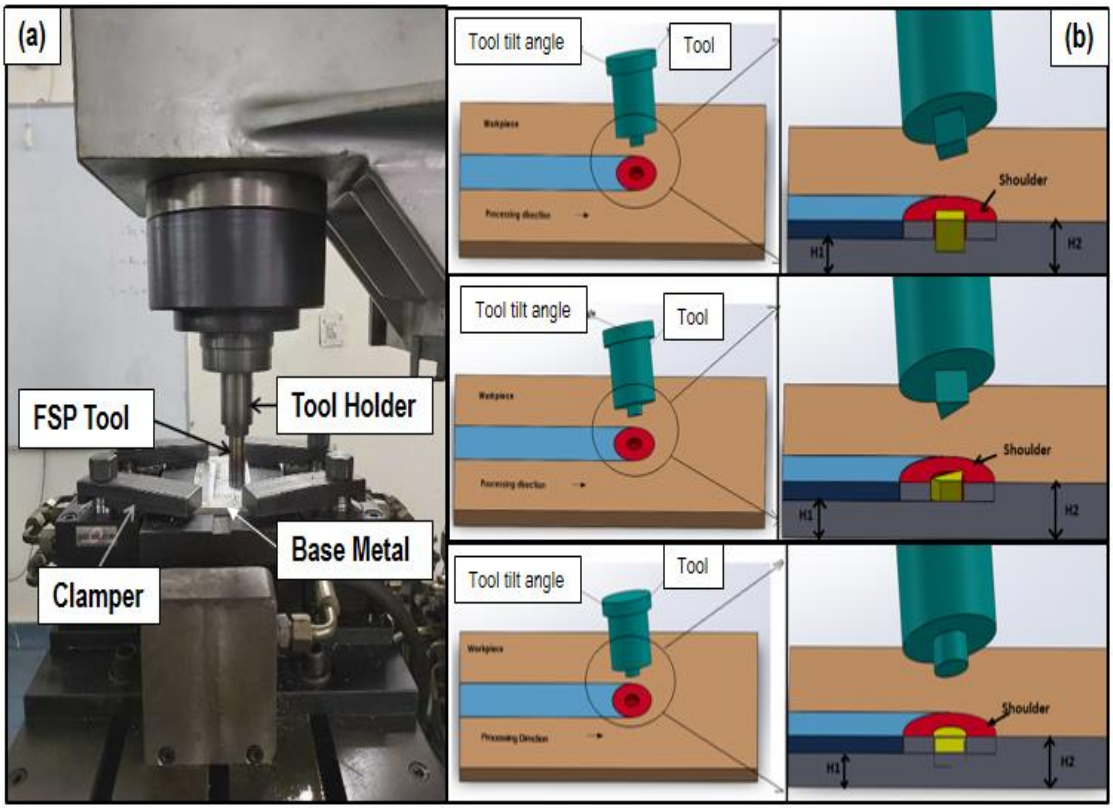

Figure 4.15-(a) FSP experimental setup (b) Schematic representation of FSP experiment with different tool pin profiles

Table 4.7: Process parameters of FSP

Process Parameters	**Value Taken**
Tool shoulder	Flat
Tool shoulder Dia	19.95mm
Tool pin profile	Square, Triangular, Circular
Tool pin length	3.5mm
Tilt angle(degree)	2^{o} constant
Tool rotational speed (rpm)	1000, 1200, 1400

In fig. 4.16 shows the FSP procedure and filling methods. In advancing side (AS) the velocity vector of tool rotation and tool traverse direction are similar and in retreating sides (RS) the velocity vector of tool rotation is opposite to tool traverse direction. In fig.4.18 shows the grooves and formation of Self-assembled monolayer (SAM) in the grooves followed by FSP procedure with different tool pins. Apart from the groove filling method, another filling method is making holes and formation of Self-assembled monolayer (SAM) in the holes followed by FSP procedure with different tool pins profiles as shown in fig. 4.17.

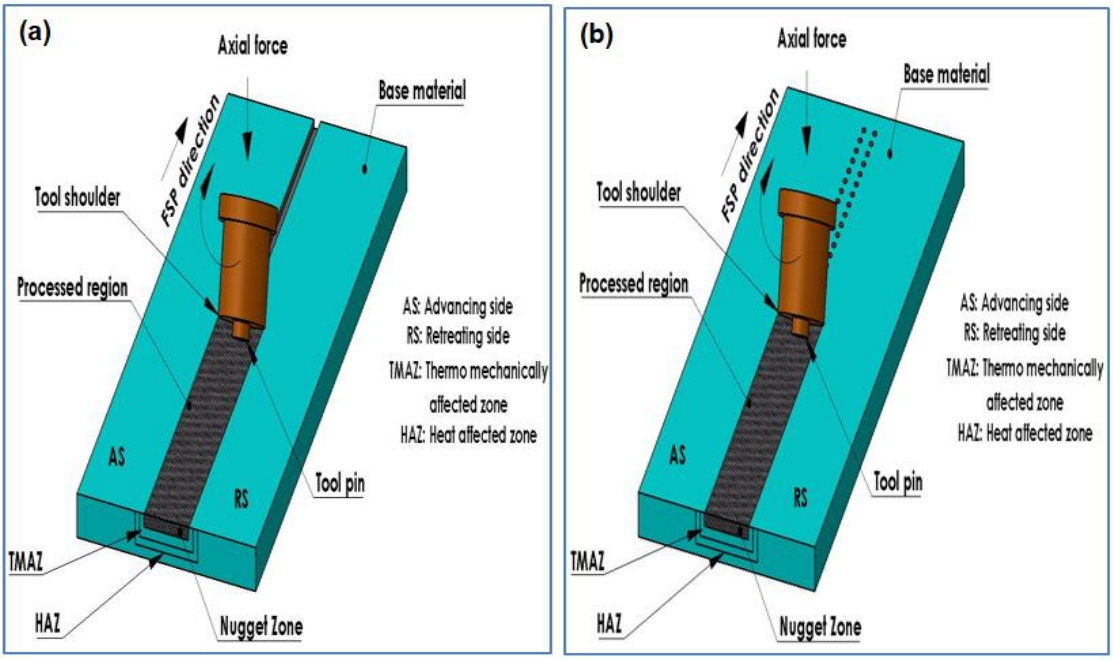

Figure 4.16-FSP procedure (a) Filling in the groove (b) Filling in the holes

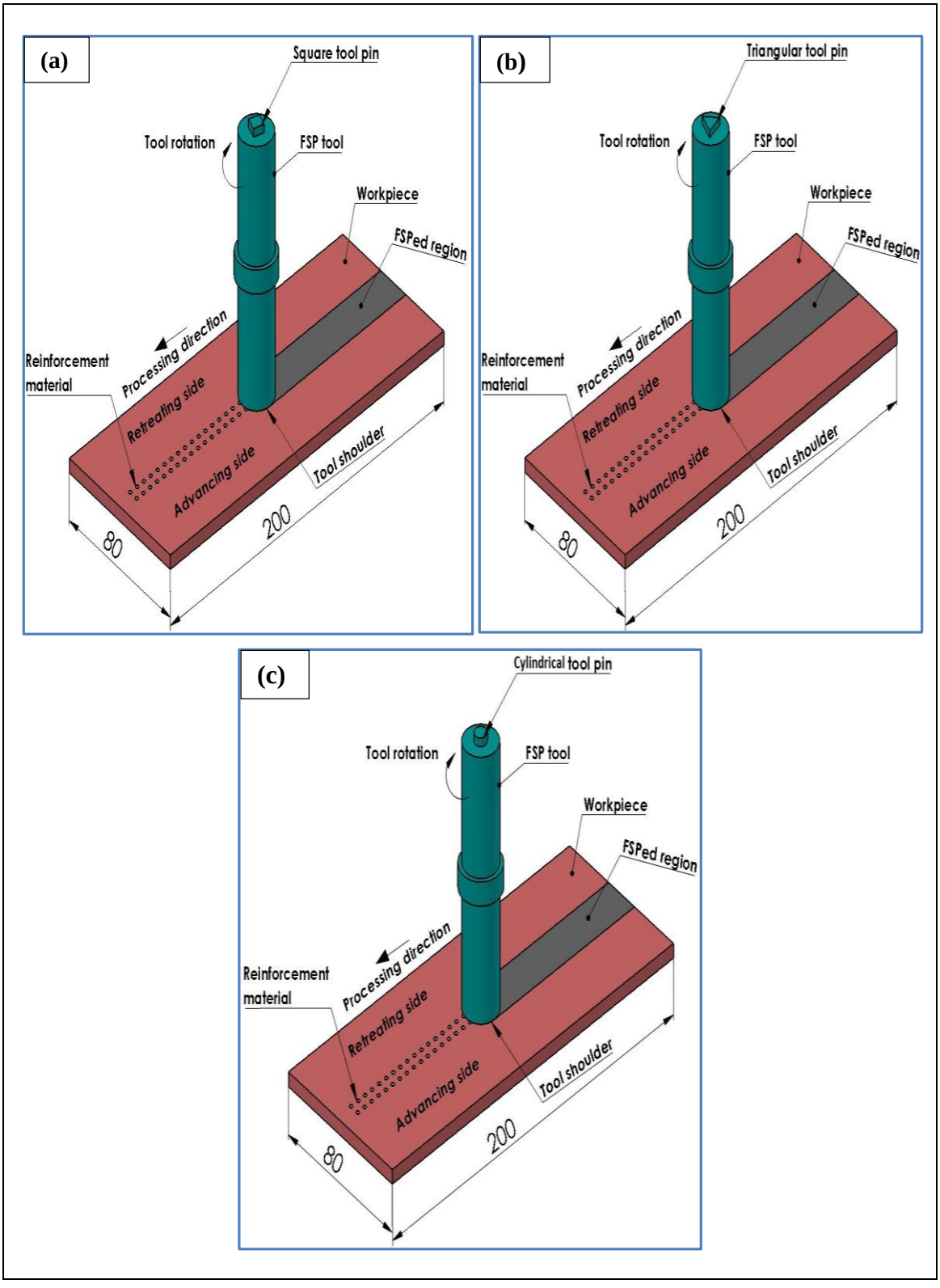

Figure 4.17-Making holes and formation of SAM in the holes followed by FSP procedure with different tool pins (a) Square tool pin profile(b) Triangular tool pin profile (c) Cylinderical tool pin profile

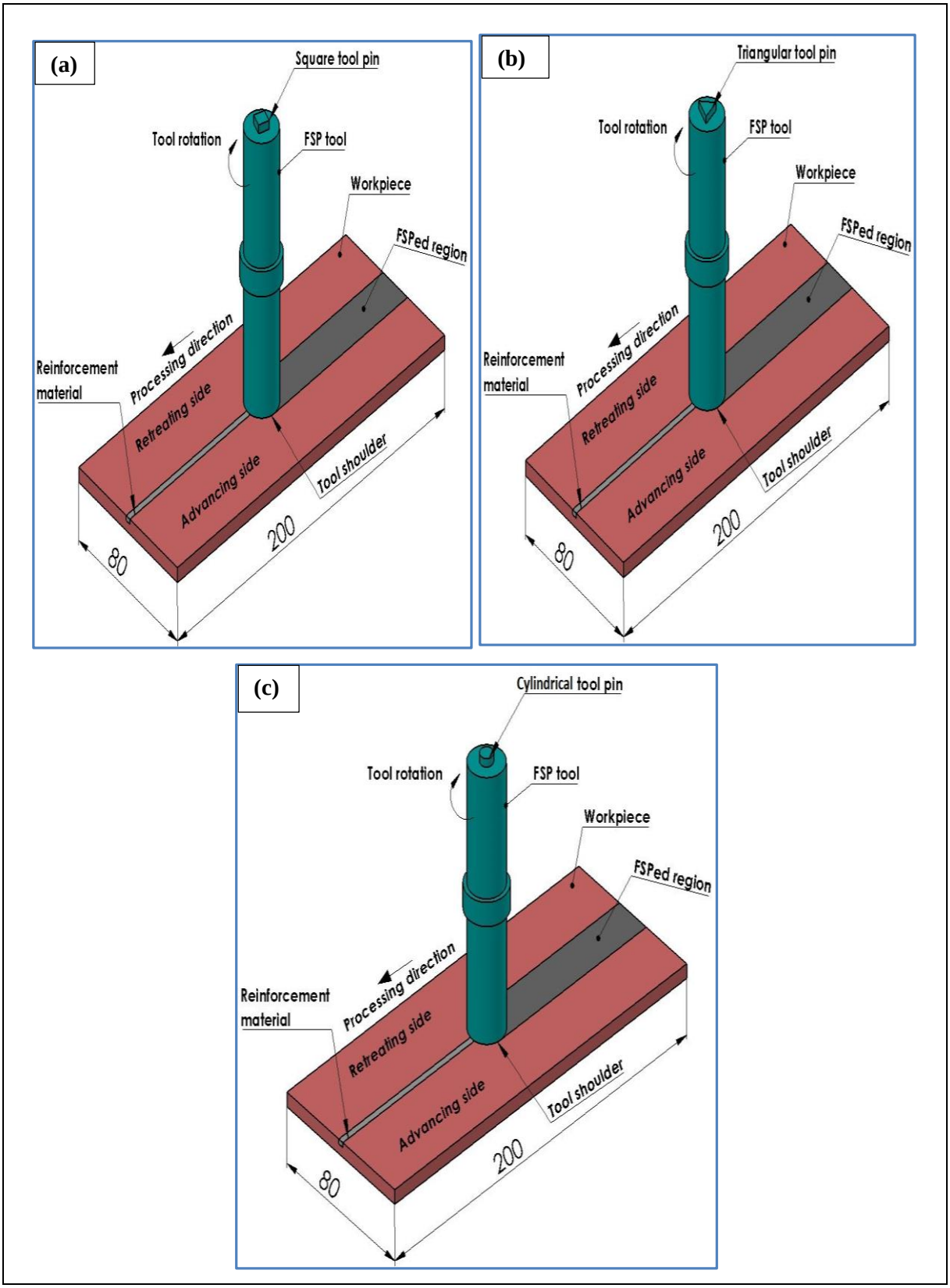

Figure 4.18-Making Grooves and formation of SAM in the grooves followed by FSP procedure with different tool pins (a) Square tool pin profile(b) Triangular tool pin profile (c) Cylinderical tool pin profile

4.5 METALLURGICAL CHARACTERIZATION OF THE SURFACE COMPOSITE

4.5.1 Microstructural characterization

The samples with the rectangular square cross section were prepared particularly for their microstructure and microhardness analysis. Such samples were cut normal to the processed line at the center of the processed or unprocessed plate. Viewing the microstructure was important because one of the most significant effects of Friction stir processing is the resultant grain structure refinement. These are translated into superior mechanical properties imparted to the composite material. However, to be able to view the microstructure, three more steps had to be performed to prepare the samples for viewing. The samples were ground and mounted with Bakelite powder in a mounting press. Then the samples were polished using different grades of emery paper (320, 400, 600, 800, 1000, 1200, 1500, 2000 grits size) followed by velvet cloth polishing using alumina suspension. Polishing machine and Olympus GX41 microscope are shown in fig. 4.19(a,b).

Figure 4.19-(a) Polishing machine (b) Olympus GX41 microscope

Microstructural characterization was carried out to determine surface morphology, uniform diffusion of reinforcement particles into the surface matrix, elemental composition of the reinforcements and matrix. Scanning Electron Microscope (Model: Hitachi S-3700N) and Field Emission Scanning Electron Microscope (FESEM) (Model: ZeissSigma300) were used for microstructural characterization of the samples (fig. 4.20 a,b). Fractured surfaces

of the tensile samples and worn surfaces of the wear-tested samples were also examined by SEM with Energy Dispersive Spectrometer (EDS) to understand the wear behaviour and mechanisms.

4.5.2 Scanning Electron Microscope (SEM)

The SEM instrument is composed of two main components, the electronic console and the electron column. The electronic console has control knobs and switches that allow for instrument adjustments such as filament current, accelerating voltage, focus, magnification, brightness and contrast. The electron microscope uses a computer system along with the electronic console, making it unnecessary to have a bulky console that houses control knobs, CRTs, and an image capture device. All the primary controls can be accessed through the computer system. The user only needs to be familiar with the GUI or software that controls the instrument rather than control knobs and switches typically found on older style scanning electron microscopes. The image that is produced by the SEM/FESEM is usually viewed on CRTs located on the electronic console, but with FEI the image can be seen on the computer monitor. Images that are captured can be saved in digital format or printed directly. The Scanning Electron Microscope (Model: Hitachi S-3700N) and Field Emission Scanning Electron Microscope (FESEM) (Model: ZeissSigma300) are shown in fig. 4.20(a,b).

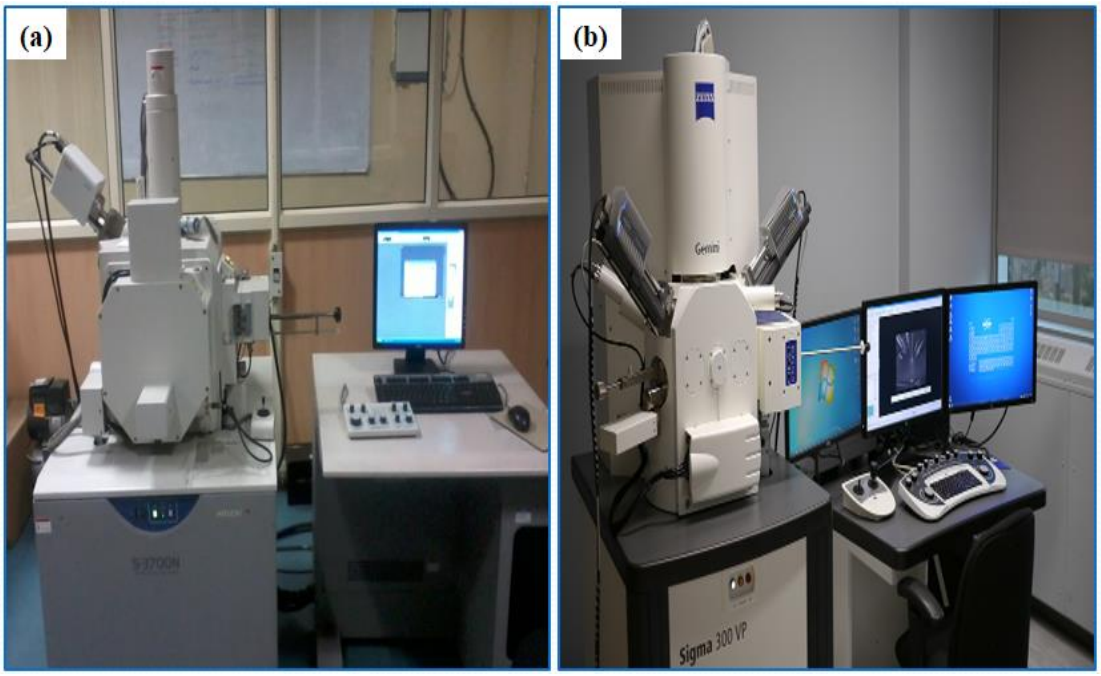

Figure 4.20-(a) Setup of Scanning Electron Microscope (Model: Hitachi S-3700N) (b) Field Emission Scanning Electron Microscope (FESEM) (Model: ZeissSigma300)

4.5.3 X-Ray Diffraction (XRD)

X-ray scattering techniques are a group of non-destructive analytical techniques that provide information about the crystallographic structure, chemical composition, and physical properties of materials. These techniques depend on the observation of the scattered intensity of an X-ray beam hitting on a sample as a function of incident and scattered angle, polarization, and wavelength or energy. XRD analysis is based on constructive interference of monochromatic x-rays and a crystalline sample. The x-rays are generated by a CRT, filtered to produce monochromatic radiation, collimated to concentrate, and directed toward the sample. The interaction of the incident rays with the sample produces constructive interference and a diffracted ray when the Bragg's law (n =2dsin) is satisfied. This law gives us the relation between the wavelength of electromagnetic radiation to the diffraction angle and the lattice spacing in a crystalline sample. X- Ray diffraction (XRD) analysis was used in the current study to determine the presence of a crystalline phase in the material. X-Ray diffraction (BRUKAR D8 ADVANCE) was used to identify the phase of B_4C nanoparticles in the surface composite shown in fig. 4.21. XRD diffractometer with Cu-Kα X-ray radiation (λ= 1.54056 Å) at room temperature. X-ray diffraction pattern for each of the samples was taken for 2θ values ranging from 10-80º. The peak position was identified from the graph and corresponding 2θ values were noted. From the Bragg's angle (2θ) values and interplanar spacing (d) were matched with the standard values of X-ray diffraction files and the phases were identified.

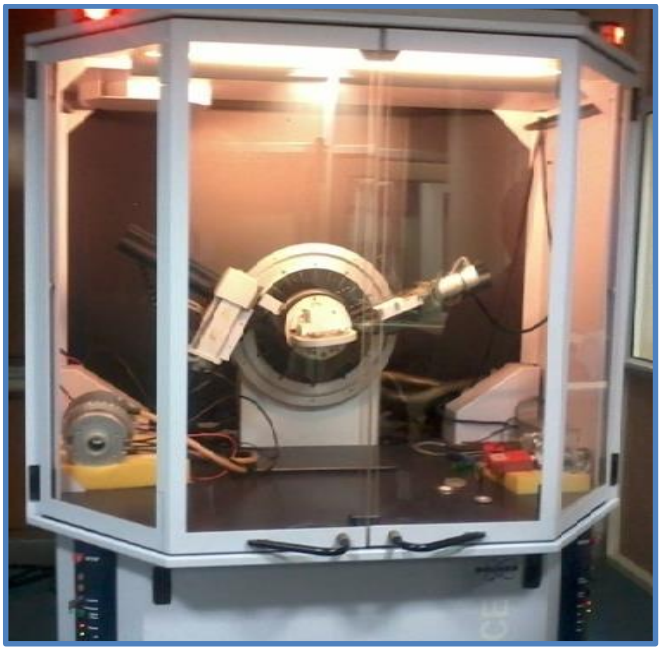

Figure 4.21-Set up of X-Ray Diffraction (Model: BRUKAR D8 ADVANCE)

4.6 MECHANICAL PROPERTIES OF THE SURFACE COMPOSITE

The characterization of the surface composites fabricated by Friction stir processing, it is accepted that grain refinement can help improve the mechanical strength and ductility of the material. Friction stir processing (FSP) as a relatively new severe plastic deformation technique can refinement of grain size and modify the matrix metal as well. As the size of the reinforcement particles are in the nano range, it is expected that strengthening mechanisms will influence the characteristics of the surface composite, and hence the overall improvement of mechanical properties like hardness, strength in the surface composites because of grain refinement is mainly governed by strengthening mechanisms. Fig. 4.22 (a,b) shows the groove and holes made on the substrate (base) metal for filling of the B_4C nanoparticles reinforcement through Self-assembled monolayer technique. Fig. 4.23 (a,b) Friction stir processed surface composite and macrograph of tensile and wear test samples extracted from the processed region. The typical tensile test samples are extracted from surface composite region are shown in fig. 4.24.

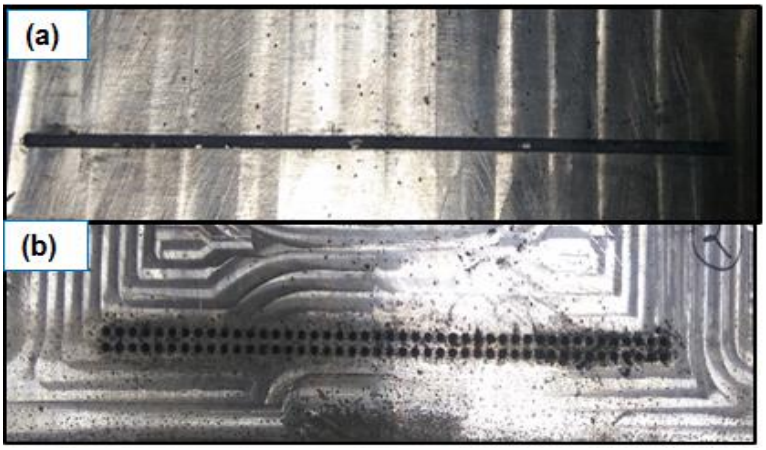

Figure 4.22(a, b)-The groove and holes for filling of the nanoparticles reinforcement

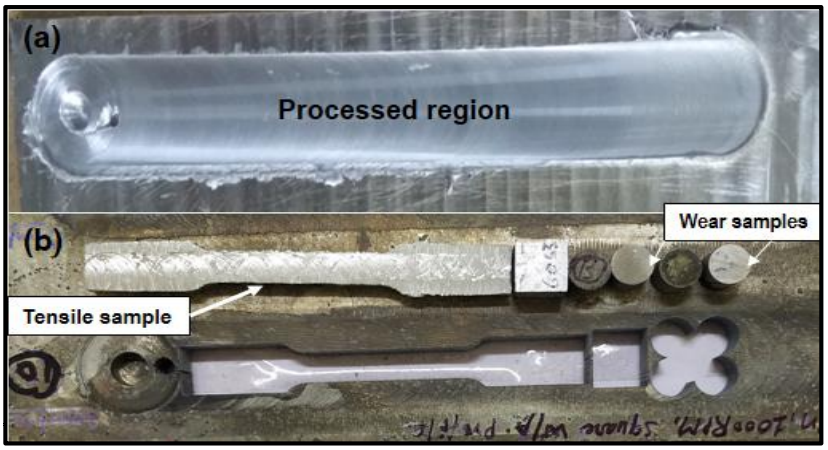

Figure 4.23 (a, b)-Friction stir processed surface and macrograph of tensile and wear test samples take out from the processed region

Figure 4.24- Tensile test samples cut from the composite region

4.6.1 Microhardness

The Fischer scope HM2000S Microhardness tester, which measures the Vickers hardness (HV) was used. Vickers hardness test is an optical method in which the size of the indentation (the diagonals) is measured. The larger the size of the indentation left by intender on the surface of a workpiece or specimen, at a predefined test force, the lower is the Vickers hardness value of the specimen. For experimental accuracy, an average of four readings was taken for each sample. Micro-hardness test was initiated at 0.300 N or 0.03kg and the dwell time was 20 seconds. The average hardness was calculated using four readings on the same load. In fig. 4.25, shows that a significant hardness variation is observed from the base metal values.

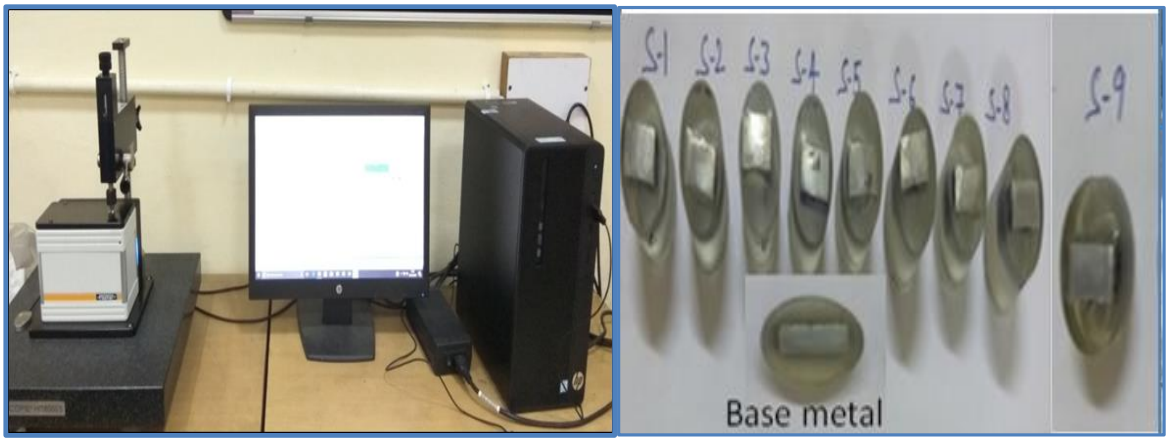

Figure 4.25-Microhardness measurements setup

4.6.2 Tensile Test

The tensile test of the base alloy and processed samples was analysed using a computer-controlled universal testing machine (Tinius Olsen H50KS) in fig. 4.26 at a constant crosshead speed of 1mm/min at room temperature. The longitudinal tensile specimens were cut from the processed region by wire-cut EDM as per ASTM: E8/E8M-011 standard. Fig. 4.27 shows the size of the tensile test samples. Mechanical properties such as Ultimate Tensile Strength (UTS) and elongation were recorded and the average of three sample testing data was reported.

The tensile testing is done by applying a longitudinal or axial load at a specific extension rate to a tensile specimen having known dimensions (gauge length and cross sectional area perpendicular to the load direction) until failure. The applied tensile load and extension are recorded during the test for the calculation of stress and strain. A range of universal standards provided by Professional societies such as American Society of Testing and Materials (ASTM) provides testing standards, which are selected based on the requirement. Each standard has a variety of test standards appropriate for different materials, dimensions and fabrication history.

Figure 4.26 -Tensile machine (Model: Tinius Olsen)

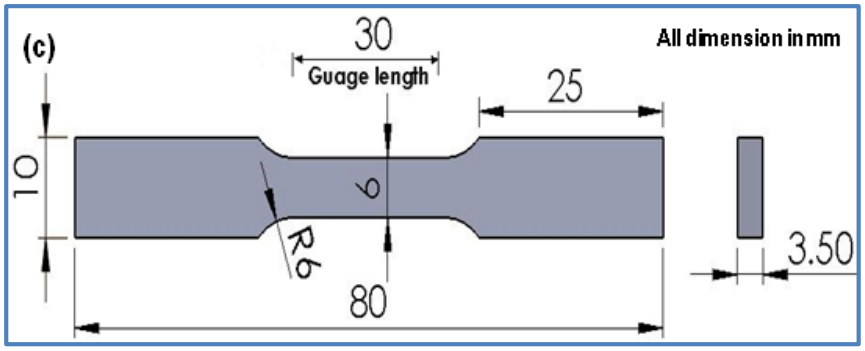

Figure 4.27-Dimension of the Sample as per ASTM standard

4.7 MEASUREMENT OF RESIDUAL STRESS

In this research study, the portable X- ray residual analyzer (PULSTEC μ-X360n, fig. 4.28) (based on cos α method), a non-destructive X-ray analyzer of PULSTEC Industrial Corporation Limited, was used for measuring the residual stress in FSPed surfaces composites and substrate metal with following specifications: tube voltage (30 kV), current (1 mA), source (Cr Ka/Ni Kb filter), and X-ray beam (wavelength = 2.29 Å, energy = 5.4 keV), Diffraction angle (2Theta) =139.528 deg, Crystal structure F.C.C, Young's modulus (E) =69.310 GPa, Poisson's ratio (v) =0.348. This analyzer could measure the stress efficiently by detecting the full Debye ring data from a single incident X-ray angle and non-goniometer stage influence on the measurement result. The X-ray signals and the distortion of Debye ring are automatically collected and saved in the computer. The diameter of the X-ray exposure was 1mm, the X-ray exposure time was 30s and the X-ray incidence angle =35.0 [deg]. The specifications Stress Analyzer set up Table 4.8**.** In fig. 4.29 shows the procedure for calculating the residual stress value and fig. 4.30 mage captured by PulsetecμX-360n stress analyzer.

Figure 4.28-Portable XRD PulsetecμX-360n stress analyzer

Table 4.8: Stress Analyzer specifications

Item	New model (μ X360n)
Collimator Size	Standard: 1mm
Maximum measurement distance (For ferrite Samples)	51 mm
X-Ray tube voltage & current	30KV/ 15mA max.
X-ray tube	Cr/Co/Cu/V/Mn
Measurement Method	Single incident angle method[cosα method]
Target Material	Ferrite, Aluminum, Nickel, Titanium, Ceramics etc.
Weight	Sensor unit : 2.4 Kg, Power Supply Unit : 6.2 kg
Sensor Unit/ Power Supply Unit Size	Sensor unit: W114 × H107× D213 (mm)Power Supply Unit : W159 × H235 × D289 (mm)
Measurement time	60 sec

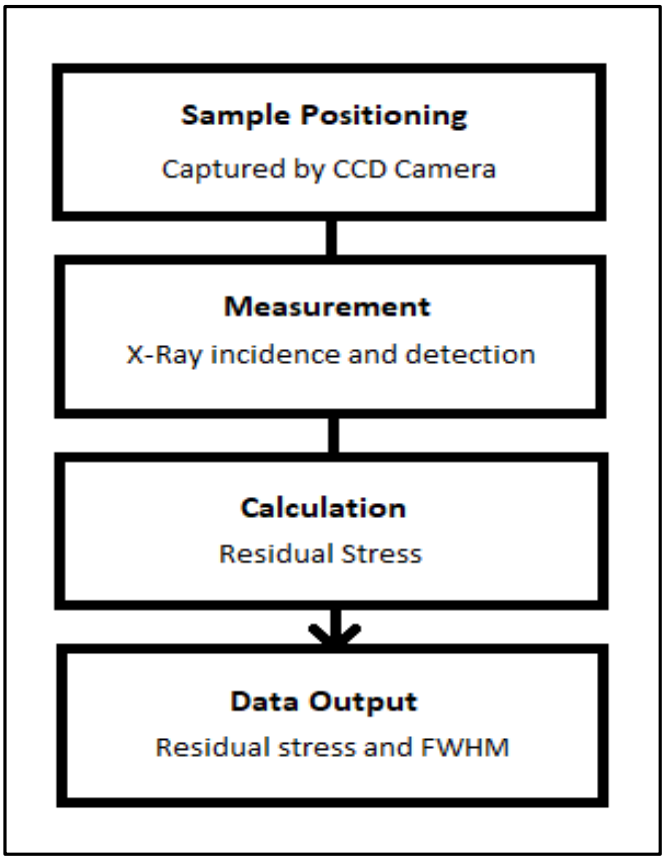

Figure 4.29-Procedure for calculating the Residual stress value

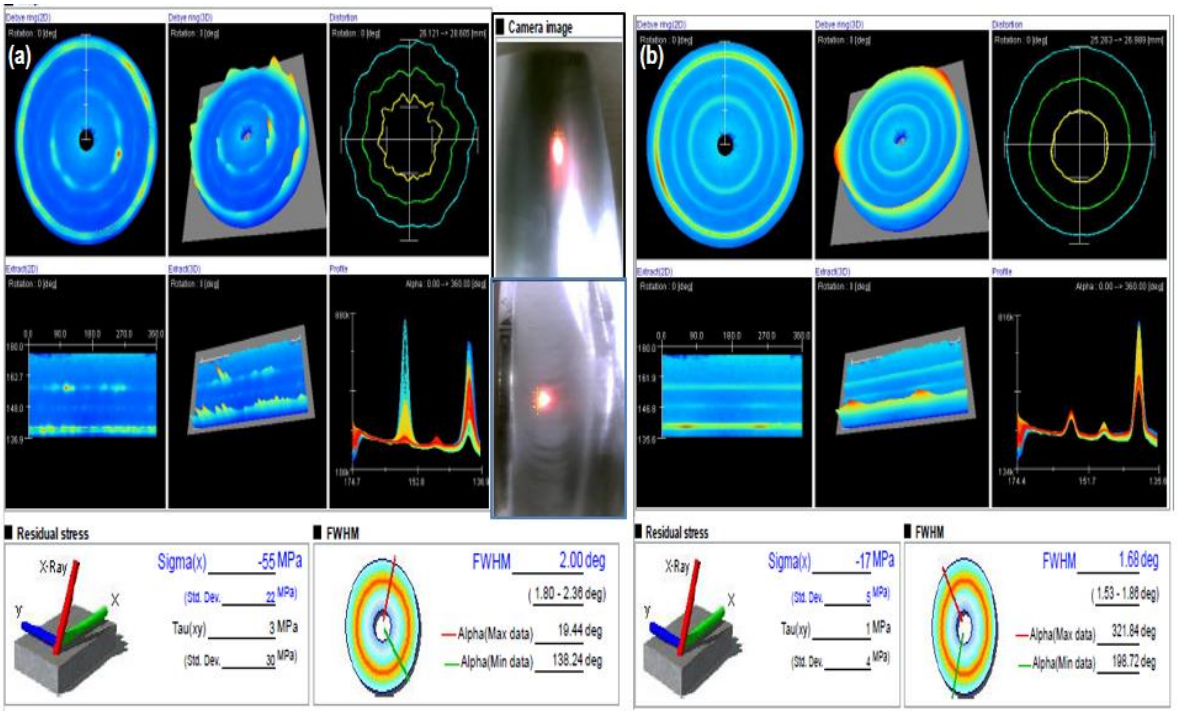

Figure 4.30-Image captured by PulsetecμX-360n stress analyzer (a) Base metal (b) FSPed sample

4.8 WEAR BEHAVIOUR OF THE SURFACE COMPOSITE

The wear behavior of the substrate or base alloy and surface composites were studied through a pin on disc tribometer (Make: DUCOM, Bangalore, India) and the tests were conducted as per ASTM G99-04 Standard. The Pin on Disk test condition of the wear test are given in table 4.9. The pin-on-disc machine setup and schematic of a pin-on-disc setup are shown in fig. 4.31, and fig. 4.32, respectively. The pin specimens of 6-10mm diameter for the wear test were cut from the processed surface, and the counter disc was made of EN-24 steel hardened to 55-60 HRC. The surface roughness (Ra) of the counter disc was measured by surface roughness tester (Make: TAYLOR HOBSON). The surface of the disc were ground on the 1500 grit emery sheet prior to the sliding wear test to maintain an initial surface roughness (Ra) of 0.2μm. A constant track diameter 100mm was used in all the tests. Prior to the wear test, the test specimens and disc were cleaned with acetone. After the wear test, the worn out surfaces were cleaned using acetone and dried before the weight loss was measured. The wear test specimens were weighed to an accuracy of 0.01mg by an electronic weighing balance (Make: SHIMADZU) before and after the test.

Table 4.9: Pin on Disc test condition

S. No.	Test condition	Values Taken
1.	RPM	319, 382, 478, 637
2.	Load (N)	20, 30, 40, 50
3.	Track diameter(mm)	30-60
4.	Pin diameter, Height(mm)	6
5.	Disc diameter(mm)	100
6.	Disc surface roughness(Ra)	0.2µm
7.	Sliding distance(m)	1000
8.	Temperature	30^{o}

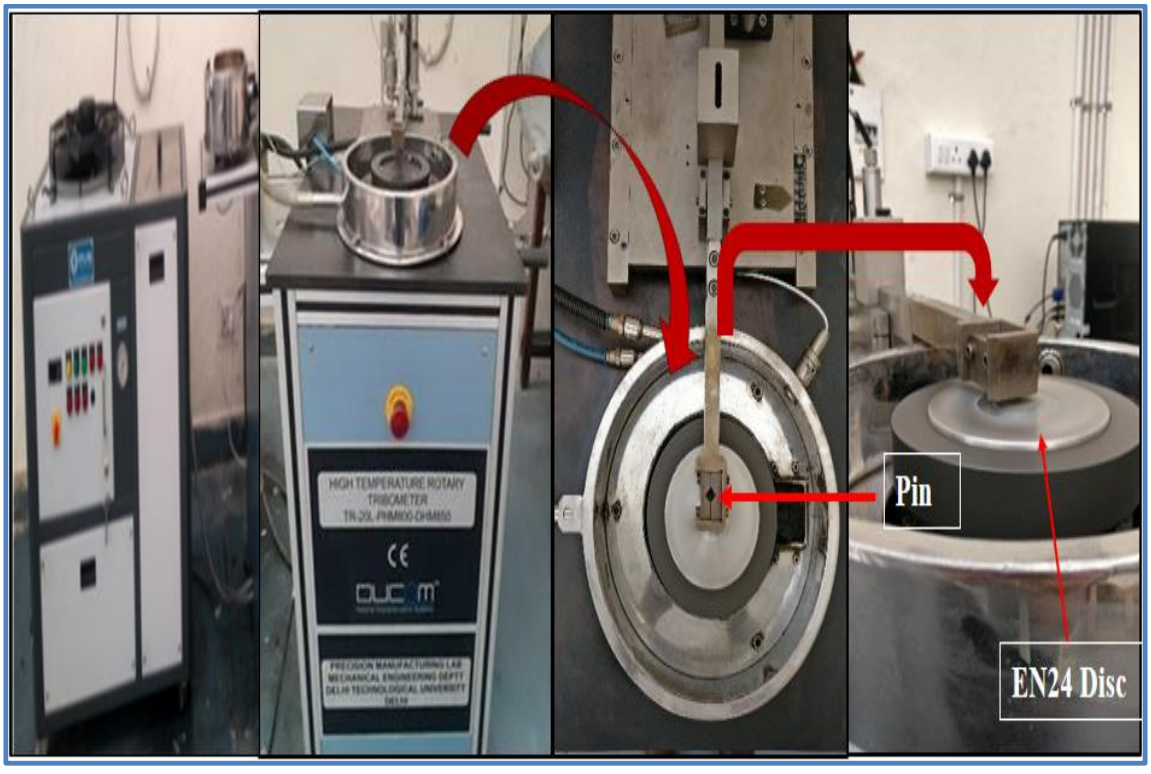

Figure 4.31- Different views of a Pin-on-Disc Tribometer

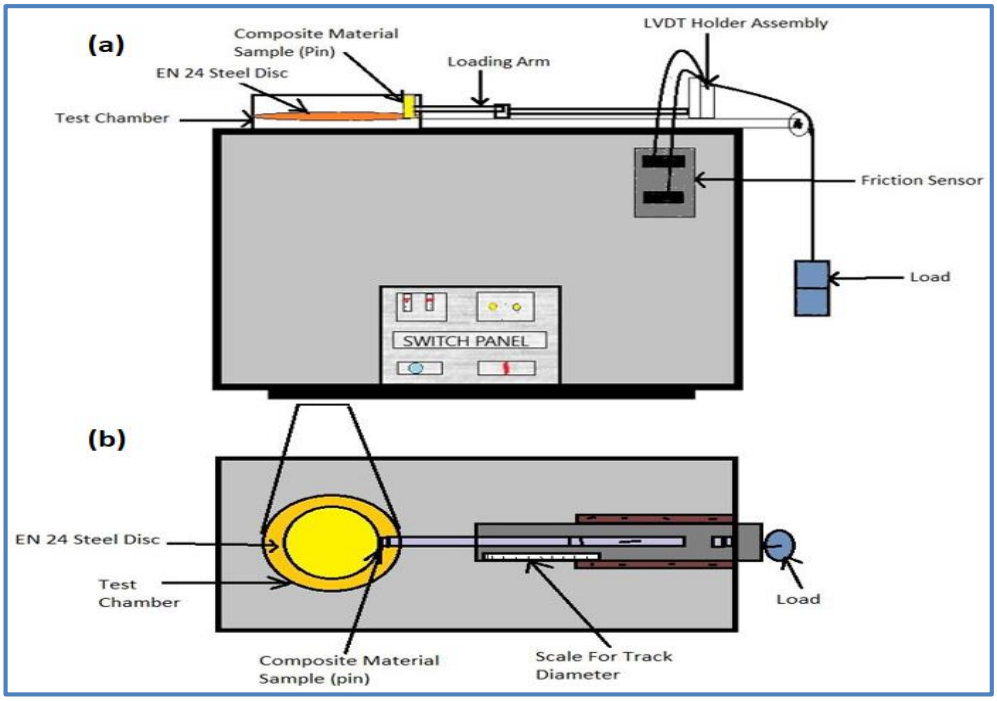

Figure 4.32-Schematic of High Temperature Pin on disc setup (a) A front view (b) A top view

4.9 SUMMARY

The surface characterization of the AA7075 substrate and B_4C nanoparticle reinforcement have been presented in this chapter. The various steps are involved preparation of substrate materials for the fabrication of surface composite have been described. The various aspects involving for preparation of substrate materials using Self-assembled monolayer (SAM) followed by fabrication surface composite through FSP method has been explained with experimental set up and schematic representation.

The metallurgical characterization procedure for fabricated surface composites are microstructure, EDX, SEM, FE-SEM, and XRD are briefly discussed. All the samples were prepared as per ASTM standards, and the test procedures are chosen as per the standards. The procedure for samples preparation and evaluating procedure of microhardness and tensile strength are explained. Tribological characterizations set up and test condition of the fabricated surface composite and base metal were also explained in this chapter. Residual stresses are induced during the friction stir processing due to severe plastic deformation of metal. The procedure of the residual measurement of the surface composite and base metal samples were also discussed in this chapter.

CHAPTER-5

RESULTS AND DISCUSSIONS

5.1 FSP PROCESS PARAMETERS OPTIMIZATION USING TAGUCHI APPROACH

5.1.1 Introduction

Self-assembled monolayer (SAM) formation over the groove and holes surface of AA7075-T6 and followed by Friction stir processing to fabricate the surface composite. The fabricated surface composites should be defects free such as cracks, tunnel defect, and so on. The selected processing parameters are significantly improved the mechanical and wear properties of obtained surface composites. The fabricated surface composite should have good mechanical and wear properties. Thus the effect of FSP processing parameters on the fabricated surface composites and contribution of each parameter on the output responses like microhardness and Ultimate strength can be investigated using ANOVA. The effects of B_4C nano reinforcement particles through Self-assembled monolayer formation followed by Friction stir processing surface composite are investigated. To study the wear behaviour of the base (substrate) metal and surface composite, wear tests performed using different normal load on a pin on disk tribometer setup (DUCOM) as per ASTM G99-04 standard. The worn out surface composite samples were subjected to scanning electron microscopy (SEM) and elemental energy dispersive X-ray spectroscopy (EDS) analyses.

In this research work, the surface has modified using B_4C nanoparticles, which is linked through the Self Assembled Monolayer (SAM) on the surface of Al-alloy. SAM is widely being used as a linking process on various surfaces [154]. Different methods have been reported for applying of reinforcement particles which initiate by preparation of grooves on the matrix metal and filled by reinforcement particles [155]**,** Matrix Hole Drilling followed up by particle reinforcement [156-159]**,** particle reinforcement with a volatile liquid mixture (methanol or acetone) applied over the matrix metal [25,160]**.** The selection of the nano particles reinforcement depends on the application of the component and compatibility of nano reinforcement and matrix metal. Authoritatively B_4C offers excellent thermal and chemical stability, neutron absorber, low density and high hardness [27,161]**.** Hence, researchers have not reported the surface modification of AA7075-T6 as a substrate through the FSP technique using B_4C nanoparticles reinforcement mixed with Di-ethyl ether (DEE).

Friction stir processing (FSP) is a new emerging, green and energy-efficient thermo-mechanical process for improvement in the material property by localized plastic deformation, which creates a microstructure with ultra-fine, equiaxed grains. It is also used to incorporate nanoparticles of Boron carbide (B_4C) into the substrate of Al7075 alloy in order to produce surface composite. A thin layer of B_4C over the surface of Al7075 alloy based matrix material through Self-Assembled Monolayer (SAM) technique followed by Friction stir processing. The major advantage of SAM is to minimize the quantity of B_4C nanoparticles used in the preparation of surface composites. The fabricated surface composites were analyzed using FESEM, SEM, XRD and residual stress studies. After the fabrication of surface composite, wear samples of cylindrical pin shape with 10mm diameter cut by wire EDM from the processed zone. Sliding speed was taken 1m/s and normal loads varying from 20, 30, 40 and 50N were preferred for conducting the wear tests with a sliding distance of 1000m. A constant track diameter 30-60 mm was utilized in all the wear tests. Worn out sample of surface composite were analyzed using scanning electron microscopy.

5.1.2 Optimization of process parameters

The experiments are conducted as per design using L_9 orthogonal array for finding out the optimum process parameters. The output responses are microhardness and Ultimate strength for input process parameters of tool traverse speed and tool rotational speed. A total of nine runs of the experiment need to be conducted using the combination of levels for finding the suitable process parameters for the fabrication of the surface composites. Three-level (40, 50, 60mm/min and 1000, 1200, 1400rpm) and Two factor (Tool traverse speed and tool rotation speed respectively) are selected for this research work using Taguchi L_9 design experiment technique. The experimental design was carried out with the help of MINITAB 17 software. Table 5.1 shows the Taguchi L_9 design matrix and experimental results of the surface composites. The values of ultimate tensile strength and microhardness of the surface composite samples with respect to varying tool traverse and tool rotational speed along with S/N ratios calculation for “larger the better” type of quality characteristic are given in table 5.2 & 5.3, 5.4 & 5.5 respectively.

Table 5.1: Design matrix and experimental results of surface composites

Nomenclature of Sample	(Factor A) Tool Traverse Speed (TTS)	(Factor B) Tool Rotational Speed (RPM)	(Response 1) Microhardness (HV)	(Response 2) Ultimate Tensile Strength
S1	40	1000	179	364
S2	40	1200	190	336
S3	40	1400	187	329
S4	50	1000	170	350
S5	50	1200	185	337
S6	50	1400	182	173
S7	60	1000	169	241
S8	60	1200	173	156
S9	60	1400	171	149

Table 5.2: Observations table for the ultimate tensile strength (MPa) and S/N ratios

Nomenclature of Sample	Tool Traverse Speed	Tool Rotational Speed	Ultimate Tensile Strength	S/N ratio
S1	40	1000	364	51.2220
S2	40	1200	336	50.5268
S3	40	1400	329	50.3439
S4	50	1000	350	50.8814
S5	50	1200	337	50.5526
S6	50	1400	173	44.7609
S7	60	1000	241	47.6403
S8	60	1200	156	43.8625
S9	60	1400	149	43.4637

Table 5.3: Response table for the S/N ratios of ultimate tensile strength (MPa) (Larger-the-better)

Level	Tool Traverse Speed	Tool Rotational Speed
1	50.70	49.91
2	48.73	48.31
3	44.99	46.19
Delta	5.71	3.73
Rank	1	2

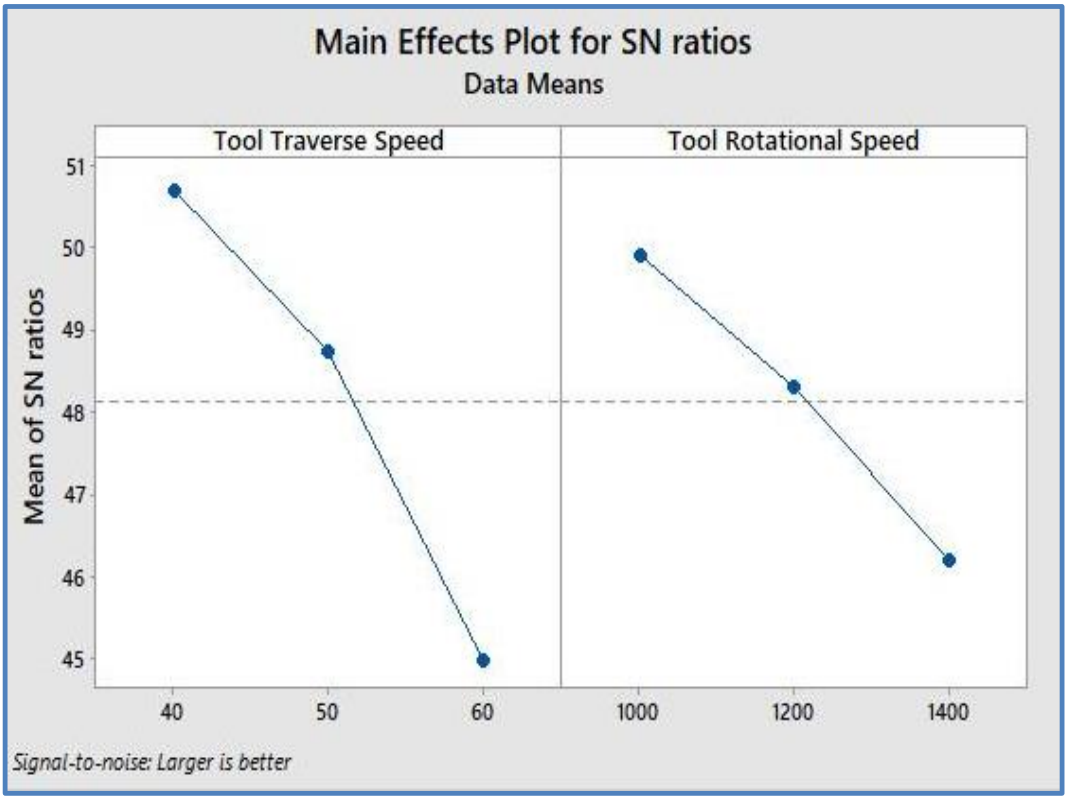

Figure 5.1: Main effects plot for mean of the S/N ratios of ultimate tensile strength

Table 5.4: Observations table for the microhardness (HV) and S/N ratios

Nomenclature of Sample	Tool Traverse Speed	Tool Rotational Speed	Microhardness (HV)	S/N ratios
S1	40	1000	179	45.0571
S2	40	1200	190	45.5751
S3	40	1400	187	45.4368
S4	50	1000	170	44.6090
S5	50	1200	185	45.3434
S6	50	1400	182	45.2014
S7	60	1000	169	44.5577
S8	60	1200	173	44.7609
S9	60	1400	171	44.6599

Table 5.5: Response table for the S/N ratios of microhardness (HV)

(Larger the better)

Level	Tool Traverse Speed	Tool Rotational Speed
1	45.36	44.74
2	45.05	45.23
3	44.66	45.10
Delta	0.70	0.49
Rank	1	2

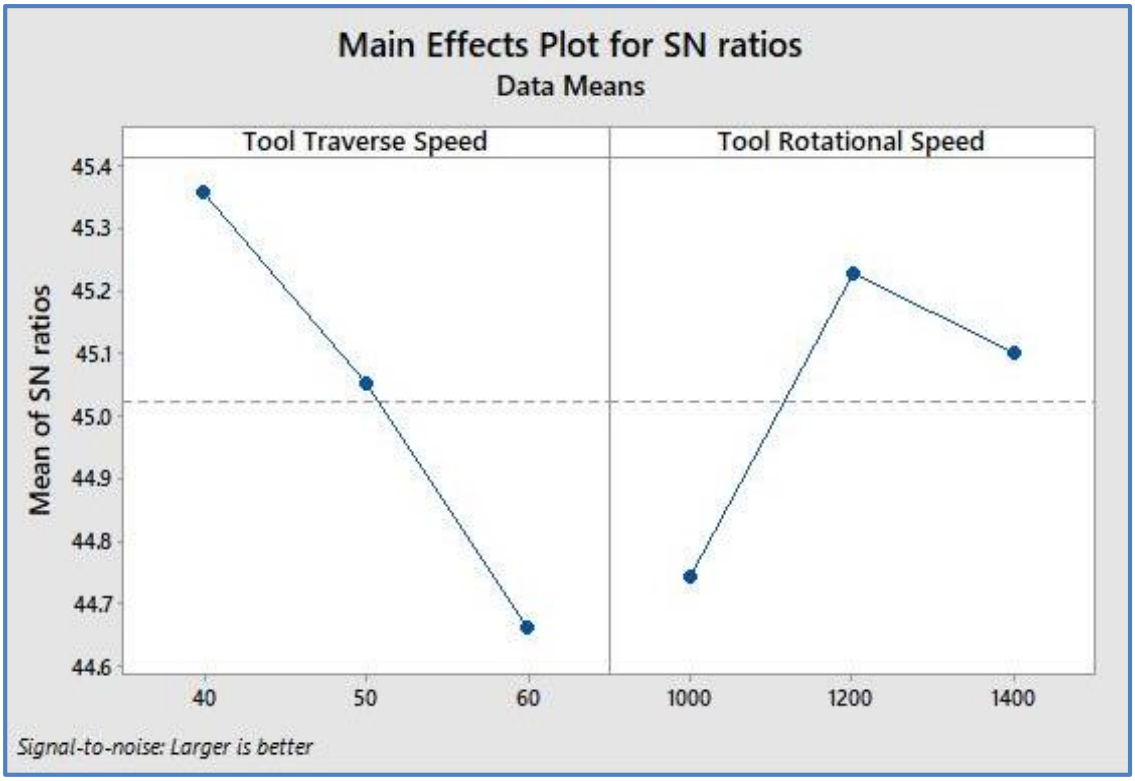

Figure 5.2: Main effects plot for mean of the S/N ratios of microhardness (HV)

In fig. 5.1 and fig. 5.2 show the main effects plot of the S/N ratios for Ultimate Tensile Strength (UTS) and Microhardness (HV), respectively, with regards to the different input parameters. The main effect plot shows how individual process parameters affect the response characteristics. An S/N ratios table for the input parameters was constructed using Taguchi with the 'larger the better' criterion for both, UTS and HV. The optimum values for UTS can be obtained at the input parameters of 40mm/min and 1000rpm, as seen in fig. 5.1. As we increase the values for TTS and RPM, the S/N ratio curve shows a decreasing trend. On the other hand, as the values of the input parameters were increased, in fig. 5.2, the optimum value of RPM was obtained at 1200rpm while for TTS it was 40mm/min as well. Hence, for HV, the optimum values were 40mm/min and 1200rpm. Since samples S1 and S2 were processed at both these combinations of values, we can note from table 5.2&5.4 that the optimum value for UTS is obtained in S1 (364) and the optimum value for HV is present at S2 (190).

5.1.3 Analysis of Variance (ANOVA)

Analysis of variance (ANOVA) is a collection of statistical models used in order to analyze the differences between group means and their associated procedures (such as "variation" among and between groups). In the ANOVA setting, the observed variance in a particular variable is partitioned into components attributable to different sources of variation. In its simplest form, ANOVA provides a statistical test of whether or not the means of several groups are equal, and therefore generalizes the solution. On doing a one –way ANOVA, we get the interval plot and individual plot between independent variable and the reference factor. We also get other information such as degree of freedom (DF) of parameter and error, F-values, S-value, standard deviation, etc.

Each of the FSP process parameter responses were estimated and significant contribution using ANOVA to understand their significance. The ANOVA responses along with the related terms are summarised in table 5.6 and 5.7. According to the ANOVA table the order of significant value of process parameters for UTS of Friction stir processed (FSPed) samples is tool traverse speed > tool rotational speed (table 5.6). The significant value of process parameters for microhardness of Friction stir processed (FSPed) samples is tool traverse speed > tool rotational speed (table 5.7). Percentage contribution of individual FSP parameter for different responses was summarised in the ANOVA.

Table 5.6: Analysis of Variance (ANOVA) for ultimate tensile strength (MPa)

Source	DF	Adj SS	Adj MS	F-Value	P-Value	Significant Value
Tool Traverse Speed	2	40050	20025	8.14	0.039	0.61195
Tool Rotational Speed	2	15553	7776	3.16	0.150	0.2376
Error	4	9844	2461			
Total	8	65446				

Regression Equation

Ultimate Tensile Strength (UTS) =270.6 + 72.4 Tool Traverse Speed (TTS) _40 + 16.1 Tool Traverse Speed (TTS) _50-88.6 Tool Traverse Speed (TTS) _60 + 47.8 Tool Rotational

Speed (TRS)__1000 + 5.8 Tool Rotational Speed (TRS)__1200 - 53.6 Tool Rotational Speed (TRS)__1400

Table 5.7: Analysis of Variance (ANOVA) for Microhardness (HV)

Source	DF	Adj SS	Adj MS	F-Value	P-Value	Significant Value
Tool Traverse Speed	2	309.56	154.778	16.39	0.012	0.6091
Tool Rotational Speed	2	160.89	80.444	8.52	0.036	0.3166
Error	4	37.78	9.444			
Total	8	508.22				

Regression Equation

Microhardness (HV**)** = 178.44 + 6.89 Tool Traverse Speed (TTS) _40 + 0.56 Tool Traverse Speed (TTS) _50 - 7.44 Tool Traverse Speed (TTS)_60 - 5.78 Tool Rotational Speed (TRS)_1000 + 4.22 Tool Rotational Speed (TRS) _1200 + 1.56 Tool Rotational Speed (TRS)_1400

Table 5.6 And 5.7, indicates that tool traverse speed as the most influential factor for ultimate tensile strength and microhardness followed by the tool rotational speed tool. In the previous literature survey, ANOVA was used to evaluate the process parameter and find out the most influencing parameter for tool rotational speed, tool profile, types of reinforcement, microhardness and UTS [100], [162]. Taguchi approach was used to establish the relation between input and output parameter and ANOVA was used to determine the significance of the parameters [141]. In another research, using ANOVA was performed to find the influence of reinforcement on the mechanical properties like hardness, % elongation, UTM and yield strength of the composite material [163]**.** It is a systematic method to determine the relationship between factors affecting a process and the output of that process. It is used to find cause-and-effect relationships. This information is needed to manage process inputs to optimize the output. DOE gives the optimized result of given experimental values or the outcome of the experiment performed [164]–[167]**.**

Table 5.6 represents ANOVA results for UTS measurement performed at 95% Confidence level in term of P-value of Tool rotational speed is more than that of Tool traverse speed and the significance value of Tool rotational speed is lesser than that of Tool traverse speed, the

tool traverse speed impacts the ultimate tensile strength (UTS) of an FSPed sample more than RPM and any change in the TTS will have a significant influence on the UTS.

The P-value is a probability that measures the evidence against the null hypothesis. Lower probabilities provide stronger evidence against the null hypothesis. To determine whether the model explains variation in the response, compare the P-value for the model to your significance level to assess the null hypothesis. The null hypothesis for the model is that the model does not explain any of the variations in the response. Usually, a significance level (denoted as α or alpha) of 0.05 works well. A significance level of 0.05 indicates a 5% risk (i.e. for a confidence level of 95%) of concluding that the model explains variation in the response when the model does not.

P-value ≤ α: The model explains variation in the response
If the p-value is less than or equal to the significance level, you conclude that the model explains variation in the response.

P-value > α: There is not enough evidence to conclude that the model explains variation in the response. If the p-value is greater than the significance level, you cannot conclude that the model explains variation in the response. You may want to fit a new model.

Since the P-value of Tool rotational speed (RPM) is more than that of Tool traverse speed (TTS) and the significance value of Tool rotational speed (RPM) is lesser than that of Tool traverse speed (TTS), which implies that TTS impacts the Microhardness of an FSPed sample more than RPM and any change in the TTS will have a significant influence on the HV.

5.1.4 Confirmation test

It is observed from the ANOVA response (table 5.6 and 5.7) for the S/N ratios of UTS and microhardness from the main effect plots (fig. 5.1 and 5.2), we can see that while the Tool rotational speed most optimum value increases to 1000 rpm (lowest value of RPM), while that for Tool traverse speed and 40 mm/min (lowest value of TTS) for ultimate tensile strength (UTS). For the optimum value for Tool traverse Speed (TTS) is 40mm/min (lowest value of TTS), while that for Tool rotational speed is 1200 rpm (middle value of RPM) for microhardness.

As we found that the optimal process parameters combination are Tool rotational speed 1000 rpm, 1200 rpm and Tool traverse speed and 40 mm/min. These parameters are selected using Taguchi orthogonal array (table 5.1).

As is evident from the Taguchi Analysis of the given (table 5.1), the optimum responses are obtained at Tool Traversal Speed = 40 mm/min and Tool Rotational Speed = 1200 rpm. This corresponds to the testing instance of sample S2, for which the values of the responses are Microhardness = 190 HV and Ultimate Tensile Strength = 336 MPa. The confirmation test of the aforementioned response values may be done by the regression equations formed by ANOVA. From the table 5.8, we can see that for both the responses, the error percentage falls under the accepted value of 5% (confidence level = 95%) and hence our regression model is valid.

Table 5.8-Comparison of the experimental and predicted values

Response	Experimental Value	Predicted value	% error
UTS	336 MPa	348.8 MPa	3.81
HV	190 HV	189.55 HV	0.24

5.1.5 Effect of tool traverse speed

Major machine variables are tool rotational speed and tool traverse speed. Tool rotational and traverse speed determine amount of heat generated in the work piece and determine the amount of heating input in the Stir Zone (SZ), which in turn affects the microstructure and grain refinement of the materials. From fig. 5.3 shows the effect of tool traverse speed on microhardness for the constant tool rotational speed at 1000rpm. The microhardness decreases with the increasing tool traverse speed from 50 to 60 mm/min.

As already stated, tool rotational and tool traverse speeds of the tool determine the heat input amount in the base metal alloy [168]**.** However, heat input is inversely proportional to grain refinement, but there must be at least the threshold heat generation to plasticize the material and hence it needs to be optimized to achieve defect free and refined stir zone [169]. Morisada et, al. [170] examined the role of traverse speed by keeping the rotational speed constant, while fabricating AZ31 alloy composites reinforced with MWCNTs. Tool traverse speed was differing from 100 to 25 mm/min. With decrease in tool traverse speed, uniform distribution of the MWCNTs was attained which can be attributed to suitability of viscosity range in the AZ31 matrix at a lesser tool traverse speed. Similar experiment was performed by Asadi et al. [171] while evaluating the microstructure and the dispersal of the SiC particles

in stir zone of the FSPed Magnesium alloy AZ91 found that decreasing the rotational speed and increasing the tool traverse speed led to a reduction in the grain size.

During surface modification through Friction Stir Processing (FSP) rotating tool moves perpendicular to the base metal alloy and the tool shoulder diameter gives sufficient forging pressure to the metal during processing. The below equation (5.1) shows the FSP heat input in the processed zone during processing ([172])

$$Q=(4\pi 2\mu\omega PD3)/3v \quad \text{.....(5.1)}$$

Where Q is the heat input, μ is the coefficient of friction between tool shoulder and the base metal, ω the tool rotational speed, P is the pressure, D is the shoulder diameter of tool, v is traverse speed of tool. As per the above equation (5.1) shoulder diameter of tool is one of the important parameter for conducting the heat input during the surface modification through Friction stir processing (FSP) and Friction stir welding.

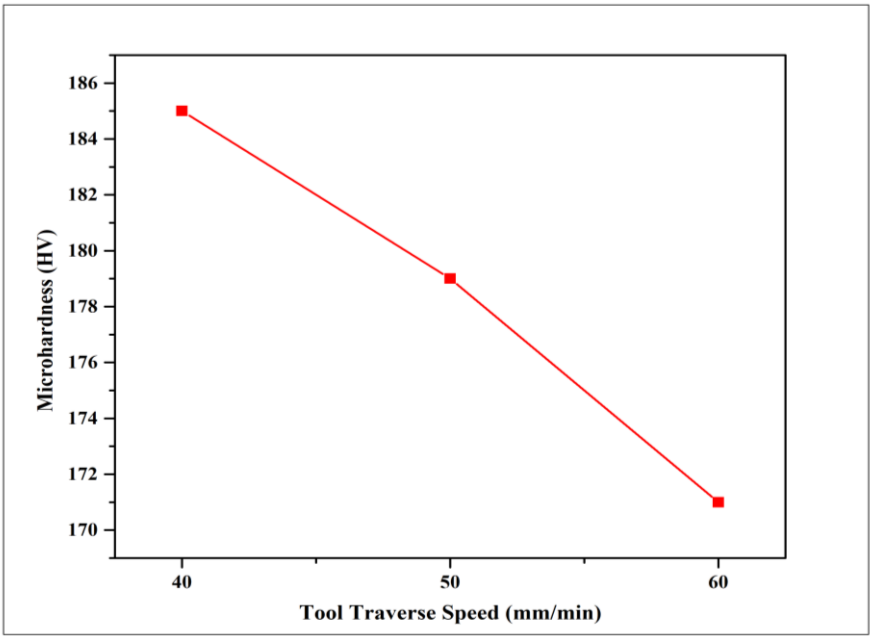

Figure 5.3-Effect of tool traverse speed on the Microhardness

Khayyamin et, al. [173] also investigated the effect of traverse speed while fabricating SiO2/AZ91 nano-composite and noticed that the increase in traverse speed led to refined grains in the stir zone and resulted in increased micro-hardness. Barmouz et, al. [174] investigated and found a very interesting result that outcome of traverse speed on grain size was reversed when the fabrication of Cu/SiC surface composites was carried out with and without SiC particles. It can be understood by the affinity of SiC particles to agglomerate at

higher traverse speeds of the tool but at lower traverse speeds SiC particles are pinned in the SZ and get a dispersed uniformly, hence in FSP of Cu without SiC particles, grain size rose with the decrease in traverse speed because of increase in heat input.

P. Vijayavel et, al. [175] produced stir cast LM25AA-5% SiCp MMCs which further processed through FSP to check the impact of tool traverse speed on strength, hardness, and ductility of FSPed LM25AA-5% SiCp MMCs. Mean grain size of zone obtained as 9.891 microns, max hardness of 116HV and increased both tensile and ductile properties are obtained in the specimen at a tool traverse speed of 40mm/min.

5.1.6 Effect of tool rotational speed

The measure of heat input to the stir zone (SZ) is controlled by tool rotational speed and traverse speed (ω and v), which thus influences the microstructure and resultant properties. There must be an adequate measure of heat input to plasticize the material despite the fact that lower heat input brings about more grain refinement [176]. In the fabrication of surface composites, the higher tool rotation speeds are more desirable for dispersal and suspension of congregations of reinforcement particles. From the fig. 5.4 shows the influence of tool rotational speed on the microhardness for constant tool traverse speed of 40mm/min. The microhardness value increases with increase in tool rotational speed from 1000rpm to 1200rpm and then decrease at rotational speed of 1400 rpm causes the tool wear at high rotational speed and agglomeration of boron carbide nanoparticle reinforcement. Similar types of results has been reported by M. Azizieh et, al. [177], at higher tool rotational speed causes more grain growth during dynamic recrystallization and decreases the microhardness. Further particle distribution and spacing between the particles affects the microhardness of material as on increasing rotational speed the inter particle distance increases leading to decrease in microhardness.

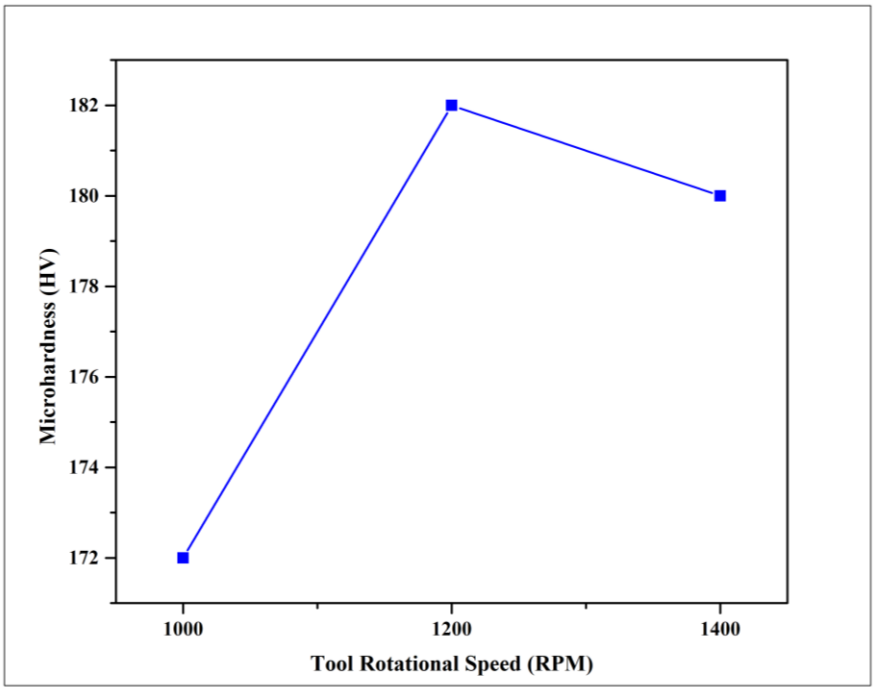

Figure 5.4-Effect of tool rotational speed on the Microhardness

Tool wear is the process of material removal during surface interaction of two materials. The material flows parallel the cylinder pin axis and give rise to wear of the tool at the early stage of the process because of two important reasons. Firstly, the reinforcing particles are rigid and harsh in nature and these particles are in micro or nano size, hence, their size makes these particles more distributed at the surface of the composite and the tool has more odds of wear. Secondly, owing to the high strain rate involved, the base material gets work hardened and affects in tool wear. Tool materials commonly utilized for FSP of softer alloys are different hard steels such as H13 steel, tungsten-based alloys, whereas cermets (WC-Co) and Poly cubic boron nitride (pcBN) find use in FSP of harder alloys. Although, pcBN is more preferred tool material for harder alloys like of steel and titanium. In another study Hajideh et, al. [178] studied the impact of tool geometry on different FSW of polyethylene–polypropylene and it was shown that the threaded cylindrical pin profile performed better compared to the other tool pin forms and imparted more uniform material flow regime while welding. Hajideh et, al. [179] in another research studied the effects of input parameters on the mechanical properties and the microstructure of the FSW joints by incorporation of copper powder into the weld zone and concluded that powder addition enhanced the strength and hardness of the joint. Ramezani et al. [180] studied the effects of rotational speed, traverse speed and pass number on the main attributes of tool wear in FSP of aluminum 7075 work piece samples with Silicon carbide (SiC) nano powder by applying response surface

method (RSM) method. Tool wear was achieved using an optical microscope by image analysis software. In fig. 5.5 shows the stir zone temperature was measured using thermal imaging camera at different tool rotational and at 40mm/min tool traverse speed.

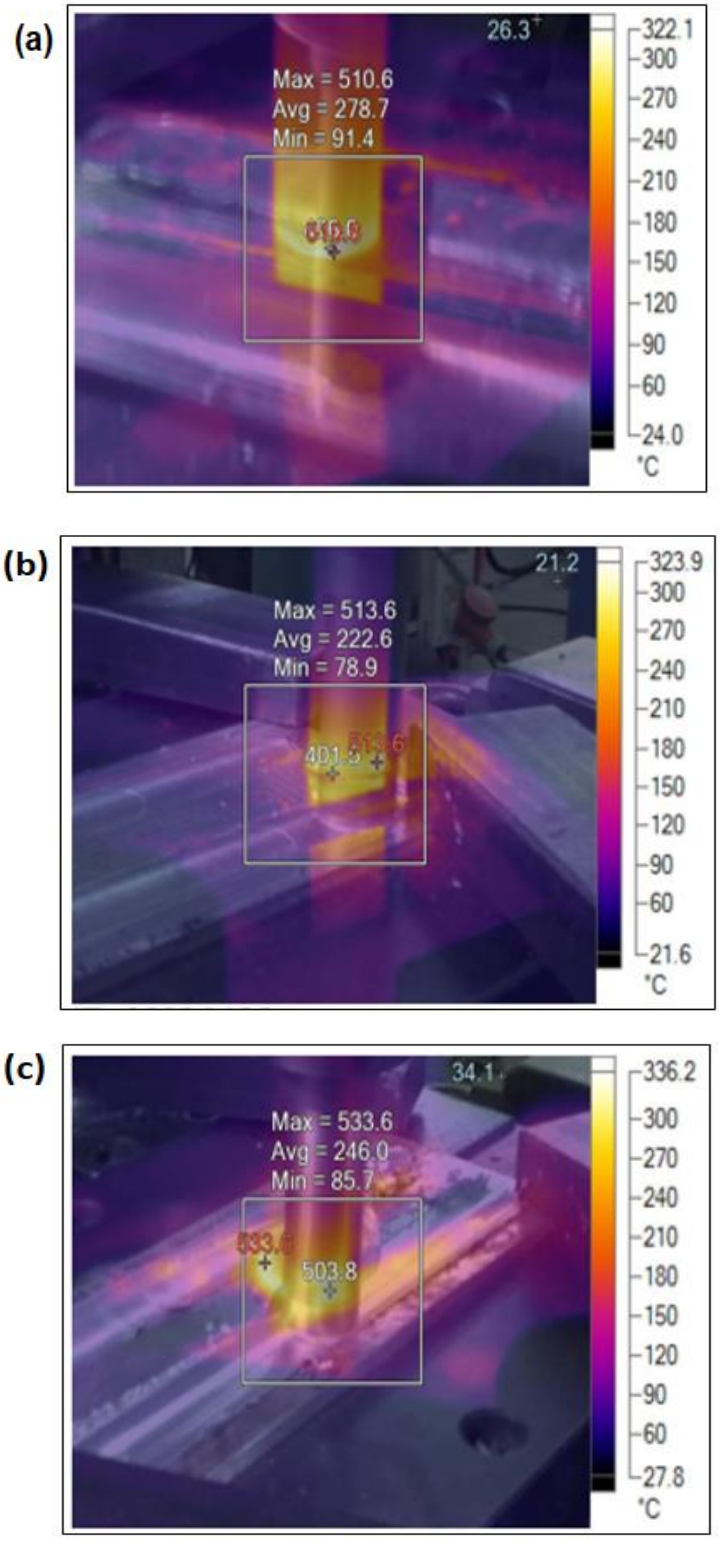

Figure 5.5-The processed zone temperature of surface composite samples at different rotational speed (a) 1000 rpm (b) 1200 rpm and (c) 1400 rpm

There are many machine parameters which influence the microstructure and grain refinement of the modified material, but the most important machine parameters in FSP are tool rotational speed and traverse speed because they are accountable for the heat input in the SZ [177] which regulates the material flow and microstructure evolution that determines the properties of the modified material. Generally, rests of the other parameters are kept constant and not varied.

Different models have been put up for the correlation of these process variables with temperature or heat produced in the stir zone.

Frigaard et al. [172] Calculated the average heat input per unit length of the specimen according to the following model, in Eq. 5.2.

$$Q = \frac{4}{3}\pi^2 \frac{\mu P N R^3}{v} \quad \ldots\ldots\ldots\ldots\ldots\ldots\ldots\ldots\ldots\ldots\ldots\ldots\ldots\ldots\ldots\ldots\ldots\ldots (5.2)$$

Where, μ denotes the coefficient of friction, P denotes the pressure, N denotes rotation per second and R is the radius of the tool. This relation shows that the heat input is directly proportional to the rotational speed and inversely proportional to the linear speed. For a given μ, R and P, it can be said that, Eq. 5.3

$$Q \propto \frac{\omega}{v} \ldots\ldots\ldots\ldots\ldots\ldots\ldots\ldots\ldots\ldots\ldots\ldots\ldots\ldots\ldots\ldots\ldots\ldots\ldots\ldots\ldots\ldots (5.3)$$

Based on experimental observations, Arbegast and Hartley, [181] proposed the following relation between the maximum temperature (Tmax) in Stir Zone and the processing parameters of rotational speed (ω) and traverse speed (v) in Eq.5.4

$$\frac{T_{max}}{T_{min}} = K \left(\frac{\omega^2}{v \times 10^4}\right)^{\alpha} \ldots\ldots\ldots\ldots\ldots\ldots\ldots\ldots\ldots\ldots\ldots\ldots\ldots\ldots\ldots\ldots\ldots\ldots (5.4)$$

Here, the constant K ranges between 0.65 and 0.75, the exponent alpha is reported to lie from 0.04 to 0.06 and Tm (◦ C) is the melting point of the alloy. The ratio between ω^2 and v is called to be the pseudo heat index.

5.1.7 Effect of tool pin profile

The basic role of tool in FSP is the generation of heat between mating surfaces by friction and transfer of applied load to workpiece as a result the workpiece material starts to deform plastically. Another function of the FSP tool is to mix the material around it uniformly. The

shoulder will control the material flow in a certain region, and the pin will generate heat and severe plastic deformation. Eventually, the friction stir tool affects the microstructure and mechanical properties. However, little knowledge about the friction stir processing tool geometry was published before, and information on friction stir welding tool could be reference to understand the tool by Thomas et, al. [70,71]. Zhao et, al. [72]**.** So, the geometry of tool such as tool pin dimensions, shoulder diameter affects the rate of heat generation, flow and proper mixing of material [78]**.**

Elangovan et, al. [73]–[75] investigated the effect of pin profile in FSP tool on the development of FSP zone in Al based MMCs using threaded cylindrical, straight cylindrical, triangular, square and tapered cylindrical pin profiles of the tool and concluded that the welds produced by tool having square pin profile when compared to other pin profiled tools are metallurgically flawless and mechanically righteous. Fujii et, al. [76] prospected that circular pin profiled tool fabricated weld with elite mechanical properties for 1050-H24 among circular with and without thread and triangular pin profiled tool used in its FSW. Hashemi et, al. [77] showed that taper threaded tool with 4 passes produced best wear resistant Al7075-T651 alloy among taper threaded, triangular and square pin profiled tools. Jamshidi et al. [182] investigated the effect of tool geometry on tribological properties of AA 6061-T6 and AA 5086-O and established that conclave shoulder and conical pin with three groves tool produced more equivalent stir zone compared to other geometries of tool used. Mahmoud et, al. [78] found that square probed tool produced better homogeneous mixture of SiC reinforced with A1050-H24 in nugget zone in contrast to other pin profiled tools. Kumar et, al. [79] investigated the role of FSW tool on weld formation and material flow to state that among pin and shoulder driven material flows, shoulder transfer the material by bulk while pin transfer layer by layer. Kumar et, al [80] studied the effect of tool pin profiles on microstructure during FSW. Various pin profiles like taper cylindrical, taper threaded and cylindrical, triangular, square, pentagonal and hexagonal, all having same shoulder diameter were utilized to fabricate the joints. It was observed that joints made by square tool pin profile showed superior mechanical properties compared to others. The efficiency of joint made by square pin profile was 85% higher than the base metal. Sameer et, al. [183] studied the impact of tool pin profiles using tungsten carbide and decided the weld quality of FSW. The profiles used were straight cylindrical, tapered cylindrical, hexagonal, triangular, and square. Joint fabricated by hexagonal pin profile showed supreme tensile strength along with 83.1% joint efficiency which was higher than the other profiles. Thube et, al. [184] utilized five different

pin profiles (straight cylindrical, tapered cylindrical, triangular, square and cone) to fabricate joints. It was observed that the tool pin designs had negligible impact on heat input and tensile properties. Straight cylindrical pin was seen to have fabricated mechanically sound weld compared to other profiles. Elangovan et, al. [73] deliberated the effect of axial force and various tool pin profiles on creation of zone through FSP in AA6061 aluminium alloy. It was originated that pin profiles partaking square section produced greater quality region of FSP having no defects. Khojastehnezhad et, al. [185] prepared Al6061/Al_2O_3-TiB_2 using friction stir processing with different tool pin profile in order to study the outcome of different pin profiles on the mechanical and tribological properties of the composite material. Square pin profile showed better distribution of particles as compared to triangular pin profiles. Kumar et, al. [82] conducted tensile test and found that tool pin profile with square shape gave better results compared to others. Manoj et, al. [186] fabricated aluminium based composites by reinforcing pine leaf ash using friction stir processing with different tool pin profiles to study its effect on tribological behaviour of the composite. It was concluded that threaded taper tool pin profile gave higher hardness and less wear rate as compared to others.

Vikrant et, al. [83] conducted hardness and tensile test on Al6082-Cu alloy and found that cylindrical threaded tool pin profile provides better result than square tool pin profile. Baruch et, al. [187] compared the effect of different tool pin profiles and found that cylindrical tool pin profile can modify the microstructure of the material more effectively. Namrata et, al. [188] utilized the different tool pin profiles i.e. cylindrical, square, triangular and tapered cylindrical pin profile to study the impact on the microstructure of FSPed AA6063/SiC composite and found that cylindrical pin provides better distribution of particles without much defects. Javad et, al. [189] developed a mathematical model to study the effect of tool pin profile on mechanical and microstructural properties, flow of material and temperature distribution of aluminium alloy in friction stir welding process. It was obtained that grain was finer and have more tensile strength in case of square tool pin profile. Suresha et, al. [190] observed that FSP tool with conical pin profile produced joints having better efficiency than square pin profiled tool. Eftekharinia et, al. [84] employed different pin profile and passes to investigate the tribological and microstructural behavior of FSPed AA6061/SiC composite and it was showed that composite produced by square pin has higher wear resistance.

5.2 CHARACTERIZATION OF FABRICATED ALUMINIUM-B_4C SURFACE COMPOSITE

5.2.1 Microstructural analysis

For microstructure observations, Olympus GX41 inverted metallurgical optical microscope has been utilized and the microstructure images were captured at 20μm. Width of the micrograph is measured as per the pixel to scale conversion according to 2 pixels per micron. Viewing the microstructure held to be imperative because of the momentous effects of the FSP technique; this was the resultant refinement of the grain structure. This would be translated into high-caliber mechanical properties imparted to the surface alteration of the material.

During surface composites fabrication using FSP, enhancement in properties and micro-structural changes are entirely dependent on the dispersal of the ceramic particles in the work piece [191]**.** However, depending upon various combinations of factors and approaches associated with composite fabrication the distribution of RPs is greatly influenced. The microstructure changes during FSP are because of thermal-mechanical effects. Like FSW, the zone of action in FSP is generally separated into a mix of heat-affected zone (HAZ), thermo-mechanically affected zone (TMAZ), stir zone (SZ), and base metal zone (BM) [192]**.** The SZ, for the most part, comprises of uniformly refined grains, which are equiaxed and smaller in size in comparison to the metal matrix composite. When FSP is performed, SZ encounters an elevated pinnacle temperature and drastic plastic deformation—this prompts microstructure transformation because of dynamic re-crystallization (DRX). (DRX) dynamic re-crystallization is generally agreed upon as the cause of grain refinement [193,194]**.** In the processing area, the segment of high-edge grain boundaries (HAGBs) is extended after the application of FSP [195]**,** which advances slippage of grain boundary, which causes the plasticity of the MMC to evidently improve.

When reinforcement particles are incorporated in the base metal plate, nucleation stimulated by the particles facilitates grain refinement during re-crystallization. The particles that stream in the vicinity of the tool are exposed to high temperatures and extreme plastic deformation, which prompts a conspicuous reduction of grain size in the zone of action. The zone agitated by the tool probe is referred to as the SZ [66]. Fine, equiaxed grains are primarily created by dynamic re-crystallization (DRX) in the SZ [74,196]**.**

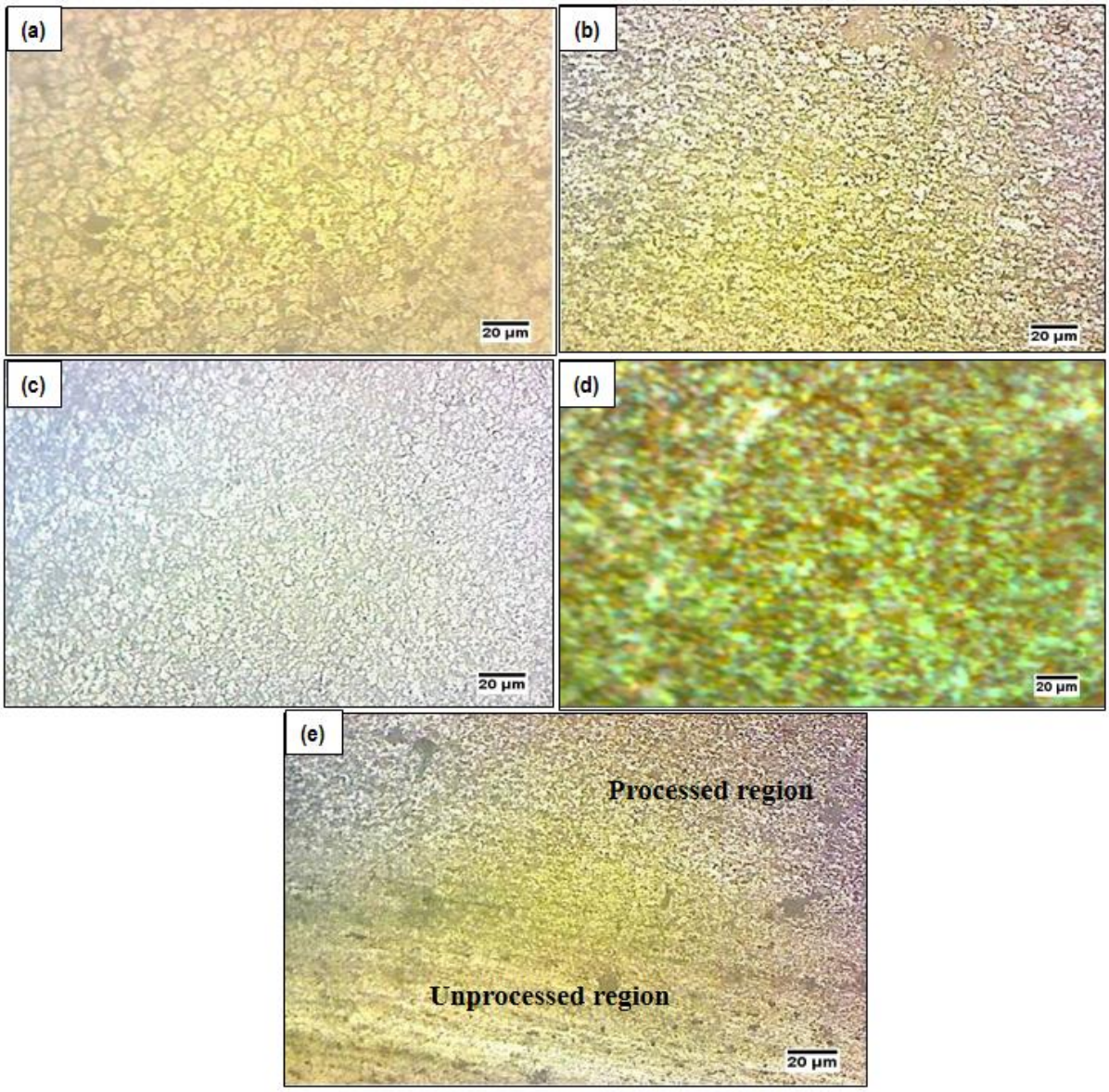

Figure 5.6 Microstructure images of different samples at 20µm (a) Unprocessed surface (base metal), (b) Friction stir processed (FSPed) w/o reinforcement (RPs) (c) Friction stir processed (FSPed) with RPs sample, S1 (d) Friction stir processed (FSPed) with RPs sample, S2(e) FSPed Sample S3, processed and unprocessed region

The rotating square, triangular and cylindrical tool pin provides a stirring action and plasticizing the matrix with the boron carbide nanoparticles in a thin layer processed through self-assembled monolayer (SAM). The grain size of the surface composite samples is further reduced due to the incorporation of B_4C nanoparticles reinforcement which act as nuclei, and their pinning effect hinder the grain growth of the base metal after dynamic re-crystallization (DRX).

As shown in fig. 5.6 (a) seen grain boundaries of base metal. In fig. 5.6 (b) Friction stir processed (FSPed) sample without reinforcement particle, extreme plastic deformation and heating due to the friction during FSP between tool and matrix metal, lead to the origination of a recrystallized ultra-fine grained microstructure in the stirred zone of surface in comparison to the unprocessed sample. On account of FSP without reinforcement, heat generation may encourage grain development [197]**.** It has also been seen that granular size in base metal itself is reduced after FSP even without the introduction of RPs to it. And when reinforcement particles were introduced to the base metal a further decrease in the size of the grains was observed. In fig. 5.6 (c) Friction stir processed (FSPed) with Reinforcement particles (RPs) sample, has shown the recrystallized ultra-fine grain structure at same scale. The microstructure of processed and unprocessed region shown in fig. 5.6 (e) the well-defined nugget zone and thermos-mechanically affected zone (TMAZ) have been recognized.

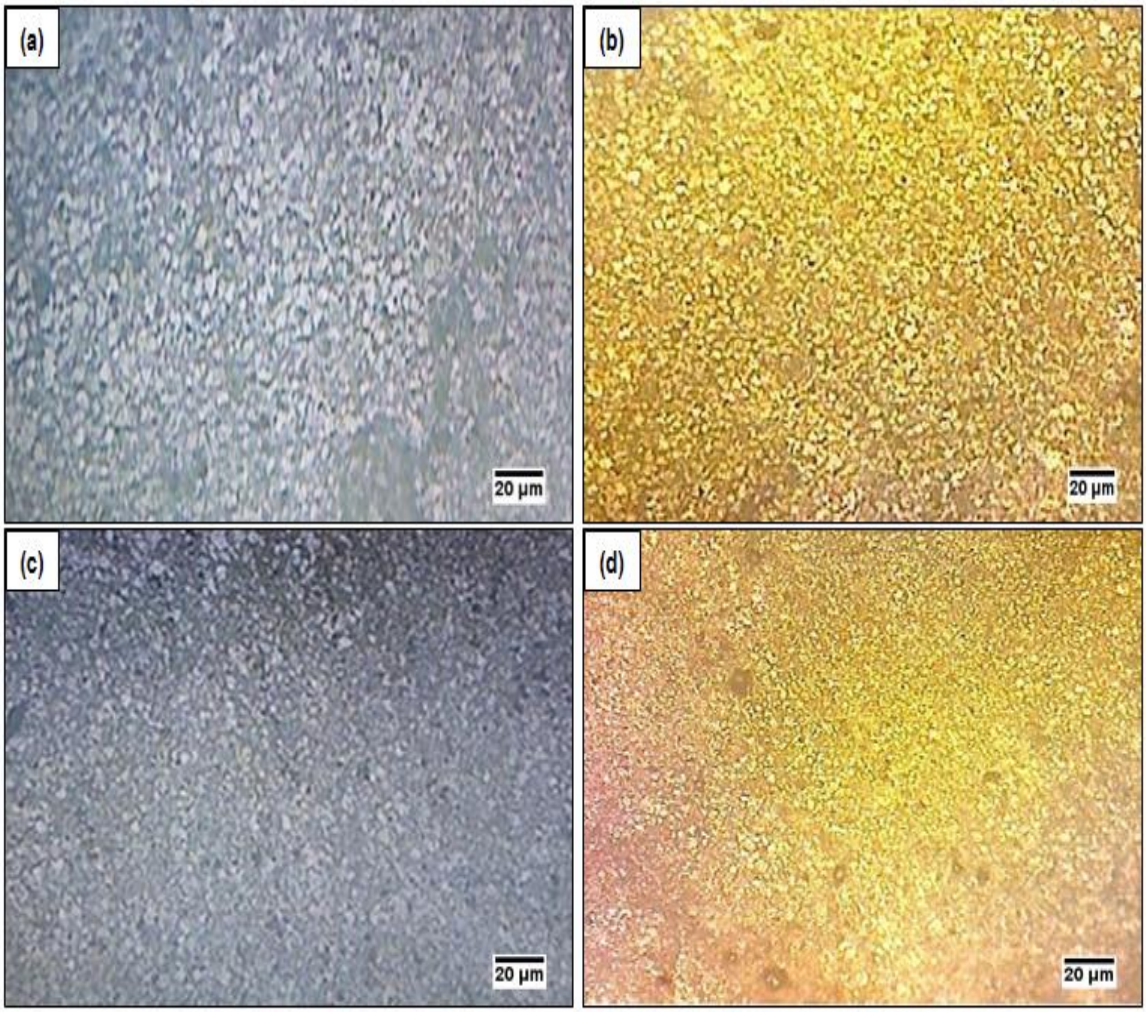

Figure 5.7-Microstructure images of different samples at 20µm (a) Friction stir processed (FSPed), S1 (b) FSPed sample, S2 (c) FSPed sample, S3 (d) Processed sample at SZ

Another significant thought identified with the size of the grain is improvement or decrease in heat input during FSP. Prevailing components affecting measurements of the grain at the time of FSP without RPs and with RPs are unique. As shown in fig. 5.7 (a-d) & fig. 5.8 (a-d), Friction stir processed (FSPed) with Reinforcement particles (RPs) and FSPed w/o reinforcement samples are clearly identified the reduction in the grain size.

Two factors affecting the size of the grain contradictorily. For starters, the elevated temperature will result in development of grains [177], [198]. Second, Reinforcement particles (RPs) may carry on like obstacles against grain boundaries subsequently confining granular development [199]**.** A generally acknowledged actuality when it comes to FSP is the predominance of pinning effect over the impact of heat inside MMCs, consequently bringing about micro-structural refinement inferable from the grain nucleation and reinforcement pinning impact [200], [201].

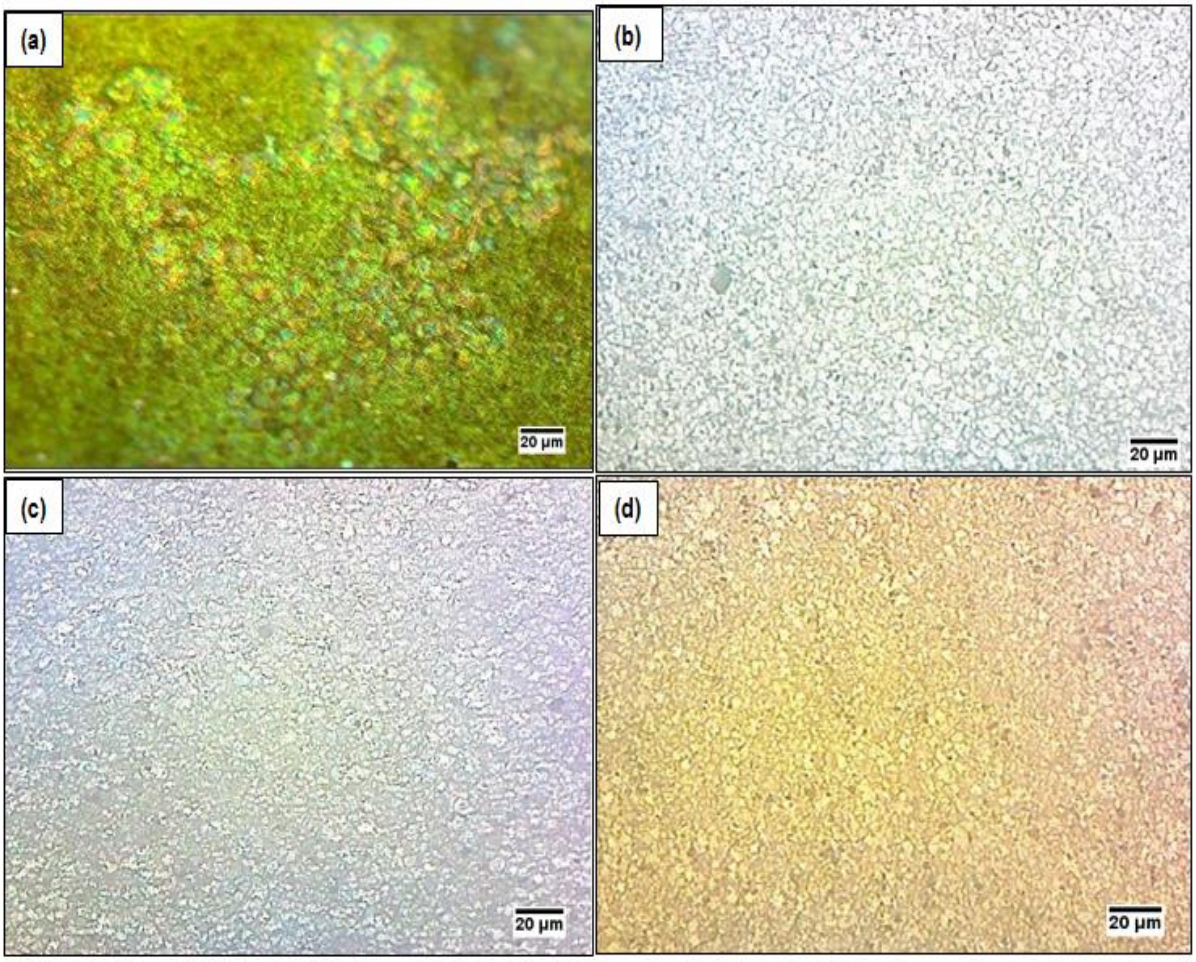

Figure 5.8 Microstructure images of different samples at 20µm (a) Friction stir processed (FSPed) w/o reinforcement sample (b) FSPed sample, S1 (c) FSPed sample, S2 (d) FSPed sample, S2

5.2.2 SEM/EDX micrograph analysis

After the fabrication of the surface composite using FSP, the samples were cut in the perpendicular direction from the processed region and then polished in different grades of emery paper followed by wet polishing. Scanning Electron Microscope (SEM) model (JSM-6510LV, JEOL JAPAN) and FESEM model (ZeissSigma300) was used to examine the homogeneous distribution of reinforcement particles. In fig. 5.9(a) represents the SEM and EDX micrograph of the base metal surfaces. In fig. 5.9(b) shows the SEM and EDX micrograph of the FSPed sample without reinforcement particles. In fig. 5.9(c) shows the SEM and EDX micrograph of the surface composite sample with a 0.5 mole concentration of B_4C nanoparticles and it has clearly shown that the B_4C particle present in the sample. The homogeneous distribution of B_4C particles can be seen in the stir zone of the processed region in the micrograph. Sharp geometries like square, triangle, and threaded pin tool wear due to more tool wear causes insufficient material flow at the higher rotational speed. At 1400rpm and some other process parameters causes more tool pin wear, due to that bad material flow and agglomeration of the nanoparticles in the surface composite. One of the authors investigated the tool pin wear of several rotational speed and constant traverse speed and he had concluded that minimum tool pin wear occurred with lower tool rotational speed. At the lowest tool rotational speed, the tool pin wear was nearly one-fourth of the higher tool rotation speed. It has been reported by Fernandez and L.E, Murr [208]. This ensures improvement in microhardness and other characteristics compared to the base metal. Due to the formation of the Self-assembled monolayer (SAM) over the surface of base metal followed by FSP. SAM technique is used to minimize the concentration of nanoparticles and obtained better properties as compared to the other reinforcement applying method.

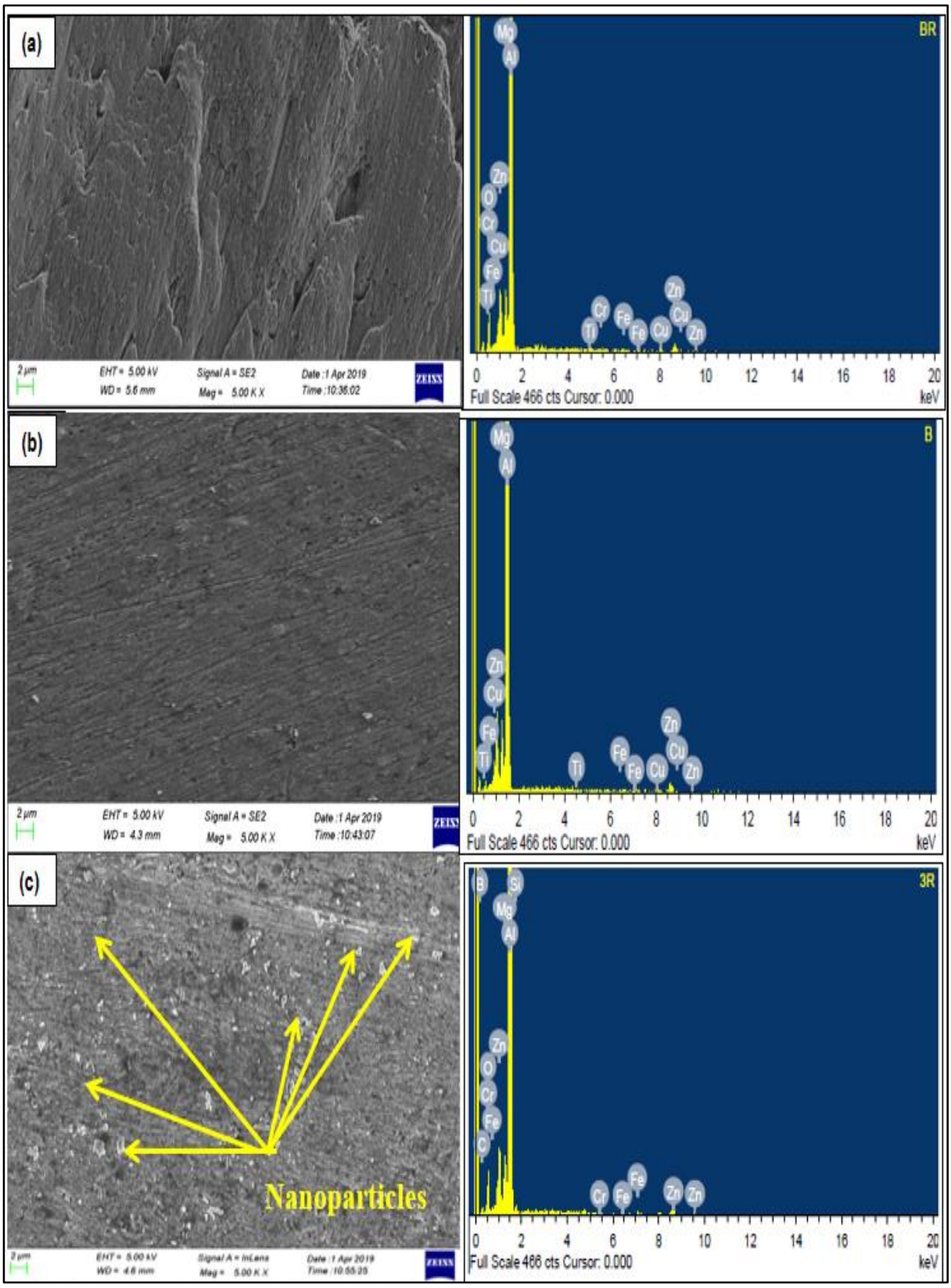

Figure 5.9-SEM/EDX micrograph of (a) Base metal (b) FSPed sample without reinforcement particles (c) FSPed sample processed at 1000rpm

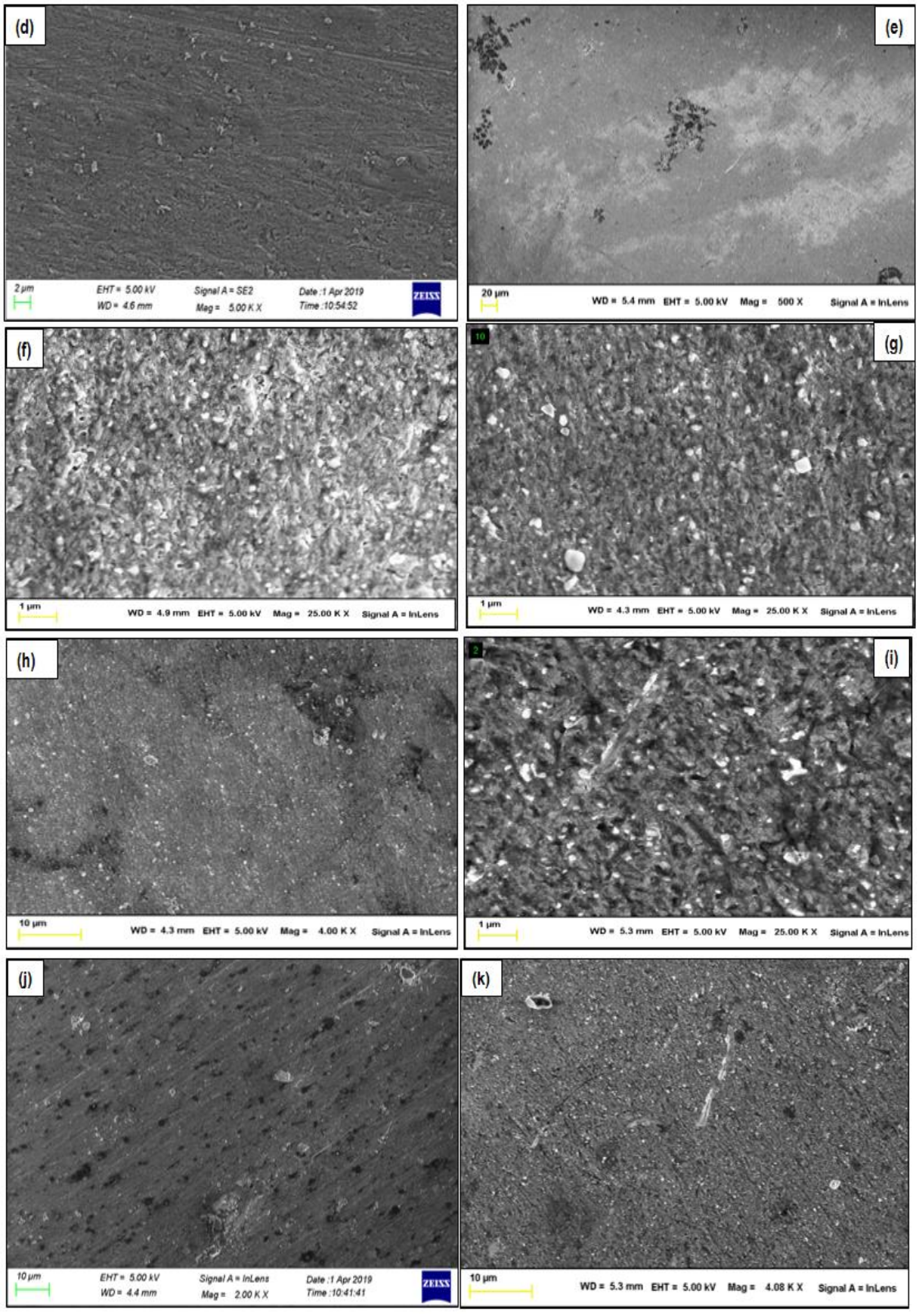

Figure 5.10-(d-k) SEM micrograph of FSPed sample processed at 1000rpm, 1200rpm, 1400rpm respectively

5.2.3 XRD analysis

X- Ray diffraction (XRD) analysis was used to determine the presence of crystalline phase into the material. X-Ray diffraction (BRUKAR D8 ADVANCE) was utilized to identify the phase of B_4C nanoparticles into a surface composite. In fig. 5.11(a) shows the XRD pattern of the substrate (base) metal. It clearly shows the presence of B_4C nanoparticles in the XRD pattern analysis of the surface composites in fig. 5.11(b). The B_4C nanoparticles were shown between 40-45^o at 2 theta angle. In the FSPed surface composite, nanoparticles can be clearly seen in the SEM micrograph also, it is also supported by a XRD pattern. The highest Al peak was present and further it was shifted towards increasing the angle. A lower peak were shown in fig. 5.12 at 40-45 degree, which was observed due to less concentration of nanoparticle using Self-assembled monolayers (SAM) technique followed by FSP method. It was observed that only two phases are present, i.e. Al and B_4C and no other diffraction peaks were detected before and after processing.

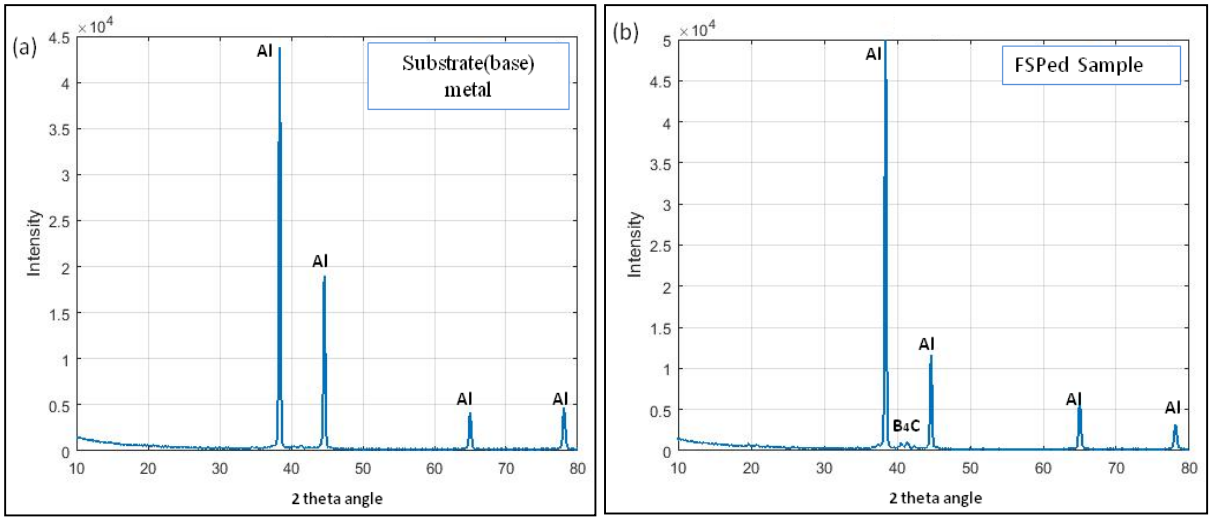

Figure 5.11-XRD analysis of (a) Base metal (b) FSPed with reinforcement particle (RPs)

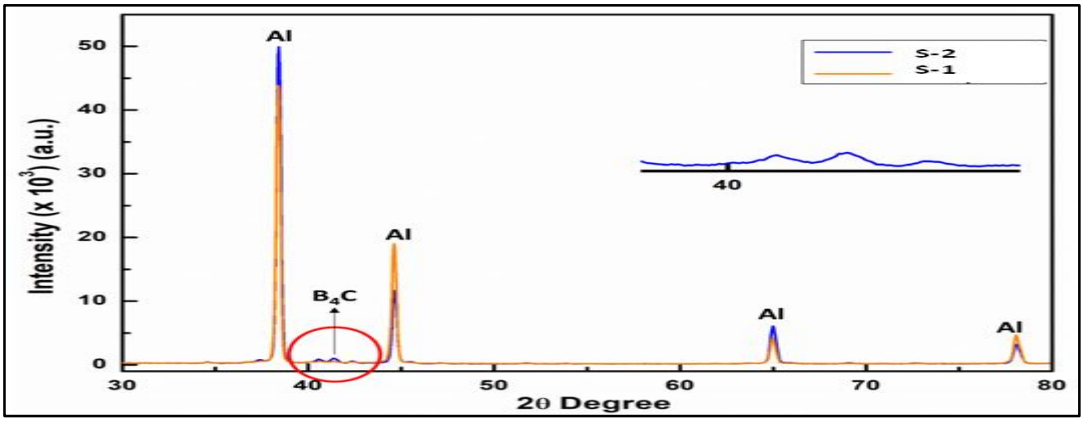

Figure 5.12-Comparision XRD analysis of FSPed without reinforcement particle (RPs) and FSPed with reinforcement particle (RPs)

5.3 MECHANICAL PROPERTIES OF FABRICATED AL-B_4C SURFACE COMPOSITE

5.3.1 Microhardness

Resistance to surface indentation is defined as hardness. Conflicting variables used for determining micro-hardness of surface composites. When the size of the grains is refined, it increases microhardness, while the increase in temperature results in annealing. Annealing overpowers the effect caused by refinement of grains resulting in decreased hardness [168]. Therefore, the increase in hardness caused by the combined effort of refinement of grains as well as homogenous reinforcement particles dispersion dictated by FSP [202]**.** The average microhardness of the base metal (BM) and friction stir processed surface composites are shown in fig. 5.13. The surface composite processed samples having zero concentration and 0.5 moles of B_4C nanoparticles concentration through self-assembled monolayer (SAM), exhibited higher hardness when compared to base metal sample. The detailed microhardness values of the friction stir processed Al-B_4C surface composite sample and base metal are presented in Table 5.9.

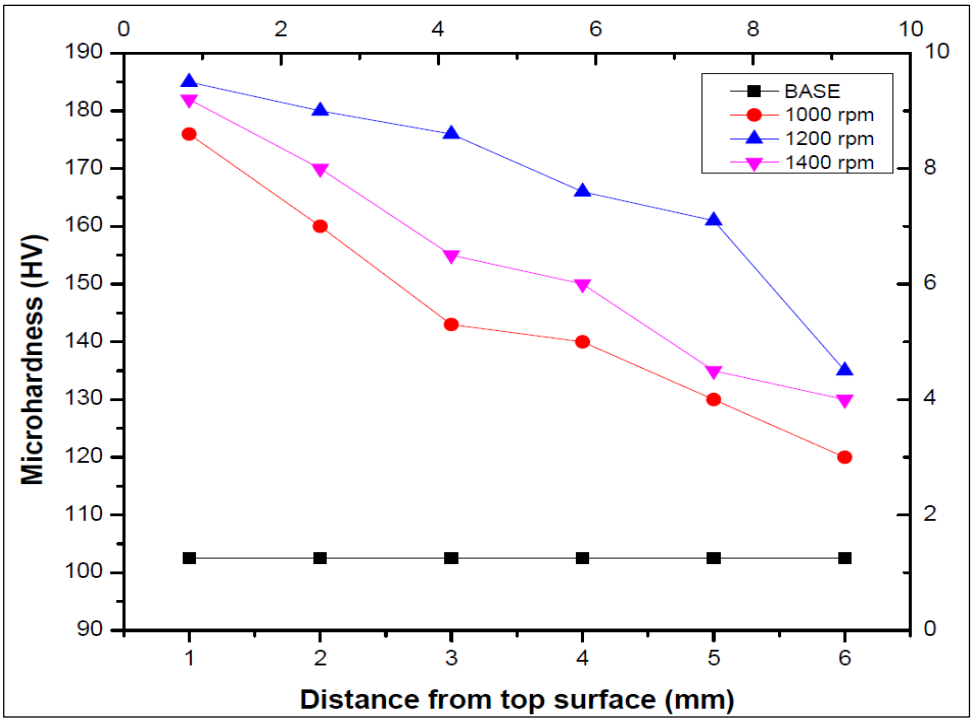

Figure 5.13-Microhardness of the base metal and Al-B_4C surface composite at distance from top surface

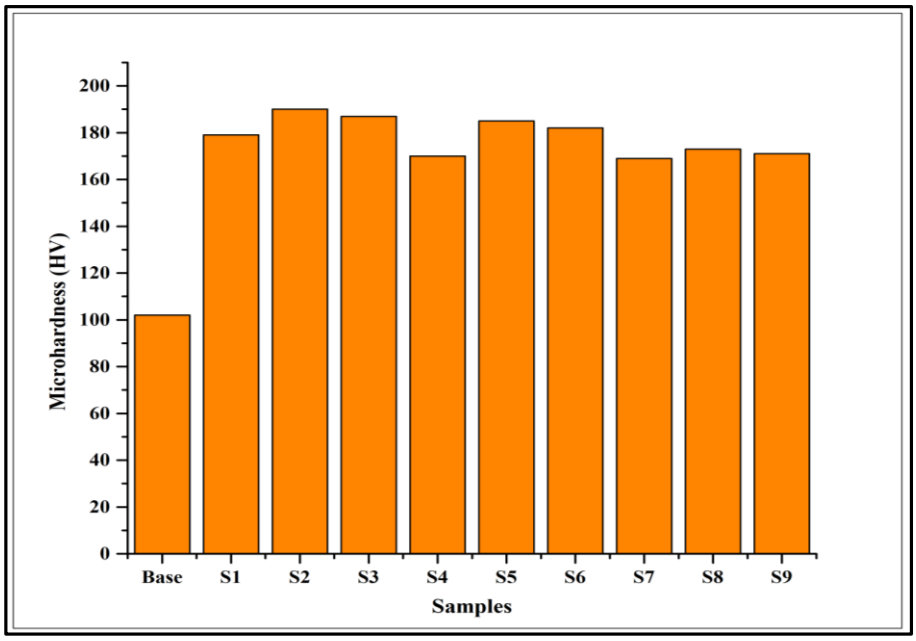

Figure 5.14-Microhardness variation in all samples of the Al-B_4C surface composites

The reduction of microhardness of the given tool is because of additional tool wear at elevated temperatures [203]. When the fabrication of nanocomposite using TIO_2 as reinforcement by friction stir processing was performed under an ambient environment, a slight nanoparticles agglomeration was obtained at 1400rpm, due to heat input exceeding and causing more tool wear and insufficient material flow and strain rate. Therefore, the performance of the tool shows decrease with consecutive increase in tool rotational speed has been explained elsewhere [180], [191]. In fig. 5.14, represents the comparison of hardness values for the Al-B_4C surface composite samples and the base metal. The pattern is to such an extent that hardness increases with an increase in tool rotational speed until 1200, after which it shows a diminishing pattern. At higher tool rotational speed causes more grain growth during dynamic recrystallization and decreases the microhardness. Further particle distribution and spacing between the particles affects the microhardness of material as on increasing rotational speed the inter particle distance increases leading to decrease in microhardness [177].

Table 5.9: Mechanical properties of Al-B_4C surface composites

Base Metal	102	494	21.5
Nomenclature of Sample	**Microhardness (HV)**	**Ultimate Stress (MPa)**	**Total Elongation (%)**

S1	179	364	15.2
S2	190	336	13.6
S3	187	329	11.9
S4	170	350	12
S5	185	337	10.5
S6	182	173	7.50
S7	169	241	10.8
S8	173	156	8.18
S9	171	149	7.12

The maximum average hardness was observed to be 190HV, which was obtained from the sample processed at 1200 rpm. This was followed by 187HV, obtained from the sample processed at 1400 rpm, and then 169HV which was obtained from the sample processed at 1000 rpm. The least average hardness for obvious reasons was of the base alloy, numerically of the order of 102HV. Due to the uniform distribution of nanoparticles at tool rotational speed 1000 to 1200rpm, results obtained increases in microhardness, but after tool rotational speed 1200 to 1400rpm microhardness has slightly decreased due to bad material flow and nanoparticles agglomeration. When the heat input exceeds a certain level and causes more tool wear and insufficient material flow, so tool wear is related to both tool geometry and high tool rotational speed. Similar results have been reported by Molla Ramezani et, al. [180].

5.3.2 Tensile properties

Friction stir processing was carried out on the self-assembled monolayer (SAM) processed surface of Al alloy at three different tool rotation speed viz. 1000 rpm, 1200 rpm, and 1400 rpm. After the fabricated surface composites through FSP, the samples are presented in fig. 5.15(a, b) were cut orthogonal to the processed region using a wire EDM setup. The tensile composite samples before and after testing and tensile sample prepared according to the ASTM standard E8M are shown in fig. 5.16 (a-c).

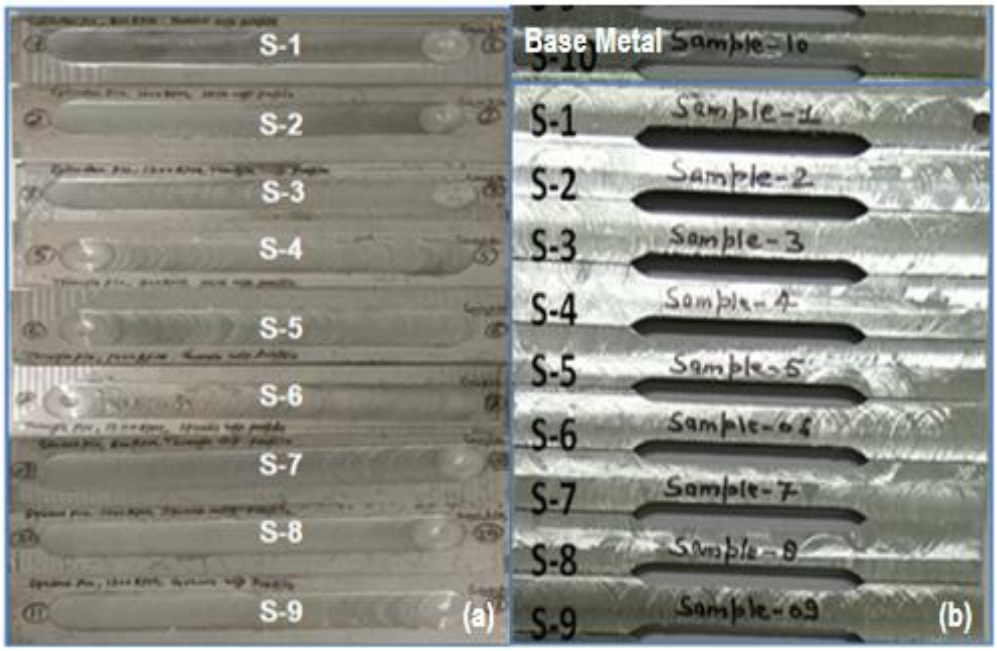

Figure 5.15-(a) FSPed samples (b) Tensile samples

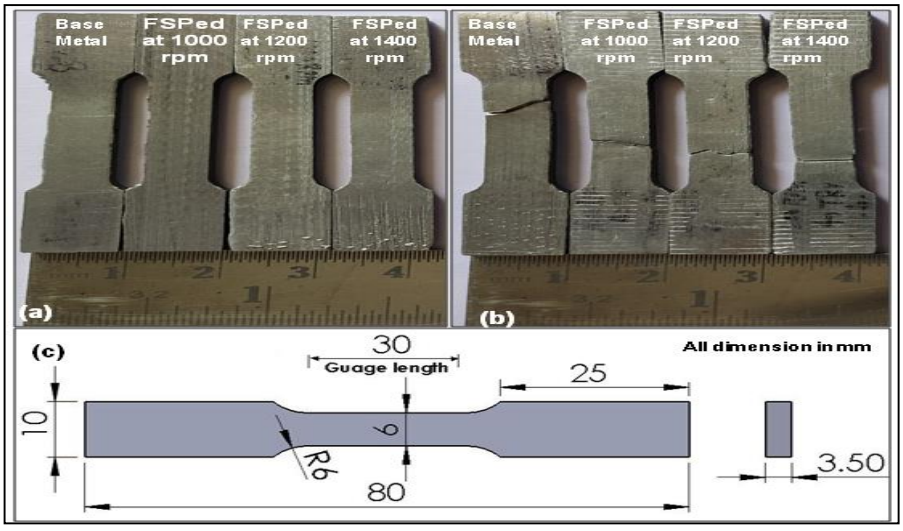

Figure 5.16-Tensile samples (a) Before fracture (b) After fracture

As the rotational speed of the FSP was incremented, it was observed that the microhardness value of the sample increased as shown in fig. 5.17. Subsequently, a decrease in the percentage elongation of the sample was observed. Yuvaraj et al. [99] have reported that percentage elongation increases when FSP was performed without particle one pass. However, the presence of hard nanoparticle in the current study contributes to decreasing the ductility of the nano surface composites. Fig. 5.18 shows the Ultimate tensile strength (UTS) and % Elongation of the surface composite samples also decreased in a similar manner due to the uniform distribution of B_4C nanoparticles, which increases the microhardness, causes a

decrease in grain size in the surface composite. The microhardness and tensile results of surface composites are presented in table 5.9.

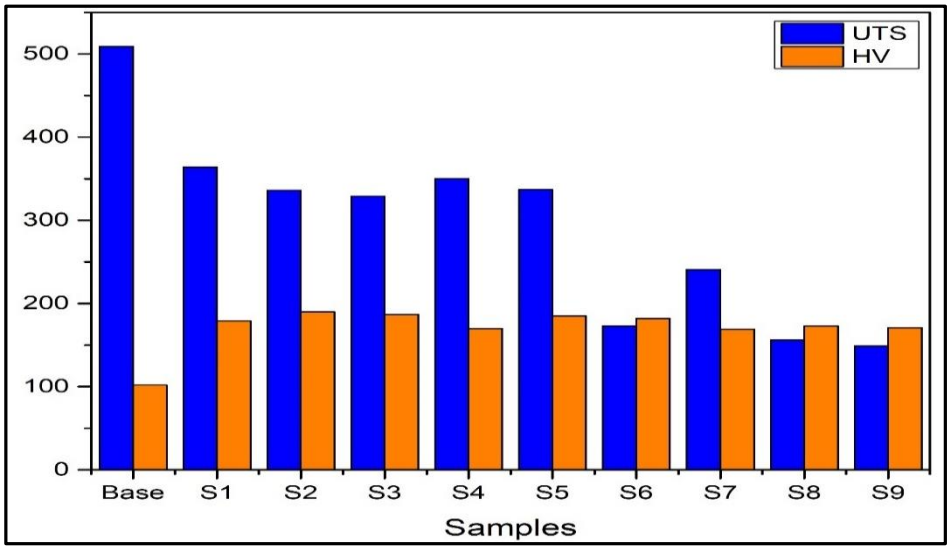

Figure 5.17-Ultimate tensile strength and Microhardness

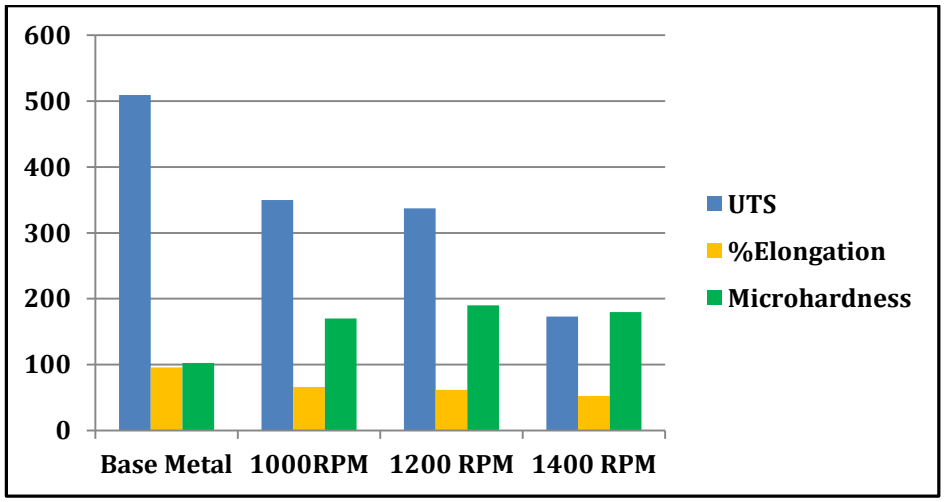

Figure 5.18-The effect of tool rpm on the Ultimate tensile strength, %Elongation and Microhardness

Fig. 5.19 shows a typical stress-strain curve of the base material, FSPed without reinforcement and the FSPed samples with a 0.5 mole concentration of boron carbide nanoparticles surface composites. The tensile test result exhibited decrease in the tensile strength of the samples S1 to S9, but increase in ductility of the sample FSP without reinforcement as compared to the base metal. Surface composites samples (S1 to S9) with a 0.5 mole concentration of boron carbide nanoparticles, strength and ductility is lowest but significantly improve its hardness as compare in base metal. This reduction in strength is a

reason for grain growth that takes place during the Friction stir process. The base metal exhibited elongation of 21.5% while the FSP without reinforcement sample showed the highest elongation of 22.4%.

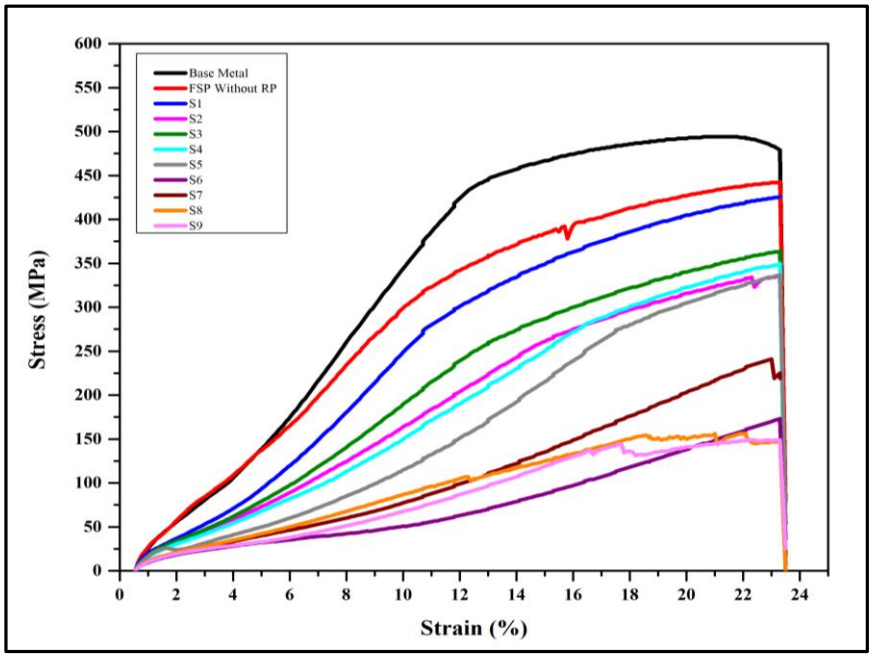

Figure 5.19-Typical stress-strain curve of samples base metal, FSPed without reinforcement particle (RPs) and FSPed with reinforcement particle (RPs) obtained from tensile test

Suri et, al. [204] have reported the effect of FSP on the mechanical properties of Al2024 alloy at 1200rpm and 1800rpm. The results pertaining to the increase and decrease in microhardness and UTS with an increment in the tool rotation speed are in-line with the ones seen in our study. Balamurugan and Mahadevan [205] investigated the effects of process parameters on the mechanical and corrosion behaviour of friction stir-claded AZ31B-magnesium alloy. They observed a uniform increase in microhardness of the FSPed sample at 500 rpm, 710 rpm, and 1000 rpm. Moustafa [206] investigated the impact of various tool rotational speeds on AA2024/Al_2O_3 and concluded that the rotational tool speed of 900 rpm improved the tensile strength after that increasing tool rpm, it shows a lower the tensile strength, and a number of passes play a significant role in improving the microhardness of the sample. The effect of tool rotation speed on the UTS of a friction stir weld stir cast AA6061–T6/AlNp composite was reported by Murugan and Kumar [207] who inferred that as a tool rotation speed increases the strength of the weld decreases and hence the value of UTS also decreases.

5.3.2.1 Fractographs analysis

Field emission scanning electron microscope (FESEM) model (ZeissSigma300) was used to examine the fracture point of a base metal, FSPed without reinforcement (RPs) samples and FSPed samples processed at different tool rotational speed. After the tensile test was carried out in UTM setup, the next stage was to cutting the sample according to the dimension of the FESEM arrangement. In fig. 5.20(a,b) FESEM fractography image with 10µm shows that the morphologies of the fracture point of base metal has a small number of dimples which indicate the maximum elongation percentage. In fig. 5.20(c,f,i) shows the fractography image with 1µm, 10µm and 20µm of the fracture point of the FSP samples processed at 1000rpm. It shows the large dimples and cleavage facets which increase the microhardness of the surface composite. In fig. 5.20(d,g,j) FESEM fractography image with 1µm, 10µm and 20µm shows the large dimples and a wide crater, which increases the microhardness of nano surface composite processed at 1200rpm. In fig. 5.20(e,h,k) the large dimples and crack formation occurred due to brittle nature of the surface composite are shown, which decrease the strength and ductility of the FSP sample processed at 1400rpm. After the fracture of the tensile test sample the area of fracture zone of the samples, which has a 0.5 mole concentration of boron carbide nano particles as reinforcement, crack formation occurred due to the brittle nature of the composite, which has significantly improved the hardness of the materials. The FESEM morphologies of nano particles reinforced surface composites exhibited finer nano particles reinforcement in the fracture zone.

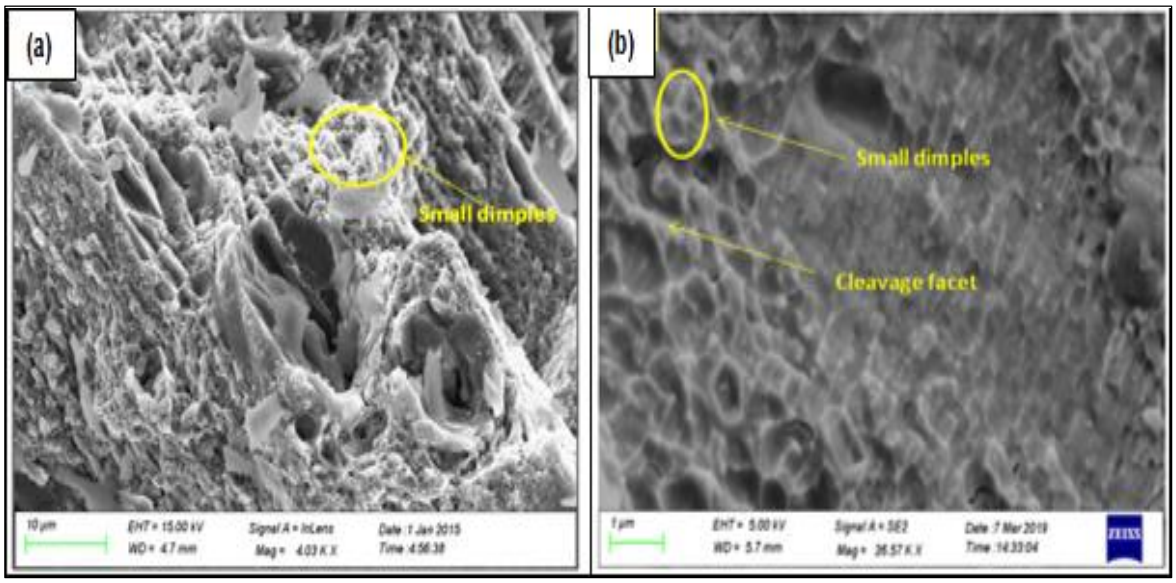

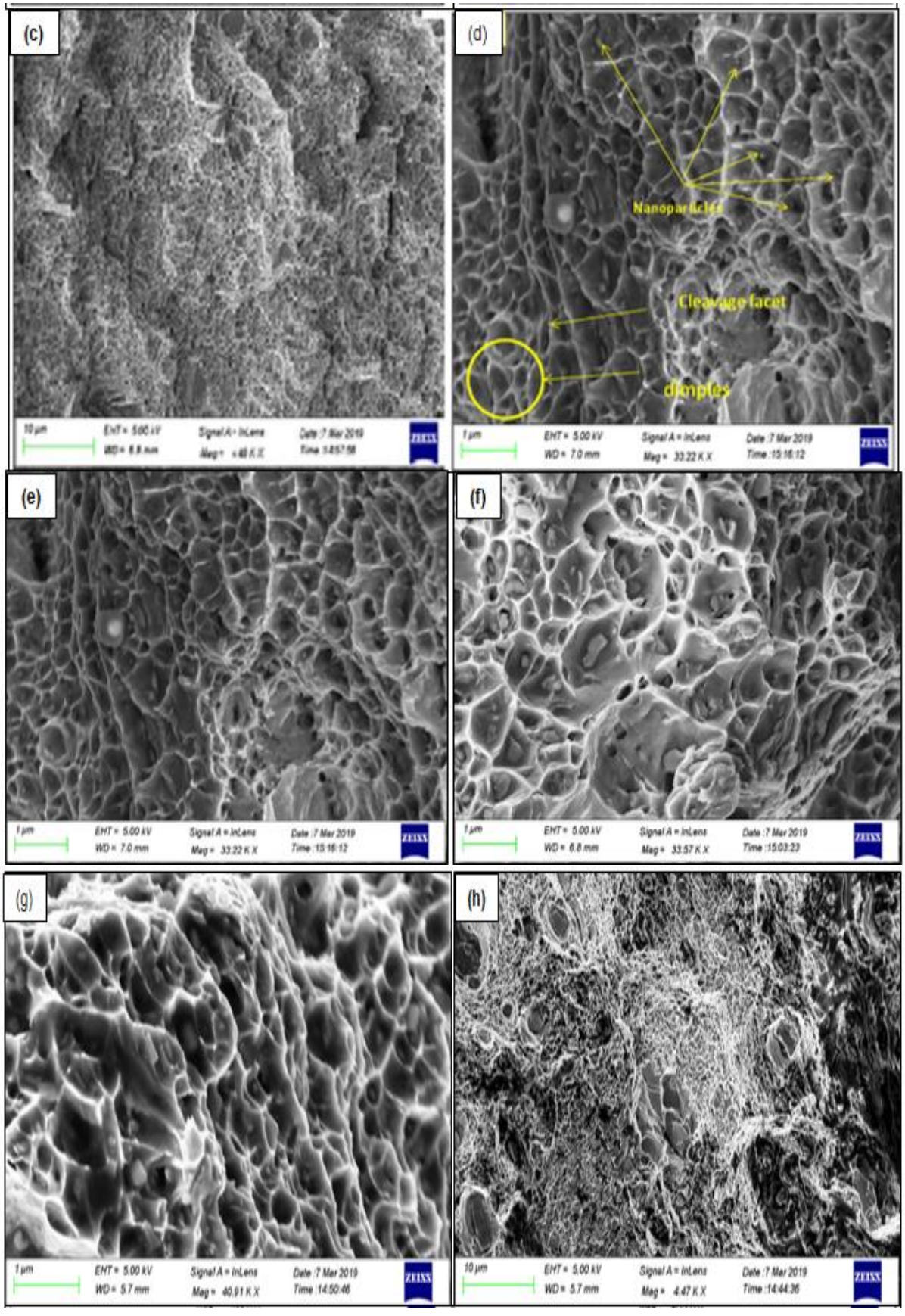
(c)
(d)
Nanoparticles
Cleavage facet
dimples
(e)
(f)
(g)
(h)

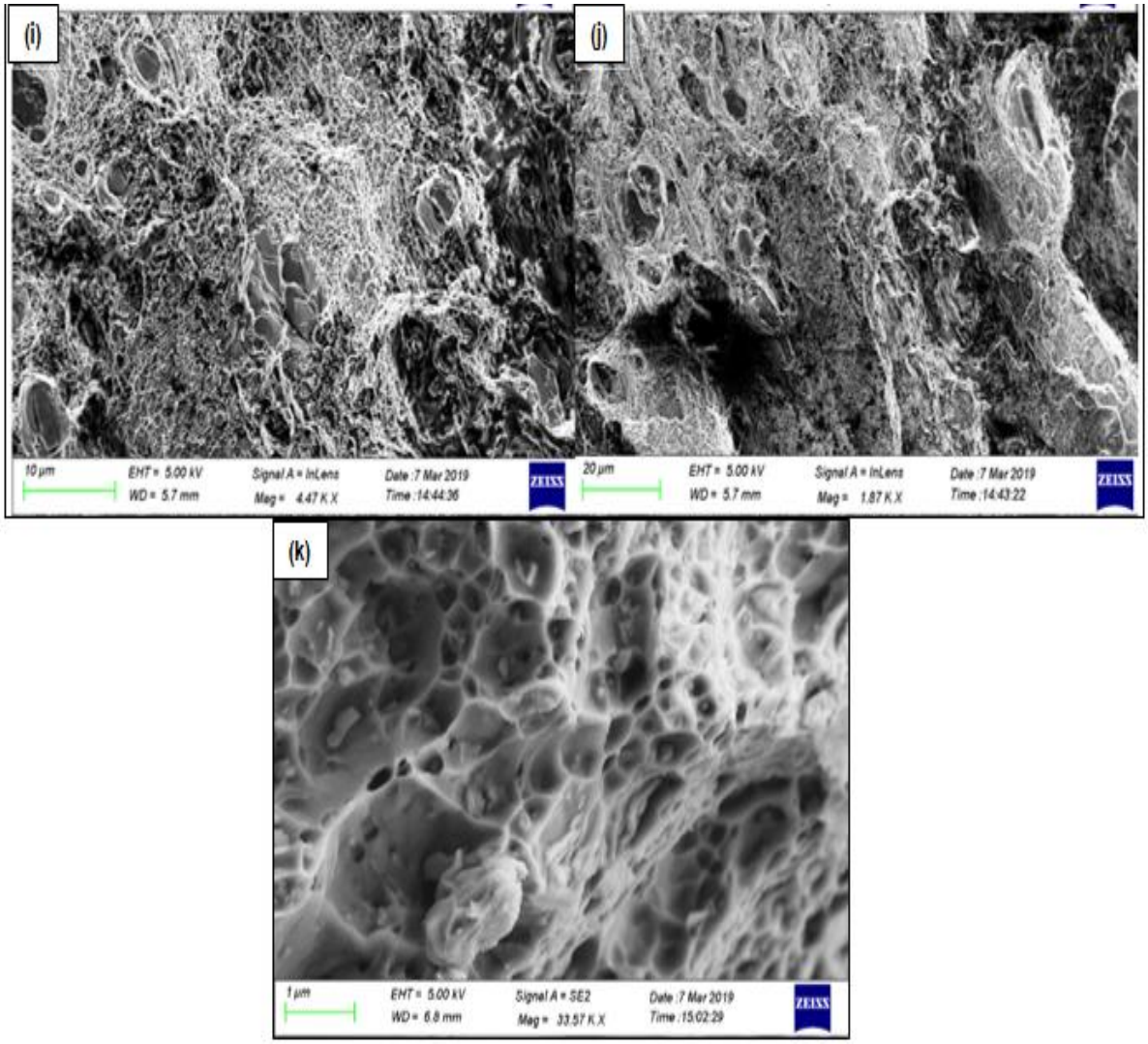

Figure 5.20-Fractographs morphologies of (a) Base metal (b) The FSPed without reinforcement particles (RPs) sample (c-k) FSPed with boron carbide reinforcement particles (RPs) samples

5.4 Residual Stresses

To measure the residual stress a non-destructive technique i.e. portable X- ray residual analyzer (PULSTEC μ-X360n) (based on cos α method), was used for the residual stress in surface composites and substrate metal with following specifications: tube voltage (30 kV), current (1 mA), source (Cr Ka/Ni Kb filter), and X-ray beam (wavelength = 2.29 Å, energy = 5.4 keV), Diffraction angle (2Theta) =139.528 deg, Crystal structure F.C.C, Young's modulus (E) =69.310 GPa, Poisson's ratio (v) =0.348. This analyzer could measure the stress efficiently by detecting the full Debye ring data from a single incident X-ray angle and Non goniometer stage influence on the measurement result. The X-ray signals and the distortion of Debye ring are automatically collected and saved in the computer. The diameter of the X-ray

exposure was 1mm, the X-ray exposure time was 30s and the X-ray incidence angle =35.0 [deg]. Residual stresses are induced during the friction stir processing due to plastic deformation of metal. This may increase or decreases the fatigue life of the fabricated composites. Hence it is very important to analyze and control it. Residual stress may be positive or negative in nature depending on the processing of the materials.

While performing XRD circular pattern was produced which is called Debye ring as depicted in fig. 5.21(a-d) along with distortion ring and XRD peak profile for base metal and friction stir processed composites at different rotational speed (1000, 1200, 1400 rpm). The concentration of residual stress are depicted by different colour mixtures such as red colour depicts maximum while blue colour represents minimum concentration [209]. On analysing diffraction intensity along the Debye ring it can be seen the intensity variation is large in case of base metal as compared to FSPed composite due to fluctuating depth of penetration of X-rays due to changing surface characteristics of base metal on the other hand less variation in intensity shows surface characteristics improvement after FSP [210, 211]. In fig. 5.21(a**)** for base metal there is a spotty distribution which depicts coarse grains in base metals and improvement can be seen in FSPed composites in fig. 5.21(b-d) due to grain refinement after FSP process [212]**.** The value of FWHM is large in base metal because of presence of high residual stress and strain while its value is less in the composite sample processed at 1000 rpm due reduction in residual stress. On the other hand FWHM increases for samples prepared at 1200 rpm and 1400 rpm due to small grain size on refinement [213]**.**

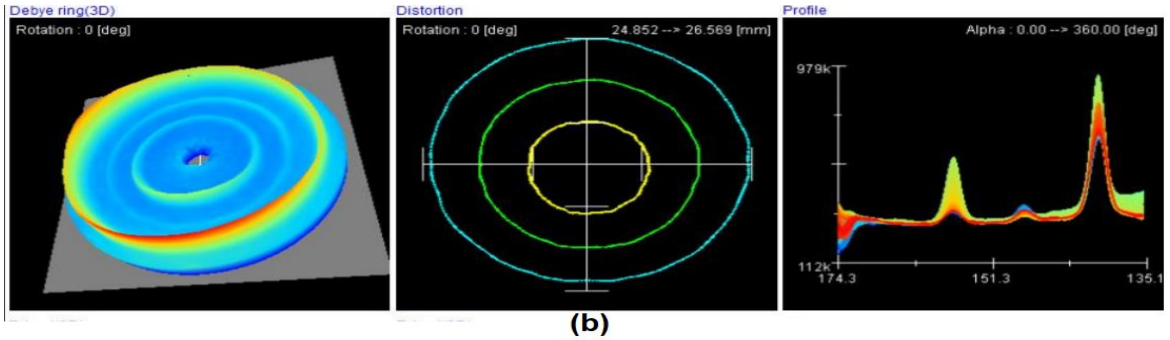

(b)

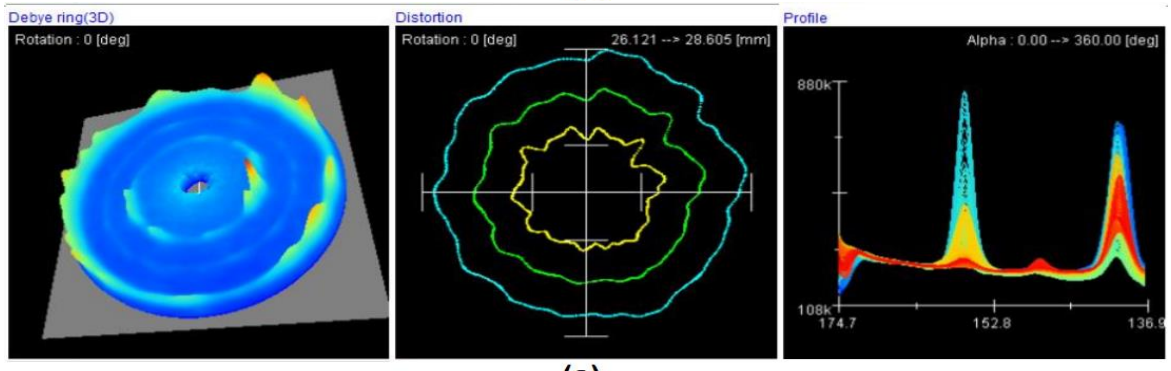

(a)

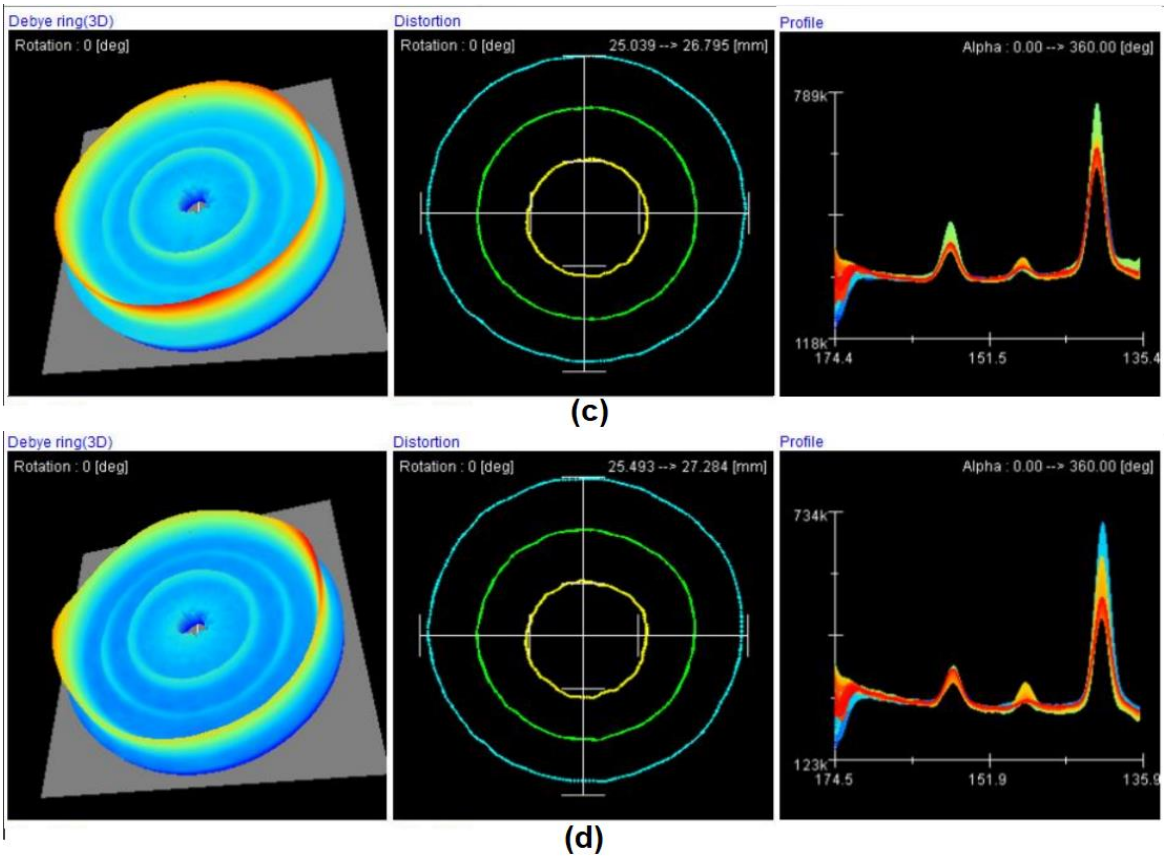

Figure 5.21-Debye ring (3D), distortion, XRD peak (a) base metal, FWHM=2 deg (b) FSPed at 1000 rpm, FWHM=1.7 deg (c) 1200 rpm, FWHM=1.75 deg (d) 1400 rpm, FWHM=1.74 deg

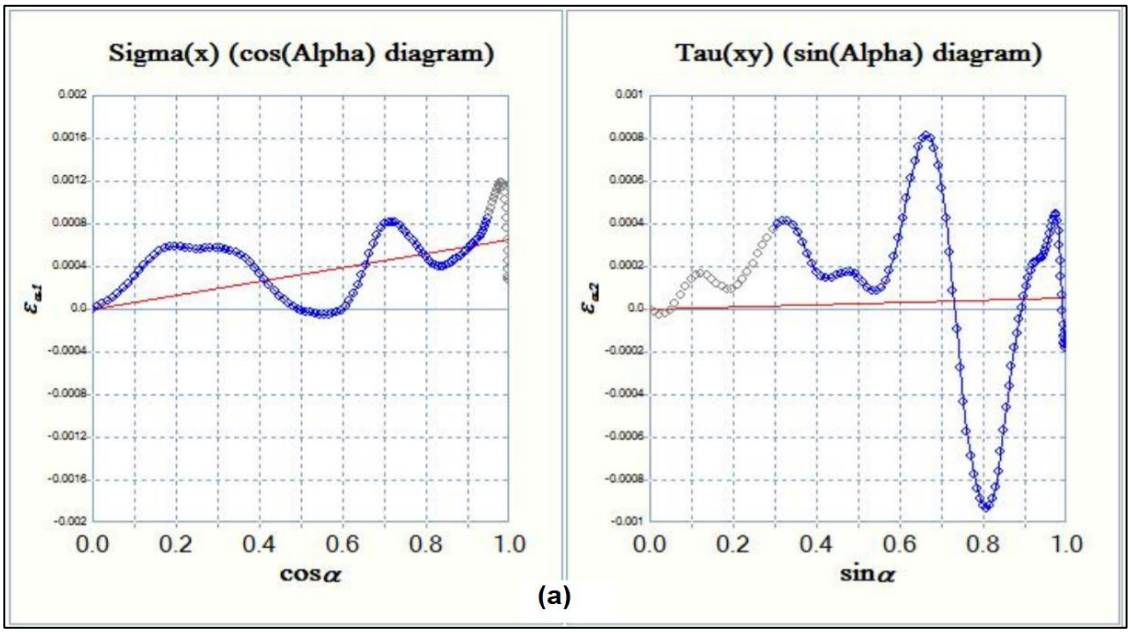

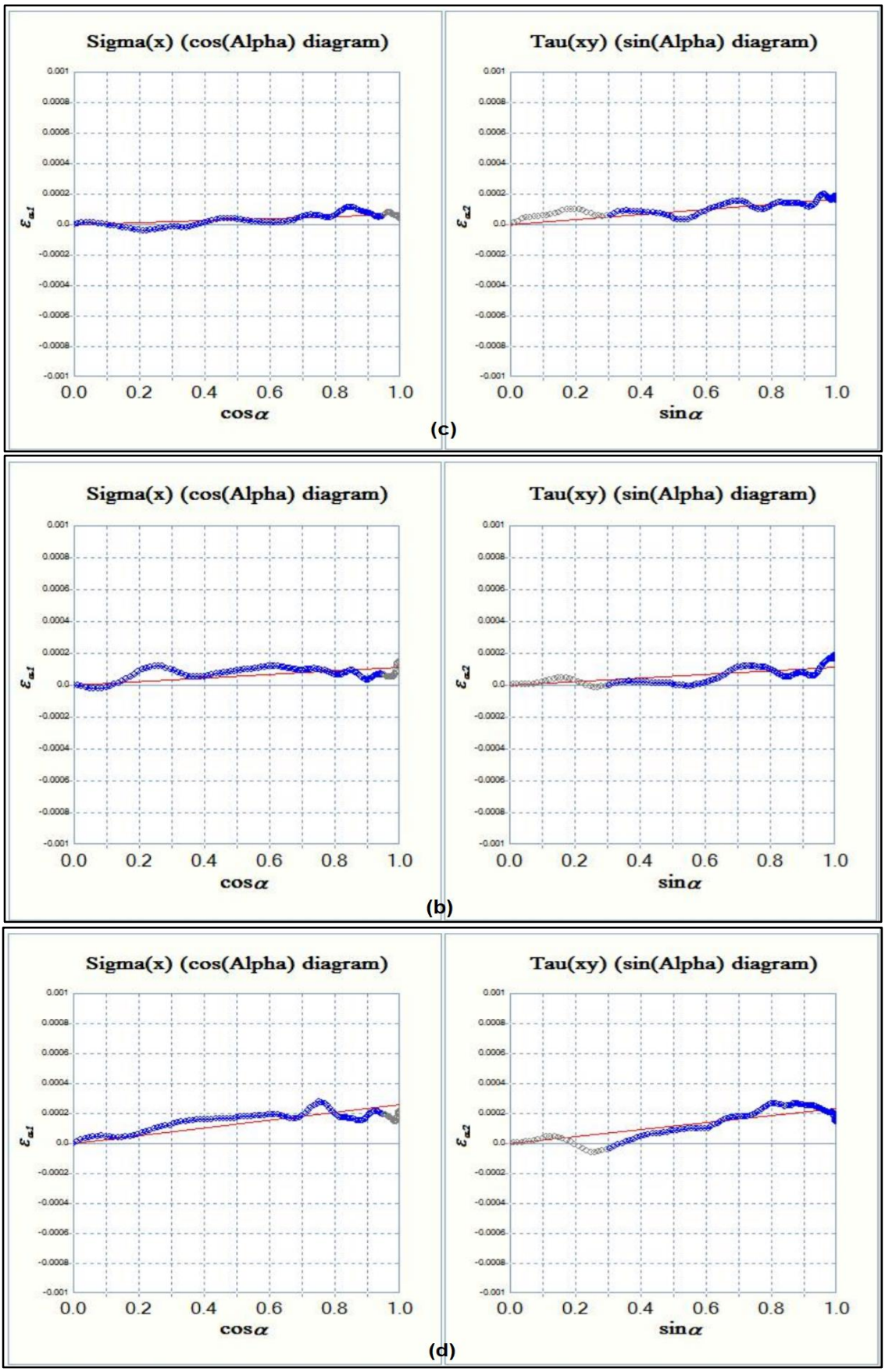

Figure 5.22- Plot of σ(x) v/s cosα, τ(xy) v/s sinα (a) base metal (b) fabricated composite at 1000 rpm (c) 1200 rpm (d) 1400 rpm

The fig. 5.22 shows the residual stress graph for the base metal and composite material**.** There is large standard deviation of residual stress in base metal due to existence of coarse grains while there is less deviation in the surface composite [214]**.** The positive slope in the graph shows the compressive nature of residual stress in all the samples. In fig. 5.23 Residual stress value of fabricated surface composites and base metal samples.

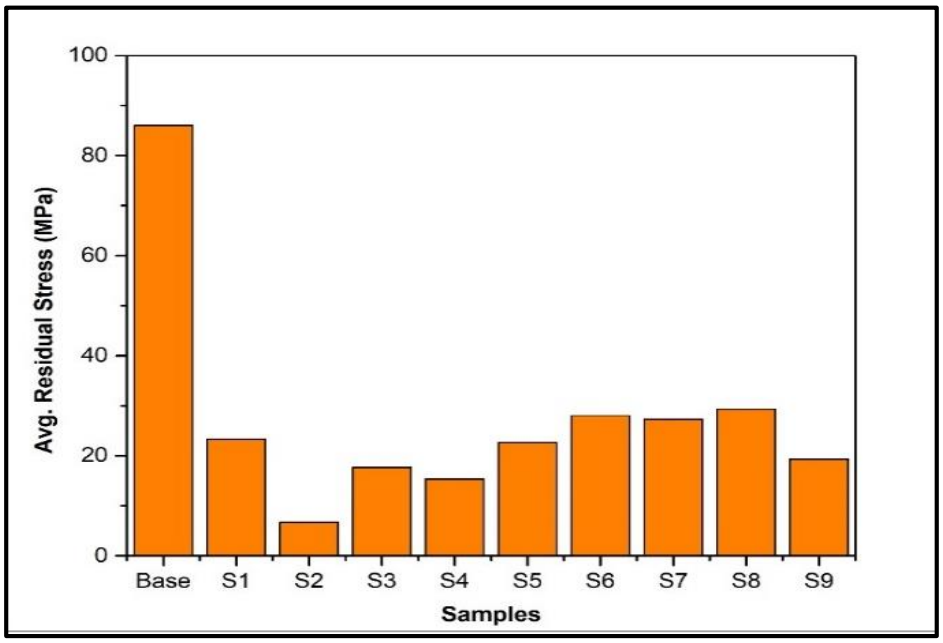

Figure 5.23-Residual stress value of fabricated surface composites and Base metal

In the research conducted by Iordachescu et, al. [215] the results of the residual stress analyses reveal that the residual stress distribution is inhomogeneous in the transverse direction of the processed layer as well as across the thickness of it. In transverse direction of the processed layer, in all specimen examined, “M” like stress distribution resulted on the plate top surface. On the FSP top surface, only compressive residual stresses were found. The maximum values of these are located at the HAZ-SZ interface. The residual stresses in other zones are smaller than these maximum values, and the parent material adjacent to the HAZ, as well as the processed layer contain small values of compressive residual stresses. With the depth increase, the “M” like stress distribution is still found at the bottom part of the processed plate, but the residual stresses values are close to those corresponding to the initial stress state of the sheet material, and are both tensile and compressive. The influence of FSP tool and process parameters, corresponding to “cold working” conditions on the residual stress distribution is explained by the increased distance between the tensile stress peaks. The magnitude of the tensile residual stresses reached in the HAZ is caused by the process heat input; the resulted wide HAZ and the lower material cooling rate produced the relatively low

magnitude of the compressive residual stresses in the processed zone. The compressive stresses can be beneficial for reducing the crack propagation speed. In the study by Weglowski et, al. [216] the effect of friction stir processing (FSP) on residual stress in a modified cast aluminium alloy AlSi9Mg is studied. The influence of rotational speed and tool type were analysed. The trepanation method was utilized to experimentally measure the residual stress. The results indicated that an increase in rotational speed causes an increase in residual stress. The region around the FSP bead was characterised by tensile residual stress fields which were balanced by compressive stresses in the parent material. A higher residual stress was observed on the advancing side than on the retreating side. Moreover, this asymmetry in residual stress distribution is due to the asymmetry in the volume of material plasticized along the advancing and retreating sides of the stir zone, generating the observed heat distribution. A higher level of residual stress was achieved with the Triflute tool than with a conventional tool. Zhao et, al. [217] conducted a research to compare the residual stresses for the parts manufactured by various metal additive process and after friction stir processing. Additive manufactured part produced via layer by layer construction leads to repeated thermal cycles and residual stresses are produced because of rapid cooling rate and large thermal gradient during manufacturing. It was observed that the FSP stir zone has comparatively low tensile stresses and rise towards the two sides of the sample and become maximum at tool shoulder edge, the residual stresses then decline and turn out to be compressive close to the two boundaries of the FSPed sample. FSP produces heat and leads to upsurge in temperature up to 80% of the melting point and residual stresses arises because of raping cooling and large thermal gradient. Khodabakhshi et, al. [218] introduced a novel processing path compounding cold gas spraying (CGS) and friction-stir processing (FSP) which was working to manufacture a compact titanium surface coating with good integrity and great mechanical property. Residual stress silhouettes presented some over-all compressive tendencies very dependent on the FSP plunge depth and transverse position. Substantial enhancement was attained by having the higher plunge depth, giving the utmost compressive residual stress amount of ~400 MPa at the forward-moving side. This may be accredited to downward materials flow instigated by the shoulder friction-stirring result.

5.5 WEAR PROPERTIES

Friction and wear can be defined as the responses of a tribological system. Coefficient of friction and wear define the state of contact of bodies not the material properties of the bodies. Aforementioned experimental data analysis between FSPed sample without (RPs) and

FSPed sample with (RPs) compared to base metal (BM) is quite distinct and characteristic. The required hypothesis of performance of FSPed sample without (RPs) and FSPed sample with (RPs) compared to base metal (BM) is keenly observed here in the wear vs. load as shown in fig. 5.24. The Friction and Wear data are in close correspondence to each other, highlighting that as load increases, friction and wear increase. FSPed sample without (RPs) and FSPed sample with (RPs) with 0.5 mole concentration of B_4C nanoparticles, here both these samples have performed better than BM in having the minimized wear, hence maximizing their durability in the quantitative process of loading the surface composite. At 20 N, the wear is quite approximately the same for FSPed sample without (RPs) and FSPed sample with (RPs) but as we progress, FSPed sample with (RPs) shows minimized wearing than FSPed sample without (RPs) sample by a safe margin showing the effectiveness of B_4C nanoparticle concentrations, whereas BM undergoes high amount of wearing which exemplifies its poor mechanical durability character. The margin of experimental wear observed here between FSPed sample without (RPs) and FSPed sample with (RPs) is appreciable using very less concentration of B_4C nanoparticles.

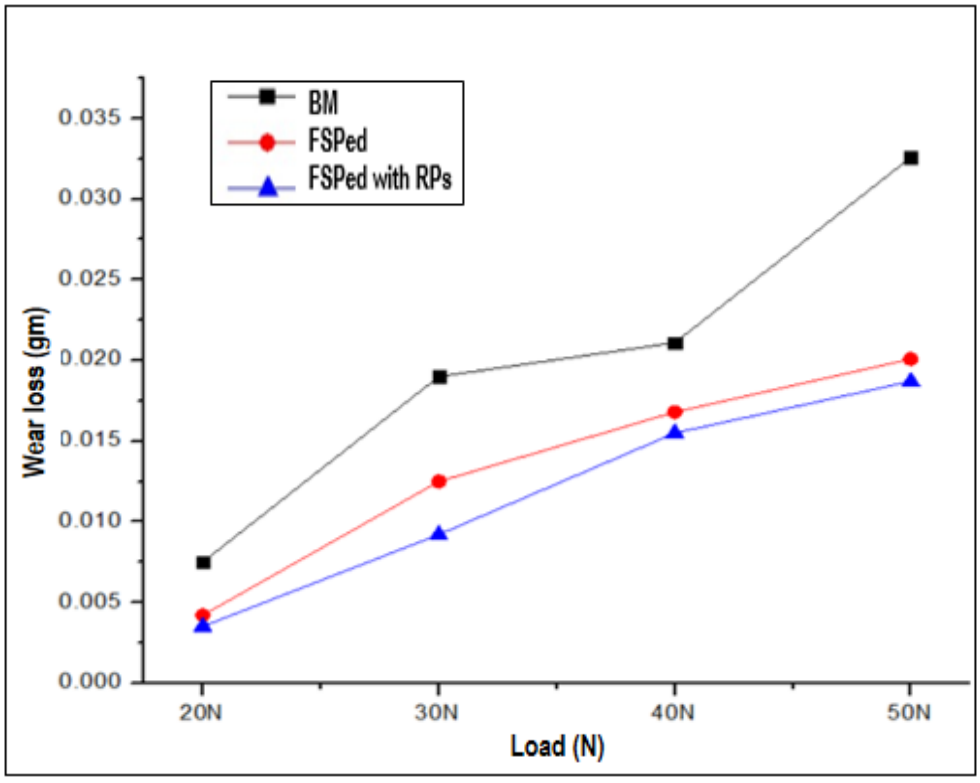

Figure 5.24-Effect of load on wear loss in gram at different sample

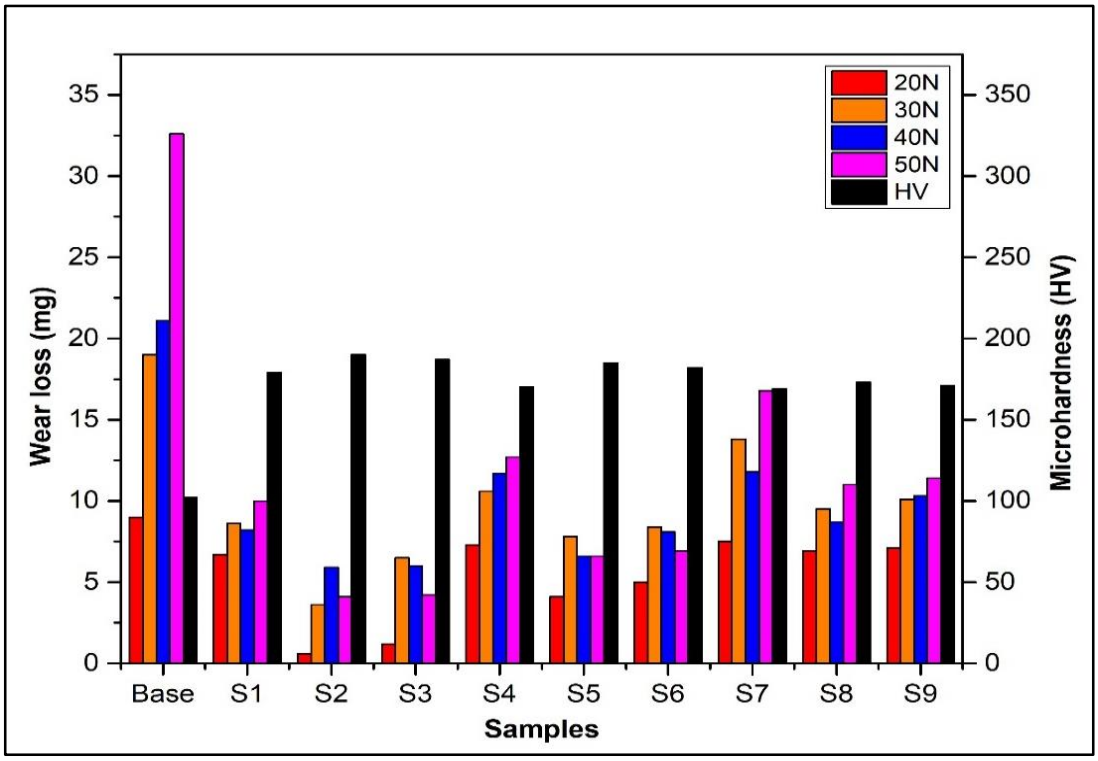

Figure 5.25-Comparison of wear loss v/s microhardness of base metal and surface Composite samples

For each of the loads i.e. 20N, 30N, 40N and 50N, the maximum wear has been observed in the base metal followed by the surface composite samples (S1, S2, and S3) at tool rotational speeds of 1000 rpm, 1200 rpm and 1400 rpm respectively. This means that wear resistance is a maximum for the FSPed sample at a tool rotation speed of 1200 rpm, followed by the FSPed sample at 1400rpm and thereafter 1000rpm. This follows the same pattern as the values from microhardness, which explains this phenomenon. As load increases wear loss increases for base metal and surface composite samples. The homogeneous dispersion of B_4C nanoparticle in the composite samples increases the hardness of the surface composite samples due to the hard B_4Creinforcement particle acts as a load bearing element. The Comparison of wear loss v/s microhardness of Base metal and surface composite samples is shown in fig. 5.25. Wear properties of the Al alloy, FSPed with reinforcement particle B_4C showed superior resistance to wear compared to unreinforced alloy**.** Anwari et, al. [219] showed this result can be attributed to the homogenous dispersion of hard B_4C particles in composite, leading to greater hardness as a result of diminishing size of grains in the Al matrix.

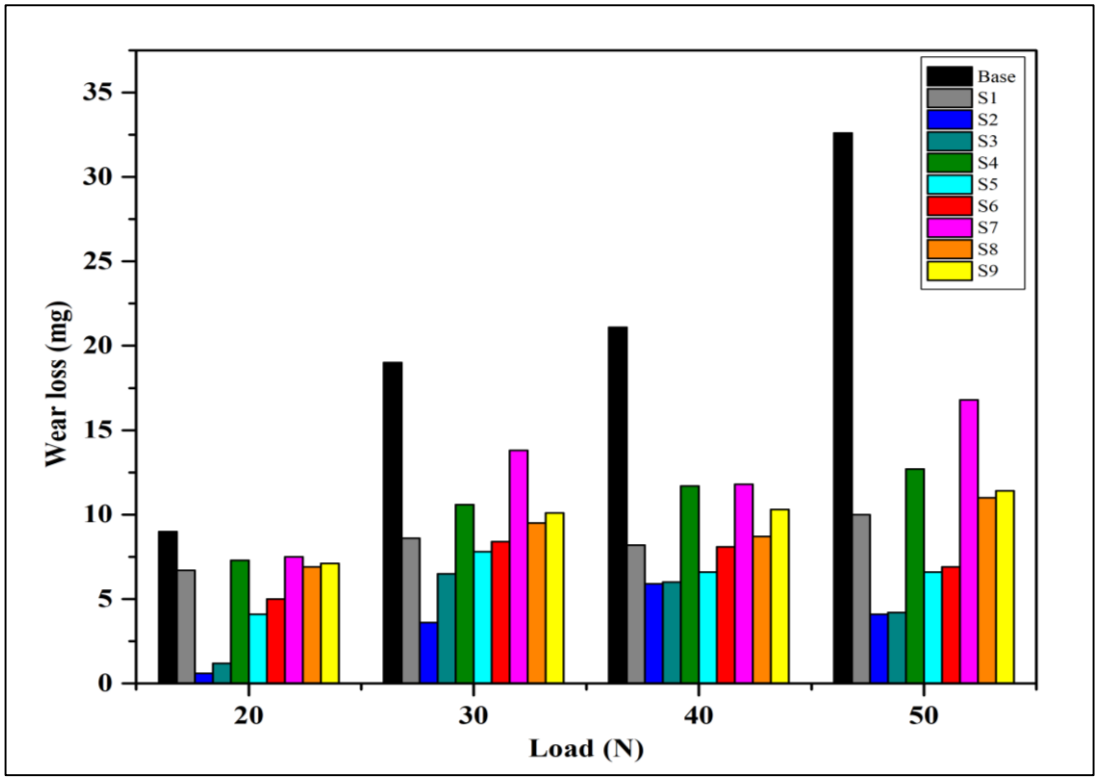

Figure 5.26-Comparison of wear loss (mg) of all the samples

The surface composite samples exhibited the lowest wear as compared to base metal alloy as shown in fig. 5.26. Composite samples have been exposed to wear tests to distinguish the wear resistance capacities of the surface composite samples and compare them with the base material just as one another to recognize the tool rotational speed as presented in table 5.1. The composite samples is attributed to higher hardness, due to the hard B_4C reinforcement particles. The improvement in the wear properties was found to be due to B_4C nanoparticles in Al5083 alloy when compared with B_4C micro particles. Nano surface composite layer was having higher wear resistance than the wear resistance of the unreinforced Al5083 alloy [99].

5.5.1 Coefficient of friction

Friction and wear are a result of complex and multiplex sets of microscopic interactions and thermo-mechanical embodiment between surfaces that are in mechanical contact and drag against each other. These synergic actions are the result of the material characteristics, the geometrical and topographical properties of the surfaces, and the accompanying physical situations under which the surfaces are subjected to the sliding action against each other, e.g., loading, temperature, atmosphere, type of contact, etc.

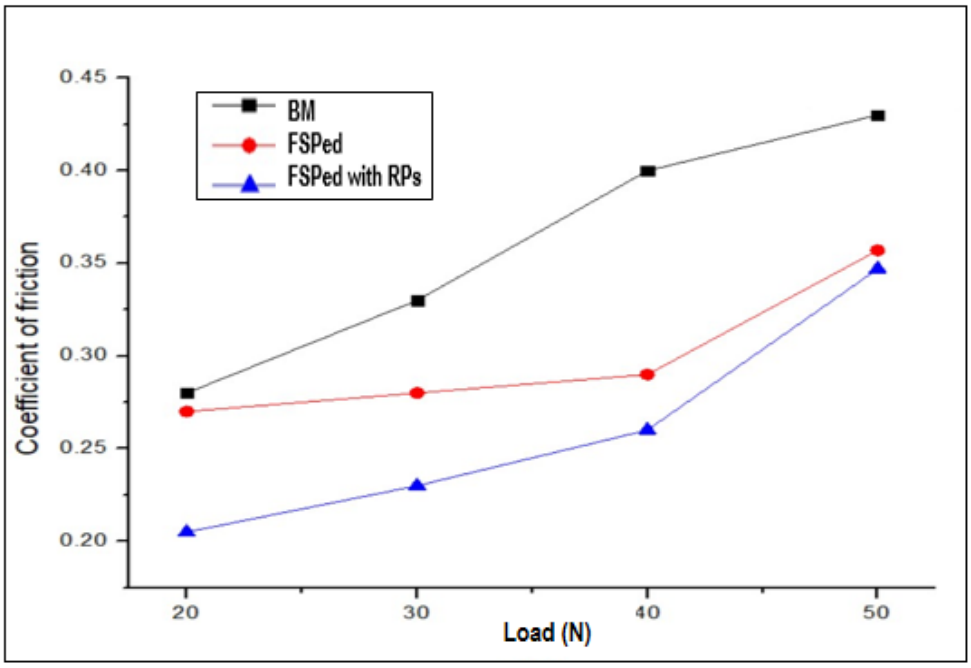

Figure 5.27-Effect of load applied on coefficient of friction at different sample

In fig. 5.27, shows the variation of the coefficient of friction of base metal (BM) and FSPed sample without reinforcement particles or with concentration of nanoparticles under four normal sliding loads. At 20N load there is large variation of friction is observed FSPed sample without reinforcement particles (RPs) and FSPed sample with reinforcement particles (RPs). The coefficient of friction samples of both the FSPed samples were lower than the base metal (BM) in all sliding loads. In base metal the coefficient of friction is linearly increase with increasing load. In the FSPed sample without reinforcement particles (RPs), initially 20N to 30N the friction coefficient is approximately same and after that friction coefficient increases with increasing load. In FSPed sample with reinforcement particles (RPs) with 0.5 moles concentration of B_4C nanoparticles, coefficient of friction value with gradually increase with increasing load is observed due to the formation of homogeneous distribution of nanoparticles.

It is observed from the fig. 5.28, that friction coefficient decreases with increases in sliding distance but on comparison of friction coefficient for base metal, FSPed sample without reinforcement particles (RPs) and FSPed sample with reinforcement particles (RPs) with 0.5 mole concentration of B_4C nanoparticles. It is also, observed that there is large fluctuation in FSPed sample with (RPs), due to the formation of hard particles in the surface composite. The friction coefficients of FSPed sample with (RPs) are lower than those of base metal alloys sample and FSPed sample without (RPs).

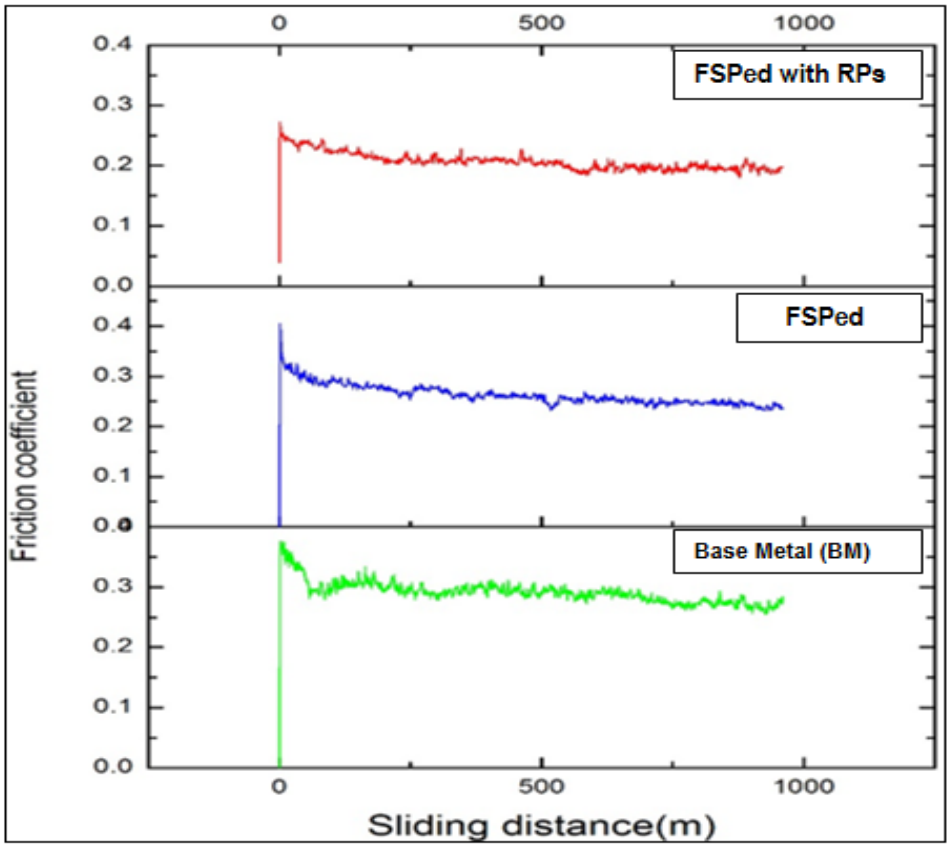

Figure 5.28-Variation of friction coefficient on sliding distance at different sample

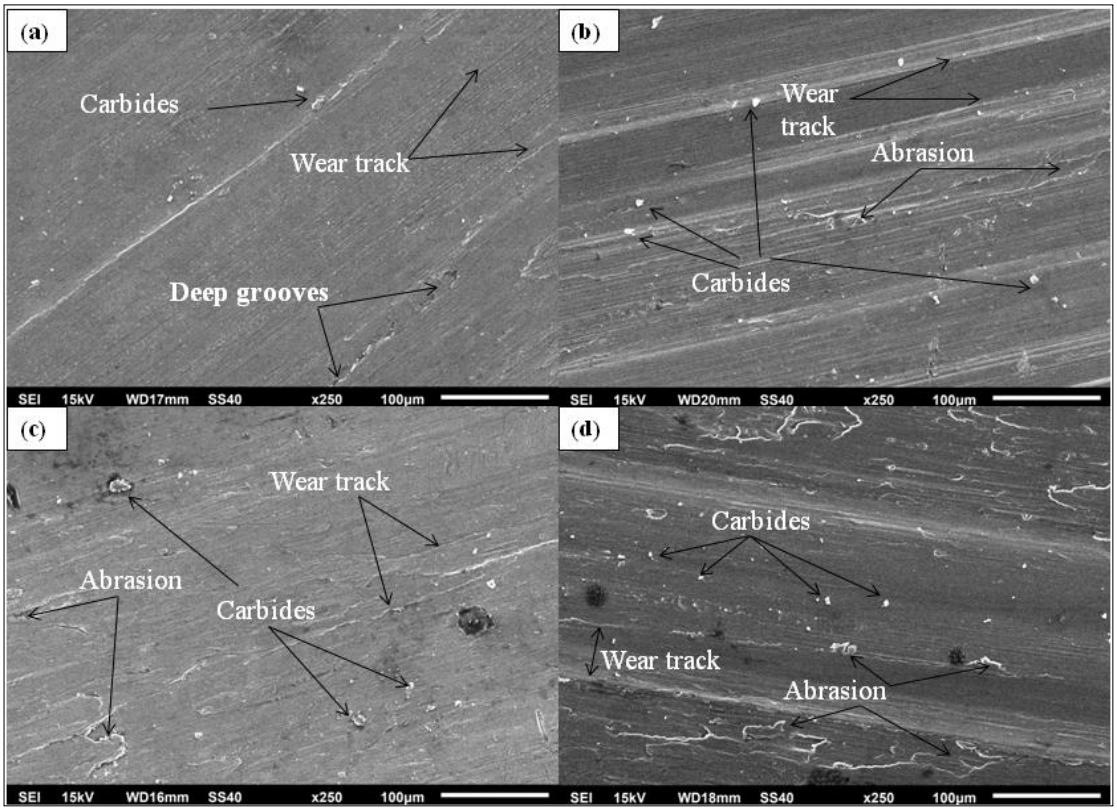

Figure 5.29-Worn-out surface morphology at 20N load (a) Base metal (b) FSPed sample at 1000 rpm (c) FSPed sample at 1200rpm (d) FSPed sample at 1400 rpm

In fig. 5.29 represents the SEM images of the worn out surface of base metal alloys and surface composite samples. The deeper groove due to high material removal has been seen in the fig. 5.29(a), base metal. While comparatively smaller scratches and carbides are seen on the other three FSPed samples process at 1000rpm 1200rpm and 1400rpm. The finer and thinner scratches in fig. 5.29(b-d) represents the difficulty in material removal due to homogeneous distribution of boron carbide nanoparticles in the FSPed sample with (RPs), 0.5 mole concentration of B_4C nanoparticles. As also seen from the wear results in the fig. 5.26 previous discussions, the base metal has the highest wear loss after that the wear loss has decrease in the FSPed samples with (RPs) at 1000rpm, 1200rpm and 1400rpm. In fig. 5.30(a-d) at 20N load and fig. 5.30(a-d) the wear tracks and carbides can be seen. It was found that the main wear mechanism is adhesive and abrasive. These results are supported by [220–222]. At high tool rotation speed at 1400rpm causes more heat and more material flow and, the tool wear effects in the material flow play a dominant role and causes poor material flow and the results nanoparticles agglomeration and make the wear properties decreases. But the wear of tool with triangular and square pin profile was much faster than the other tools pin profiles which was showed by Li et, al. [223].

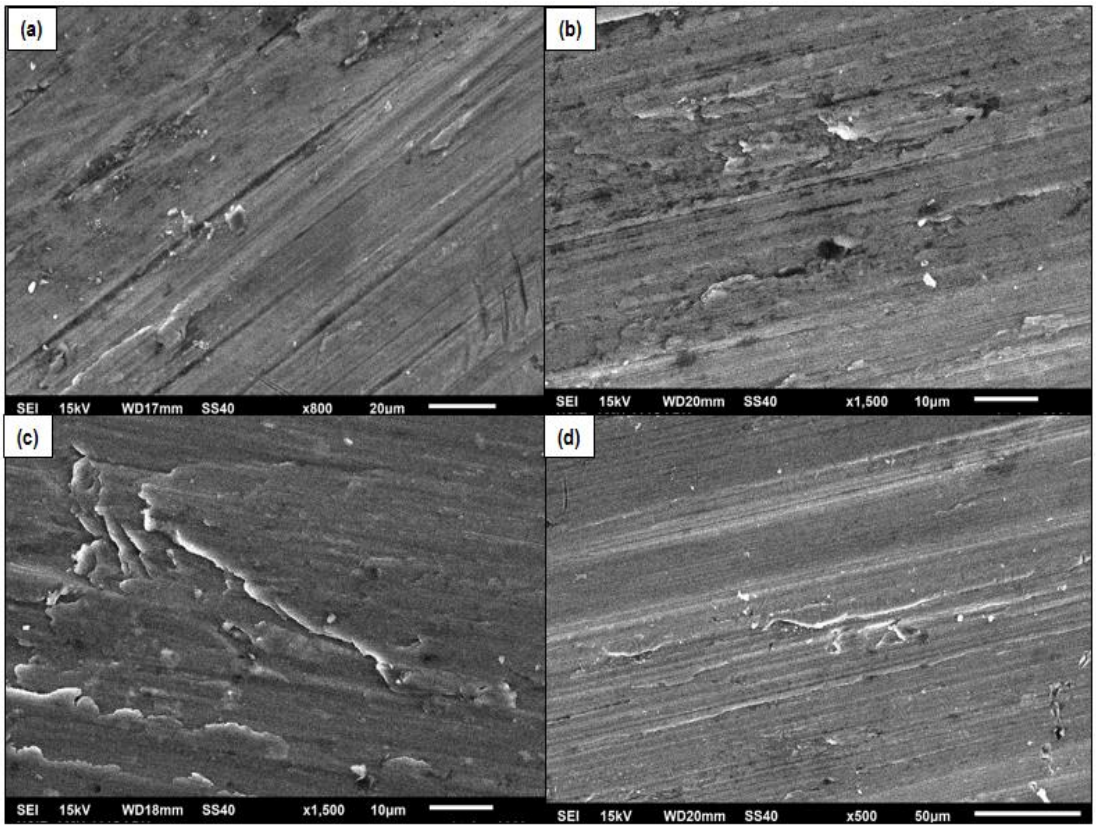

Figure 5.30-Worn-out surface morphology at 50N load (a) Base metal (b) FSPed sample at 1000 rpm (c) FSPed sample at 1200rpm (d) FSPed sample at 1400 rpm

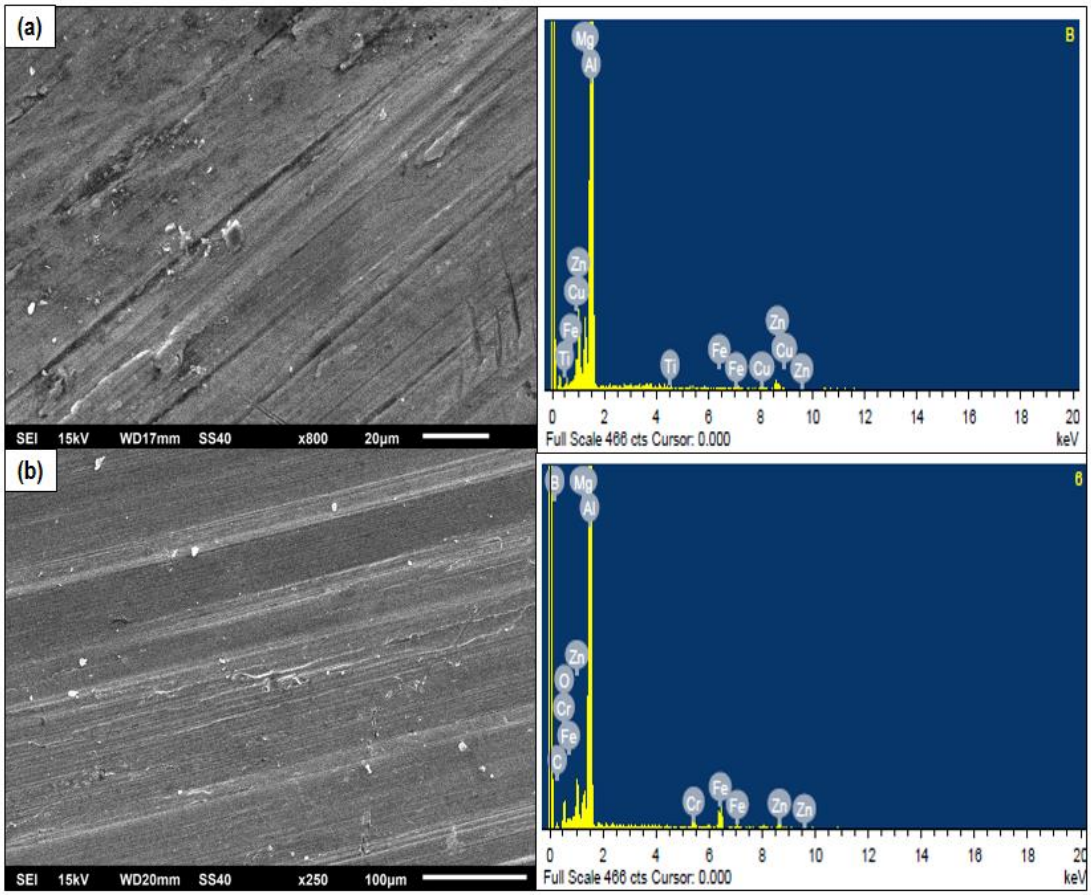

Figure 5.31- SEM with EDS Profile of worn-out surface (a) Base metal (b) FSPed sample with Reinforcement particles (RPs)

The SEM with EDS profile of a worn-out surface of base material and the FSPed sample with Reinforcement particles (RPs) at 50N load are shown in fig. 5.31(a,b) respectively. The primarily peaks of aluminum alloy with oxygen and iron peaks are observed.

5.6 SUMMARY

This chapter details upon the findings of the various mechanical, microstructural and tribological testing done on the Friction stir processed surface composite. Taguchi and ANOVA were used to determine the factor affecting the microhardness and UTS of the surface composite, as well as determine their optimum processing values. It was found that Tool Traverse Speed has a higher influence on both the properties and the optimum processing parameters for UTS are 40mm/min and 1000 rpm while for microhardness they are 40mm/min and 1200 rpm. After this, confirmatory tests were conducted for both these properties and the effect of tool traverse speed, tool rotational speed and tool pin profile were investigated thoroughly. The mechanical characterization of the fabricated Al-B_4C surface composite was also done. The microstructure of the FSPed samples were studied and

compared in order to justify the change in properties on the basis of microstructural changes. The microhardness, tensile strength as well as the Fractographs after tensile testing were studied for the same.

For the characterization of these samples, SEM/EDX and XRD analysis of the samples was done to observe the homogeneous distribution of the reinforcement particles and to identify the phase of the nanoparticles in the surface composite respectively.

The residual stresses of the surface composite were studied as well. The residual stresses decreased after Friction stir processing primarily due to the resultant grain refinement. The Debye rings and the variation in their intensity were used to make the given conclusions.

In the end, the wear properties of the samples were tested using a pin-on-disc tribometer. The variation of wear with regards to changing loads was studied. The base metal showed the maximum wear while the surface composite had a significantly improved wear resistance. The coefficient of friction for these samples was also studied. The main wear mechanisms were adhesive and abrasion. The coefficient of friction increased with increasing load, but was altogether less than the corresponding base metal sample.

CHAPTER 6
CONCLUSIONS AND FUTURE SCOPE

6.1 CONCLUSIONS

The surface modification of the AA7075 substrate using B_4C nanoparticles reinforcement has been carried out successfully. In the present research work we have fabricated the surface composite with minimizing the hard B_4C nanoparticles using Self-assembled monolayer (SAM) followed by fabrication surface composite through a relatively new solid-state processing technique i.e.FSP method. Hence, researchers have not reported the surface modification of AA7075 processed through Self-assembled monolayer (SAM) technique using B_4C nanoparticles reinforcement mixed with Di-ethyl ether (DEE) followed by Friction stir processing.

The preliminary trials were useful in selecting the levels and factor of FSP process parameters using design of experiments. The optimization of maximizing the hardness and UTS was carried out through Taguchi approach.

After the Friction stir processed of AA7075/B_4C nanoparticle surface composite has been processed through Self-assembled monolayer technique various mechanical, microstructural and tribological testing has been done. This work has also underscored on the impacts of tool rotational speed in the FSP procedure on the mechanical and wear resistance of the prepared surface composite.

An experimental and simulation study was carried out on residual stresses developed due to the machining of H13 tool steel. The specimens were made in the shape of FSP tool with two different probes i.e. circular, taper circular. The following conclusions have been derived from the present research work.

1. The residual stress measured by X-Ray stress analyzer was found to be maximum in a tapered circular and least in circular probe profile. This can be attributed to the fact that more machining processes were done in tapered circular probe in comparison to cylinder probe. The difference in residual stress between the cylinder probe and Taper cylinder probe as analyzed by X-Ray stress Analyzer was 53 MPa.

2. Experimental readings validate the simulation results for the tapered circular and circular probe with the error values lying in an acceptable range. The errors can be minimized by improving the mesh quality.
3. With the help of Taguchi technique, optimum condition was obtained to achieve the maximum value of microhardness. Increase in tool rotation speed from 1000 rpm to 1200 rpm led to increase in hardness (HV) value but further increase to 1400 rpm decreased the hardness (HV) value. Thus, 1200rpm is the optimal choice.
4. Noteworthy, uniform distribution of nanoparticles has been found in the surface composite inside the stirred zone is achieved by using FSP methodology that causes exceptional plastic deformation and recrystallization due to frictional heating and were indicative of the presence of B_4C nanoparticle.
5. The average hardness for the surface composites has been found to be more than that of the substrate (base) metal. The trend is such that hardness increases with an increase in tool rotation speed up to 1200, after which it shows a decreasing trend.
6. FESEM fractography images, EDS composition and XRD pattern confirms the presence of boron carbide nanoparticles as reinforcement particles in surface composite.
7. The FESEM and SEM micrograph of the FSPed sample with reinforcement particles at 1000, 1200 and 1400 rpm reinforced with boron carbide nanoparticles exhibit the homogeneous distribution and agglomeration of reinforcement particle. The FSPed sample with reinforcement particles obtained higher hardness as compared to the base metal (BM) hardness.
8. Significant grain refinement occurs in the FSP procedure to the intense plastic deformation recrystallization, which occurs due to frictional heating during FSP. This results in the generation of a recrystallized fine-grained microstructure within the stirred zone.
9. Frictional and wear analysis highlights the mechanical durability and surface characteristics of base metal, FSPed sample without reinforcement particles(RPs) and FSPed sample with reinforcement particles(RPs).
10. Experimental data suggests that FSPed sample with reinforcement particles (RPs) has the least wearing and frictional coefficient due to the effective application and processing of B_4C nanoparticles compared to FSPed sample without reinforcement particles (RPs). Base metal has been reported to have least durability and highest frictional coefficient.

11. For the 20, 30, 40 and 50N load, as tool rotation speed increases from 1000 rpm to 1200 rpm, the wear resistance increases, after which a decrease in wear resistance is observed at 1400 rpm due to bad material flow and nanoparticle agglomeration.

6.2 FUTURE SCOPE

1. Fabrication of surface composite with minimizing the reinforcement particles through Self-assembled monolayer (SAM) followed by FSP can be applied to other alloy and combination of hybrid reinforcement particles in order to obtained better mechanical properties of the materials.
2. Further investigations on increasing the concentration of reinforcement particles and the effect of higher concentration of reinforcement particles on mechanical microstructure and wear properties of the fabricated composite might be advantageous.
3. Though many models have been made to characterize mechanical and wear properties of fabricated composite, not many studies have used of optimization techniques like ANN and RSM. There's a lot of scope to consider the various process parameters of FSP and study their impact on the characteristics of the thus fabricated composites.
4. More thickness Al alloy plates can be processed by employing different types of tool pin profiles with multi-pass process with changed shoulder diameter.
5. Further studies may be done on the fabricated surface composites like creep, fatigue strength and bending strength tests.

REFERENCES

[1] O. N. Çelik, M. Ulutan, H. Gaşan, Ü. Er, and S. Buytoz, "Effects of graphite content on the microstructure and wear properties of an AISI 8620 steel surface modified by tungsten inert gas (TIG)," *Surf. Coatings Technol.*, vol. 206, no. 6, pp. 1423–1429, Dec. 2011, doi: 10.1016/j.surfcoat.2011.09.009.

[2] A. de Damborenea, J., Navas, C., García, J., Arenas, M., & Conde, "Corrosion–erosion of TiN-PVD coatings in collagen and cellulose meat casing," *Surf. Coatings Technol.*, vol. 201, no. 12, pp. 5751–5757, 2007, doi: 10.1016/j.surfcoat.2006.10.009.

[3] A. Fotovvati, B., Namdari, N., & Dehghanghadikolaei, "On Coating Techniques for Surface Protection: A Review," *J. Manuf. Mater. Process.*, vol. 3, no. 1, p. 28, 2019, doi: 10.3390/jmmp3010028.

[4] A. Prengel, H., Pfouts, W., & Santhanam, "State of the art in hard coatings for carbide cutting tools," *Surf. Coatings Technol.*, vol. 102, no. 3, pp. 183–190, 1998, doi: 10.1016/s0257-8972(96)03061-7.

[5] T. Tański and K. Labisz, "Electron Microscope Investigation of PVD Coated Aluminium Alloy Surface Layer," *Solid State Phenom.*, vol. 186, pp. 192–197, Mar. 2012, doi: 10.4028/www.scientific.net/SSP.186.192.

[6] R. K. Annavarapu, S. Kim, M. Wang, A. J. Hart, and H. Sojoudi, "Explaining Evaporation-Triggered Wetting Transition Using Local Force Balance Model and Contact Line-Fraction," *Sci. Rep.*, vol. 9, no. 1, p. 405, Dec. 2019, doi: 10.1038/s41598-018-37093-6.

[7] H. Sojoudi *et al.*, "Stable Wettability Control of Nanoporous Microstructures by iCVD Coating of Carbon Nanotubes," *ACS Appl. Mater. Interfaces*, vol. 9, no. 49, pp. 43287–43299, Dec. 2017, doi: 10.1021/acsami.7b13713.

[8] S. K. Nemani and H. Sojoudi, "Barrier Performance of CVD Graphene Films Using a Facile P3HT Thin Film Optical Transmission Test," *J. Nanomater.*, vol. 2018, pp. 1–11, 2018, doi: 10.1155/2018/9681432.

[9] H. Sojoudi *et al.*, "Micro-/Nanoscale Approach for Studying Scale Formation and Developing Scale-Resistant Surfaces," *ACS Appl. Mater. Interfaces*, vol. 11, no. 7, pp. 7330–7337, Feb. 2019, doi: 10.1021/acsami.8b18523.

[10] K. K. Gleason, "Overview of Chemically Vapor Deposited (CVD) Polymers," in *CVD Polymers*, Weinheim, Germany: Wiley-VCH Verlag GmbH & Co. KGaA, 2015, pp. 1–11.

[11] A. Z. Abidin *et al.*, "Preparation and characterization of CVD-TiN-coated carbon fibers for applications in metal matrix composites," *Thin Solid Films*, vol. 589, pp. 479–486, Aug. 2015, doi: 10.1016/j.tsf.2015.06.022.

[12] M. Mori *et al.*, "Development of long YBCO coated conductors by multiple-stage CVD," *Phys. C Supercond. its Appl.*, vol. 445–448, pp. 515–520, Oct. 2006, doi: 10.1016/j.physc.2006.04.046.

[13] A. Ramanathan, P. K. Krishnan, and R. Muraliraja, “A review on the production of metal matrix composites through stir casting – Furnace design, properties, challenges, and research opportunities,” *J. Manuf. Process.*, vol. 42, pp. 213–245, Jun. 2019, doi: 10.1016/j.jmapro.2019.04.017.

[14] L. Pawlowski, *The Science and Engineering of Thermal Spray Coatings*, 2nd ed. Hoboken, NJ, USA: John Wiley & Sons, 2008.

[15] A. Tyagi, R. S. Walia, and Q. Murtaza, “Tribological behavior of HVOF carbon coating for wear resistance applications,” *Mater. Res. Express*, vol. 6, no. 12, p. 125606, Nov. 2019, doi: 10.1088/2053-1591/ab555d.

[16] S. Kumar, R. Singh, and M. S. J. Hashmi, “Metal matrix composite: a methodological review,” *Adv. Mater. Process. Technol.*, vol. 6, no. 1, pp. 13–24, Jan. 2020, doi: 10.1080/2374068X.2019.1682296.

[17] S. Abedrabbo *et al.*, “Ion beam mixing for processing of nanostructure materials,” *J. Electron. Mater.*, vol. 35, no. 5, pp. 834–839, May 2006, doi: 10.1007/BF02692536.

[18] Q. Su, F. Wang, B. Cui, M. A. Kirk, and M. Nastasi, “Temperature-dependent ion-beam mixing in amorphous SiOC/crystalline Fe composite,” *Mater. Res. Lett.*, vol. 4, no. 4, pp. 198–203, Oct. 2016, doi: 10.1080/21663831.2016.1174164.

[19] G. S. Was, “Ion beam modification of metals: Compositional and microstructural changes,” *Prog. Surf. Sci.*, vol. 32, no. 3–4, pp. 211–332, Jan. 1989, doi: 10.1016/0079-6816(89)90005-1.

[20] F. Machalett and P. Seidel, “Focused Ion Beams and Some Selected Applications,” in *digital Encyclopedia of Applied Physics*, Weinheim, Germany: Wiley-VCH Verlag GmbH & Co. KGaA, 2019, pp. 1–39.

[21] G. Dearnaley, “The effects of ion implantation upon the mechanical properties of metals and cemented carbides,” *Radiat. Eff.*, vol. 63, no. 1–4, pp. 1–15, Jan. 1982, doi: 10.1080/00337578208222820.

[22] N. Yuvaraj, S. Aravindan, Vipin, "Comparison studies on mechanical and wear behavior of fabricated aluminum surface nano composites by fusion and solid state processing," *Surf. Coatings Technol.*, vol. 309, pp. 309–319, Jan. 2017. doi.org/10.1016/j.surfcoat.2016.11.076.

[23] M. Islak, S., Buytoz, S., & Karagoz, “Microstructural development on AISI 1060 steel by FeW/B_4C composite coating produced by using tungsten inert gas (TIG) process,” *Indian J. Eng. Mater. Sci.*, vol. 19, pp. 253–259, 2012.

[24] Y. Gan, D. Solomon, and M. Reinbolt, “Friction Stir Processing of Particle Reinforced Composite Materials,” *Materials (Basel).*, vol. 3, no. 1, pp. 329–350, Jan. 2010, doi: 10.3390/ma3010329.

[25] A. Kurt, I. Uygur, and E. Cete, “Surface modification of aluminium by friction stir processing,” *J. Mater. Process. Technol.*, vol. 211, no. 3, pp. 313–317, Mar. 2011, doi: 10.1016/j.jmatprotec.2010.09.020.

[26] N. A. Patil, S. R. Pedapati, O. Bin Mamat, and A. M. Hidayat Syah Lubis, “Effect of SiC/Fly Ash Reinforcement on Surface Properties of Aluminum 7075 Hybrid

Composites," *Coatings*, vol. 10, no. 6, p. 541, Jun. 2020, doi: 10.3390/coatings10060541.

[27] R. Butola, L. Tyagi, R. M. Singari, Q. Murtaza, H. Kumar, D. Nayak, "Mechanical and wear performance of Al/SiC surface composite prepared through friction stir processing", *Material Research Express*, Vol. 8, no. 1, pp. 016520, Jan. 2021 doi.org/10.1088/2053-1591/abd89d.

[28] M. Rosso, "Ceramic and metal matrix composites: Routes and properties," *J. Mater. Process. Technol.*, vol. 175, no. 1–3, pp. 364–375, Jun. 2006, doi: 10.1016/j.jmatprotec.2005.04.038.

[29] I. A. Ibrahim, F. A. Mohamed, and E. J. Lavernia, "Particulate reinforced metal matrix composites — a review," *J. Mater. Sci.*, vol. 26, no. 5, pp. 1137–1156, Mar. 1991, doi: 10.1007/BF00544448.

[30] A. V. Muley, S. Aravindan, and I. P. Singh, "Nano and hybrid aluminum based metal matrix composites: an overview," *Manuf. Rev.*, vol. 2, p. 15, Aug. 2015, doi: 10.1051/mfreview/2015018.

[31] R. S. Mishra, Z. Y. Ma, and I. Charit, "Friction stir processing: A novel technique for fabrication of surface composite," *Mater. Sci. Eng. A*, vol. 341, no. 1–2, pp. 307–310, 2003, doi: 10.1016/S0921-5093(02)00199-5.

[32] R. Butola, Q. Murtaza, and R. M. Singari, "Formation of Self-Assembled Monolayer and Characterization of AA7075-T6/B 4 C Nano-ceramic surface composite using Friction Stir Processing," *Surf. Topogr. Metrol. Prop.*, vol. 8, no. 2, p. 025030, Jun. 2020, doi: 10.1088/2051-672X/ab96db.

[33] R. Butola, R. M. Singari and Q. Murtaza, "Mechanical and wear behaviour of Friction stir processed surface composite through Self-Assembled Monolayer Technique. *Surface Topography: Metrology and Properties"*, Vol. 8, no. 4, pp. 045007, June. 2020, doi.org/10.1088/2051-672X/abbcb8

[34] R. T.P.D., R. Pillai, and C. Pai, "Reinforcement coatings and interfaces in aluminium metal matrix composites," *J. Mater. Sci.*, vol. 33, pp. 3491–3503, 1998, doi: 10.1023/A:1004674822751.

[35] M. A. Atwater, L. N. Guevara, K. A. Darling, and M. A. Tschopp, "Solid State Porous Metal Production: A Review of the Capabilities, Characteristics, and Challenges," *Adv. Eng. Mater.*, vol. 20, no. 7, p. 1700766, Jul. 2018, doi: 10.1002/adem.201700766.

[36] Y. Liu, L. F. Chen, H. P. Tang, C. T. Liu, B. Liu, and B. Y. Huang, "Design of powder metallurgy titanium alloys and composites," *Mater. Sci. Eng. A*, vol. 418, no. 1–2, pp. 25–35, Feb. 2006, doi: 10.1016/j.msea.2005.10.057.

[37] R. S. Mishra, T. R. Bieler, and A. K. Mukherjee, "Superplasticity in powder metallurgy aluminum alloys and composites," *Acta Metall. Mater.*, vol. 43, no. 3, pp. 877–891, Mar. 1995, doi: 10.1016/0956-7151(94)00323-A.

[38] G. Abouelmagd, "Hot deformation and wear resistance of P/M aluminium metal matrix composites," *J. Mater. Process. Technol.*, vol. 155–156, pp. 1395–1401, Nov. 2004, doi: 10.1016/j.jmatprotec.2004.04.223.

[39] A. M. A. E.-M. G. Abouelmagd, “Characterization of P/M aluminum composite reinforced with Fe, Ni and Ti,” in *Proceedings of the 5th International Conference on Measurement and Control of Granular Materials, XI AN China*, 2000, pp. 69–76.

[40] Tokaji, Shiota, and Kobayashi, “Effect of particle size on fatigue behaviour in SiC particulate-reinforced aluminium alloy composites,” *Fatigue Fract. Eng. Mater. Struct.*, vol. 22, no. 4, pp. 281–288, Apr. 1999, doi: 10.1046/j.1460-2695.1999.00163.x.

[41] S. J. Zhu, L. M. Peng, Q. Zhou, Z. Y. Ma, K. Kuchařová, and J. Čadek, “Creep behaviour of aluminium strengthened by fine aluminium carbide particles and reinforced by silicon carbide particulates — DS Al–SiC/Al4C3 composites,” *Mater. Sci. Eng. A*, vol. 282, no. 1–2, pp. 273–284, Apr. 2000, doi: 10.1016/S0921-5093(00)00757-7.

[42] L. Zhen and S. B. Kang, “Deformation and fracture behavior of two Al-Mg-Si alloys,” *Metall. Mater. Trans. A*, vol. 28, no. 7, pp. 1489–1497, Jul. 1997, doi: 10.1007/s11661-997-0211-6.

[43] *Metal Handbook: Powder Metallurgy*, 9th ed. ASM, 1984.

[44] T. Ozben, E. Kilickap, and O. Çakır, “Investigation of mechanical and machinability properties of SiC particle reinforced Al-MMC,” *J. Mater. Process. Technol.*, vol. 198, no. 1–3, pp. 220–225, Mar. 2008, doi: 10.1016/j.jmatprotec.2007.06.082.

[45] M. Razavi, A. R. Farajipour, M. Zakeri, M. R. Rahimipour, and A. R. Firouzbakht, “Production of Al 2 O 3 –SiC nano-composites by spark plasma sintering,” *Boletín la Soc. Española Cerámica y Vidr.*, vol. 56, no. 4, pp. 186–194, Jul. 2017, doi: 10.1016/j.bsecv.2017.01.002.

[46] K. Dash, D. Chaira, and B. C. Ray, “Synthesis and characterization of aluminium–alumina micro- and nano-composites by spark plasma sintering,” *Mater. Res. Bull.*, vol. 48, no. 7, pp. 2535–2542, Jul. 2013, doi: 10.1016/j.materresbull.2013.03.014.

[47] V. Mamedov, “Spark plasma sintering as advanced PM sintering method,” *Powder Metall.*, vol. 45, no. 4, pp. 322–328, Dec. 2002, doi: 10.1179/003258902225007041.

[48] J. Bhatt, N. Balachander, S. Shekher, R. Karthikeyan, D. R. Peshwe, and B. S. Murty, “Synthesis of nanostructured Al–Mg–SiO2 metal matrix composites using high-energy ball milling and spark plasma sintering,” *J. Alloys Compd.*, vol. 536, pp. S35–S40, Sep. 2012, doi: 10.1016/j.jallcom.2011.12.062.

[49] H. Abdoli, H. Asgharzadeh, and E. Salahi, “Sintering behavior of Al–AlN-nanostructured composite powder synthesized by high-energy ball milling,” *J. Alloys Compd.*, vol. 473, no. 1–2, pp. 116–122, Apr. 2009, doi: 10.1016/j.jallcom.2008.05.069.

[50] M. S. El-Eskandarany, M. Omori, T. Hirai, T. J. Konno, K. Sumiyama, and K. Suzuki, “Synthesizing of nanocomposite WC/MgO powders by mechanical solid-state reduction and subsequent plasma-activated sintering,” *Metall. Mater. Trans. A*, vol. 32, no. 1, pp. 157–164, Jan. 2001, doi: 10.1007/s11661-001-0111-0.

[51] D. Zhou, H. Wang, and X. Yao, “Sintering Behavior and Dielectric Properties of Bi 3

NbO 7 Ceramics Prepared by Mixed Oxides and High-Energy Ball-Milling Methods," *J. Am. Ceram. Soc.*, vol. 90, no. 1, pp. 327–329, Jan. 2007, doi: 10.1111/j.1551-2916.2006.01407.x.

[52] H. Xiong, Y. Wu, Z. Li, X. Gan, K. Zhou, and L. Chai, "Comparison of Ti(C, N)-based cermets by vacuum and gas-pressure sintering: Microstructure and mechanical properties," *Ceram. Int.*, vol. 44, no. 1, pp. 805–813, Jan. 2018, doi: 10.1016/j.ceramint.2017.10.003.

[53] Y. Gao *et al.*, "Mechanical properties and microstructure of WC-Fe-Ni-Co cemented carbides prepared by vacuum sintering," *Vacuum*, vol. 143, pp. 271–282, Sep. 2017, doi: 10.1016/j.vacuum.2017.06.028.

[54] X. Zhang, S. Liang, H. Li, and J. Yang, "Mechanical and optical properties of transparent alumina obtained by rapid vacuum sintering," *Ceram. Int.*, vol. 43, no. 1, pp. 420–426, Jan. 2017, doi: 10.1016/j.ceramint.2016.09.175.

[55] B. Šuštaršič, L. Kosec, M. Jenko, and V. Leskovšek, "Vacuum sintering of water-atomised HSS powders with MoS2 additions," *Vacuum*, vol. 61, no. 2–4, pp. 471–477, May 2001, doi: 10.1016/S0042-207X(01)00161-0.

[56] M. Oghbaei and O. Mirzaee, "Microwave versus conventional sintering: A review of fundamentals, advantages and applications," *J. Alloys Compd.*, vol. 494, no. 1–2, pp. 175–189, Apr. 2010, doi: 10.1016/j.jallcom.2010.01.068.

[57] E. T. Thostenson and T.-W. Chou, "Microwave processing: fundamentals and applications," *Compos. Part A Appl. Sci. Manuf.*, vol. 30, no. 9, pp. 1055–1071, Sep. 1999, doi: 10.1016/S1359-835X(99)00020-2.

[58] H. Peng, W. R. Tinga, U. Sundararaj, and R. L. Eadie, "Microwave Sintering Process Model," *J. Microw. Power Electromagn. Energy*, vol. 38, no. 4, pp. 243–258, Jan. 2003, doi: 10.1080/08327823.2003.11688503.

[59] M. P. Reddy *et al.*, "Enhanced performance of nano-sized SiC reinforced Al metal matrix nanocomposites synthesized through microwave sintering and hot extrusion techniques," *Prog. Nat. Sci. Mater. Int.*, vol. 27, no. 5, pp. 606–614, Oct. 2017, doi: 10.1016/j.pnsc.2017.08.015.

[60] P. Ashwath, .J. Joel, M. Anthony Xavior, and H. G. Prashantha Kumar, "Effect of SiC and Al2O3 particles addition to AA 2900 and AA 2024 MMC's synthesized through microwave sintering," *Mater. Today Proc.*, vol. 5, no. 2, pp. 7329–7336, 2018, doi: 10.1016/j.matpr.2017.11.402.

[61] S. Sebastian and V. Suyamburajan, "Microstructural analysis of diffusion bonding on copper stainless steel," *Mater. Today Proc.*, Aug. 2020, doi: 10.1016/j.matpr.2020.07.244.

[62] M. Ghosh, K. Bhanumurthy, G. B. Kale, J. Krishnan, and S. Chatterjee, "Strength of the Diffusion Bonded Joints between CP Ti and 304 Stainless Steel Processed below and above .BETA.-Transus," *ISIJ Int.*, vol. 44, no. 2, pp. 388–395, 2004, doi: 10.2355/isijinternational.44.388.

[63] X.-P. Zhang, L. Ye, Y.-W. Mai, G.-F. Quan, and W. Wei, "Investigation on diffusion

bonding characteristics of SiC particulate reinforced aluminium metal matrix composites (Al/SiCp-MMC)," *Compos. Part A Appl. Sci. Manuf.*, vol. 30, no. 12, pp. 1415–1421, Dec. 1999, doi: 10.1016/S1359-835X(99)00040-8.

[64] Shamsipur, A., kashani-Bozorg S.F., Hanzaki Z.A., "Fabrication of Ti/Sic surface nano-composite layer by friction stir processing", *International Journal of Modern Physics, Conference Series*, 5, 367–374.

[65] C. J. Thomas, W.M, Nicholas, E.D, Needham, J.C., Murch, J., Temple-smith, P., Dawes, "Friction Stir Butt Welding," PCT/GB92/02203, 1991.

[66] R. S. Mishra and Z. Y. Ma, "Friction stir welding and processing," *Mater. Sci. Eng. R Reports*, vol. 50, no. 1–2, pp. 1–78, Aug. 2005, doi: 10.1016/j.mser.2005.07.001.

[67] R. NANDAN, T. DEBROY, and H. BHADESHIA, "Recent advances in friction-stir welding – Process, weldment structure and properties," *Prog. Mater. Sci.*, vol. 53, no. 6, pp. 980–1023, Aug. 2008, doi: 10.1016/j.pmatsci.2008.05.001.

[68] R. Mishra, R.S., Mahoney, M.W., Sato, Y., Hovanski, Y., Verma, *Friction stir welding and processing VI*. New Jersey: Wiley, 2011.

[69] F. Nascimento, T. Santos, P. Vilaça, R. M. Miranda, and L. Quintino, "Microstructural modification and ductility enhancement of surfaces modified by FSP in aluminium alloys," *Mater. Sci. Eng. A*, vol. 506, no. 1–2, pp. 16–22, Apr. 2009, doi: 10.1016/j.msea.2009.01.008.

[70] S. D. Thomas W.M., Nicholas E.D., Smith, "Aluminium 2001-Processings of the TMS," *Alum. Automot. Join. Sess.*, p. 213, 2001.

[71] J. Thomas, WM and Dolby, RE and David, SA and DebRoy, T and Lippold, JC and Smartt, HB and Vitek, "Proceedings of the Sixth International Conference on Trends in Welding Research," *Pine Mt. GA, ASM Int.*, pp. 203–211, 2003.

[72] Y. Zhao, S. Lin, L. Wu, and F. Qu, "The influence of pin geometry on bonding and mechanical properties in friction stir weld 2014 Al alloy," *Mater. Lett.*, vol. 59, no. 23, pp. 2948–2952, Oct. 2005, doi: 10.1016/j.matlet.2005.04.048.

[73] K. Elangovan, V. Balasubramanian, and M. Valliappan, "Influences of tool pin profile and axial force on the formation of friction stir processing zone in AA6061 aluminium alloy," *Int. J. Adv. Manuf. Technol.*, vol. 38, no. 3–4, pp. 285–295, Aug. 2008, doi: 10.1007/s00170-007-1100-2.

[74] K. Elangovan and V. Balasubramanian, "Influences of tool pin profile and tool shoulder diameter on the formation of friction stir processing zone in AA6061 aluminium alloy," *Mater. Des.*, vol. 29, no. 2, pp. 362–373, Jan. 2008, doi: 10.1016/j.matdes.2007.01.030.

[75] K. Elangovan and V. Balasubramanian, "Influences of pin profile and rotational speed of the tool on the formation of friction stir processing zone in AA2219 aluminium alloy," *Mater. Sci. Eng. A*, vol. 459, no. 1–2, pp. 7–18, Jun. 2007, doi: 10.1016/j.msea.2006.12.124.

[76] H. Fujii, L. Cui, M. Maeda, and K. Nogi, "Effect of tool shape on mechanical properties and microstructure of friction stir welded aluminum alloys," *Mater. Sci.*

Eng. A, vol. 419, no. 1–2, pp. 25–31, Mar. 2006, doi: 10.1016/j.msea.2005.11.045.

[77] R. Hashemi and G. Hussain, "Wear performance of Al/TiN dispersion strengthened surface composite produced through friction stir process: A comparison of tool geometries and number of passes," *Wear*, vol. 324–325, pp. 45–54, Feb. 2015, doi: 10.1016/j.wear.2014.11.024.

[78] E. R. I. Mahmoud, M. Takahashi, T. Shibayanagi, and K. Ikeuchi, "Effect of friction stir processing tool probe on fabrication of SiC particle reinforced composite on aluminium surface," *Sci. Technol. Weld. Join.*, vol. 14, no. 5, pp. 413–425, Jul. 2009, doi: 10.1179/136217109X406974.

[79] K. Kumar and S. V. Kailas, "The role of friction stir welding tool on material flow and weld formation," *Mater. Sci. Eng. A*, vol. 485, no. 1–2, pp. 367–374, Jun. 2008, doi: 10.1016/j.msea.2007.08.013.

[80] A. Kumar and L. S. Raju, "Influence of Tool Pin Profiles on Friction Stir Welding of Copper," *Mater. Manuf. Process.*, vol. 27, no. 12, pp. 1414–1418, Dec. 2012, doi: 10.1080/10426914.2012.689455.

[81] O. P. Abolusoro, E. T. Akinlabi, and S. V. Kailas, "Impact of tool profile on mechanical behavior and material flow in friction stir welding of dissimilar aluminum alloys," *Materwiss. Werksttech.*, vol. 51, no. 6, pp. 725–731, Jun. 2020, doi: 10.1002/mawe.202000002.

[82] A. Kumar, "Optimization of process parameter for AA6061 alloy during friction stir processing," *Mater. Today Proc.*, Jan. 2020, doi: 10.1016/j.matpr.2020.01.120.

[83] V. Yadav, V. Kumar, and V. Tiwari, "Effect of tool pin profile on mechanical properties of Al6082 and Al6082-Cu composite by friction stir processing," *IOSR J. Mech. Civ. Eng.*, vol. 11, no. 3, pp. 07–11, 2014, doi: 10.9790/1684-11340711.

[84] H. Eftekharinia, A. A. Amadeh, A. Khodabandeh, and M. Paidar, "Microstructure and wear behavior of AA6061/SiC surface composite fabricated via friction stir processing with different pins and passes," *Rare Met.*, vol. 39, no. 4, pp. 429–435, Apr. 2020, doi: 10.1007/s12598-016-0691-x.

[85] S. Rathee, S. Maheshwari, A. N. Siddiquee, and M. Srivastava, "A Review of Recent Progress in Solid State Fabrication of Composites and Functionally Graded Systems Via Friction Stir Processing," *Crit. Rev. Solid State Mater. Sci.*, vol. 43, no. 4, pp. 334–366, 2018, doi: 10.1080/10408436.2017.1358146.

[86] N. J. Panaskar and A. Sharma, "Surface Modification and Nanocomposite Layering of Fastener-Hole through Friction-Stir Processing," *Mater. Manuf. Process.*, vol. 29, no. 6, pp. 726–732, Jun. 2014, doi: 10.1080/10426914.2014.892619.

[87] P. Fu, C. Jiang, X. Wu, and Z. Zhang, "Surface Modification of 304 Steel Using Triple-Step Shot Peening," *Mater. Manuf. Process.*, vol. 30, no. 6, pp. 693–698, Jun. 2015, doi: 10.1080/10426914.2015.1004702.

[88] S. Selvakumar, I. Dinaharan, R. Palanivel, and B. Ganesh Babu, "Characterization of molybdenum particles reinforced Al6082 aluminum matrix composites with improved ductility produced using friction stir processing," *Mater. Charact.*, vol. 125, pp. 13–22,

Mar. 2017, doi: 10.1016/j.matchar.2017.01.016.

[89] M. Nattapat, S. Marimuthu, A. M. Kamara, and M. R. N. Esfahani, “Laser Surface Modification of Carbon Fiber Reinforced Composites,” *Mater. Manuf. Process.*, vol. 30, no. 12, pp. 1450–1456, Dec. 2015, doi: 10.1080/10426914.2015.1019097.

[90] M. A. García-Bernal, R. S. Mishra, R. Verma, and D. Hernández-Silva, “Influence of friction stir processing tool design on microstructure and superplastic behavior of Al-Mg alloys,” *Mater. Sci. Eng. A*, vol. 670, pp. 9–16, Jul. 2016, doi: 10.1016/j.msea.2016.05.115.

[91] J. S. de Jesus, A. Loureiro, J. M. Costa, and J. M. Ferreira, “Effect of tool geometry on friction stir processing and fatigue strength of MIG T welds on Al alloys,” *J. Mater. Process. Technol.*, vol. 214, no. 11, pp. 2450–2460, Nov. 2014, doi: 10.1016/j.jmatprotec.2014.05.012.

[92] V. L. Srinivas, M. Zammerudhin, M. R. Kumar, B. R. Sankar, and K. Ravindra, “Parametric Analysis of Friction Stir Welding on AA6061,” *Int. J. Mech. Eng. Res.*, vol. 3, no. 5, pp. 557–564, 2013.

[93] I. Radisavljevic, A. Zivkovic, V. Grabulov, and N. Radovic, “Influence of pin geometry on mechanical and structural properties of butt friction stir welded 2024-T351 aluminum alloy,” *Hem. Ind.*, vol. 69, no. 3, pp. 323–330, 2015, doi: 10.2298/HEMIND131206020R.

[94] A. P. A.Ramesh, Dr. M Indira Rani, “Influence of tool design on the mechanical properties in friction stir welding of AA6082-T6 aluminum alloy,” *Eng. Sci. Technol. an Int. J.*, vol. 7, no. 6, p. 5, 2016.

[95] D. Venkateswarlu, N. R. Mandal, M. M. Mahapatra, and S. P. Harsh, “Tool design effects for FSW of AA7039,” *Weld. J.*, vol. 92, no. 2, 2013.

[96] Y. Bozkurt and Z. Boumerzoug, “Tool material effect on the friction stir butt welding of AA2124-T4 Alloy Matrix MMC,” *J. Mater. Res. Technol.*, vol. 7, no. 1, pp. 29–38, Jan. 2018, doi: 10.1016/j.jmrt.2017.04.001.

[97] A. Kumar, M. M. Mahapatra, P. K. Jha, N. R. Mandal, and V. Devuri, “Influence of tool geometries and process variables on friction stir butt welding of Al–4.5%Cu/TiC in situ metal matrix composites,” *Mater. Des.*, vol. 59, pp. 406–414, Jul. 2014, doi: 10.1016/j.matdes.2014.02.063.

[98] Y. N. Zhang, X. Cao, S. Larose, and P. Wanjara, “Review of tools for friction stir welding and processing,” *Can. Metall. Q.*, vol. 51, no. 3, pp. 250–261, Jul. 2012, doi: 10.1179/1879139512Y.0000000015.

[99] N. Yuvaraj, S. Aravindan, and Vipin, “Fabrication of Al5083/B4C surface composite by friction stir processing and its tribological characterization,” *J. Mater. Res. Technol.*, vol. 4, no. 4, pp. 398–410, 2015, doi: 10.1016/j.jmrt.2015.02.006.

[100] R. Butola, R. M. Singari, and Q. Murtaza, “Fabrication and optimization of AA7075 matrix surface composites using Taguchi technique via friction stir processing (FSP),” *Eng. Res. Express*, vol. 1, no. 2, p. 025015, Oct. 2019, doi: 10.1088/2631-8695/ab4b00.

[101] B. Ratna Sunil, T. S. Sampath Kumar, U. Chakkingal, V. Nandakumar, and M. Doble, "Nano-hydroxyapatite reinforced AZ31 magnesium alloy by friction stir processing: a solid state processing for biodegradable metal matrix composites," *J. Mater. Sci. Mater. Med.*, vol. 25, no. 4, pp. 975–988, Apr. 2014, doi: 10.1007/s10856-013-5127-7.

[102] B. Ratna Sunil, T. S. Sampath Kumar, U. Chakkingal, V. Nandakumar, and M. Doble, "Friction stir processing of magnesium–nanohydroxyapatite composites with controlled in vitro degradation behavior," *Mater. Sci. Eng. C*, vol. 39, pp. 315–324, Jun. 2014, doi: 10.1016/j.msec.2014.03.004.

[103] C. LEE, J. HUANG, and P. HSIEH, "Mg based nano-composites fabricated by friction stir processing," *Scr. Mater.*, vol. 54, no. 7, pp. 1415–1420, Apr. 2006, doi: 10.1016/j.scriptamat.2005.11.056.

[104] M. Yang, C. Xu, C. Wu, K. Lin, Y. J. Chao, and L. An, "Fabrication of AA6061/Al2O3 nano ceramic particle reinforced composite coating by using friction stir processing," *J. Mater. Sci.*, vol. 45, pp. 4431–4438, 2010.

[105] H. R. Akramifard, M. Shamanian, M. Sabbaghian, and M. Esmailzadeh, "Microstructure and mechanical properties of Cu/SiC metal matrix composite fabricated via friction stir processing," *Mater. Des.*, vol. 54, pp. 838–844, Feb. 2014, doi: 10.1016/j.matdes.2013.08.107.

[106] G. M. Reddy, A. S. Rao, and K. S. Rao, "Friction Stir Surfacing Route: Effective Strategy for the Enhancement of Wear Resistance of Titanium Alloy," *Trans. Indian Inst. Met.*, vol. 66, no. 3, pp. 231–238, Jun. 2013, doi: 10.1007/s12666-013-0254-x.

[107] A. Mertens, A. Simar, H.-M. Montrieux, J. Halleux, F. Delannay, and J. Lecomte-Beckers, "Friction stir processing of magnesium matrix composites reinforced with carbon fibres: Influence of the matrix characteristics and of the processing parameters on microstructural developments. Mg 2012," 2012.

[108] T. Wang, W. Guo, L. Wan, and S. Lv, "Microstructure and surface mechanical property of AZ31 Mg/SiCp surface composite fabricated by Direct Friction Stir Processing," *Mater. Des.*, vol. 59, pp. 274–278, 2014, doi: 10.1016/j.matdes.2014.02.067.

[109] F. García-Vázquez, B. Vargas-Arista, R. Muñiz, J. C. Ortiz, H. H. García, and J. Acevedo, "The Role of Friction Stir Processing (FSP) Parameters on TiC Reinforced Surface Al7075-T651 Aluminum Alloy," *Soldag. Inspeção*, vol. 21, no. 4, pp. 508–516, Dec. 2016, doi: 10.1590/0104-9224/si2104.10.

[110] O. N. Sert A., Celik, "Wear behavior of SiC-reinforced surface composite Al7075-T651 aluminum alloy produced using friction stir processing," *Indian J. Eng. Mater. Sci.*, vol. 21, pp. 35–43, 2014, [Online]. Available: http://nopr.niscair.res.in/handle/123456789/27448.

[111] H. G. Rana, V. J. Badheka, and A. Kumar, "Fabrication of Al7075 / B4C Surface Composite by Novel Friction Stir Processing (FSP) and Investigation on Wear Properties," *Procedia Technol.*, vol. 23, pp. 519–528, 2016, doi: 10.1016/j.protcy.2016.03.058.

[112] H. Bisadi and A. Abasi, "Fabrication of Al7075/TiB2 Surface Composite Via Friction

Stir Processing," *Am. J. Mater. Sci.*, vol. 1, no. 2, pp. 67–70, Aug. 2012, doi: 10.5923/j.materials.20110102.10.

[113] S. F. Kashani-Bozorg, K. Jazayeri, M. Rusop, and T. Soga, "Formation of Al/B4C Surface Nano-composite Layers on 7075 Al Alloy Employing Friction Stir Processing," in *AIP Conference Proceedings*, 2009, pp. 715–719, doi: 10.1063/1.3160241.

[114] D. S. C. Mouli, K. A.Sarath, and R. R. U. Maheswara, "Improvement of Hardness of Aluminium 7075 Metal Matrix Composite with Silicon Carbide Powder by Friction Stir Processing," *Int. J. Eng. Technol. Sci. Res.*, vol. 4, no. 9, pp. 432–439, 2017.

[115] M.-H. Ku, F.-Y. Hung, T.-S. Lui, and L.-H. Chen, "Embrittlement Mechanism on Tensile Fracture of 7075 Al Alloy with Friction Stir Process (FSP)," *Mater. Trans.*, vol. 52, no. 1, pp. 112–117, 2011, doi: 10.2320/matertrans.M2010315.

[116] R. R and M. N, "Microstructure and Metallurgical Properties of Aluminium 7075 – T651 Alloy / B4c 4 % Vol. Surface Composite by Friction Stir Processing," *Int. J. Adv. Mater. Manuf. Charact.*, vol. 3, no. 1, pp. 301–305, Mar. 2013, doi: 10.11127/ijammc.2013.02.055.

[117] K. A. Al-Ghamdi, G. Hussain, and R. Hashemi, "Fabrication of metal-matrix AL7075T651/TiN nano composite employing friction stir process," *Proc. Inst. Mech. Eng. Part B J. Eng. Manuf.*, vol. 231, no. 8, pp. 1319–1331, Jun. 2017, doi: 10.1177/0954405415596695.

[118] N. Singh, J. Singh, B. Singh, and N. Singh, "Wear behavior of B4C reinforced AZ91 matrix composite fabricated by FSP," *Mater. Today Proc.*, vol. 5, no. 9, pp. 19976–19984, 2018, doi: 10.1016/j.matpr.2018.06.364.

[119] H. A. Deore, A. Bhardwaj, A. G. Rao, J. Mishra, and V. D. Hiwarkar, "Consequence of reinforced SiC particles and post process artificial ageing on microstructure and mechanical properties of friction stir processed AA7075," *Def. Technol.*, vol. 16, no. 5, pp. 1039–1050, Oct. 2020, doi: 10.1016/j.dt.2019.12.001.

[120] M. Akbari, M. H. Shojaeefard, P. Asadi, and A. Khalkhali, "Hybrid multi-objective optimization of microstructural and mechanical properties of B 4 C/A356 composites fabricated by FSP using TOPSIS and modified NSGA-II," *Trans. Nonferrous Met. Soc. China*, vol. 27, no. 11, pp. 2317–2333, Nov. 2017, doi: 10.1016/S1003-6326(17)60258-9.

[121] M. Paidar, O. O. Ojo, H. R. Ezatpour, and A. Heidarzadeh, "Influence of multi-pass FSP on the microstructure, mechanical properties and tribological characterization of Al/B4C composite fabricated by accumulative roll bonding (ARB)," *Surf. Coatings Technol.*, vol. 361, pp. 159–169, Mar. 2019, doi: 10.1016/j.surfcoat.2019.01.043.

[122] M. Navaser and M. Atapour, "Effect of Friction Stir Processing on Pitting Corrosion and Intergranular Attack of 7075 Aluminum Alloy," *J. Mater. Sci. Technol.*, vol. 33, no. 2, pp. 155–165, Feb. 2017, doi: 10.1016/j.jmst.2016.07.008.

[123] O. M. Ikumapayi, E. T. Akinlabi, J. D. Majumdar, and S. A. Akinlabi, "Characterization of high strength aluminium–based surface matrix composite reinforced with low-cost PKSA fabricated by friction stir processing," *Mater. Res.*

Express, vol. 6, no. 10, p. 106554, Aug. 2019, doi: 10.1088/2053-1591/ab395b.

[124] R. Abrahams, J. Mikhail, and P. Fasihi, "Effect of friction stir process parameters on the mechanical properties of 5005-H34 and 7075-T651 aluminium alloys," *Mater. Sci. Eng. A*, vol. 751, pp. 363–373, Mar. 2019, doi: 10.1016/j.msea.2019.02.065.

[125] I. Sudhakar, G. Madhusudhan Reddy, and K. Srinivasa Rao, "Ballistic behavior of boron carbide reinforced AA7075 aluminium alloy using friction stir processing – An experimental study and analytical approach," *Def. Technol.*, vol. 12, no. 1, pp. 25–31, Feb. 2016, doi: 10.1016/j.dt.2015.04.005.

[126] A. Singh and A. Agrawal, "Investigation of surface residual stress distribution in deformation machining process for aluminum alloy," *J. Mater. Process. Technol.*, vol. 225, pp. 195–202, Nov. 2015, doi: 10.1016/j.jmatprotec.2015.05.025.

[127] W. Jomaa, V. Songmene, and P. Bocher, "An Investigation of Machining-Induced Residual Stresses and Microstructure of Induction-Hardened AISI 4340 Steel," *Mater. Manuf. Process.*, vol. 31, no. 7, pp. 838–844, May 2016, doi: 10.1080/10426914.2015.1070431.

[128] K. Punitharani, N. Murugan, and S. M. Sivagami, "Finite element analysis of residual stresses and distortion in hard faced gate valve," *J. Sci. Ind. Res. (India).*, vol. 69, no. 2, pp. 129–134, 2010.

[129] R. Mertens, B. Vrancken, N. Holmstock, Y. Kinds, J.-P. Kruth, and J. Van Humbeeck, "Influence of Powder Bed Preheating on Microstructure and Mechanical Properties of H13 Tool Steel SLM Parts," *Phys. Procedia*, vol. 83, pp. 882–890, 2016, doi: 10.1016/j.phpro.2016.08.092.

[130] D. Ulutan and T. Ozel, "Machining induced surface integrity in titanium and nickel alloys: A review," *Int. J. Mach. Tools Manuf.*, vol. 51, no. 3, pp. 250–280, Mar. 2011, doi: 10.1016/j.ijmachtools.2010.11.003.

[131] W. Li, P. J. Withers, D. Axinte, M. Preuss, and P. Andrews, "Residual stresses in face finish turning of high strength nickel-based superalloy," *J. Mater. Process. Technol.*, vol. 209, no. 10, pp. 4896–4902, Jun. 2009, doi: 10.1016/j.jmatprotec.2009.01.012.

[132] N. C. Tâmpu, B. Chiriţă, E. Herghelegiu, and G. Brabie, "Influence of the cutting regime on the residual stresses generated by carbon steel milling," *Indian J. Eng. Mater. Sci.*, vol. 21, no. 3, pp. 283–288, 2014.

[133] Y. Ma, P. Feng, J. Zhang, Z. Wu, and D. Yu, "Prediction of surface residual stress after end milling based on cutting force and temperature," *J. Mater. Process. Technol.*, vol. 235, pp. 41–48, Sep. 2016, doi: 10.1016/j.jmatprotec.2016.04.002.

[134] B. Li, X. Jiang, J. Yang, and S. Y. Liang, "Effects of depth of cut on the redistribution of residual stress and distortion during the milling of thin-walled part," *J. Mater. Process. Technol.*, vol. 216, pp. 223–233, Feb. 2015, doi: 10.1016/j.jmatprotec.2014.09.016.

[135] S. Caruso, J. C. Outeiro, D. Umbrello, and R. M'Saoubi, "Modeling and experimental validation of the surface residual stresses induced by hard machining of AISI H13 tool steel," *Int. J. Mater. Form.*, vol. 3, no. S1, pp. 515–518, Apr. 2010, doi:

10.1007/s12289-010-0820-2.

[136] O. Bhatkar, S. Sakharkar, V. Mohan, and R. Pawade, “Residual Stress Analysis in Orthogonal Cutting of AISI 1020 Steel,” 2017, doi: 10.2991/iccasp-16.2017.17.

[137] K. Chandrasekaran, P. Marimuthu, K. Raja, and A. Manimaran, “Machinability study on AISI410 with different layered inserts in CNC turning during dry conditions,” *Indian J. Eng. Mater. Sci.*, vol. 20, no. 5, pp. 398–404, 2013.

[138] J. C. Outeiro, D. Umbrello, and R. M’Saoubi, “Experimental and numerical modelling of the residual stresses induced in orthogonal cutting of AISI 316L steel,” *Int. J. Mach. Tools Manuf.*, vol. 46, no. 14, pp. 1786–1794, Nov. 2006, doi: 10.1016/j.ijmachtools.2005.11.013.

[139] A. Attanasio, E. Ceretti, and C. Giardini, “3D FE MODELLING OF SUPERFICIAL RESIDUAL STRESSES IN TURNING OPERATIONS,” *Mach. Sci. Technol.*, vol. 13, no. 3, pp. 317–337, Aug. 2009, doi: 10.1080/10910340903237806.

[140] M. Hribersek, F. Pusavec, J. Rech, and J. Kopac, “Modeling of machined surface characteristics in cryogenic orthogonal turning of inconel 718,” *Mach. Sci. Technol.*, vol. 22, no. 5, pp. 829–850, Sep. 2018, doi: 10.1080/10910344.2017.1415935.

[141] R. Butola, J. kumar, V. khanna, P. Ali, and V. Khanna, “Effecton Surface Properties OF Mild Steel During Dry Turning & Wet Turning On Lathe,” *Mater. Today Proc.*, vol. 4, no. 8, pp. 7892–7902, 2017, doi: 10.1016/j.matpr.2017.07.125.

[142] R. Butola, Q. Murtaza, and R. M. Singari, “Advances in Computational Methods in Manufacturing,” *Lect. Notes Multidiscip. Ind. Eng.*, pp. 337–348, 2019.

[143] P. J. Withers and H. K. D. H. Bhadeshia, “Residual stress. Part 2 – Nature and origins,” *Mater. Sci. Technol.*, vol. 17, no. 4, pp. 366–375, Apr. 2001, doi: 10.1179/026708301101510087.

[144] W. M. Thomas, K. I. Johnson, and C. S. Wiesner, “Friction Stir Welding – Recent Developments in Tool and Process Technologies,” *Adv. Eng. Mater.*, vol. 5, no. 7, pp. 485–490, Jul. 2003, doi: 10.1002/adem.200300355.

[145] A. Chaudhary, A. Kumar Dev, A. Goel, R. Butola, and M. S. Ranganath, “The Mechanical Properties of Different alloys in friction stir processing: A Review,” *Mater. Today Proc.*, vol. 5, no. 2, pp. 5553–5562, 2018, doi: 10.1016/j.matpr.2017.12.146.

[146] P.S. Prevéy, “X-Ray Diffraction Residual Stress Techniques,” in *Materials Characterization*, ASM International, 1986, pp. 380–392.

[147] B. Cullity, “Elements of X-ray diffraction, Addison,” *Wesley Mass*, 1978.

[148] K. TANAKA and Y. AKINIWA, “Diffraction Measurements of Residual Macrostress and Microstress Using X-Rays, Synchrotron and Neutrons,” *JSME Int. J. Ser. A*, vol. 47, no. 3, pp. 252–263, 2004, doi: 10.1299/jsmea.47.252.

[149] K. Oh-Ishi and T. R. McNelley, “The influence of friction stir processing parameters on microstructure of as-cast NiAl bronze,” *Metall. Mater. Trans. A*, vol. 36, no. 6, pp. 1575–1585, Jun. 2005, doi: 10.1007/s11661-005-0249-2.

[150] R. Butola, Q. Murtaza, and R. M. Singari, “An experimental and simulation validation of residual stress measurement for manufacturing of friction stir processing tool,” *Indian J. Eng. Mater. Sci.*, vol. 27, pp. 826–836, 2020.

[151] R. Butola, P. Chandra, K. Bector and R. M Singari, "Fabrication and multi-objective optimization of friction stir processed aluminium based surface composites using Taguchi approach. *Surface Topography: Metrology and Properties*", Vol. 9, pp. 025044, 2021, doi.org/10.1088/2051-672X/ac0ba3.

[152] M. Khakbiz and F. Akhlaghi, “Synthesis and structural characterization of Al–B4C nano-composite powders by mechanical alloying,” *J. Alloys Compd.*, vol. 479, no. 1–2, pp. 334–341, Jun. 2009, doi: 10.1016/j.jallcom.2008.12.076.

[153] Y. Mazaheri, M. Meratian, R. Emadi, and A. R. Najarian, “Comparison of microstructural and mechanical properties of Al–TiC, Al–B4C and Al–TiC–B4C composites prepared by casting techniques,” *Mater. Sci. Eng. A*, vol. 560, pp. 278–287, Jan. 2013, doi: 10.1016/j.msea.2012.09.068.

[154] D. Wang, Y. Ni, Q. Huo, and D. E. Tallman, “Self-assembled monolayer and multilayer thin films on aluminum 2024-T3 substrates and their corrosion resistance study,” *Thin Solid Films*, vol. 471, no. 1–2, pp. 177–185, Jan. 2005, doi: 10.1016/j.tsf.2004.06.158.

[155] N. Yuvaraj, S. Aravindan, and Vipin, “Wear Characteristics of Al5083 Surface Hybrid Nano-composites by Friction Stir Processing,” *Trans. Indian Inst. Met.*, vol. 70, no. 4, pp. 1111–1129, 2017, doi: 10.1007/s12666-016-0905-9.

[156] M. Komarasamy, R. S. Mishra, J. A. Baumann, G. Grant, and Y. Hovanski, “Processing, Microstructure and Mechanical Property Correlation in Al-B4C Surface Composite Produced via Friction Stir Processing,” in *Friction Stir Welding and Processing VII*, Cham: Springer International Publishing, 2013, pp. 39–46.

[157] Q. Liu, L. Ke, F. Liu, C. Huang, and L. Xing, “Microstructure and mechanical property of multi-walled carbon nanotubes reinforced aluminum matrix composites fabricated by friction stir processing,” *Mater. Des.*, vol. 45, pp. 343–348, Mar. 2013, doi: 10.1016/j.matdes.2012.08.036.

[158] D. R. Ni, J. J. Wang, Z. N. Zhou, and Z. Y. Ma, “Fabrication and mechanical properties of bulk NiTip/Al composites prepared by friction stir processing,” *J. Alloys Compd.*, vol. 586, pp. 368–374, Feb. 2014, doi: 10.1016/j.jallcom.2013.10.013.

[159] Z. Du, M.-J. Tan, J.-F. Guo, and J. Wei, “Friction stir processing of Al–CNT composites,” *Proc. Inst. Mech. Eng. Part L J. Mater. Des. Appl.*, vol. 230, no. 3, pp. 825–833, Jun. 2016, doi: 10.1177/1464420715571189.

[160] R. . Mishra, Z. . Ma, and I. Charit, “Friction stir processing: a novel technique for fabrication of surface composite,” *Mater. Sci. Eng. A*, vol. 341, no. 1–2, pp. 307–310, Jan. 2003, doi: 10.1016/S0921-5093(02)00199-5.

[161] K. Kalaiselvan, N. Murugan, and S. Parameswaran, “Production and characterization of AA6061–B4C stir cast composite,” *Mater. Des.*, vol. 32, no. 7, pp. 4004–4009, Aug. 2011, doi: 10.1016/j.matdes.2011.03.018.

[162] M. Srivastava, A. N. Siddiquee, S. Rathee, and S. Maheshwari, “Optimisation of friction stir processing parameters to fabricate AA6063/SiC surface composites using Taguchi technique,” *Int. J. Mater. Prod. Technol.*, vol. 58, no. 1, p. 16, 2019, doi: 10.1504/ijmpt.2019.10017760.

[163] R. Butola, C. Pratap, A. Shukla, and R. S. Walia, “Effect on the Mechanical Properties of Aluminum-Based Hybrid Metal Matrix Composite Using Stir Casting Method,” *Mater. Sci. Forum*, vol. 969, pp. 253–259, Aug. 2019, doi: 10.4028/www.scientific.net/MSF.969.253.

[164] R. Butola, R. Jain, P. Bhangadia, A. Bandhu, R. S Walia, and Q. Murtaza, “Optimization to the parameters of abrasive flow machining by Taguchi method,” *Mater. Today Proc.*, vol. 5, no. 2, pp. 4720–4729, 2018, doi: 10.1016/j.matpr.2017.12.044.

[165] R. Butola, Q. Murtaza, R. S. Walia, and P. Kumar, “Two start and Three Start Helical Abrasive Flow Machining for Brittle Materials,” *Mater. Today Proc.*, vol. 4, no. 2, pp. 3685–3693, 2017, doi: 10.1016/j.matpr.2017.02.263.

[166] R. Kumar, R. P. Singh, and R. Kataria, “Study on mechanical properties of fabricated hybrid natural fibre polymeric composites,” *Int. J. Mater. Prod. Technol.*, vol. 60, no. 1, pp. 73–91, 2020, doi: 10.1504/IJMPT.2020.108490.

[167] S. Kanwar, R. M. Singari, R. Butola, "Comparison of Genetic Algorithm and Taguchi technique for surface roughness of natural fiber reinforced polymer composites", *SAE Int. J. of Mater. Manuf.*. 14(2):141-151, April. 2021

[168] A. Dolatkhah, P. Golbabaei, M. K. Besharati Givi, and F. Molaiekiya, “Investigating effects of process parameters on microstructural and mechanical properties of Al5052/SiC metal matrix composite fabricated via friction stir processing,” *Mater. Des.*, vol. 37, pp. 458–464, May 2012, doi: 10.1016/j.matdes.2011.09.035.

[169] M. Barmouz and M. K. B. Givi, “Fabrication of in situ Cu/SiC composites using multi-pass friction stir processing: Evaluation of microstructural, porosity, mechanical and electrical behavior,” *Compos. Part A Appl. Sci. Manuf.*, vol. 42, no. 10, pp. 1445–1453, Oct. 2011, doi: 10.1016/j.compositesa.2011.06.010.

[170] Y. Morisada, H. Fujii, T. Nagaoka, and M. Fukusumi, “MWCNTs/AZ31 surface composites fabricated by friction stir processing,” *Mater. Sci. Eng. A*, vol. 419, no. 1–2, pp. 344–348, Mar. 2006, doi: 10.1016/j.msea.2006.01.016.

[171] P. Asadi, G. Faraji, and M. K. Besharati, “Producing of AZ91/SiC composite by friction stir processing (FSP),” *Int. J. Adv. Manuf. Technol.*, vol. 51, no. 1–4, pp. 247–260, Nov. 2010, doi: 10.1007/s00170-010-2600-z.

[172] Ø. Frigaard, Ø. Grong, and O. T. Midling, “A process model for friction stir welding of age hardening aluminum alloys,” *Metall. Mater. Trans. A*, vol. 32, no. 5, pp. 1189–1200, May 2001, doi: 10.1007/s11661-001-0128-4.

[173] D. Khayyamin, A. Mostafapour, and R. Keshmiri, “The effect of process parameters on microstructural characteristics of AZ91/SiO2 composite fabricated by FSP,” *Mater. Sci. Eng. A*, vol. 559, pp. 217–221, Jan. 2013, doi: 10.1016/j.msea.2012.08.084.

[174] M. Barmouz, M. K. Besharati Givi, and J. Seyfi, “On the role of processing parameters in producing Cu/SiC metal matrix composites via friction stir processing: Investigating microstructure, microhardness, wear and tensile behavior,” *Mater. Charact.*, vol. 62, no. 1, pp. 108–117, Jan. 2011, doi: 10.1016/j.matchar.2010.11.005.

[175] P. Vijayavel, V. Balasubramanian, and I. Rajkumar, “Effect of Tool Traverse Speed on Strength, Hardness, and Ductility of Friction-Stir-Processed LM25AA-5% SiCp Metal Matrix Composites,” *Metallogr. Microstruct. Anal.*, vol. 7, no. 3, pp. 321–333, Jun. 2018, doi: 10.1007/s13632-018-0442-5.

[176] M. A. Moghaddas and S. F. Kashani-Bozorg, “Effects of thermal conditions on microstructure in nanocomposite of Al/Si3N4 produced by friction stir processing,” *Mater. Sci. Eng. A*, vol. 559, pp. 187–193, Jan. 2013, doi: 10.1016/j.msea.2012.08.073.

[177] M. Azizieh, A. H. Kokabi, and P. Abachi, “Effect of rotational speed and probe profile on microstructure and hardness of AZ31/Al2O3 nanocomposites fabricated by friction stir processing,” *Mater. Des.*, vol. 32, no. 4, pp. 2034–2041, Apr. 2011, doi: 10.1016/j.matdes.2010.11.055.

[178] M. Rezaee Hajideh, M. Farahani, S. A. D. Alavi, and N. Molla Ramezani, “Investigation on the effects of tool geometry on the microstructure and the mechanical properties of dissimilar friction stir welded polyethylene and polypropylene sheets,” *J. Manuf. Process.*, vol. 26, pp. 269–279, Apr. 2017, doi: 10.1016/j.jmapro.2017.02.018.

[179] M. Rezaee Hajideh, M. Farahani, and N. Molla Ramezani, “Reinforced Dissimilar Friction Stir Weld of Polypropylene to Acrylonitrile Butadiene Styrene with Copper Nanopowder,” *J. Manuf. Process.*, vol. 32, pp. 445–454, Apr. 2018, doi: 10.1016/j.jmapro.2018.03.010.

[180] N. Molla Ramezani, B. Davoodi, M. Aberoumand, and M. Rezaee Hajideh, “Assessment of tool wear and mechanical properties of Al 7075 nanocomposite in friction stir processing (FSP),” *J. Brazilian Soc. Mech. Sci. Eng.*, vol. 41, no. 4, p. 182, Apr. 2019, doi: 10.1007/s40430-019-1683-1.

[181] W. J. Arbegast, P. J. Hartley, and J. M. Vitek, “Friction Stir Weld Technology Development at Lockheed Martin Michoud Space System - An Overview, International conference; 5th, Trends in welding research,” in *Trends in welding research, TRENDS IN WELDING RESEARCH -INTERNATIONAL CONFERENCE-, International conference; 5th, Trends in welding research*, 1999, pp. 541–546, [Online]. Available: https://www.tib.eu/de/suchen/id/BLCP%3ACN031929209.

[182] H. Jamshidi Aval, S. Serajzadeh, A. H. Kokabi, and A. Loureiro, “Effect of tool geometry on mechanical and microstructural behaviours in dissimilar friction stir welding of AA 5086–AA 6061,” *Sci. Technol. Weld. Join.*, vol. 16, no. 7, pp. 597–604, Oct. 2011, doi: 10.1179/1362171811Y.0000000044.

[183] M. D. Sameer and A. K. Birru, “Effect of Tool Pin Profiles Using Tungsten Carbide Tool on Microstructure and Tensile Properties of Friction Stir Welded AA 6082-T6 Thin Aluminium Alloy Joints,” in *Advances in Additive Manufacturing and Joining. Lecture Notes on Multidisciplinary Industrial Engineering. Springer, Singapore*, Springer, 2020, pp. 475–486.

[184] R. S. Thube, “Effect of Tool Pin Profile and Welding Parameters on Friction Stir

Processing Zone, Tensile Properties and Micro-hardness of AA5083 Joints Produced by Friction Stir Welding," *Int. J. Eng. Adv. Technol.*, vol. 3, no. 5, pp. 2249–8958, 2014.

[185] V. M. Khojastehnezhad, H. H. Pourasl, and R. Vatankhah Barenji, "Effect of tool pin profile on the microstructure and mechanical properties of friction stir processed Al6061/Al 2 O 3 —TiB 2 surface hybrid composite layer," *Proc. Inst. Mech. Eng. Part L J. Mater. Des. Appl.*, vol. 233, no. 5, pp. 900–912, May 2019, doi: 10.1177/1464420717715048.

[186] M. K. Gupta, "Effects of tool pin profile and feed rate on wear performance of pine leaf ash/Al composite prepared by friction stir processing," *J. Adhes. Sci. Technol.*, pp. 1–13, Jul. 2020, doi: 10.1080/01694243.2020.1800290.

[187] J. Baruch L, R. Raju, and V. Balasubramanian, "Effect of Tool Pin Profile on Microstructure and Hardness of Friction Stir Processed Aluminum Die Casting Alloy," *Eur. J. Sci. Res.*, vol. 70, 2012.

[188] N. Gangil, S. Maheshwari, and A. N. Siddiquee, "Influence of tool pin and shoulder geometries on microstructure of friction stir processed AA6063/SiC composites," *Mech. Ind.*, vol. 19, no. 2, p. 211, Sep. 2018, doi: 10.1051/meca/2018010.

[189] J. Marzbanrad, M. Akbari, P. Asadi, and S. Safaee, "Characterization of the Influence of Tool Pin Profile on Microstructural and Mechanical Properties of Friction Stir Welding," *Metall. Mater. Trans. B*, vol. 45, no. 5, pp. 1887–1894, Oct. 2014, doi: 10.1007/s11663-014-0089-9.

[190] C. N. Suresha, B. M. Rajaprakash, and S. Upadhya, "A Study of the Effect of Tool Pin Profiles on Tensile Strength of Welded Joints Produced Using Friction Stir Welding Process," *Mater. Manuf. Process.*, vol. 26, no. 9, pp. 1111–1116, Sep. 2011, doi: 10.1080/10426914.2010.532527.

[191] F. Khodabakhshi, A. P. Gerlich, A. Simchi, and A. H. Kokabi, "Cryogenic friction-stir processing of ultrafine-grained Al–Mg–TiO2 nanocomposites," *Mater. Sci. Eng. A*, vol. 620, pp. 471–482, Jan. 2015, doi: 10.1016/j.msea.2014.10.048.

[192] G. K. Padhy, C. S. Wu, and S. Gao, "Friction stir based welding and processing technologies - processes, parameters, microstructures and applications: A review," *J. Mater. Sci. Technol.*, vol. 34, no. 1, pp. 1–38, Jan. 2018, doi: 10.1016/j.jmst.2017.11.029.

[193] B. Ratna Sunil, "Different strategies of secondary phase incorporation into metallic sheets by friction stir processing in developing surface composites," *Int. J. Mech. Mater. Eng.*, vol. 11, no. 1, 2016, doi: 10.1186/s40712-016-0066-y.

[194] U. Ramamurty, J. C. McNulty, M. Steen, and L. B. Li, "Fatigue in Ceramic Matrix Composites," in *Reference Module in Materials Science and Materials Engineering*, Elsevier, 2017.

[195] A. Tamadon, D. Pons, K. Sued, and D. Clucas, "Thermomechanical Grain Refinement in AA6082-T6 Thin Plates under Bobbin Friction Stir Welding," *Metals (Basel).*, vol. 8, no. 6, p. 375, May 2018, doi: 10.3390/met8060375.

[196] F. Khodabakhshi, A. P. Gerlich, and P. Švec, “Fabrication of a high strength ultra-fine grained Al-Mg-SiC nanocomposite by multi-step friction-stir processing,” *Mater. Sci. Eng. A*, vol. 698, pp. 313–325, Jun. 2017, doi: 10.1016/j.msea.2017.05.065.

[197] G. Faraji and P. Asadi, “Characterization of AZ91/alumina nanocomposite produced by FSP,” *Mater. Sci. Eng. A*, vol. 528, no. 6, pp. 2431–2440, Mar. 2011, doi: 10.1016/j.msea.2010.11.065.

[198] M. Abbasi Gharacheh, A. H. Kokabi, G. H. Daneshi, B. Shalchi, and R. Sarrafi, “The influence of the ratio of ‘rotational speed/traverse speed’ (ω/v) on mechanical properties of AZ31 friction stir welds,” *Int. J. Mach. Tools Manuf.*, vol. 46, no. 15, pp. 1983–1987, Dec. 2006, doi: 10.1016/j.ijmachtools.2006.01.007.

[199] M. M. El-Rayes and E. A. El-Danaf, “The influence of multi-pass friction stir processing on the microstructural and mechanical properties of Aluminum Alloy 6082,” *J. Mater. Process. Technol.*, vol. 212, no. 5, pp. 1157–1168, May 2012, doi: 10.1016/j.jmatprotec.2011.12.017.

[200] Y. Morisada, H. Fujii, T. Nagaoka, K. Nogi, and M. Fukusumi, “Fullerene/A5083 composites fabricated by material flow during friction stir processing,” *Compos. Part A Appl. Sci. Manuf.*, vol. 38, no. 10, pp. 2097–2101, Oct. 2007, doi: 10.1016/j.compositesa.2007.07.004.

[201] R. Butola, D. Pandit, C. Pratap, P. Chandra. "Two decades of friction stir processing–a review of advancements in composite fabrication", *J. Adhes. Sci. Technol*, Vol. 35, pp. 1–38, 2021, doi: 10.1080/01694243.2021.1938835

[202] H. Izadi, R. Sandstrom, and A. P. Gerlich, “Grain Growth Behavior and Hall–Petch Strengthening in Friction Stir Processed Al 5059,” *Metall. Mater. Trans. A*, vol. 45, no. 12, pp. 5635–5644, Nov. 2014, doi: 10.1007/s11661-014-2492-x.

[203] P. Sahlot, K. Jha, G. K. Dey, and A. Arora, “Quantitative wear analysis of H13 steel tool during friction stir welding of Cu-0.8%Cr-0.1%Zr alloy,” *Wear*, vol. 378–379, pp. 82–89, May 2017, doi: 10.1016/j.wear.2017.02.009.

[204] A. Suri, A. Sahai, K. H. Raj, and N. K. Gupta, “Impact and Tensile testing of Al2024 Alloy Processed by Friction Stir Processing,” *Procedia Eng.*, vol. 173, pp. 679–685, 2017, doi: 10.1016/j.proeng.2016.12.145.

[205] K. Balamurugan, “Investigation on the Effects of Process Parameters on the Mechanical and Corrosion Behaviour of Friction Stir-Cladded AZ31B Magnesium Alloy,” *Arab. J. Sci. Eng.*, vol. 40, pp. 1647–1655, 2015.

[206] E. Moustafa, “Effect of Multi-Pass Friction Stir Processing on Mechanical Properties for AA2024/Al2O3 Nanocomposites,” *Materials (Basel).*, vol. 10, no. 9, p. 1053, Sep. 2017, doi: 10.3390/ma10091053.

[207] N. Murugan and B. Ashok Kumar, “Prediction of tensile strength of friction stir welded stir cast AA6061-T6/AlNp composite,” *Mater. Des.*, vol. 51, pp. 998–1007, Oct. 2013, doi: 10.1016/j.matdes.2013.05.012.

[208] G. . Fernandez and L. . Murr, “Characterization of tool wear and weld optimization in the friction-stir welding of cast aluminum 359+20% SiC metal-matrix composite,”

Mater. Charact., vol. 52, no. 1, pp. 65–75, Mar. 2004, doi: 10.1016/j.matchar.2004.03.004.

[209] A. Tyagi, S. Pandey, R. S. Walia, Q. Murtaza, and R. S. Mishra, "Characterization and parametric optimization of % change in residual stress of Mo composite coating using Taguchi approach," *Mater. Res. Express*, vol. 6, no. 12, p. 125623, Jan. 2020, doi: 10.1088/2053-1591/ab6252.

[210] B. Wang and S. Qu, "Comparison of residual stress before and after shot peening on the surface of a Ti-6Al-4V titanium alloy by μ-X360n equipment," *IOP Conf. Ser. Mater. Sci. Eng.*, vol. 397, p. 012112, Aug. 2018, doi: 10.1088/1757-899X/397/1/012112.

[211] R. Butola, N. Choudhary, R. Kumar, P. K Mouria, M. Zubair, R. M. Singari, "Measurement of residual stress on H13 tool steel during machining for fabrication of FSW/FSP tool pins", *Materials Today: Proceedings,* Vol 43, Part 1, pp. 256-262. 2021, doi.org/10.1016/j.matpr.2020.11.656

[212] K. Tanaka, "X-ray measurement of triaxial residual stress on machined surfaces by the cosα method using a two-dimensional detector," *J. Appl. Crystallogr.*, vol. 51, no. 5, pp. 1329–1338, Oct. 2018, doi: 10.1107/S1600576718011056.

[213] M. Vashista and S. Paul, "Correlation between full width at half maximum (FWHM) of XRD peak with residual stress on ground surfaces," *Philos. Mag.*, vol. 92, no. 33, pp. 4194–4204, Nov. 2012, doi: 10.1080/14786435.2012.704429.

[214] K. Bector, M. Singh, D. Pandey R. Butola, R. M. Singari, "Study of residual stresses in multi-pass friction stir processed surface composites", *Advances in Materials and Processing Technologies*, vol. 6, doi.org/10.1080/2374068X.2021.1939983

[215] M. Iordachescu, J. Hervías, D. Iordachescu, J. Porro, and E. Scutelnicu, "Residual stress analysis of friction stir processed AA6061," *Weld. World*, vol. 52, 2008.

[216] M. Weglowski, P. Sedek, and C. Hamilton, "The effect of process parameters on residual stress in a friction stir processed cast aluminium alloy ALSi9Mg," vol. 64, pp. 301–309, 2016.

[217] L. Zhao, J. G. Santos Macías, A. Dolimont, A. Simar, and E. Rivière-Lorphèvre, "Comparison of residual stresses obtained by the crack compliance method for parts produced by different metal additive manufacturing techniques and after friction stir processing," *Addit. Manuf.*, vol. 36, p. 101499, Dec. 2020, doi: 10.1016/j.addma.2020.101499.

[218] F. Khodabakhshi, B. Marzbanrad, A. Yazdanmehr, H. Jahed, and A. P. Gerlich, "Tailoring the residual stress during two-step cold gas spraying and friction-stir surface integration of titanium coating," *Surf. Coatings Technol.*, vol. 380, p. 125008, Dec. 2019, doi: 10.1016/j.surfcoat.2019.125008.

[219] S. R. Anvari, F. Karimzadeh, and M. H. Enayati, "Wear characteristics of Al–Cr–O surface nano-composite layer fabricated on Al6061 plate by friction stir processing," *Wear*, vol. 304, no. 1–2, pp. 144–151, Jul. 2013, doi: 10.1016/j.wear.2013.03.014.

[220] L. Tyagi, R. Butola, and A. K. Jha, "Mechanical and tribological properties of

AA7075-T6 metal matrix composite reinforced with ceramic particles and aloevera ash via Friction stir processing," *Mater. Res. Express*, vol. 7, no. 6, 2020, doi: 10.1088/2053-1591/ab9c5e.

[221] R. Butola, L. Tyagi, L. Kem, M. S. Ranganath, and Q. Murtaza, "Mechanical and Wear Properties of Aluminium Alloy Composites: A Review," Springer, Singapore, 2020, pp. 369–391.

[222] L.Tyagi, R. Butola, L. Kem, R. M Singari. "Comparative analysis of response surface methodology and artificial neural network on the wear properties of surface composite fabricated by friction stir processing", *Journal of Bio- and Tribo-Corrosion*. Vol. 7,pp. 36, 2021. doi.org/10.1007/s40735-020-00469-1

[223] K. Li, X. Liu, and Y. Zhao, "Research Status and Prospect of Friction Stir Processing Technology," *Coatings*, vol. 9, no. 2, pp. 129, Feb. 2019, doi: 10.3390/coatings9020129

LIST OF PUBLICATIONS

International Journals

1. **Ravi Butola**, Ranganath M. Singari and Qasim Murtaza. Mechanical and wear behaviour of Friction stir processed surface composite through Self-Assembled Monolayer Technique. *Surface Topography: Metrology and Properties* Vol.8 (4), 2020, pp. 045007. https://doi.org/10.1088/2051-672X/abbcb8 **(SCIE) (IF-2.038)**

2. **Ravi Butola**, Qasim Murtaza and Ranganath M.Singari. Formation of Self-Assembled Monolayer and Characterization of AA7075-T6/B_4C Nano-ceramic surface composite using Friction Stir Processing. *Surface Topography: Metrology and Properties,* Vol. 8(2), 2020, pp. 025030. https://doi.org/10.1088/2051-672X/ab96db (**SCIE) (IF-2.038)**

3. **Ravi Butola**, Qasim Murtaza and Ranganath M. Singari. An experimental and simulation validation of residual stress measurement for manufacturing of friction stir processing tool. *Indian Journal of Engineering & Materials Sciences.* Vol. 27(4), 2020, pp. 826-836. **(SCI) (IF-0.88)**

4. **Ravi Butola**, Prakash Chandra, Kartikeya Bector and Ranganath M. Singari. Fabrication and multi-objective optimization of friction stir processed aluminium based surface composites using Taguchi approach. *Surface Topography: Metrology and Properties*, Vol. 9, (2) pp. 025044. https://doi.org/10.1088/2051-672X/ac0ba3 **(SCIE) (IF-2.038)**

5. **Ravi Butola**, Ranganath M. Singari Qasim Murtaza and Lakshay Tyagi. Comparison of response surface methodology with artificial neural network for prediction of the tensile properties of friction stir-processed surface composites. *Proceedings of the Institution of Mechanical Engineers, Part E: Journal of Process Mechanical Engineering*. https://doi.org/10.1177/09544089211036833 (Published Online) (**SCI) (IF-1.620)**

6. **Ravi Butola,** Lakshay Tyagi, Ranganath M. Singari, Qasim Murtaza, Harish Kumar, Dhiraj Nayak. Mechanical and wear performance of Al/SiC surface composite prepared through friction stir processing, *Material Research Express*, Vol.8 (1) (2021) pp. 016520. https://doi.org/10.1088/2053-1591/abd89d **(SCIE) (IF-1.620)**

7. Lakshay Tyagi, **Ravi Butola**, Avinash Kumar Jha. Mechanical and tribological properties of AA7075-T6 metal matrix composite reinforced with ceramic particles and aloevera ash via Friction stir processing. *Material Research Express*, Vol.7 (6), 2020, pp. 066526. https://doi.org/10.1088/2053-1591/ab9c5e **(SCIE) (IF-1.620)**

8. **Ravi Butola**, Deepak Pandit, Chandra Pratap, Prakash Chandra. Two decades of friction stir processing–a review of advancements in composite fabrication, *J. Adhes. Sci. Technol*., pp. 1–38, Vol. 35, 2021. https://doi: 10.1080/01694243.2021.1938835 **(SCI) (IF-2.077)**

9. **Ravi Butola**, Ranganath M. Singari, Qasim Murtaza. Fabrication and optimization of AA7075 matrix surface composites using Taguchi technique via friction stir processing

(FSP). *Engineering Research Express.* Vol. 1(2), (2019) pp. 025015. https://doi.org/10.1088/2631-8695/ab4b00 **(SCOPUS)**

10. **Ravi Butola,** Susheem Kanwar, Lakshay Tyagi, Ranganath M. Singari, Mohit Tyagi. Optimizing the machining variables in CNC turning of aluminum based hybrid metal matrix composites. SN Applied Sciences (2020) 2:1356. https://doi.org/10.1007/s42452-020-3155-8. **(SCOPUS), (ESCI)**

11. Anubhav Coyal, N. Yuvaraj, **Ravi Butola**, Lakshay Tyagi. An experimental analysis of tensile, hardness and wear properties of aluminium metal matrix composite through stir casting process. SN Applied Sciences (2020)2:892. https://doi.org/10.1007/s42452-020-2657-8, **(SCOPUS), (ESCI)**

12. **Ravi Butola**, Ranganath M. Singari, Qasim Murtaza. A Review on Surface Modification of Aluminium Alloy using Friction Stir Processing, *International Journal for Research in Applied Science & Engineering Technology (IJRASET)*, Vol. 7(4), 2019.

13. Susheem Kanwar, **Ravi Butola**, Ranganath M. Singari. Comparison of Genetic Algorithm and Taguchi technique for surface roughness of natural fiber reinforced polymer composites. *SAE International Journal of Materials and Manufacturing*. 14(2):141-151, 2021. **(SCOPUS), (ESCI)**.

14. Lakshay Tyagi, **Ravi Butola**, Luckshaya Kem, Ranganath M Singari. Comparative analysis of response surface methodology and artificial neural network on the wear properties of surface composite fabricated by friction stir processing. In Press. Journal of Bio- and Tribo-Corrosion. Vol. 7, 36 (2021). https://doi.org/10.1007/s40735-020-00469-1 **(SCOPUS)**

15. **Ravi Butola**, Ravi Pratap Singh, Naman Choudhary, K.K.S. Mer, Jitendra Bhaskar, Ranganath M. Singari. Fabrication of FSW Tool Pins through Turning of H13 Tool Steel: A Comparative Analysis for Residual Stresses. Journal of Advanced Manufacturing Systems. https://doi.org/10.1142/S0219686722500135 (**SCOPUS), (ESCI)**

16. **Ravi Butola**, N. Yuvaraj, Ravi Pratap Singh, Lakshay Tyagi, Faim Khan. Evaluation of Microhardness and Wear properties of Al 6063 composite reinforced with Yttrium Oxide using Stir casting process. World Journal of Engineering. https://doi.org/10.1108/WJE-12-2020-0645. (**SCOPUS), (ESCI)**

17. Mridul Gupta, Mushin Ahmad Khan, **Ravi Butola** & Ranganath M. Singari. Advances in applications of Non-Destructive Testing (NDT): A review, Advances in Materials and Processing Technologies, (2021) https://doi:10.1080/2374068X.2021.1909332 (**SCOPUS), (ESCI)**

18. Shourya Sahdev, Himanshu Kumar, **Ravi Butola**, Ranganath M. Singari. Evaluating the effect of process parameters on FSP of AL5083 alloy using ANSYS. Annales de Chimie - Science des Matériaux. 2021, Vol. 45, No. 2, pp. 113-120. https://doi.org/10.18280/acsm.450203. (**SCOPUS), (ESCI)**

19. Kartikeya Bector, Mrinal Singh, Divya Pandey, **Ravi Butola**, Ranganath M. Singari. Study of residual stresses in multi-pass friction stir processed surface composites. Advances in Materials and Processing Technologies, (2021) Vol. 6 https://doi.org/10.1080/2374068X.2021.1939983 (**SCOPUS), (ESCI)**

20. **Ravi Butola**, Chander Pratap, Anurag Shukla, Ravinder Walia. Effect on the mechanical properties of aluminum-based hybrid metal matrix composite using stir casting method. *Mater Sci Forum*. Vol. 969, (2019), 253–259, https://doi.org/10.4028/www.scientifc.net/msf.969.253 Scientific. Net **(SCOPUS)**

21. Anubhav Coyal, Narayan Yuvaraj **Ravi Butola**, Kapil Dev Pandey, Tusharjeet Singh Kalra**,** Microstructure and Mechanical Properties of Synthesized Aluminium Composite using Stir Casting Process *IJAPIE*-2019-04-237, Vol4 (2), 01-06 https://doi.org/10.35121/ijapie201904237

22. **Ravi Butola**, Ranganath MS, Ashwani Bandhu, Ravinder Walia. Characteristics and Properties of different reinforcement in hybrid aluminium composites: a review, *Int. J. Adv. Product Ind.* Eng.-SI-MM, (2017) 511:71–80.

International Conference Proceedings

1. Anshul Chaudhary, Kumar Dev A, Anshul Goel, **Ravi Butola**, Ranganath M.S. The Mechanical properties of different alloys in friction stir processing: a review, *Materials Today: Proceeding* 5(2):5553–5562(2018). https://doi.org/10.1016/j.matpr.2017.12.146, **Elsevier (SCOPUS)**

2. **Ravi Butola**, Aahan Malhotra, Mukesh Yadav, Ranganath MS, Qasim Murtaza, Prakash Chandra. Experimental Studies on Mechanical Properties of Metal Matrix Composites Reinforced with Natural Fibres Ashes. *SAE Technical Paper* 2019-01-1123, https://doi.org/10.4271/2019-01-1123, **SAE (SCOPUS)**

3. **Ravi Butola**, Rishabh Jain, Priyesh Bhangadia, Ashwani Bandhu, Ravinder Walia, Qasim Murtaza, Optimization to the parameters of abrasive flow machining by Taguchi method, *Materials Today: Proceedings* 5(2018)4720–4729. https:doi.org/10.1016/j.matpr.2017.12.044 **Elsevier (SCOPUS)**

4. **Ravi Butola**, Qasim Murtaza, Ravinder Walia. Two start and Three Start Helical Abrasive Flow Machining for Brittle Materials, *Materials Today: Proceedings* 4(2017)3685-3693. https://doi.org/10.1016/j.matpr.2017.02.263 **Elsevier (SCOPUS)**

5. **Ravi Butola**, Jitendra kumar, Vaibhav khanna, Parvesh Ali, Vishesh Khanna. Effect on Surface Properties OF Mild Steel during Dry Turning & Wet Turning on Lathe, *Materials Today: Proceedings* 4 (2017) 7892–7902 https://doi.org/10.1016/j.matpr.2017.07.125 **Elsevier (SCOPUS)**

6. Shantilal Meena, **Ravi Butola**, Qasim Murtaza, Hardik Jayantilal, M.S Niranjan. Metallurgical Investigations of Microstructure and Micro hardness across the various zones in Synergic MIG Welding of Stainless steel. *Materials Today: Proceedings* 4, 2017, 8240–8249. https://doi.org/10.1016/j.matpr.2017.07.166 **Elsevier (SCOPUS)**

7. Mukesh Yadav, Deepak Kumar, **Ravi Butola**, Ranganath M.Singari. Effect of the impact strength of glass fibre reinforced plastic composite using wet layup process, *Materials Today: Proceedings.* 2020, pp. 919-924. https://doi.org/10.1016/j.matpr.2020.03.077 **Elsevier (SCOPUS)**

8. Ishant Khurana, Chandra Pratap, Shubhender Singh, Ankit Bansal, **Ravi Butola.** Experimental analysis of different GSM of glass fibre using Dynamic Mechanical Analysis. *Materials Today: Proceedings*. Vol. 25 (4), 2020, pp. 946-951 https://doi.org/10.1016/j.matpr.2020.04.332 **Elsevier (SCOPUS)**

9. **Ravi Butola**, Naman Choudhary, Ravi Kumar, Pradeep Kumar Mouria, Mohammad Zubair, Ranganath M. Singari. Measurement of residual stress on H13 tool steel during machining for fabrication of FSW/FSP tool pins. Materials Today: Proceedings, Vol 43, Part 1, 2021, 256-262. https://doi.org/10.1016/j.matpr.2020.11.656 **Elsevier (SCOPUS)**

Book Chapter

1. **Ravi Butola**, Qasim Murtaza, Ranganath M.Singari, Advances in Computational Methods in Manufacturing, *Lecture Notes on Multidisciplinary Industrial Engineering*. Springer (Eds: R. Narayanan, S. Joshi, U. Dixit), Singapore, 2019, pp.337-348. https://doi.org/10.1007/978-981-32-9072-329, **Springer (SCOPUS)**

2. **Ravi Butola**, Tyagi L., Kem L., Ranganath M.S., Murtaza Q. (2020) Mechanical and Wear Properties of Aluminium Alloy Composites: A Review. In: Sharma V., Dixit U., Sørby K., Bhardwaj A., Trehan R.(eds) Manufacturing Engineering. *Lecture Notes on Multidisciplinary Industrial Engineering.* Springer, Singapore. https://doi.org/10.1007/978-981-15-4619-8_28 **Springer (SCOPUS)**

3. Kartikeya Bector, Mrinal Singh, Divya Pandey, **Ravi Butola**, Ranganath M. Singari. (2021). A Review on the Fabrication of Surface Composites via Friction Stir Processing and Its Modeling Using ANN. In R. M. Singari, K. Mathiyazhagan, & H. Kumar (Eds.), *Advances in Manufacturing and Industrial Engineering.* (pp. 1–11). Lecture Notes in Mechanical Engineering, Springer, Singapore. https://doi.org/10.1007/978-981-15-8542-5_1 **Springer (SCOPUS)**

4. Saurav Kumar Gupta, Chauhan S., Shivam, **Ravi Butola.** (2021) Development and Properties of Aluminium-Based Metal Matrix Composite: A Review. In: Kumar A., Pal A., Kachhwaha S.S., Jain P.K. (eds) Recent Advances in Mechanical Engineering. Lecture Notes in Mechanical Engineering. Springer, Singapore. https://doi.org/10.1007/978-981-15-9678-0_82 **Springer** (**SCOPUS)**

International Conferences Presented

1. **Ravi Butola**, Qasim Murtaza and Ranganath M. Singari. CNC Turning and Simulation of Residual Stress Measurement on H13 Tool Steel. 2nd International Conference on Computational Methods in Manufacturing (ICCMM -2019) at IIT Guwahati, 8-9 March 2019.

2. **Ravi Butola**, Ranganath M. Singari, Qasim Murtaza. A Review on Surface Modification of Aluminium Alloy using Friction Stir Processing. International Conference on Advanced Production and Industrial engineering (ICAPIE 2018), 5-6, October, 2018.

3. **Ravi Butola**, Lakshay Tyagi, Lakshay Kem, Ranganath M.Singari, Qasim Murtaza. Mechanical and Wear Properties of Aluminium Alloy Composites: A Review. 6th International Conference on Production and Industrial Engineering, (CPIE-2019) during June 08-10th, 2019 at Dr. B R Ambedkar National Institute of Technology, Jalandhar Punjab.

4. Anubhav Coyal, Narayan Yuvaraj **Ravi Butola**, Kapil Dev Pandey, Tusharjeet Singh Kalra. Microstructure and Mechanical Properties of Synthesized Aluminium Composite using Stir Casting Process International Conference on Advance Production and Industrial Engineering (ICAPIE)-2019 at Delhi Technological University, New Delhi.

5. Kartikeya Bector, Aranyak Tripathi, Divya Pandey, **Ravi Butola**, and Ranganath M. Singari. A Review on the Fabrication of Surface Composites via Friction Stir Processing and Its Modeling Using ANN. 4th International Conference on Advanced Production and Industrial Engineering (ICAPIE 2019) at DITE Delhi, 20-21 December 2019.

6. Kartikeya Bector, **Ravi Butola** and Ranganath M.S. Effect of the processing parameters on the microhardness of Friction stir processed surface composite and its prediction using Artificial neural network. 1st International Conference on Energy, Materials Sciences and Mechanical Engineering (EMSME - 2020) at NIT Delhi, 31st October-1st November 2020.

7. **Ravi Butola**, Naman Choudhary, Ravi Kumar, Pradeep Kumar Mouria, Mohammad Zubair, Ranganath M. Singari. Measurement of residual stress on H13 tool steel during machining for fabrication of FSW/FSP tool pins. 1st International Conference on Energy, Materials Sciences and Mechanical Engineering (EMSME - 2020) at NIT Delhi, 31st October-1st November 2020.

8. Faim Khan, N. Yuvaraj, **Ravi Butola,** Lakshay Tyagi and Luckshaya Kem and. Analysis of tribological properties of Aluminium metal matrix composite fabricated by Stir casting method. International Conference on Industrial and Manufacturing Systems (CIMS-2020) held on October 09-11, 2020 at Dr. B R Ambedkar National Institute of Technology, Jalandhar, Punjab, India.

9. **Ravi Butola**, Anshul Chaudhary, Pankaj Raj Meena, and Shanti Lal Meena. Optimization of Aluminium based metal matrix Surface composite using Taguchi technique via Friction stir processing. International Conference on Industrial and Manufacturing Systems (CIMS-2020) held on October 09-11, 2020 at Dr. B R Ambedkar National Institute of Technology, Jalandhar, Punjab, India.

10. Ravi Kumar, **Ravi Butola**, Naman Choudhary, Mohammad Zubair, Optimization of FSP Process Parameters of surface composites using GRA and Taguchi Approach. 3rd International Conference on Computational & Experimental Methods in Mechanical Engineering (ICCEMME-2021)" organized by Department of Mechanical Engineering G. L. Bajaj Institute of Technology & Management, Greater Noida, India, which will be held on Feb 11-13, 2021

CURRICULUM VITAE

MR. RAVI BUTOLA has obtained his B.Tech Degree from College Of Technology, G.B. Pant University of Agriculture and Technology, Pantnagar, Uttarakhand, India, and Master Degree in Production Engineering from Delhi Technological University (Formerly Delhi College of Engineering), Delhi, India. Since 2014, he has been working as an Assistant Professor in the Department of Mechanical Engineering, Delhi Technological University (Formerly Delhi College of Engineering), Delhi, India. He has also worked as Lecturer in G.B.P.E.C Ghurdauri, Pauri Garhwal, Uttarakhand, and as an Assistant Professor at Shivalik College of Engineering, Dehradun, Uttarakhand. He is actively engaged in teaching and research. He has eight year of teaching experience. He has published more than 30 research papers in International Journal and Conferences Proceedings and 4 Book chapters. He has guided 5 M.Tech students. He is currently working in the area of surface modification and composite materials.